Final Report

Delivery System for Cirrus Cloud Thinning

DSE Group 11

Technische Universiteit Delft

TU Delft

THIS PAGE IS INTENTIONALLY LEFT BLANK.

Final Report

Delivery System for Cirrus Cloud Thinning

by

DSE Group 11

Group Members:	M.D.N. Aalberse	4279611
	E.A. Ebbens	4492277
	S.J. van den Eijkel	4351150
	C.A. ‘t Hooft	4440625
	N. Schiettekatte	4485610
	M.V. Sickler	4354052
	A. Stienstra	4374886
	M.A.S. Stol	4237323
	J.F.A. Vlasblom	4365526
	M. Zupanič	4440560
Staff Members:	Dr. S.J. Hulshoff	Tutor
	J.P. Pinto Leite MSc.	Coach
	Ir. O. Stroosma	Coach

TU Delft

Acknowledgements

Our team would like to express our great appreciation to our supervisor Steven Hulshoff and our coaches Olaf Stroosma and Pedro Pinto Leite. Their professional advice has been essential for our group. Next to this, the guidance of the OSCC, OSSA's and PMSE TA's has been a great help in this learning experience. Furthermore, we are grateful for the help of associate professor David L. Mitchell of the Desert Research Institute in Reno for his expertise in the field of Cirrus Cloud Thinning.

Contents

List of Figures

List of Tables

[2] Retrieved from; http://www.aerospaceweb.org/question/airfoils/q0041.shtml [05-04-2018]

Executive Overview

Introduction
Global warming is a pressing issue mankind is currently facing. The Earth is warming at an alarming rate and climate models show that this warming is expected to continue if no sufficient action is taken. Although moving to clean power sources is the only long term sustainable solution, it is proving difficult to achieve this transition in a reasonable time. Due to this rising issue, geo-engineering is investigated as a possible method to temporarily halt global warming in case of a climate catastrophe. The geo-engineering method investigated in this project is called Cirrus Cloud Thinning. Its purpose will be to allow more time for mankind to reduce the greenhouse gas emissions. However, it cannot be seen as a solution to climate change as a whole.

The mission of this project is to design a delivery system to temporarily protect mankind from the detrimental effects of global warming, through Cirrus Cloud Thinning, in the event of a global climate catastrophe. This mission is achieved by performing the preliminary design of a system to deliver ice nuclei which prevent homogeneous cirrus formation for the purpose of climate engineering, by 10 students in 10 weeks.

Operations
The mission is performed with a large fleet of aircraft, the operation of this fleet is done from four different airports in the Northern and Southern hemispheres. The airports chosen for this mission are Ushuaia, Christchurch, Svalbard and Thule. They have been chosen for their location, capacity, ability to expand and local weather conditions. A noise restriction study was done for the airports to ensure that operation from these bases is possible. For each of the chosen airports changes to the infrastructure are needed to accommodate the ACT fleet. To further support the operation maintenance and ground crew is needed at the airports. Flight operators can control up to six aircraft at the same time, as the aircraft do most of the operation autonomously. Weather effects, both for the airports and at cruise altitudes, were investigated, at altitude polar jets in particular could have a large effect on the mission.

Payload Subsystem Design
One of the most important aspects of the mission is an accurate injection of the ice nuclei (IN) into the troposphere. To ensure that this can be done consistently, a detailed payload subsystem was designed. A concentration of 35 particles per litre will be maintained by injecting IN into the upper 3 kilometres of the troposphere by the seeding aircraft each week. This is based on the assumption that the dispersion will be 10 kilometres in width and 1 kilometre in height. The IN material chosen for the seeding is bismuth tri-iodide, as this material is relatively inexpensive, has a low effectivity threshold and is not toxic for the environment. However, bismuth tri-iodide has not been used for this purpose before and thus the system is also made compatible with silver iodide to guarantee success of the mission.

The material is transported in a solution form consisting of bismuth tri-iodide and ethanol, which is combusted before dispersion into the troposphere. The chemical reaction in this combustion chamber is given in the following relation: $C_2H_5OH + 3O_2 \rightarrow 2CO_2 + 3H_2O$. The combustion chamber volume is determined to be 2.8 litres, and will be placed at the tail end of the fuselage. A pump will be placed between the storage tank and combustion chamber to regulate the flow, which is 4.37 grams per second at 10 kilometres altitude.

To ensure that the desired concentration of IN in the cirrus clouds is maintained an Ultra-High Sensitivity Aerosol Spectrometer is installed, which can accurately measure the particle concentration. The overall effect of CCT however is monitored using the CALIPSO, GOES-16, and GOES-17 satellites. Together they can observe how cirrus clouds and aerosols in the atmosphere behave.

In case of urgency, a possibility of integrating the system into existing aircraft was investigated. There are several options to integrate the payload subsystem into existing aircraft. For example, the cabin content of a passenger aircraft could be replaced by the payload system using bleed air for passengers for the payload system. However, integrating the payload subsystem into existing aircraft will likely result in an inefficient

system, as the range of most aircraft is significantly less, thus resulting in a very large amount of aircraft to fulfil the mission. It can be used however for initial testing purposes.

Aircraft Design

The most driving requirement for the aircraft design identified was the 14,000 km minimal range. As the aircraft will most likely be governmental or internationally owned, it does not have to adhere to the EASA or FAA regulations. Consequently, the constraints on wing loading and thrust come from operational aspects like base airport operational procedures. The two most constraining requirements found in the thrust and wing loading diagrams were the sea level climb rate and stall speed with high lift devices (HLD's). The last iteration gave the W/S of 4150 N/m^2 and T/W of 0.215.

It was decided that the aircraft should be unmanned based on lower operating cost, higher reliability, better operational flexibility and system weight. The aircraft incorporates a single fuselage because of the high technology readiness level (TRL), simplicity and good performance in cross-wind conditions. It was decided to use a single engine for high fuel efficiency and low maintenance cost. Since the aircraft is unmanned and is mostly operating over non-populated regions, the safely in case of an engine failure was not of high priority. The turbofan engine is mounted on top of the fuselage to avoid the injection of foreign objects from the runway and allows for a shorter landing gear. It was also decided that in combination with this engine position a V-tail offers the best performance, since the engine and the tail can be moved almost independently to control the centre of gravity.

For range performance an aspect ratio of 15 was chosen which is slightly higher than regional turboprop aircraft. A taper ratio of 0.4 was chosen since it offers almost elliptical lift distribution. The wings were kept unswept because of the low cruise Mach number and good structural characteristics. NACA $65_2$416 was selected since it offered the best compromise of performance out of all examined airfoils. The $C_{L_{max}}$ in clean configuration at landing is approximately 1.2. To achieve the stall speed of 60m/s with MTOW, HLD's had to be implemented. However, the complexity of HLD's had to be as low as possible to reduce weight and maintenance. Therefore, single slotted flap system was designed and incorporated.

The preliminary fuselage and empennage sizing were optimised to minimise zero-lift drag. First, the fuselage volume budget was estimated based on the required payload, fuel that did not fit in the wing and avionics. Moreover, a constraint was placed on the fuselage slenderness ratio for structural considerations. The V-tail fin dihedral of 50° could be obtained from the ratio of the required horizontal and vertical tail surface. The selected engine is GE Honda HF120 which provides sufficient thrust at sea level and at cruising altitude. It will run on jet-B fuel because of the low freezing point. After the main components of the aircraft were sized a more detail drag estimation was obtained and the drag polar was constructed.

The landing gear positioning and sizing in parallel with the wing positioning since the main landing gear is attached to the wing. The final iteration gave 20% of the static load on the nose landing gear and 80% of the load onto the main landing gears. The nose gear has a single strut and the main landing gear incorporates two struts. Each strut has one wheel.

The class II weight estimation was done with the method for general aviation described by Raymer [74]. The flight envelope gave the most constraining load was a positive gust load which gave a factor of 3.9, including a 50% margin. To perform the iterations, the outputs of class II weight estimation were fed back to class I weight estimation and aircraft sizing together with better estimates of other performance parameters, such as L/D. The iterations were performed until the two consecutive OEW results differed for less than 1%.

A more detailed tail design was done using the stability parameters of the Arctic Tern. First, the longitudinal stability was analysed. To control the CG range and the required tail surface size the wing had to be positioned. The optimum stabiliser size and wing position were found with the scissor plot, the static stability margin incorporated was 5%. To size the ailerons a constant roll rate of 45° in 1.4 s was taken for the requirements. The differential ailerons were incorporated to reduce adverse yaw. For the vertical stabiliser and rudder it was found that with the current vertical stabiliser the aircraft is directionally stable in all operational flight regimes. The rudder was sized based on the de-crab manoeuvre in cross-wind landing with the side-slip angle of 30°.

The analysis of the electrical consumption of the aircraft result in 8.9 kVA required power. The CCT Arctic

Tern will have a ram air turbine in case of engine loss. The fuel system incorporates many redundancies since it is crucial for the aircraft to be able to shift the fuel weight in between tanks. Moreover, a fuel jettison system is included to be able to quickly reduce weight for emergency landing.

Table 1: Final values for the aircraft parameters

Parameter	Value
Mass & Balance	
MTOW	4323 kg
OEW	1378 kg
Maximum fuel weight	2650 kg
Maximum payload weight	297 kg
Most forward c.g. position	13 MAC%
Most aft c.g. position	38 MAC%
Fuselage dimensions	
Fuselage length	7.90 m
Fuselage diameter	0.935 m
Nosecone length	0.468 m
Tailcone length	2.34 m
XLEMAC	3.80 m
Landing gear	
Nose gear position from nose	0.49 m
Main gear position from nose	4.27 m
Wheel base	3.78 m
Main landing gear track	1.23 m
Nose gear tire diameter	0.46 m
Main gear tire diameter	0.54 m

Parameter	Value
Wing dimensions	
Surface area	10.2 m^2
Aspect Ratio	15
Span	12.4 m
Taper ratio	0.4
MAC	0.88 m
Quarterchord sweep angle	0°
Airfoil	NACA65_2416
Empennage dimensions	
Configuration	V-tail
Dihedral	50°
Surface area	4 m^2
Aspect ratio	2.5
Span	2.24 m
Taper ratio	0.3
Leading edge sweep angle	40°
Control surfaces	
High-lift device type	Single-slotted flap
Aileron surface area	0.33 m^2 per wing
Total ruddervator surface area	0.86 m^2

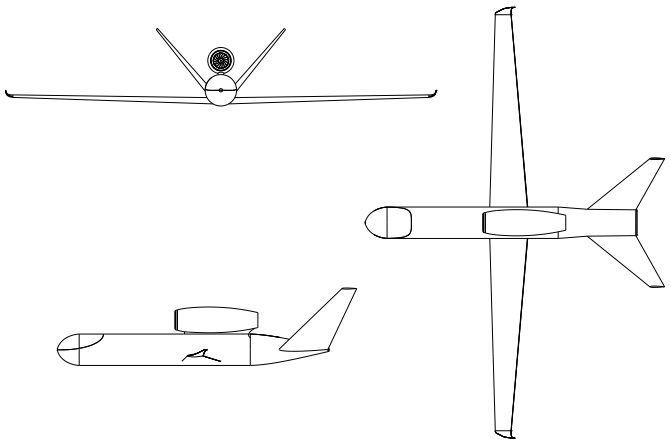

Figure 1: Drawing of the aircraft from three perspectives.

Aircraft Performance

XFLR5 was used for the aerodynamic analysis, a model was built which consists of the wing and tail section, neglecting the fuselage and wing tips. Resulting in a trim angle of -2.1° for the tail for maximum range. This resulted in the trim point occurring at 1.4° and a maximum L/D of 26.3, however, this value is expected to be an overestimation due to the model omitting the fuselage.

Subsequently, T7 analysis was performed in XFLR5 to determine stability and control characteristics of the aircraft. Furthermore, the response of the Arctic Tern to the short period, phugoid, dutch roll, and spiral motion were evaluated. For the short period, phugoid, and dutch roll, the Arctic Tern is stable and adheres to the level 2 Cooper-Harper handling requirements. This is acceptable for the Arctic Tern since there is an autopilot system

in place. The spiral mode is unstable, but because of the large time constant this is considered acceptable since there is enough time to counter this motion.

The structural analysis of the aircraft focuses on the preliminary design of the fuselage and wing. First, carbon fibre reinforced plastic (CFRP) was selected as the material to be used in these sections. Aluminium alloys, titanium alloys, and glass reinforced polymers were all considered too. They were evaluated primarily on material weight, strength, and cost. The loading diagrams can then be produced for the aircraft critical loading cases. A stress analysis is then performed on these cases, at which point it is possible to come up with a detailed design of the wingbox so that the critical loads are met. This includes the number of stringers, stringer area, skin thickness, and the maximum stresses and deflections the wingbox can endure. Aeroelasticity was also evaluated. This was done in two parts: static aeroelasticity and dynamic aeroelasticity. The AT1 met the requirements established by analysing the two most significant static aeroelasticity effects, torsional divergence and control reversal. Meanwhile, the AT1's design was not analysed in detail to flutter but due to the coinciding centre of gravity and flexural centre of the wing, flutter is not expected to be a problem.

The AT1's flight performance was analysed for all the scenarios it will encounter during its mission. This involved evaluating all phases of the flight profile: start-up and taxi, take-off, climb, transit departure, seeding, transit return, descent, climb to transit/loiter altitude, transit, loiter, descent, landing, and taxi. The flight performance was then linked to the requirements to make sure the AT1 could perform its mission. The distance travelled, fuel burnt, and time taken for each phase were estimated, as well as the AT1's service ceiling.

The final aspect of performance analysis was evaluating whether or not the aircraft could perform in all weather conditions. The potential causes of failure considered were low temperatures, low visibility, cross-winds, and the presence of ice.

Reliability, Availability, Maintainability and Safety Characteristics
During the design of ACT the required availability level of the system has to be considered during all different phases of the project. These characteristics combined determine the availability of the system. A failure mode analysis is performed to map the different function that can fail and their causes using top-down approach. After this analysis a redundancy philosophy is set-up to account for failure modes that are found to be both critical and likely to happen. Redundancies are mostly implemented in the flight control, measurement and communication subsystems of the aircraft, as these are vital to the mission performance.

Compliance Matrix
The compliance matrices have shown that all requirements set at the beginning phase of the project have been met. However, there are some requirements that can only be conformed to at a more detailed phase of the project, for example the training of the maintenance personnel. Three requirements were identified as killer requirements at the beginning stages of the project and are therefore not achieved in the design phase, as expected. The killer requirements were found to be STK-CUS-05, STK-CUS-06, and STK-CUS-15. These are related to the initial development cost, annual operating cost, and all-weather operations respectively.

Market Analysis
Market analysis is a method to understand the competition as well as the interests and opinions of the customer and stakeholders, which are important aspects of any engineering project. The market analysis includes the investigation of potential users and buyers, suppliers, competition, funding and the public opinion.

Since CCT is a very costly mission, and the seeding airspace is territorial, it would be most feasible for collaboration between governments to execute such a mission. The customer will most likely be a multi-national organisation such as the United Nations. The funding for such an expensive mission could be provided by participating nations. The amount of funding contributed by each country could be proportional to their contribution to climate change, for example the amount of greenhouse gases emitted. The public is polarised on this topic, caused by both the potential positive and negative effects of CCT.

All the chosen external suppliers have been chosen to be reliable partners active throughout the aerospace industry. Several back-up suppliers, with similar products and capacities, are identified in case one of the suppliers is no longer available. The competition for a similar mission is estimated to be small. Companies pursuing different geo-engineering techniques, for example stratospheric aerosol injection, could pose a po-

tential competitor. The other source of competition will arise from other CCT projects. This could be done using existing aircraft or example, however after analysing the yearly and initial cost of implementing CCT with existing aircraft it was found that the yearly operational costs would be 2 to 3 times as high compared to the AT1 and half a billion euros more on the initial cost. To counter all possible competition, the CCT project will have to have the best combination of performance, sustainability and cost.

Sensitivity Analysis
A sensitivity analysis was performed to show the robustness of the design to certain changes in parameters. These parameters can either be performance variables that were assumed such as L/D and dispersion area or user requirements such as the seeding latitude and seeding interval. Since ACT consists of a fleet of aircraft, most of the problems can be solved by scaling the fleet. Of course this will increase the cost of the system, therefore a change in variable is plotted over the total cost. A change in seeding area from 60°to 45°was investigated in more detail. In general an increase in area, either by a change in dispersion width, depth or requirements by a factor of two also causes an increase of cost by a factor of two. A recommendation is made to model the seeding performance more accurately to be able to better estimate the cost.

Technical Risk Assessment
During the more detailed design phase of the project more risks were identified. These risks were then analysed, mapped and mitigated to ensure that they reduce the chance of project failure, delay or financial issues. These risks include competitors, project development time, modification of airports, controllability of the aircraft, range, aircraft take-off and landing performance, weather effects of the flight path, IN dispersion rate, and the performance of bismuth tri-iodide. These are divided into four main risk categories: payload, operations, aircraft, and project development. The risks are analysed based on their likelihood and severity, after which these are mitigated where possible.

Verification and Validation
To ensure the validity of the models that were made for the design and evaluation of the aircraft, verification and validation on these models were done.

The class II weight estimation has been verified with hand calculations for each component and for the complete model. The estimation has been validated by inserting the dimensions of the Gulfstream G550 and comparing the estimated operational empty weight with the actual operational empty weight. A discrepancy of 8.9% which was acceptable in this design stage.

The fuselage length optimisation model has been verified with limit tests which showed expected results and with hand calculations. As the fuselage length optimisation consists of three modules, each module was validated. The first module is calculating the dimensions of the fuselage such that it has a volume equal to the required volume. The module was validated by inputting the final dimensions into an external volume calculator for geometric shapes and comparing the volume with the required volume. The second module calculates the empennage size from statistics. The dimensions of six reference aircraft have been used to calculate the empennage size and these have been compared with their actual empennage size. The horizontal tail surface estimation was found to have a standard deviation in discrepancy of 10.4% and the vertical tail surface estimation was found to have a standard deviation of the discrepancy of 9.9%. The zero-lift drag estimation was the final module and has been validated with the dimensions and zero-lift drag coefficient of the Boeing 727-100. The discrepancy of the zero-lift drag was found to be an overestimate of 14.6%. This was considered acceptable in this design stage.

The scissor plot, used to position the wing and design the empennage in more detail, has been verified with hand calculations. Furthermore, the scissor plot has been validated by comparing the results with reference aircraft. It was shown that the location of the wing was very similar to reference aircraft, with a maximum discrepancy of 4.6%. The tail size was found to be within the range of the reference aircraft.

A more detailed drag estimation has been verified and validated with the same method as the drag estimation for the fuselage length optimisation. A discrepancy of 1.25% was found for the zero-lift drag estimation using the Boeing 727-100 as reference aircraft.

The structural analysis model has been verified with hand calculations at the critical points. The validation

should be done by testing or using a Finite Element Method (FEM). At this stage, the structural analysis model is validated using a mass approximation and comparing the calculated mass of the structure with the statistical mass of the structure. A discrepancy of 13% was found.

The cost analysis of the aircraft has been validated with different cost estimations. The RDT&E cost was estimated to be €8.8M, while the alternative cost estimations were found to estimate the cost at €6.1M and €8.7M. The cost estimation is therefore agreeing with the alternative models and gives a conservative estimate. The maintenance cost has been proven to be hard to estimate. Commercial airliner maintenance cost has been used as reference and the cost estimation for the maintenance is found to be within the bounds of the maintenance cost of commercial airliners.

Resource Allocation, Budget and Cost Breakdown
To analyse the feasibility of ACT a detailed cost analysis was made to analyse the cost of the mission. These cost were split up in the initial cost, Annual cost and end of life cost. The main contributor for the initial cost of the aircraft was determined to be the manufacturing of the fleet. The biggest contributor to the annual cost was determined to be the maintenance cost, this estimate however caries a lot of uncertainty and should therefore be re-evaluated. The end of life cost only consist of the salvage value of the fleet, this was determined to be an income instead of a cost. An overview of the cost is given in table 2.

Table 2: Summary of the mission cost analysis

Initial cost	€ 2.02 B	**Annual Cost**	€ 762 M	**End-of-life cost**	€ -18.8 M
R&D	€ 423 M	Fixed cost	€ 609 M	Salvage value	€ -18.8 M
Manufacturing	€ 1.46 B	Variable costs	€ 83.5 M		
Setup operations	€ 136 M	Unforeseen costs	€ 69.6 M		

For the future design phases of the AT1 a number of budgets were made. The most important budgets were determined to be the mass and volume budget. The mass budget is based on the Class II weight estimations and the volume budget is based on conceptual estimates. To make sure the design stays within the budgets a strategy of contingencies will be used. These contingencies are based on the level of detail in the different components of the design.

Sustainable Development
To limit the amount of resources, time and money used to complete the CCT mission successfully a sustainable development strategy is set-up. The sustainability of the project is evaluated on three different aspects: economic, environmental and social sustainability. When applying this method during the different phases of the project, economic, environmental, and social criteria have to be considered and, if possible, design choices can be graded on performance with respect to these criteria. An optimally managed project is such that all three indicators are respected. To assess the economic sustainability a market analysis is performed to investigate the market presence and economic feasibility. For the environmental sustainability the CO_2 emissions from manufacturing and operations are estimated with CES Edupack. As expected most of the CO_2 emissions are from the operational part of the project. An important factor to consider for social sustainability is the support of society for the CCT mission, especially since some areas in the world might have to deal with increasing rainfall.

Post-DSE Planning
During the DSE, the conceptual and preliminary design of the CCT delivery system have been performed, this is followed by the detailed design phase that starts after the DSE. In this phase, both the fully integrated option, the AT1 aircraft, and the modular payload systems that can be mounted on existing aircraft will be developed. Immediately after the DSE lab-tests as well as in-situ measurements using existing weather modification aircraft will be initiated to determine the final dispersion characteristics and effect of cloud seeding on CCT. The findings from the tests are used to drive the detailed design and eliminate factors of uncertainty in the assumptions for the preliminary design. The detailed design phase is followed by the production phase, test and certification phase and operational phase, which are partly running in parallel. The AT1 including the fully integrated payload delivery system is expected to have its prototype available 4,5 years after initiation of the detailed design phase which allows for start of the flight test program. The flight test program is projected to be completed in one full year. This implies that the start of operations is foreseen in Q1 2024 if the detailed

design phase is initiated in Q3 2018. As the temperature rise may progress at a rate that calls for action earlier than starting operations in 2024 a modular payload system is developed concurrently with the AT1. The prototype of the modular system is expected to be developed in 2,5 years, allowing seeding operations to commence in Q1 2022 after testing and physical integration of the modular system if the development is started as well in Q3 2018.

Conclusion
A total of 205 aircraft is needed for the ACT mission to seed the area by flying 786 sorties per week. Operating from the following airports: Ushuaia in Argentina, Christchurch in New Zealand, Svalbard in Norway, and Thule in Greenland. These airports were chosen based on their location, capacity, ability to expand and local weather conditions. The IN material chosen was bismuth tri-iodide as this material is relatively cheap, has a lower effectivity threshold and is not toxic for the environment. A weekly concentration of 35 particles per litre has to be maintained in the upper three kilometres of the troposphere. The yearly amount of bismuth tri-iodide required was found to be 422 tons. The material is transported in a solution form consisting of bismuth tri-iodide and ethanol, which is combusted before dispersion into the troposphere. To ensure that the desired concentration of IN in the cirrus clouds is maintained an Ultra-High Sensitivity Aerosol Spectrometer is installed. The overall effect of CCT is monitored using the CALIPSO, GOES-16, and GOES-17 satellites. A modular payload system is designed to integrate in existing aircraft for a short term implementation of CCT.

The driving design factor for the aircraft was the long minimum range of 14,000 km. This resulted in an aircraft with a high aspect ratio of 15, and a wing surface area of 10.2 m^2. This wing design ensures a good lift to drag ratio performance. The engine selected to ensure that the required thrust can be provided given a preferable low operational empty weight is the GE Honda HF120, providing a thrust of 9.1kN at sea level. This turbofan engine will run on jet-B fuel to ensure the fuel doesn't freeze at the low temperatures during aerial operation. With this engine placed on top of the fuselage a V-tail was found to offer the best performance. Resulting in an aircraft with an operational weight of approximately 1378 kg and ability to carry and inject a maximum of 296 kg of IN-ethanol solution per flight.

Using a mission cost analysis it was found that the initial cost is approximately €2 billion, the annual cost was approximated to be €762 million, and the end-of-life cost to be an income of €19 million. The initial costs of the project are relatively high compared to other possible solutions, such as equipping existing aircraft with a modular CCT seeding system. However, due to the highly specific nature of the mission no existing aircraft will be able to surpass the performance of the AT1 in terms of operations cost and environmental impact.

Nomenclature

α	Angle of attack [rad]
$\bar{x}_{ac}$	x-position of aerodynamic centre [m]
$\bar{x}_h$	x-position of horizontal tail [m]
$\bar{x}_{np}$	x-position of neutral point [m]
β	Prandtl-Glauert compressibility correction factor [-]
β	Side-slip angle [rad]
δr	Rudder deflection [rad]
δ_a	Aileron deflection [rad]
$\dot{m}$	Fuel mass flow [kg/s]
$\dot{m}$	Mass flow [kg/s]
$\dot{m}_F$	Fuel mass flow rate [kg/s]
$\dot{m}_{PL}$	Payload mass flow rate [kg/s]
$\dot{q}$	Heat flow [W]
ϵ	Down-wash angle [rad]
η	Airfoil efficiency factor [-]
η_{cc}	Combustion efficiency [-]
η_{comp}	Compression efficiency [-]
γ	Specific heat ratio [-]
γ_{cl}	Climb angle for initial climb [degrees]
$\Lambda_{0.25c}$	Quarter chord sweep [rad]
$\Lambda_{0.5c}$	*Half chord sweep [rad]
Λ_{hinge_line}	HLD's hinge line sweep [rad]
$\overline{\frac{L}{D}}$	Mean Lift over drag [-]
$\overline{V}_{to}$	Average speed during take-off [m/s]
Π_{comp}	Compression ratio [-]
ψ	Overturn angle [rad]
ρ	Air density [kg/m^2]
ρ	Density [kg/m^3]
σ	Fuselage side-wash angle [rad]
σ	Stress [N/m^2]
T	angle of the V-tail with respect to the horizon when the pitch is zero [rad]
τ	Control surface effectiveness [-]
τ	Shear stress [N/m^2]
A	Area combustion chamber [m^2]
A	Enclosed area [m^2]
A	Wing aspect ratio [-]
a	Speed of sound [m/s]
$a_{ellipse}$	Semi-major axis ellipse [m]
B_{area}	Area of a boom [m^2]
$b_{ellipse}$	Semi-minor axis ellipse [m]
c	Wing chord [m]
C_D	Aircraft drag coefficient [-]
C_L	Aircraft lift coefficient [-]
C_l	Airfoil lift coefficient [-]
C_m	Moment coefficient [-]
C_{D_0}	Zero-lift drag coefficient [-]
C_{d_0}	Airfoil zero-lift drag coefficient [-]
$C_{D_{misc}}$	Miscellaneous zero-lift drag coefficient [-]
C_{l_p}	First derivative of roll moment with respect to roll rate [Nm/s]
$C_{L_{\alpha_h}}$	First derivative of the horizontal tail lift coefficient with respect to angle of attack [-]
$C_{L_{\alpha_{A-h}}}$	First derivative of aircraft without the horizontal tail lift coefficient with respect to angle of attack [-]
$C_{L_{\alpha_v}}$	First derivative of the vertical stabiliser lift coefficient with respect to the angle of attack [-]
C_{l_α}	First derivative of airfoil lift coefficient with respect to angle of attack [-]
$C_{l_{\delta a}}$	First derivative of roll moment with respect to aileron deflection [Nm]
C_{m_α}	First derivative of moment coefficient with respect to the angle of attack [-]
$C_{n_{\beta_{fuselage}}}$	First derivative of the yaw moment with respect to the side-slip angle - contribution of the fuselage[Nm]
$C_{n_{\beta_{VT}}}$	First derivative of the yaw moment with respect to the side-slip angle - contribution of the vertical tail[Nm]
$C_{n_{\beta_{wing}}}$	First derivative of the yaw moment with respect to the side-slip angle - contribution of the wing[Nm]
C_{n_β}	First derivative of the aircraft yaw moment with respect to the side-slip angle [Nm]
$C_{n_{\delta r}}$	First derivative of the aircraft yaw moment with respect to the rudder deflection [Nm]
$c_{p,g}$	Specific heat of a gas [$JK^{-1}kg^{-1}$]]
c_p	Specific heat [$JK^{-1}kg^{-1}$]
e	Oswald efficiency factor [-]
ec	Distance from flexural point to aerodynamic

	centre [m]
G	Modulus of rigidity [GPa]
g	Gravitational acceleration [m/s^2]
h	Sphere height [m]
h_{scr}	Screen height [m]
I	Moment of Inertia [m^4]
J	Torsional stiffness [m^4]
K	Aircraft induced drag factor [-]
k	Load factor [-]
L	Lift force [N]
L	Reference distance between point of pressure and farthest boundary in loading direction [m]
L_a	Sound pressure level [-]
L_{A-h}	Lift of the aircraft without the horizontal stabiliser [N]
L_{DN}	Day-night average sound level [dB]
l_{fus}	Length of the fuselage [m]
l_n	Distance from nose to main landing gear [m]
l_n	Distance from nose to nose landing gear [m]
l_v	Vertical stabiliser arm [m]
M	Bending moment [N/m]
M	Mach number [-]
M_{dd}	Drag divergence Mach number [-]
MAC	Mean aerodynamic chord length [m]
$MTOW$	Maximum take-off weight [kg]
OEW	Operational empty weight [kg]
P	Pressure [Pa]
P	Steady roll rate [rad/s]
P_a	Available power [W]
P_m	Load on the main landing gear [N]
P_n	Load on the nose landing gear [N]
Q	Flow function [$kgK^{0.5}/m^2kPas$]
q	Shear flow [N/m]
$q_{s,0}$	Correcting shear flow [N/m]
R	Range [m]
R	Specific gas constant for air [$Jkg^{-1}K^{-1}$]
r	Sphere Radius [m]
R_{cl}	Radius for initial climb [m]
ROC_{sc}	Rate of climb at service ceiling [m/s]
S_h	Horizontal tail reference area [m^2]
S_v	Vertical tail reference area [m^2]
S_z	Shear force [N]
S_{vtail}	Reference area of the V-tail [m^2]
SEL	Sound exposure level [-]
SFC	Specific Fuel Consumption [kg/Ns]
SM	Stability margin [-]
Swf	Wing area affected by HLD's [m^2]
T	Temperature [K]
T	Thrust [N]
t	Thickness [m]
t	Time [s]
T_0	Temperature at sea level [K]
T_r	Required power [W]
T_0	Temperature at sea level [K]
T_{fl}	Flame temperature [K]
V	Aircraft true airspeed [m/s]
V	Volume [m^3]
V_h	Airflow velocity at the horizontal stabiliser [m/s]
V_{cc}	Volume combustion chamber [l]
V_{cruise}	Cruise speed [m/s]
V_{div}	Divergence speed [m/s]
$V_{fuselage}$	Fuselage volume [m^3]
$V_{max,dd}$	Maximum speed due to drag divergence limit [m/s]
V_{rev}	Reversal speed [m/s]
V_{stall}	Stall speed [m/s]
V_{to}	Take-off speed [m/s]
V_{VT}	Volume coefficient of the vertical stabiliser [-]
W	Weight of the aircraft [N]
w	Contrail width [m]
X_h	Horizontal tail arm from the nose [m]
X_v	Vertical tail arm from the nose [m]
$X_{aft,cg}$	Most far aft position of aircraft CG [m]
X_{cg}	Location of the centre of gravity from the nose [m]
x_{LEMAC}	Length from the nose to the leading edge of the mean aerodynamic chord [m]
X_w	Location of the main landing gear attachment point in the wing from the nose [m]
y	Span-wise wing position [m]
y_{MAC}	Span-wise position of the mean aerodynamic chord [m]
Y_{MLG}	Main landing gear track [m]

1 Introduction and Project Objective

Global warming is a pressing issue mankind is currently facing. The Earth is warming at an alarming rate and climate models show that this warming is expected to continue if no sufficient action is taken. Although moving to clean power sources is the only long term sustainable solution, it is proving difficult to achieve this transition in a reasonable time. Due to this rising issue, geo-engineering is investigated as a possible method to temporarily halt global warming in case of a climate catastrophe. The geo-engineering method investigated in this project is called Cirrus Cloud Thinning. Its purpose will be to allow more time for mankind to reduce the greenhouse gas emissions. However, it cannot be seen as a solution to climate change as a whole.

Cirrus cloud thinning (CCT) is a method which uses Ice Nuclei (IN) to thin cirrus clouds, thereby increasing the Earth's albedo. This increase in Earth's radiation into space decreases the global temperature of the planet. State-of-the-art climate simulations have shown that CCT could have the potential to temporarily reduce global temperatures substantially if performed effectively. However, CCT may have some negative effects. People might view CCT as a long term solution instead of the temporary measure it is. This might cause people to reduce their efforts in developing sustainable technologies, causing greenhouse gas emissions to continue growing. As a result, the cooling effect of CCT might become ineffective and no real solutions remain. CCT might also have unanticipated effects, such as changes in wind or sea currents. Therefore, these have to be monitored extensively. Furthermore, increased rainfall in certain areas might occur [82, 83]. The goal of this project is to investigate the feasibility of an in-air delivery system capable of effectively performing this type of geo-engineering.

In order to perform CCT, a fleet of aircraft has been designed capable of both transporting the IN to the desired altitude as well as seeding the IN in the troposphere. Furthermore, a system has to be designed capable of both supporting and maintaining this fleet of aircraft. This system was aptly named 'ACT' for Aerial Cloud Thinning, the aircraft that operate in this system have been named 'AT1' after the Arctic Tern, a bird that breeds in the polar regions and migrates between the two poles.

The different parts of the preliminary design of the system are presented in a series of reports. In these reports, the scope is limited to the technical aspects of the mission. Both a quantitative and qualitative analysis will be performed and presented in the reports. The political and ethical difficulties will briefly be discussed but will not be elaborated upon. In this series of reports, the first report is the project plan report which gives an overview of both the scope of the project as well as the planning and organisational aspects of the project [43]. In the second report [33], the baseline for the project was developed including the design options and requirements. The third report is the midterm report [34], here a design concept was chosen and a preliminary design investigating its feasibility was performed. Finally, in this report, a more detailed design of the aircraft will be presented which follows up on the preliminary design of the previous report [34].

A realistic operational scenario is determined from which an appropriate fleet size and range are determined. With this fleet size and range the preliminary aircraft design can be started. The design choices for both the design of the aircraft as well as the operational aspects of the mission will be investigated. For a clear vision of the project a mission need statement and project objective statement are determined as follows;

Mission Need Statement

A delivery system needs to be designed to temporarily protect mankind from the detrimental effects of global warming, through Cirrus Cloud Thinning, in the event of a global climate catastrophe.

Project Objective Statement

To perform the preliminary design of a system to deliver ice nuclei which prevent cirrus formation for the purpose of climate engineering, by 10 students in 10 weeks.

The final report is structured as follows. First, the market analysis is done analysing the potential users and buyers, suppliers, competition, funding, and the public opinion. This is done in chapter 2. Secondly, an updated version of the functional breakdown structure and functional flow diagram are presented in chapter 3 based on the current stage of the design process. Thirdly, the operations concept is worked out in chapter 4, concerning the operational, logistical aspects, as well as the noise emissions of the mission. Next, the payload subsystem design development, choice of IN material, and modular system is elaborated upon in chapter 5. Subsequently, in chapter 6 the aircraft is designed including the sizing of the wings, tail, fuselage, ailerons, landing gear, and engine selection. In chapter 7 the aircraft performance is analysed on its aerodynamic performance, stability and control, structural characteristics, aeroelasticity, and the flight performance. Following this, the communications and navigation system that the aircraft will be equipped with are considered in chapter 8. Subsequently, the reliability, availability, maintainability and safety characteristics are discussed in chapter 9. Resource allocation and budget and cost breakdown of the mission are elaborated upon in chapter 10. For a successful execution of the project a technical analysis is performed to decrease the likelihood of project failure, delay or financial issues in chapter 11. Following this, the sustainability development strategy for the mission development is reviewed in chapter 12. Chapter 13 analyses the results from the different subsystems to ensure a feasible design, by performing a verification and validation analysis. The compliance matrices confirming the requirements set in the initial stages of the project are presented in chapter 14. These are followed by a sensitivity analysis in chapter 15 where the sensitivity to the seeding requirements and aircraft performance are investigated. Subsequently the project design and development logic and post-DSE planning is presented in chapter 16. Finally, the conclusion and recommendation are discussed in chapter 17.

2 Market Analysis

In this chapter a market analysis for the CCT system will be performed. Market analysis is a method to understand the competition as well as the interests and opinions of the customer and stakeholders, which are important aspects of engineering projects. Section section 2.1 will discuss the potential users and buyers, section 2.3 will analyse the market environment, section 2.5 will discuss possibilities for funding and section 2.6 will briefly discuss the public opinion.

2.1. Potential Users and Buyers

Global warming is pressing issue for mankind, it must be confronted by the world's most influential countries, especially concerning geo-engineering and CCT. The fleet performing CCT will have to deliver IN in territorial airspace above the 60th north parallel. Here most land is owned by Canada, Russia and the United States of America. For the airspace below the 60th south parallel there will be less territorial problems since there are less territorial claims and according to the Antarctic Treaty System every piece of land below the 60th south parallel is a scientific preserve with freedom of scientific investigation[1]. Due to these constraints it would be challenging for a single party or government to perform CCT individually. It is more feasible for a big consortium of governments to execute CCT in collaboration, or hire a private company to execute CCT. A possible governmental consortium that has the political power and influence to start CCT is the United Nations. Assuming that a consortium of governments decide to execute the CCT mission, more resources are needed than just money. The governments will have to work together with the private and academic sector to get the required knowledge and equipment to complete the CCT mission successfully.

2.2. Suppliers

During the design of the mission and aircraft multiple external suppliers have been identified. These are for instance Droplet Measurement Technologies where the payload measurement systems will be ordered. The landing gear tyres will be delivered by Goodyear. Honda, who will provide the jet-engine, and Honeywell who will be responsible for the various communication and navigational systems. A more elaborate description on which exact systems are delivered can be found in the according sections. All of these suppliers are market leaders delivering products throughout the aerospace industry and thus very reliable partners. The competition in the sector is very small which makes the risk that one of these companies will go bankrupt or ceases their operations due to another reason is fairly small. However the risk this happening must always be accounted for and different suppliers will have to be identified. The aircraft engine for instance could be supplied by Pratt & Whitney instead of Honda as they produce an engine with a similar performance to the one chosen, therefore eliminating the possibility that there would be no engines available.

2.3. Competition

The UN may request proposals to lower the global temperature. This would then lead to a worldwide public tender. As with most large engineering projects, there will be several proposals to solve the need for global warming reduction and prevention. Current concepts for radiation management can be found in figure 2.1. As a result, the competition is expected to be companies that aim to mitigate the greenhouse gas concentrations in the atmosphere. CCT however will have direct impact on the climate which is a huge benefit over geological storage or afforestation since these are long term solutions, but can not be implemented in a short time. Competition of implementation of CCT in existing aircraft is discussed in section 2.4.

[1] Retrieved from: https://www.state.gov/documents/organization/81421.pdf [26-06-2018]

Compared to stratospheric aerosols this project will be cheaper and less harmful to the environment directly [1]. A company that might present itself as a direct competitor is Weather Modification Inc.[2], this is a company that is already active in the weather modification industry. For now, mostly focused on increased precipitation and mitigating hail damages. However systems used to do so might also be used to seed the IN. These kind of companies could however also be an opportunity since a lot of research and knowledge in the subject is required, and could thus provide for the CCT system. As the mission of the project is to decrease the global temperatures, there are little financial constraints. The mission cost however could be reduced significantly if other companies are able to provide valuable information or support in acquiring the mission goals. Therefore these companies will be seen as allies instead of competition.

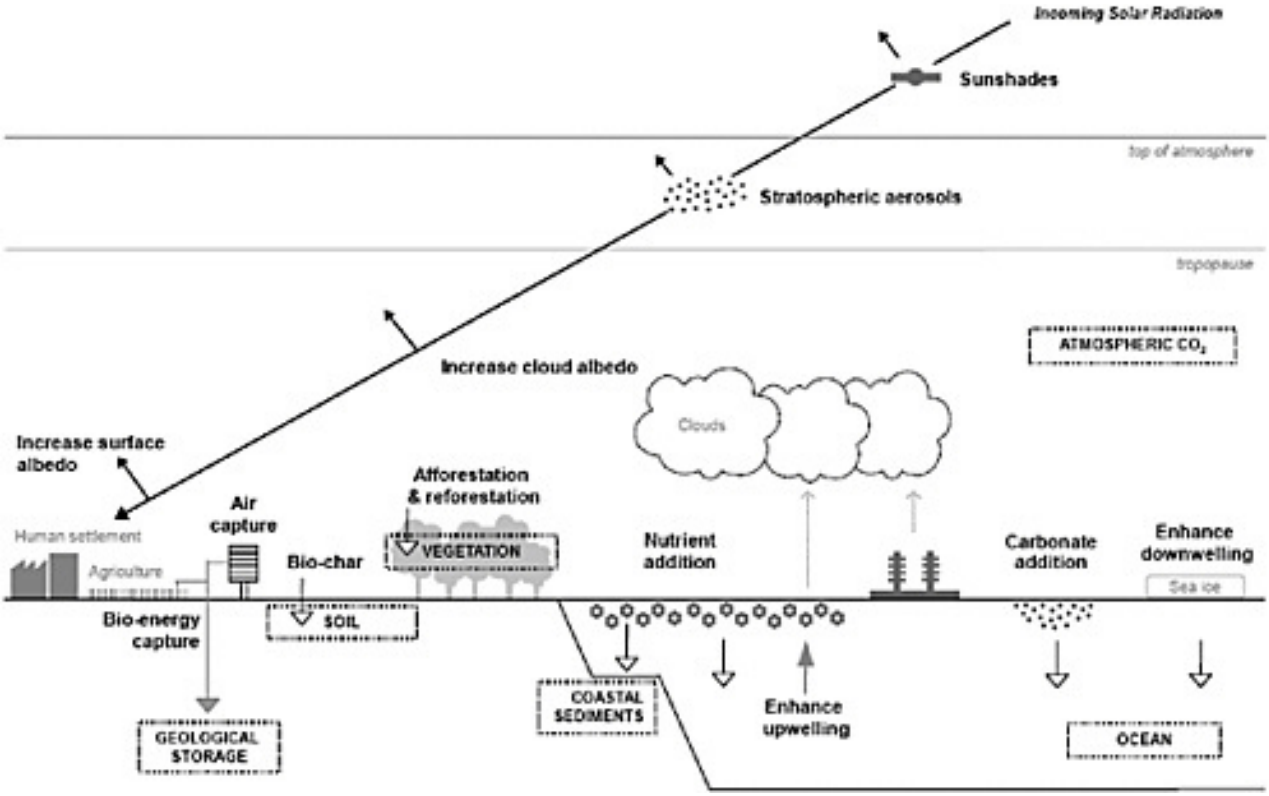

Figure 2.1: Radiation Management Options [17]

Since the market specialised in geo-engineering is still modest, it is challenging to predict if there will be competition. Financial driven companies are expected to be disinterested in this project as it requires high investment in new technologies, high risks and low returns. The competitive environment will therefore most likely consist of only a few companies presenting a feasible plan for the likely public tender. To ensure that this project will prevail over these other options it must be ensured that it has the best balance between cost, safety, and performance.

2.4. CCT Implementation in Existing Aircraft

The biggest competitor for the ACT mission could potentially be a company that also wants to use CCT as a mean to temporarily reduce the temperature on earth, but will do so with existing aircraft. The main benefit of this system is that it will be almost directly implementable. Three aircraft that would be able to perform the seeding for (almost) the entire seeding area were analysed on their initial and operational costs. As well as the performance of pilots on such long flights.

Three aircraft were found to be most optimal for the mission. These selected aircraft are the Dassault Falcon

[2]Retrieved from: http://www.weathermodification.com/cloud-seeding.php [19/06/2018]

8X, Gulfstream G650, and the yet to be released Bombardier Global 8000. These are all long range business jets with a service ceiling well above the minimum 10km. The jets were analysed as they come from the factory. The extra range acquired by adding more fuel and stripping the plane of unnecessary weight is assumed to be countered by the fact that the aircraft will have to fly below their designed cruise height and thus the drag will increase significantly. Therefore it is assumed that it will have the same range at 10km height as their designed cruise height of 15km. It is important to note that only the Global 8000 will be able to seed the entire area from the selected airports, the other two will need to leave certain areas unseeded.

The range was used to calculate the required amount of sorties. With this information the total required amount of aircraft is calculated. This information can be found in table 2.1. For the initial cost per aircraft a value of 30% of the listed unit price was assumed. This way an extremely opportunistic estimation could be made on the initial cost of the existing aircraft option. When this is compared to the conventional initial cost estimation of the AT1 found in section 10.1, which was found to be close to 2 billion euros, the existing aircraft solution is about half a billion more expensive. And this does not include changes required to the airport. It must however be stated that this already is a very optimistic estimate with a high chance of not meeting the assumption, whereas for the Arctic Tern estimation it is very likely that the estimation will be met or the initial costs might even be lower. Also changes needed to be made to the existing aircraft and the purchase of the separate dispersion system are not taken into account in this assumption.

For the existing aircraft only the fuel costs were analysed for the operational costs and can be found in table 2.1. This was done because after the calculation of the annual fuel cost based on the required amount of sorties the fuel cost was already found to be equal to the annual cost of the AT1 as can be seen in section 10.1. This was 10 times more than the annual fuel cost of the Arctic Tern. Pilot costs, maintenance costs, other personnel, and other operational costs should still be added to this assumption. It is therefore fair to assume that the total annual operational cost of the existing aircraft will be at least twice as high as the AT1.

Table 2.1: Cost Analysis for Existing Aircraft

	Range (km)	Ceiling (km)	Min fleetsize	Sorties/ Week	30% Unit Price (€)	Total Initial Cost (€)	Total Annual Fuel Cost (€)
Global 8000	14631	15545	98	967	17.7M	2.586B	656M
G650	12964	15545	103	1146	17.1M	2.651B	703M
Falcon 8X	11945	15545	108	1293	14.7M	2.376B	626M

The exhausting environments for the pilots must also not be forgotten. Even though the selected aircraft fly with mach 0.85 considerably faster than the AT1, they still have to fly a total time of about 13 hours to complete a sortie. This would require at least 3 pilots to be on board of the aircraft[3]. In combination with the long flight hours and the constant flight paths the job will be extremely boring. Almost similar to long-term space missions it will be the main challenge to keep the pilots sharp and focused. To make sure that the pilots wont fall asleep an designated rest area must be available in each aircraft so that the pilots can rest according to the regulations.

In the end this will not be feasible on the long run as it will cost too much. The only feasible option for such a system would be to span the time for the ACT mission to be fully developed and operational.

2.5. Funding

A project with the complexity and magnitude of the continuous execution of cirrus cloud thinning requires an immense starting capital and working capital for operations. Acquisition for the funding of the project is expected to be challenging as the project will have no to very little return on investment (ROI). This is because the aircraft provide in a public need and will have very little value after their lifetime. An estimation of the salvage value of the aircraft at end of life can be found in section 10.1.3.

As a result, the project funds will have to mostly be sourced from government bodies and public pools. The

[3]http://work.chron.com/duty-limitations-faa-pilot-17646.html

investment may be shared among several governments. A potential source of funding could be the United Nations (UN). Specifically, the United Nations Framework Convention on Climate Change (UNFCCC) could set up a framework for the implementation of CCT for the United Nations. The project could be funded with contributions from every UN member with an amount proportional to a measure of their contribution to global warming. As the funding has to be provided from public pools and government bodies, the political and public approval may play an important role. The political and public approval of the project will likely increase as the climate effects of global warming increase, the uncertainty of the effects of CCT reduces and its benefits become more known.

2.6. Public Opinion

A survey with 3105 participants published by Mercer [61] suggests that 72% of the people are ”somewhat” or ”strongly” supporting research in solar radiation management. This article is however highly debated by some organisations since one of the authors is an open supporter and owner of a geo-engineering company [31]. It is thus clear that despite the possibility of a majority of the people in favour of geo-engineering research, one should be aware of the fierce public debate that will accompany it. For this reason it is important to emphasise that CCT is only a temporarily measure in the case that the amount of negative effects of global warming become so big that immediate action is required to bridge the time for a long time solution to take into effect.

An important factor influencing the public opinion are the side effects and uncertainty of CCT. The side effects of CCT will negatively affect part of the population. Because of this ethical dilemma the public is polarised on this topic. For instance, countries in South Asia and South-East Asia could potentially experience more precipitation due to CCT [48]. The water management infrastructure in these regions is insufficient to handle the current levels of rain, let alone an increased amount after CCT. Should CCT be considered as a temporarily measure, the required support and infrastructure development for these countries to cope with the increased precipitation have to be considered, such as flood defence systems. Furthermore, the effects of CCT are still very uncertain and there is a chance of unexpected effects occurring globally. However, the public opinion is expected to shift when CCT is considered to be used, as CCT is only to be used in climate emergencies.

3 Functional Analysis

In this chapter, the functional analysis of the system is presented. The functional analysis is performed in the baseline report [33] and was updated to meet the progress of the project. First, the functional breakdown is provided and described in section 3.1 after which the functional flow diagram is presented in section 3.2.

3.1. Functional Breakdown

To obtain an overview of the functions of the system a functional breakdown structure (FBS) was created. The FBS was also used to get an insight as to what additional (sub)system requirements the design had to meet. The FBS represents hierarchically the functions that the product or system must perform in the form of an AND tree. It was chosen to have a FBS of both the fleet operations and the individual sortie. These diagrams have been elaborated to a level of detail that is detailed enough to form the subsystem requirements, but general enough to not impose design solutions. The FBS for the entire fleet of aircraft can be seen in figure 3.1. Within the operation of the fleet the individual sortie and monitoring of the sorties are identified as functions. Performing the individual sortie is further developed in figure 3.2. The monitoring of sortie communicating the flight path, monitoring the fleet to avoid collisions, and assist the aircraft in landing and take-off. The support for the fleet includes maintenance of the fleet and the various logistical functions such as providing payload and fuel, which can only be done after setting up the proper infrastructure.

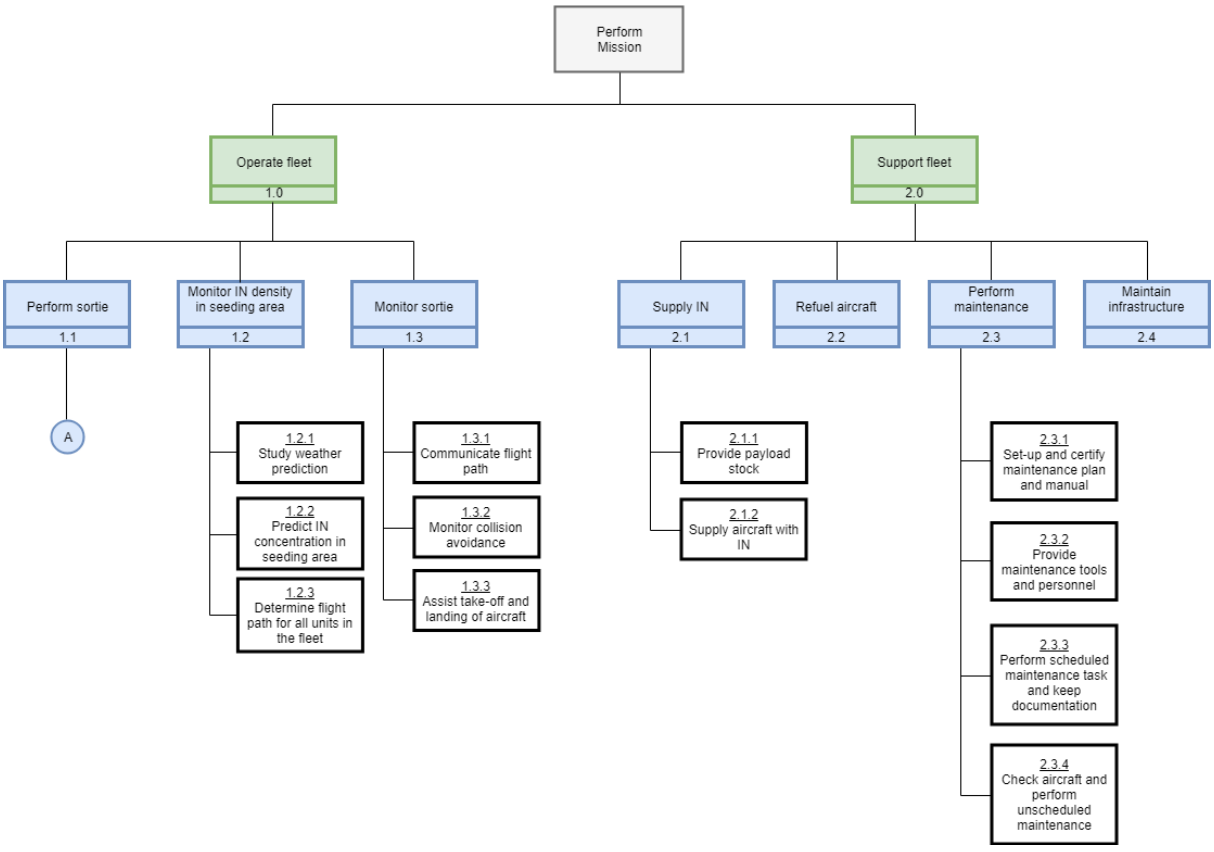

Figure 3.1: Functional breakdown structure of the entire fleet

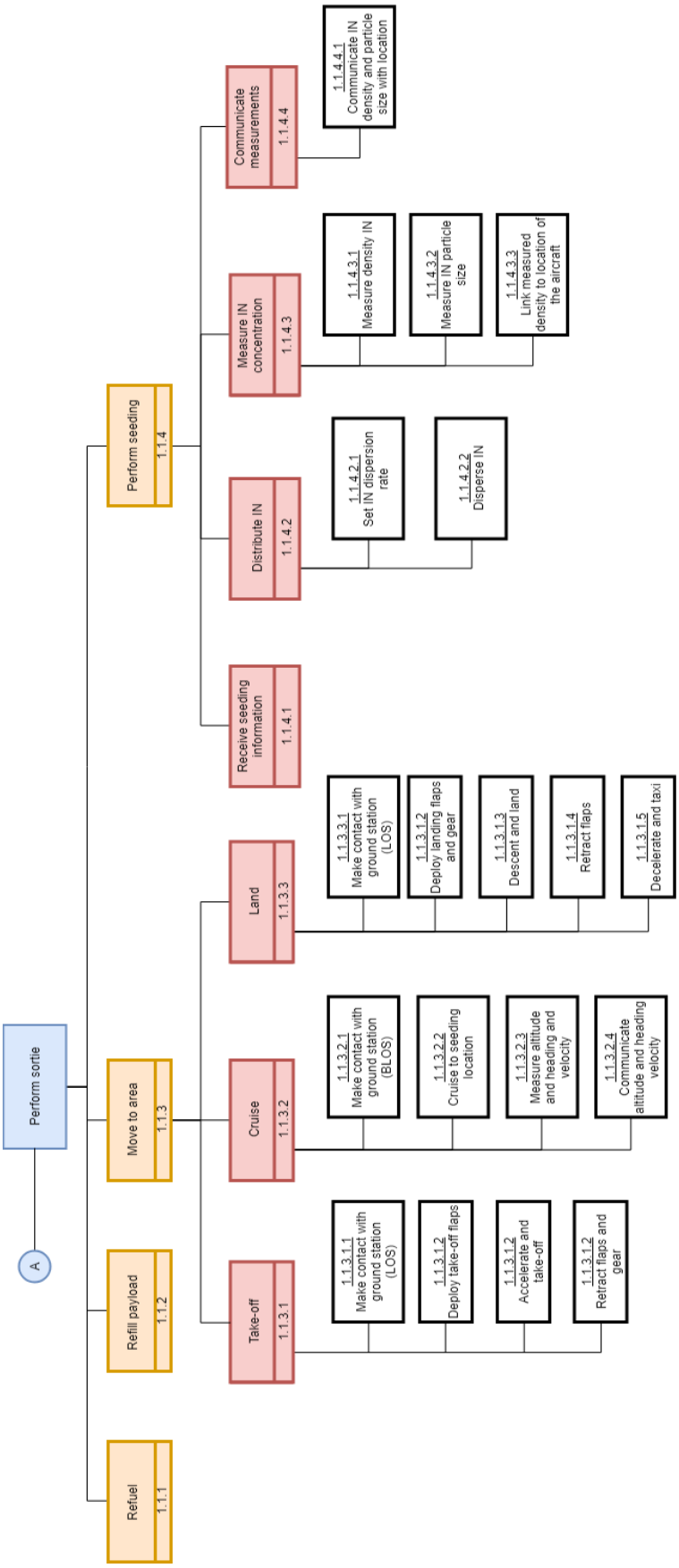

Figure 3.2: Functional breakdown structure of one sortie

From the FBS of the individual sortie in figure 3.2 it can be seen that the payload and fuel will be required for each sortie. 'Moving to seeding area' is separated into take-off, land, and cruise to and within the seeding area. It can be seen that function 1.1.4, on 'Perform Seeding', would require information on how much should be seeded. Function 1.1.4.3, labelled 'Distribute IN', is identified as one of the key functions of the system.

3.2. Function Flow Diagrams

Following the FBS, a Functional Flow Diagram (FFD) is created to get an overview of the sequence of the functions of the system which is displayed in figure 3.3. The FFD presents the same functions as the FBS, however the FFD shows the functions in a chronological order and where the process loops occur. This means that it is immediately clear which functions are interdependent, which is important later in the design process. In essence, the CCT mission consists of two parallel functions - operating the fleet and supporting the fleet. The operation of the fleet consists of simultaneous sorties corresponding to each aircraft within the fleet. The sortie itself is separated into performing and monitoring of IN density and the sortie itself, which occur in parallel. Performing the sortie is a sequential process, including reception of fuel and payload, positioning of the aircraft to the seeding area and perform seeding. The sequence of the last two functions is further dissected. Moving to the seeding area and back to base are a straight forward sequences. The seeding itself, however, is a feedback loop consisting of receiving seeding information, distributing the IN, measuring the IN concentration and communicating the measurements back to base.

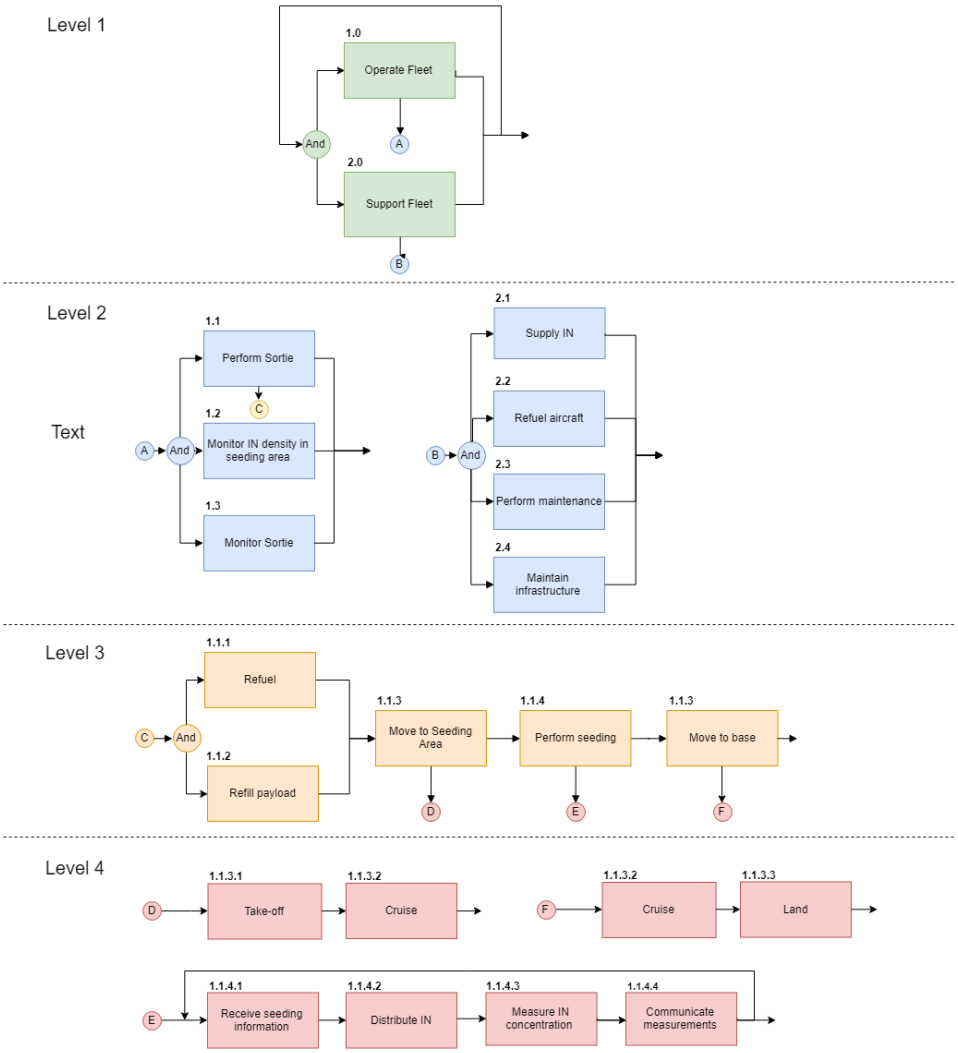

Figure 3.3: Functional Flow Diagram

4 Operations Concept

The ACT mission is performed with a large fleet of aircraft designed for injection of IN into the atmosphere over the poles. The operation of this fleet is done using four different airports in the northern and southern hemisphere. The selection of the airports is discussed in section section 4.2. The airport capacity and weather conditions were extensively studied to determine whether the fleet operations are possible from the chosen locations. To successfully perform the CCT mission a volume stretching from the trophopause to 3 km below has to be seeded, which is at around 7 to 10 kilometres altitude, on both the Northern and the Southern hemisphere above 60 degrees latitude.[40] The seeding is done during late fall, winter and early spring on each side of the globe. Therefore the fleet of seeding aircraft will alternate between the North and South Pole. To determine the mission profile for the AT1 the total range needed to cover this area is first determined, with which the range of one aircraft and the size of the fleet was determined. A total of 136 aircraft is needed for the ACT mission to seed the area by flying 786 sorties per week. To account for maintenance the fleet size is increased to 205. This means each of the aircraft will perform 200 flights per year. The mission profile for the aircraft is described in section 4.4. To support this fleet of aircraft infrastructure and personnel is needed. The expansion of the airfields and logistical support is discussed in section 4.3.

4.1. Operations and Logistics Concept Description

During the conceptual design phase of the project 4 operational concepts were established. They are briefly discussed in section 4.1.2. An extensive trade-off was done in an earlier stage of this project. Conventions for naming different distances throughout this report are presented first in section 4.1.1.

4.1.1. Distance Nomenclature

To ensure consistency, a convention for naming different distances important to the ACT mission was established. These distances are illustrated in figure 4.1, and a description of the separate terms is provided below.

- **Seeding range** - Distance covered whilst seeding takes place by a single aircraft during one sortie.
- **Transit range** - Distance flown from the base to the seeding area and back during one sortie. Transit range is defined as the total distance covered minus the seeding range by a single aircraft during one sortie.
- **Total range** - Entire distance covered by one aircraft in one sortie. It is obtained by summing transit range and seeding range.
- **Seeding coverage** - Seeding distance covered by entire fleet in one week.
- **Transit coverage** - Transit distance covered by the entire fleet in one week. Essentially, the distance that is covered by the entire fleet in a week with the seeding coverage subtracted.
- **Total coverage** - Total distance done by the entire fleet in a week. It can be obtained by summing transit coverage and seeding coverage.

4.1.2. Operations concept description

In order to cover the seeding area in the most optimal way, four operational concepts were set up. Sketches of the concepts can be seen in figure 4.2(a). The first concept consists of a fleet of aircraft that performs conventional operations. They take off, seed, and then land again. The second concept has a fleet of continuously flying and seeding aircraft which are refuelled by a fleet of refuelling aircraft. The third concept consists of a mother-ship which transports a fleet of drones to the seeding area. These drones are then released, after

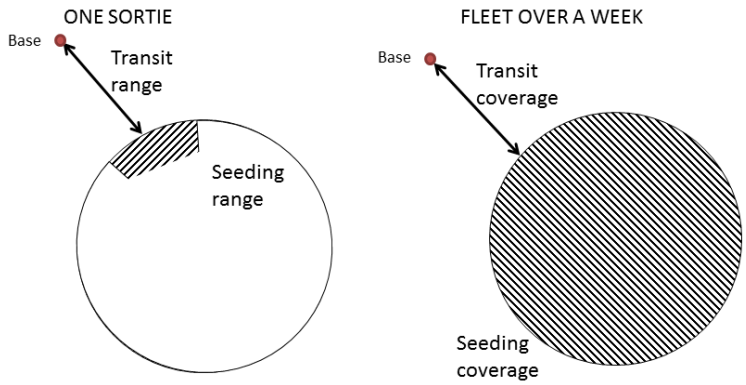

Figure 4.1: Distance naming convention

which they seed and then return back to the mother-ship. The fourth concept also has a mother-ship. In this concept however the drones do not return to the mother-ship but they are disposed instead. After an elaborate trade-off which can be found in the midterm report[34], The first concept was chosen for its high TRL and good maintainability compared to the other concepts.

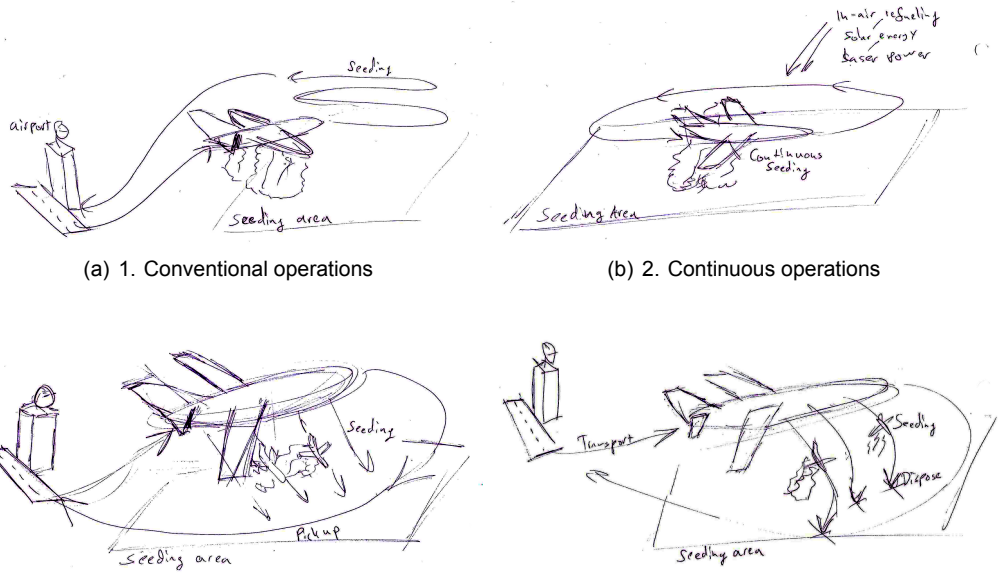

(a) 1. Conventional operations

(b) 2. Continuous operations

(c) 3. Mother-ship with reusable drones

(d) 4. Mother-ship with disposable drones

Figure 4.2: Operations concepts

4.1.3. Operations fleet sizing

After the conventional concept was chosen for ACT, the aircraft needed to be designed. To determine the requirements for the aircraft the mission needed to be designed first to get the payload mass, required total range, etc. This was done by defining the requirements for the entire fleet and then scaling the fleet and aircraft such that it is able to perform the mission. This method uses the first class weight estimations to estimate the aircraft weight and fuel usage per aircraft. These are then related to a cost function which is minimised in order to get the most optimal relation between aircraft and fleet size. A more detailed description of this model in given in the mid-term report [34]. The result for the class I weight estimations are given in section 6.1. The V&V procedures for this model is discussed in section 13.1. When the final range of the aircraft is determined the minimal final fleet size required can be determined. The fleet size is found by first setting the amount

of sorties which is the seeding coverage divided by the range of one aircraft. Next the number of aircraft is determined by using the endurance of one sortie and time available in one week.

4.2. Airport Operations

In this section, the airports that were selected in the midterm report [34] are further analysed on their capacity, ability to expand, possible noise constraints, and local weather. These parameters are very important to the design since they might impose constraints.

4.2.1. Selected Airports

The airports that were selected and will be further analysed are Ushuaia in Argentina, Christchurch in New Zealand, Svalbard in Norway and Thule in Greenland. Thule was discarded in the project plan [35] since it is an US Air Force base. However, after consulting the customer it was decided that this should not pose a problem. Therefore, it was decided to drop Pevek Airport in favour of Thule Air Base since Thule has more capacity and better infrastructure.

Table 4.1: General info per airport

	THU [1]	LYR [2]	USH [3]	CHC [4]
Runway Length	3047m	2319m	2800m	3288m
Runway Type	Asphalt	Asphalt	Asphalt	Asphalt
Elevation	77m	27m	22m	37m
Min. Temperature	-28°C	-17°C	-2°C	3°C

Table 4.1 shows some relevant information on the selected airports and some constraints such as maximum take-off length. The elevation at all bases is less than 100 metres mean sea-level. The temperature of -65$^{\circ}C$ for which the aircraft is designed is far lower than the temperature extremes recorded at the bases. However, de-icing facilities for both the runway and the aircraft should be made available.

Crosswind Conditions Crosswind is an import issue that has to be investigated when selecting the airports since this might constrain the design of the aircraft. figure 4.3(a), figure 4.3(b), figure 4.3(c), and figure 4.3(d)show the windroses for the selected airports [5]. It is worth noticing that the occurrence percentage scale varies between airports.

From these figures it is clear that aircraft will experience high winds during landing. For Thule, Svalbard and Christchurch this wind is mostly in the direction of the runway. For Ushuaia however, wind speeds are above 10 m/s, 22 % of the time and are not always aligned with the runway. Other airports in Cape Horn were analysed as potential substitutes, but were found to have the same wind problems. Crosswind landing performance will therefore drive the design. Also, a strategy for dealing with diverted flight had to be established. This can be found in section 7.11.

4.2.2. Airport capacity

Airport capacity is an important factor to investigate since each airport will have to be able to handle around 103 aircraft and 393 sorties each week. The use of existing facilities instead of building new facilities will

[1] Retrieved from https://web.archive.org/web/20160805103115/https://naviair-public.sharepoint.com/AIM%20Documents/AIP%20Gr%C3%B8nland/AIP%20PART%203%20-%20FLYVEPLADSER%20(AD)/AD%202%20AERODROMES/Thule%20(BGTL)(MIL)/BG_AD_2_BGTL_en.pdf [03-07-2018]

[2] Retrieved from https://web.archive.org/web/20120611143342/https://www.ippc.no/norway_aip/current/AIP/AD/ENSB/EN_AD_2_ENSB_en.pdf [03-07-2018]

[3] Retrieved from https://web.archive.org/web/20090419234013/http://www.cra.gov.ar/dta/ais/aip/docs/244.pdf [03-07-2018]

[4] Retrieved from http://www.aip.net.nz/pdf/NZCH_AD2.pdf [03-07-2018]

[5] Retrieved from: https://www.enviroware.com/METAR/METAR_WindRoses_201_maps.html [06-06-2018]

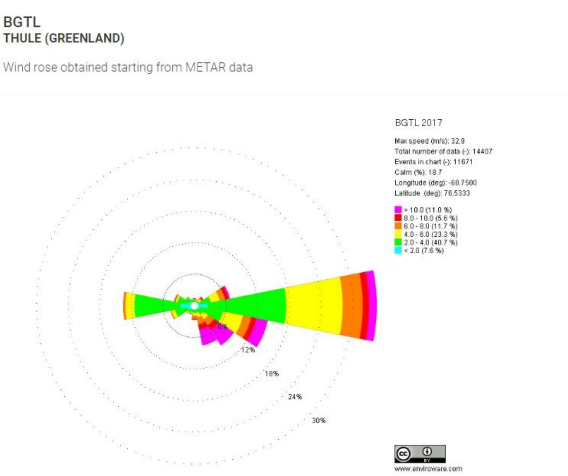

(a) Thule Air Base (RWY 08/26)

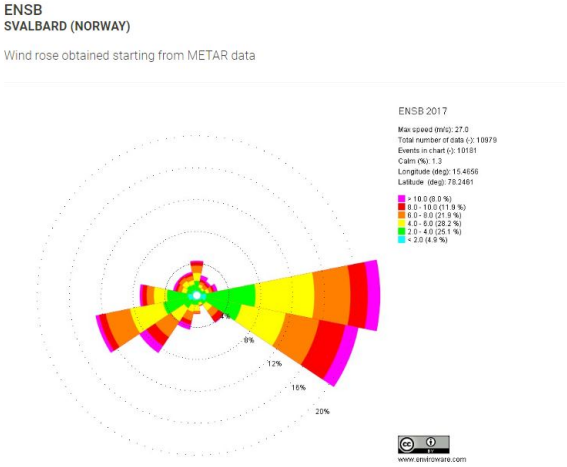

(b) Svalbard Longyearbyen Airport (RWY 10/28)

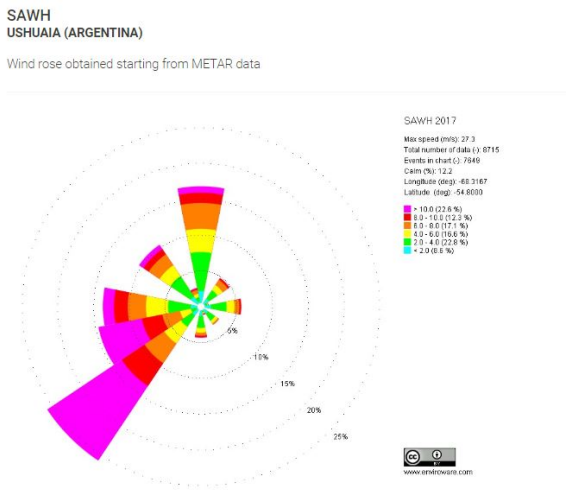

(c) Ushuaia Airport (RWY 07/25)

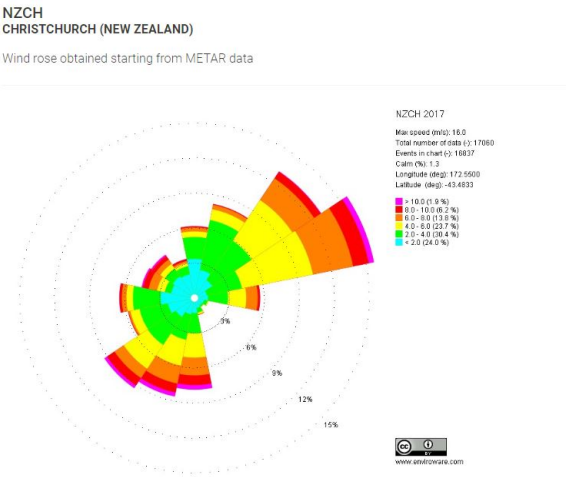

(d) Christchurch Airport (RWY02/20)

Figure 4.3: Windroses for selected airports

drastically decrease the cost of the whole system. Each airport will be analysed on their capacity, facilities, ability to expand and other relevant infrastructure.

Thule Air Base: Very limited information on Thule Air Base is available since it is a US Air Force Base. Images of the field show a number of hangars but it is unsure how many flights the airport already handles. Facilities of the airport will need to be updated when ACT will operate from Thule. Furthermore, the airport is very remote since the water around the base is frozen 9 months of the year [6]. Therefore, payload delivery has to be done during summer months or via the air.

Svalbard: Svalbard mostly handles domestic flights to Norway but regular charter flights also operate from the field. 154261 passengers were handled by the airport in 2014 [7]. When 'ACT' will operate form the field, the airport needs to be able to handle significantly more flights. Fortunately, there is a lot of space around the airfield to expand. Since the airport is located on an island and is surrounded by ice most of the time, the payload will have to be transported to the airport in summer by ships or during winter by air.

Ushuaia: Ushuaia airport mostly handles seasonal passenger flights. Airport movements are very limited and so are the facilities. The airport has a very small passenger terminal and can only handle two aircraft on the ramp at the same time [8]. If ACT will operate from this field, the airfield will most definitely need to expand. Fortunately, the airport is situated in a remote area where expansion will probably not inflict with the residential areas. The airport is accessible both via the road or by boat. However, since Ushuaia's location is so remote, it might be better to transport the payload to the airfield via the air.

Christchurch: Christchurch International Airport currently handles 107,822 movements per year and is the largest of the selected airports. Traffic consists mostly of domestic and international passenger flights, but general aviation also flies from the field. If 'ACT' will fly from Christchurch, the airport will almost definitely need to expand. Luckily, there is enough room to expand on the western side of the field. There is no night curfew restricting airport operations. The infrastructure around the airfield is made for passengers and so it will be no problem to transport the payload to the field.

4.2.3. Noise Restrictions

Noise pollution is one of the most pressing issues facing airport growth, the negative health effects of exposure to prolonged noise are becoming more clear, while the aviation industry is growing rapidly. This must be taken into consideration when evaluating the suitability of the selected airports. Aircraft traffic in the selected airports will drastically increase with the inclusion of the AT1 take-offs and landings, so following an overview of the metrics used to measure aircraft noise, each airport will be evaluated for the ACT system in addition to the existing operations taking place. When analysing noise limitations, only the noise pollution surrounding the airport due to taking-off and landing will be considered. Noise pollution from climb, cruise, and descent will not be considered, but should be explored in later stages of the design process.

In order to evaluate the ACT system, the noise produced by an AT1 must be quantified. The Cirrus Vision SF50 might be the most similar production aircraft to the AT1, so it can be assumed the two aircraft have similar sound characteristics. The similarities lie in the SF50 also being a light aircraft with one similarly sized turbofan engine mounted on top of the fuselage. The European Aviation Safety Agency have compiled a database of noise level for a number of aircraft, including the SF50 [7].

The SF50 is loudest when approaching, relative to lateral or fly-over measurements, for which it has an effective perceived noise (EPN) of 80.3 dB [7]. This is significantly lower than common passenger aircraft. For instance, the EPN of the A320-211 is 96.1 dB and for the B737-200 it reaches 99.1 dB. This metric for measuring noise, the perceived noise, is a 10 second burst of steady noise that has the same amount of sound energy as the event measured.

The airports measure noise in a different way from aircraft. The day-night average sound level, L_{DN}, can be

[6] Retrieved from http://download.militaryonesource.mil/12038/Plan%20My%20Move/Thule%20Information.pdf [06-06-2018]
[7] Retrieved from: http://media.avinor.no/documents/trafikkstatistikk-desember-2014-42080 [05-06-2018]
[8] Retrieved from http://www.aeropuertoushuaia.com/en/airport.php [06-06-2018]

used to find the average noise pollution over a 24-hour period. This is generally considered the best metric to evaluate airport noise exposure [2]. The day-night average can be found by taking the logarithm of the sum of sound exposure of significant events over the course of the day, such as landings or take-offs. To account for aircraft noise having a greater nuisance during night-time, heavier weights can be applied to events occurring between 22:00 and 07:00. Furthermore, this metric is A-weighted, meaning it accounts for how differences in frequency effect the perceived loudness measured by humans. The equation for this can be seen below [22], where L_a is the sound pressure level, SEL is the sound exposure level, and $w(t)$ is the weight of the event which accounts of the night-time. Between 07:00 and 22:00 the weight is 1, and for the other times the weight is 10.

$$L_{DN} = 10log\left[\frac{1}{86400}\int_0^{86400} w(t)10^{\frac{L_A(t)}{10}}dt\right] = -49.5 + 10log\left[\sum_{i=1}^{N} 10^{(SEL_i+Wi)/10}\right] \tag{4.1}$$

Inconveniently, the metric used to measure the noise produced by the aircraft, SEL, is not related to the metrics to measure noise at airports, EPN. Due to nature of the day-night average metric, to maintain the same day-night average after doubling the number of events, the average SEL of the events must decrease by 3 dB.

Thule Air Base in Greenland does not have any nearby residents, thanks to the American's forcibly relocating the inhabitants of the local town in order for the military airports to expand. This results in noise pollution not being an issue for aircraft taking-off and landing here. As discussed in this subsection's introduction, once the aircraft is at its cruise altitude, its sound pollution is minimal. Therefore, any noise pollution surrounding Thule does not have to be considered.

Christchurch Airport has the most established noise pollution measures in place of chosen airports. This is partly due to the airport being located only a few kilometres from the city of Christchurch. Much like the FAA, Christchurch airport impose a 65 dB limit for the day-night average [8] that cannot be exceeded outside the noise limit. This noise limit is shown in the figure 4.4.

Christchurch Airport currently handles 266 daily movements, with the most common aircraft used being the Airbus A320, followed by the ATR 72. The European Aviation Safety Agency aircraft noise database used earlier also includes both these aircraft. The effective perceived noise (EPN) of the A320-211 is 96.1 dB, and 94.2 dB for the ATR 72-212. As discussed, the EPN of the AT1 can be assumed to be 80.3 dB.

Figure 4.4: The 65 dB noise limit at Christchurch Airport

Rough calculations will be performed to estimate the impact of the ACT system on the day-night average at

Christchurch. This is done by assuming the day-night average at Christchurch reaches 63 dB, slightly under their limit of 65 dB, with the same sound exposure level for each movement. Using these assumptions in equation (4.1), the SEL of each movement reached up to 84.2 dB. These events are assumed to be carried out by Christchurch's most used aircraft, the A320. Using the same relationship between the two aircraft for both the SEL and EPN, the SEL of the AT1 can be found. The EPN of the AT1 is 10% lower than for the A320, meaning the SEL of the AT1 can be assumed to be 77.7 dB. Filling in these values into equation (4.1), weighting the nighttime flights, the day-night average becomes 63.6 dB, only slightly larger than without the ACT system and still below the limit.

This indicates that the addition of the Arctic Tern movements will not drastically increase the noise pollution around Christchurch Airport. However, many assumptions were made to come to this conclusion, so it is recommended that further research be carried out to better measure the noise produced by the AT1 aircraft and how that will effect noise pollution at the selected airports.

Svalbard may have an issue with noise pollution as well. Longyearbyen, Svalbard's largest town with a population of just over 2000 people, lies a few kilometres from the airport. To make matters worse, after the introduction of the ACT system, the daily events Svalbard will handle will increase approximately 10-fold, bringing the total daily events to around 105 movements.

Comparing Svalbard Airport incorporating the ACT system of aircraft to the current operations at Christchurch, it is possible to estimate the magnitude of the noise pollution. Christchurch handles 266 movements per day, significantly more than the 105 of Svalbard with ACT. Furthermore, the aircraft landing and taking-off at Christchurch are louder, as established earlier in this subsection. Christchurch imposes a strict 65 dB noise limit, a mere few hundred meters from the runway. Since Christchurch accommodates more aircraft which are also louder than AT1 while still not breaking the sound limit, it is determined that aircraft noise pollution will not be an issue for operations at Svalbard. In addition, there are hills acting as physical obstacles between the airport and the town of Svalbard, further reducing the issue of noise pollution.

Ushuaia Airport is situated just over two kilometres from the edge of the town of Ushuaia. Much like Svalbard Airport, Ushuaia does not handle many movements daily. Due to the many similarities between these two airports, the same conclusion drawn for Svalbard can be applied here. That is, if Christchurch can cope with their current capacity, while not breaking the 65 dB limit set by the FAA, then so can Ushuaia. The only aspect that would require further research would be the effect of the bay on noise travel. Unlike Christchurch, a bay lies between the airport and the town of Ushuaia. The water or ice may carry the sound better, and result in greater aircraft noise pollution. Further research should be conducted to investigate whether this effect is enough to break the noise limit.

4.2.4. Diversion airports

When the aircraft is unable to land at one of the operational bases due to the weather or conditions on the ground, the aircraft should be able to divert to a different nearby airport. For each airport which ACT will operate from, diversion airports are selected. The contingency on runway length for the diversion airports can be less than the operational bases, as the risk does not have to be as low. As such, the minimum required runway length is chosen to be 1 kilometre. Furthermore, the diversion airports do not require to have expansion capabilities, extensive infrastructure, and large airport capacities compared to the operational bases. The final selection of diversion airports and their distance from the operational base is given in table 4.2.

Table 4.2: Airports used for diversions if the aircraft can not land on the operational bases, and their distance from the respective operational airport.

Operational airport	Diversion airport	Diversion distance
Thule	Arctic Bay	614 km
Svalbard Longyear	Banak	952 km
Ushuaia	Hermes Quijida	124 km
Christchurch	Dunedin	328 km

All four diversion airports have a runway length of more than one kilometre and sufficient runway conditions.

The Arctic Bay has the worst runway condition with a gravel runway, however the tires of the CCT Arctic Tern are capable of landing with these conditions.

At the four operational bases, the aircraft land using pilot-in-the-loop, through line-of-sight (LOS) communication at an operating tower at the airport. The diversion airports have to handle the AT1 movements in a manner; the latency is too high with beyond line-of-sight (BLOS), rendering it impossible for the operator to land the aircraft. The goal is to have the operators land the AT1s at the diversion airports using LOS, while stationed at the operating base. To achieve this, an operator capable of handling AT1 movements will be stationed at the four diversion airports. Since the diversion airports will only be used when the weather conditions are too severe for the AT1, something that will not occur often

The use of diversion airports will require additional initial development costs. This will go towards all the necessary technology to aid landing, such as an instrument landing system, to make sure the aircraft can position itself with regards to the runway and communicate with the operator. Furthermore, the operator's salary will contribute to the annual upkeep costs.

4.3. Logistics and Ground Support

This section discussed needed expansion of the airports and the estimated cost for these projects. Apart from changes in infrastructure a maintenance plan was set-up and an estimate for the number of needed support crew was made.

4.3.1. Maintenance

To achieve the required availability of the system regular maintenance checks have to be performed on the aircraft. After each of the flights the aircraft is checked, refuelled, reloaded and de-iced if necessary before the next flight.

More extensive maintenance is performed with regular intervals. A rough estimate is made to determine the amount of spare aircraft needed to meet the mission requirements while also maintaining the fleet. As the AT1 is a relatively small aircraft flying at subsonic speed and carrying no passengers the assumed number of maintenance hours per check is significantly lower than for larger commercial aircraft. Moreover, all of the aircraft in the fleet are the same type which speeds up the maintenance process further. More information on the full maintenance plan and different checks that are performed is given in section 9.2. For the AT1 is assumed that type 'A' checks have to be performed every 500 flight hours and 60 man hours are needed for one check, type 'C' check are performed every 24 months and take 3000 hours, type 'D' checks are performed every 5 years and take up to 25000 man hours. The number of personnel needed to perform the maintenance tasks is estimated by finding relation between the number of aircraft added to the fleet and the cost for maintenance personnel, as described in the cost breakdown in chapter 10, and the cost per worker. From this relation, the optimal number of crew member is found to be 900. The fleet size is multiplied by 1.5 to account for maintenance which results in 205 aircraft.

4.3.2. Infrastructure

During the selection of the airports the capacity and option to expand were taken into account. During operation of the ACT fleet the aircraft fly sorties with an endurance of around 30 hours, the turn-around time of an aircraft is 1 hour. Per week, each aircraft is on the ground for 4.88 hours, excluding maintenance time. Over the whole fleet this means that two or three aircraft are on the ground being refuelled, reloaded and checked at each of the airports, assuming the fleet is divided equally over the two bases. To be able to service the ACT aircraft each of the airports will be expanded. This is necessary because of the number of added aircraft movements to perform the mission. At each of the airports a runway, apron, control tower and maintenance hangar are build to provide proper ground support for the system. The runways should meet the landing and take-off requirements as determined when analysing the aircraft performance in chapter 7. The aprons should be able to accommodate the three aircraft at any time to keep the turn around time the aircraft under one hour.

From the control tower both the monitoring of the fleet and IN density is monitored. The estimated cost for the expansion of the airports can be seen in table 4.3. The assumed cost were found by studying details on similar expansions, for instance the recent redesign of Christchurch Airport.

Table 4.3: Infrastructure expansion cost

Object	Cost [USD]
Runway	10M$
Apron	15M$
Control Tower	6M$
Maintenance Hangar	10M$

4.3.3. Personnel

Apart from accommodating the fleet, it also has to be maintained. Estimates for the amount of personnel needed for maintenance are made when setting up the maintenance plan as discussed in section 9.2. Next to maintenance crew, people are needed to refuel and reload the aircraft. Working with 2 people per aircraft that means 10 people are needed for all aircraft on the ground.

For the control of the aircraft a crew with operators is needed that monitor the aircraft flight path and the IN density in the seeding area. By studying different drone mission and experiments it is found that six aircraft can be controlled by one controller [37]. This is based on the assumption that the aircraft performs the mission autonomously, except in case of emergency, for instance, when extreme weather conditions occur during landing or take-off. The total number of operators is presented in table 4.4 together with the rest of the ground and maintenance crew.

Table 4.4: Crew numbers and cost per hour

Type of personnel	Number	Cost per working hour [36]
Maintenance crew	900	52.12
Ground crew	10	83.26
UAV operator	22	78.21
Ground station supervisor	2	110.03

4.4. Mission Profile

As the bases for the North Pole operations are inside the seeding area, while at the South Pole transit to the area is required, two different mission profiles are considered. To optimise the operations specific to each of the profiles, the seeding coverage has to be determined and the average transit range has to be estimated. This calculation has been presented in the midterm review [34]. It is assumed that the dispersion width of the IN is 10 km. Consequently, to cover the entire seeding area the fleet has to cover $3.43 \cdot 10^6$ km. Moreover, the dispersion height of a contrail is assumed to be 1 km as described in section 5.2. Similar to the dispersion width, this can be refined in the detailed design phase. Since the IN have to be delivered in a 3 km altitude range, the entire seeding coverage has to be multiplied by 3. Therefore, the seeding coverage is $10.3 \cdot 10^6$ km.

In order to accurately estimate the required range of the aircraft, the average transit range to reach the seeding area must be studied. To do this, the distance from the base locations decided in section 4.2 to the seeding area were utilised. In the northern hemisphere, the airports that are suitable for CCT mission are located within the seeding area. Therefore, the transit coverage includes the take-off and climb, furthermore transit might be necessary to reach an unseeded part on the seeding area. As this transit will not be sizing for the aircraft range it is not considered here. In the southern hemisphere, the transit range is significant. It was estimated by taking the direct distance from Christchurch to the seeding area and back. A 10% safety margin

was added, resulting in a minimal transit range estimate of 4000km per sortie. Thus, the mission profile for the operation on the northern hemisphere consists of taxi, take-off, climb, transit before seeding, seeding cruise, transit back to base, descent, diversion, loitering, landing and taxi again. To make optimal use of the flying hours per sortie the aircraft flight path should be optimised such that the ratio of the transit range over the seeding range is minimal.

As on both the northern and southern hemisphere, there are two bases and two seeding coverage concepts, they all need to be considered. For both of the poles the operations can be done from one base to the other or operating from one base and returning. As the South Pole is the sizing situation for this mission the two concepts are discussed in more detail. Sketches of both, closest base and base-to-base flying can be seen in figure 4.5 and figure 4.6. For the closest base concept the seeding area is split in two parts, depending on whichever base is closer. The fleet is also split over two bases and the aircraft seed the area closest to the base. For the base-to-base concept an aircraft takes of from one base, seeds, and then proceeds to land on the other base. Both concepts are considered executable and could both be favourable when taking into account external effects such as weather.

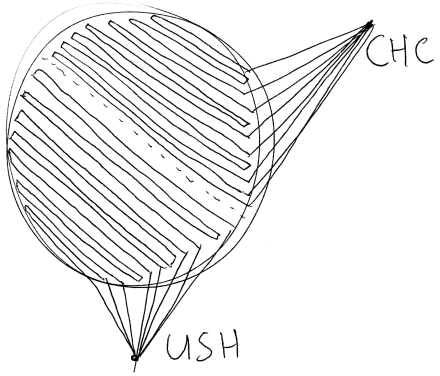

Figure 4.5: Flight pattern based on closest base

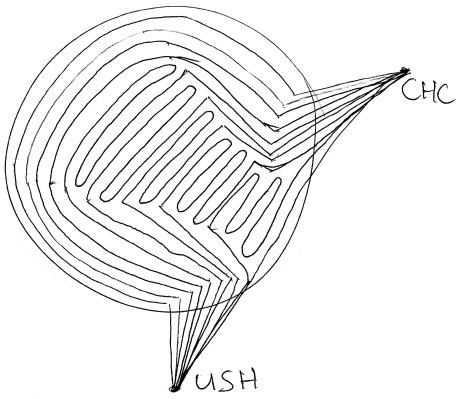

Figure 4.6: Flight pattern based on base-to-base operations

4.5. Flight Path Optimisation

Unlike regular passenger and cargo aircraft operations that focus on 'simple' transportation from A and B, the mission is to cover a certain area (the seeding area) within a certain time. Therefore, the most optimal route to cover this area needs to be computed, including the process to minimise the transit range. Creating such a model is beyond the scope of this project. This section describes the objectives and constraints that would be needed. In the the midterm report [34] several existing models have been studied to get a general sense of how such an algorithm works. The first step to optimise the flight path is to identify the seeding area and divide the area into a series of nodes. The nodes are spaced with the dispersion width, so 10km apart.

Objective

The objective of the algorithm is to minimise the total coverage of the fleet, and thus covering all of the seeding area in the most efficient manner. Doing this it will minimise the amount of fuel used and the time needed to cover the total area. The model should minimise the number of nodes, and thus distance, touched to cover all the nodes. Constraints are presented next that pose restrictions on how the model does the optimisation.

Constraints

The route of the fleet has to comply with the following constraints:

- **Cover all nodes:** In order to cover the entire seeding area all nodes need to be covered by the fleet.
- **Return to base:** All aircraft need to return to a base for refuelling, payload reloading, and maintenance.
- **Minimise turns:** The route should minimise the amount of corners the aircraft has to fly, this is because the aircraft is not able to seed optimally when its is performing a turn.
- **Fleet size:** The route has to take the limited fleet size into account, it should not be assumed that more aircraft are flying than the amount of aircraft in the fleet.
- **Aircraft range:** The aircraft can not fly further than its maximum range. This means the sum of the distances between the nodes connected by a single aircraft can not be larger than the remaining range of the aircraft. However, all units in the fleet should be used to their maximum capacity, if the aircraft do not fly their full range the fleet is oversized.
- **Seeding time:** The seeding has to be performed every week, therefore the time it takes to perform the seeding should be less than the available time in a week.
- **Constant Seeding:** The transit range should be minimised.
- **Reduce touching covered nodes:** The flight pattern should be optimised to avoid nodes being crossed by multiple aircraft in a single seeding week.
- **Reaction to change in density:** Due to weather in the seeding area the seeding density of certain areas will change unpredictably during operations. The nodes in these areas should be blocked and the path of the fleet changed so that no double seeding is done.

4.5.1. Effect of weather at cruise altitude

The prevailing winds at the latitude and altitude must be considered. The most notable weather phenomenons that will effect the mission are the polar vortex and polar jet streams, occurring at the 60° and -60° latitude, between an altitude of 9km and 12 km. The polar jet stream is a fast, narrow current of air, flowing from west to east. The rest of the wind at that altitude also flows from west to east due to the polar vortex, but decreases in speed with increasing latitude. Despite the rare occurrence of the jet stream meandering below the 60° latitude, the wind patterns are generally consistent [79]. Due to this consistency, two things should be considered: how to use the prevailing winds to ACT's advantage, and the effects of the polar jet stream on the aircraft's performance.

Compared to passenger aircraft, for example, which benefit from flying in the direction of an air current to save time, the ACT mission will not be able to use the weather as effectively. The payload will also be carried by the wind, and since the wind is consistently going from the west to east, decreasing in speed with increasing latitude, the aircraft will still have to seed the same amount as if there was no wind.

The polar jet stream will have wind currents travelling up to 400 km/h, while the air next to the polar jet stream may be travelling significantly slower. The large difference in speeds causes clean air turbulence (CAT) [27], which can cause the aircraft to suddenly lose altitude. This does not usually pose a safety risk, especially since the aircraft is unmanned. For CCT, the aircraft will have to regain control and potentially divert its flight path to avoid encountering CAT again. Closely studying the daily locations of the polar jet streams before determining the flight path will also help avoiding the border between the jet stream and normal air, thus saving time and fuel, as well as reduce accident risk.

At the operational altitude the strong winds will move the IN through the seeding area. The flight path algorithm should take the current weather forecast into account to predict the movement of the IN. Apart from the prediction the current IN concentration can be determined with the sensors carried by seeding aircraft. The current concentrations and predicted concentration combined should given an overview of where seeding is needed to maintain the required density at all times. In the flight path model the nodes that have the required density should be inactive, and a new path should be selected for all active units.

4.5.2. Accounting for weather at the bases

The effect of weather also has to be taken into account while determining the optimal route. Both weather at the airports and weather in the seeding area affect the mission. As discussed in section 4.2 strong cross wind may occur at Ushuaia airport, which might halt the operation from this base. Due to the range limit

of the aircraft some parts of the seeding area are unreachable from Christchurch airport. As reseeding is only needed once per week, the effect of not being able to seed due to weather can be countered looking at weather forecasts to make sure that the unreachable area is seeded when possible.

5 Payload Concept

This chapter describes the payload system designed for ACT. First the IN concentration and replenishment strategy for effective CCT are discussed in section 5.1, followed by the IN dispersion characteristics in section 5.2 and IN material selection in section 5.3, which have been previously reported in the midterm report. In section 5.4 the chosen injection system is chosen and elaborated upon. Next, in section 5.5 the design and specifications of the components of the payload subsystem are discussed which are: the combustion system, pumping system, storage tank and pipes. The subsystem descriptions are concluded with a graphical representation of the payload system lay-out. Then, the monitoring system including a testing strategy and operations initiation strategy are presented in section 5.6. A description of possible use of the payload system as a modular system to be mounted on existing aircraft is described in section 5.7. Finally, the compatibility of the payload system with silver iodide is analysed in section 5.8.

5.1. IN Concentration and Replenishment Strategy

In this section first the IN seeding concentration is discussed, after which the replenishment strategy will be elaborated upon.

IN concentration
It is required that a minimum IN seeding concentration of 15 particles per litre in the specified seeding area must be sustained, to ensure effective CCT. The optimal concentration of IN is 18 particles per litre [82], and CCT will be most efficient if this concentration is kept constant at all time. Since the half-life time is one week, the concentration would ideally be restored every day [63]. This will however result in a huge increase in fleet size, fuel consumption and other costs compared to seeding fewer times per week. Therefore, the impact of higher seeding concentrations on the performance of CCT has to be considered.

Storelvmo et al. [83] have researched the possible IN concentration range and the reduction in net cloud forcing related to these concentrations. The concentrations have been varied from 0 to 1500 particles per litre. The results of this study are presented in figure 5.1.

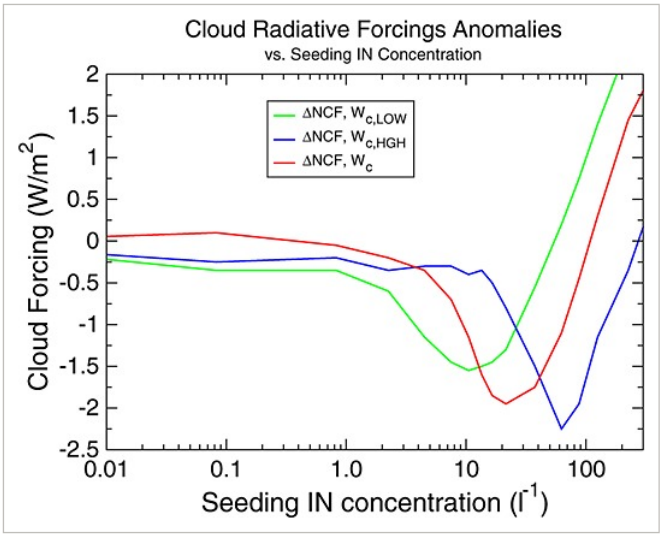

Figure 5.1: Net cloud forcing as a function of seeding concentration [83]

It can be seen from figure 5.1 (W_c function) that the net cloud forcing at a concentration of 15 particles per litre corresponds to approximately the same net cloud forcing when seeding at a concentration of 35 particles per litre. Every seeding concentration in between this, results in a more effective cloud forcing. The difference between the optimum seeding concentration and the minimum seeding concentration is only a few percent, therefore, it is not sustainable to have an aircraft resupply each day to increase the effectiveness by only a small percentage. It is more sustainable to resupply once a week, and have the effectiveness reduced by a small percentage simultaneously reducing the cost significantly.

Considering that the half-life time is approximately one week [63], a seeding concentration of at least 15 particles per litre has to be sustained at all time, a seeding concentration of at least 30 particles per litre has to be achieved at the beginning of a week. After one week, the concentration is then reduced to 15 particles per litre. To include contingency, the seeding concentration will be restored to 35 particles per litre each week. This will allow for extra time if incidentally resupply does not occur within one week.

Replenishment strategy
The initial seeding payload weight will be driving for the aircraft design. The aircraft should be designed to seed a concentration of 35 particles per litre at the start of the seeding period.

After the initial seeding of 35 particles per litre, the aircraft should reseed approximately with 18 particles per litre after one week as the half-life time is one week. This is however very inefficient, as the aircraft will be heavier than when it is designed to have an initial seeding potential of less than 35 particles per litre. The aircraft OEW reduces if the initial seeding potential is reduced and less fuel is required. This will take more weeks before the required initial seeding concentration is achieved, but reduces the OEW and thus cost. Different seeding strategies are stated in table 5.1.

As it is required that seeding should occur during late fall until early spring, strategies which take longer than three weeks to achieve the concentration of 35 particles per litre are not considered. As there should also be a margin to increase the seeding concentration due to deviating dispersion or half-life time changes, the aircraft should be able to seed at least 20 particles per litre into the seeding area. Looking at the different strategies in table 5.1, it is concluded that the aircraft will have a seeding potential of 24 particles per litre. After one week, the initial seeding concentration of 35 particles per litre is then achieved. The concentration can be increased to 48 particles per litre if that is required due to unexpected changes. This will result in a lower OEW and thus less fuel is required than when the aircraft is designed for a seeding potential of 35 particles per litre.

Table 5.1: Optional seeding strategies

Aircraft seeding potential [l^{-1}]	No. of weeks before initial concentration of 35 l^{-1}	Maximum initial concentration [l^{-1}]
20	3	40
24	1	48
28	1	56
32	1	64
35	0	70

5.2. Dispersion of IN

To ensure adequate atmospheric concentrations when seeding, it is important to determine the dispersion ”area” of the seeding material when released from the seeding aircraft. As described in the midterm report [34], the dispersion of the IN is assumed to act similar to aircraft contrails in agreement with the project principal tutor. Even though Schumann et al. [80] describes an elaborate review of available data of contrail development from in-situ measurements and remote observations, and Unterstrasser and Görsch [87] allows for determining a basic relation of aircraft wingspan to contrail plume radius, the level of detail is insufficient to determine solid dispersion characteristics as AT1’s design differs vastly from daily operating airline aircraft for which the contrail prediction simulation and observation are derived. Therefore the preliminary design of the CCT system is performed assuming a dispersion width of 10 km and dispersion height of 1 km which is retrieved from Schumann et al. [80]. In section 5.6 a description is given on how the actual dispersion area

will be established and how the design will be changed if necessary.

5.3. IN Material

For the IN material selection, several materials were considered. Studies show that the following materials can be used as IN: dust [75], soot [18], minerals covered with sulphate [9], biological debris [71], volcanic ash [23], sea salt [97], silver iodide [50], lead iodide [50] and finally bismuth tri-iodide [63]. From these materials only sea salt, soot, silver iodide and bismuth tri-iodide are considered, since the other materials are not feasible on a large scale, the material has negative environmental impacts or the material is toxic.Soot, sea salt, silver iodide and bismuth tri-iodide have been analysed further.

After the analysis of soot, it became clear that soot has a net warming effect. Soot warms the Earth by absorbing sunlight and radiating it into the atmosphere. It reduces Earth's albedo, while an increase is desired for CCT [11]. Wagner et al. [94] have investigated the behaviour of sea salt as IN at lower temperatures. The conclusion is that sea salt fully deliquesces at temperatures above -53^{o}C and nucleates ice homogeneously. This is unwanted and critical for the mission, as heterogeneous nucleation is required in order to successfully perform CCT.

Two promising materials remain, silver iodide and bismuth tri-iodide. Silver iodide has already been proven to be an effective IN in weather modification programs [50]. However, silver iodide is very expensive, it is toxic when dissolved in water and it can also affect clouds at lower altitudes, which will increase local rainfall. Bismuth tri-iodide has a lower effectivity threshold, which makes it favourable as it does not affect clouds at lower altitudes [63]. Also, it is twelve times cheaper than silver iodide. The disadvantage of bismuth tri-iodide is that the effect on the environment is unknown, although it is known not to be toxic. Also, it is corrosive so extra measures must be taken for the design of the payload subsystem.

Considering the aforementioned aspects, bismuth tri-iodide will be the best material for the mission, because silver iodide is twelve times more expensive, it is toxic to aquatic life and it has other (possible) environmental impacts. However, since silver iodide is proven to be an effective IN, the system will also be made compatible with silver iodide. This will be done to ensure that the system can still perform CCT should bismuth tri-iodide not be suitable to perform its function properly. This will be discussed in section 5.8.

An estimation of the payload weight can be obtained using the method described in the Midterm Report [34]. It is found that 422 tons of bismuth tri-iodide is required on a yearly basis. This will have an annual cost of 17 million dollars. Seeding will take place weekly and the particle size is assumed to be 0.1 μm, which is the same as the mean particle size which is obtained after combustion of silver iodide dissolved in acetone in weather modification programs[62].

5.4. Injection System

In this section, the injection system will be elaborated upon. The chosen method is stated and the corresponding process is discussed.

5.4.1. Injection Method

In the Midterm Report [34] it was determined that the IN material will be dissolved in an ethanol solution and evaporated by ignition. This will be done using a combustion chamber which will evaporate the ethanol solution leaving aerosol form. A bismuth tri-iodide solubility of $3.5g/100ml$ is required for this combustion. 180,000 kg of payload has to be injected into the troposphere each week [34].

5.4.2. Combustion Process

For the chosen injection method, the ethanol solution must be ignited to transform the dissolved bismuth tri-iodide into aerosol particles. For this process three aspects must be present: fuel, oxygen and heat. The ethanol solution can be seen as the fuel and heat can be added by means of a spark. Furthermore, oxygen must be supplied for a complete combustion. The chemical reaction that will take place is shown in equation (5.1)

$$C_2H_5OH + 3O_2 \rightarrow 2CO_2 + 3H_2O \tag{5.1}$$

This reaction can be used to determine the amount of oxygen that is required for the combustion. For each molecule of ethanol, three oxygen molecules are required. The aircraft is flying at Mach 0.6 during cruise and the dispersion width and depth are 10 and 1 km, respectively. The injection and combustion rate can be determined using this information. As a result, the combustion rate will be 4.26 grams of solution per second at an altitude of 10 km. This can be scaled to other altitudes, if required. As the molar mass of ethanol is 46.07 g/mole, 0.108 moles of ethanol is required. Three times as much oxygen is necessary for a complete combustion. As a result, 10.4 grams of oxygen per second is required for this process. The mass percentage of oxygen in the air is 23.1%[1]. At an altitude of 10 km, this will require an air supply of 93 litres per second for a stoichiometric combustion.

To supply the required air for combustion, several options must be considered. One option is to store the oxygen in a tank which is located in the aircraft. However, looking at the ethanol and oxygen supply rates determined above, this will approximately triple the payload weight, which is undesired as this will increase the aircraft size and consequently the cost significantly. Another option is to have an inlet on the aircraft. Air can flow into this inlet and be transported to the combustion chamber. The last option is to tap air from the engine, which is called bleed air. Airliners use this option to control the environment in the cabin and refresh the air in the cabin multiple times during a flight [4]. Air is tapped after the compression stage which is still upstream of the combustion chamber of the jet engine. Air will then be transported from the engine to the combustion chamber. The last option will be chosen as the inlet of the second option will increase drag, while for the first option only a small adaptation to the engine should be made. The engine chosen in section 6.8 allows a maximum of 7.14 kg of air per minute to be tapped from the engine at 10 km altitude [5], without affecting the thrust performance. For the combustion, only 2.3 kg of air per minute is required for stoichiometric combustion. The performance will not be affected by this, as the maximum thrust at 10 km altitude is still almost 40% higher than the required thrust.

Ethanol has a minimum ignition temperature of $16.6°$C [47]. As the aircraft is flying at minimal temperatures of $-60°$C, the ethanol solution has to be heated in order to be ignited. The melting temperature of ethanol is $-114°$C, which is beyond the temperature range to which the aircraft is exposed. Therefore, no phase transition will have to be accounted for. The ethanol solution will be heated to $25°$C, to allow for a cooling margin. The heating will be done by including a heater in the pump, which will be explained in section 5.5. The heat flow required can be calculated with equation (5.2) [13].

$$\dot{q} = c_p \dot{m} \Delta T \tag{5.2}$$

Here, c_p is the specific heat of ethanol which is 2.44 $JK^{-1}g^{-1}$[13], $\dot{m}$ is the mass ethanol mass flow and ΔT is the required temperature increase. As a result, 883 W has to be supplied for the worst case scenario. This amount will probably be less depending on the actual temperature.

5.5. Payload System Components

In this section the payload components are described. First, a preliminary sizing of the storage tank and combustion chamber is performed. After that, a pump which transports the ethanol solution from the storage tank to the combustion chamber is chosen and the corresponding pipes are presented.

[1]Retrieved from: https://www.engineeringtoolbox.com/air-composition-d_212.html [06/06/18]

5.5.1. Combustion System

For the combustion chamber, first the materials are chosen after which the combustion chamber is sized.

Combustion chamber material

In the combustion chamber of a jet engine the material consists mostly of an alloy which is able to maintain its material characteristics at high temperatures. Haynes 188 is such a material which has a yield strength of 131 MPa at $1000°C$[2]. It has been used in jet engines frequently, where a temperature of 1400 K after combustion is not exceptional [52]. This makes it a reliable material to use in the combustion chamber. Although this material has a good corrosion resistance at higher temperatures, the chamber will be covered with a layer of Monel 400 because of its excellent resistance to many corrosive environments[3].

Combustion chamber sizing

The method used to come to the preliminary design of the combustion chamber is based on the method described in Walsh and Fletcher [95]. The compression ratio of the jet engine is 24[4]. Since the air is not bled at the end of the compressor, a compression ratio of 20 is assumed. This value should be updated accordingly when detailed information of the engine is available. The temperature after compression can be determined with equation (5.3) [58].

$$T_2 = T_1 + \frac{T_1}{\eta_{comp}} \left(\Pi_{comp}^{(\gamma-1)/\gamma} - 1 \right) \quad (5.3) \qquad \dot{m} = \frac{\dot{m}_f \cdot LHV \cdot \eta_{cc}}{c_{p.g}(T_3 - T_2)} \quad (5.4)$$

T_1 and the pressure are determined according to ISA standards at an altitude of 10 km, the efficiency η_{comp} is assumed to be 0.85 and γ is 1.4 for air[59]. As a result the temperature T_2 is 578 K after compression. The temperature after combustion should be limited so the material will not melt. This temperature T_3 has been set to 1200 K, as the material characteristics of Haynes 188 will degrade at higher temperatures. The corresponding required air mass flow is determined with equation (5.4) [58]. Here, $\dot{m}_f$ is the fuel mass flow, LHV is the lower heating value of ethanol, which is 29.7 MJ/kg[13]. η_{cc} is the combustion efficiency, which is assumed to be 0.99 and the specific heat of a hot gas $c_{p,g}$ is 1150 J/kg/K[13]. The required air mass flow is 0.148 kg/s. This is higher than the allowed air that may be bled from the engine, as was stated in section 5.4.2. Therefore, the air temperature should be decreased after it is bled from the engine. In section 7.14 a heating/cooling system of the aircraft is described which is able to cool the air to 328 K, which will then be used to heat the fuselage. This results in an air mass flow of 0.110 kg/s, which is within the bounds of the maximum air to be bled. The volume of the combustion chamber V_{cc} can be determined with equation (5.5) [95].

$$Loading = \frac{\dot{m}}{V_{cc} p^{1.8} 10^{0.00145(T_2-400)}} \quad (5.5) \qquad A = \frac{\dot{m}\sqrt{T_{fl}}}{Qp} \quad (5.6)$$

Here, the loading represents the combustor loading, which is preset by the design guidelines to 1 $kg/s\ atm^{1.8}\ m^3$ [95]. $\dot{m}$ is the mass flow, and p is the pressure in atm. The combustion chamber volume is then 2.84 litres. Next, the length and diameter ratio has to be determined. The circular surface area of the combustion chamber is calculated with equation (5.6) [95].

The maximum flame temperature T_{fl} of ethanol is 2355 K and p is the pressure in kPa (whereas in equation (5.5) the pressure was in atm, but the method is verified by Walsh and Fletcher [95]). Q is the flow function, which is 1.3609 $kg\sqrt{K}/m^2 kPa\ s$ at an exit Mach of 0.02. This is the lower end of the design guidelines from Walsh and Fletcher [95]. As a result, the area circular area is 0.0074 m^2, the radius is 0.049 m and the length is 0.38 m.

[2]Retrieved from: http://www.hightempmetals.com/techdata/hitempHaynes188data.php [06/06/18]
[3]Retrieved from: http://www.specialmetals.com/assets/smc/documents/alloys/monel/monel-alloy-400.pdf [06/06/18]
[4]Retrieved from: http://world.honda.com/HondaJet/Background/TurbofanEngine/ [06/06/18]

The minimum thickness of Haynes 188 is 0.4 mm[5]. The yield strength is 131 MPa at $1000°$C and the radius is 0.049 m. Using equation (5.10), the maximum pressure that the combustion chamber can withstand is 1 MPa. The maximum possible pressure is 0.53 MPa, which is considerably lower than 1 MPa, also after including a safety factor of 1.5. Therefore, the minimum possible thickness will also be the thickness of the combustion chamber.

To minimise the heat the aircraft structure will be exposed to, a casing around the combustion chamber will be placed. In between these, air flows to dissipate the heat generated by the combustion chamber, as was determined previously in this section. The material that will be used for this casing is the titanium alloy Ti6Al4V, because of its frequent application in jet engines and high melting temperature of $1650°$C[6]. The diameter will be 1.5 times the diameter of the combustion chamber and it will have a thickness of 0.8 mm as this is the minimum thickness and the structure does not have to carry loads.

The combustion chamber mass will be 0.44 kg, which only consists of the skin. Taking a contingency of 30% for more detailed design considerations, a mass of 0.57 kg is obtained. Including the casing as well, a total mass of 1.2 kg is found.

Combustion Chamber Location

In the midterm report [34] two options for the placement of the combustion chamber were discussed. First, mounting the combustion chamber below the wing as wing pods and secondly, placing the combustion chamber in the tail end of the fuselage. Placing the combustion chamber as wing pods is discarded as this creates additional drag and will thus influence the range of the aircraft negatively. As a consequence, the combustion chamber will be placed at tail end of the fuselage. This configuration will also minimise the risk of payload material interaction with the aircraft, as it disperses immediately behind the aircraft. The combustion chamber is located as an extension of the fuselage, halfway outside the aircraft, hence integration the combustion chamber in the fuselage. Although it is determined in section 7.3.1 that carbon fibre reinforced plastic (CFRP) will be the main material in the aircraft, this will not be used around the combustion chamber. CFRP does not perform well at high temperatures and therefore, the material around the combustion chamber will also consist of titanium, just as the combustion chamber housing. The transition from CFRP to titanium can be implemented as described in Möller et al. [66]. It is stated here that normally rivets or bolts are used, but a CFRP-metal novel joint configuration is more favourable as it reduces structural weight. This joint configuration requires a thermal, laser based joining process.

5.5.2. Pumping System

The ethanol solution must be transported from the storage tank to the combustion chamber. To do this a pump is required. In the midterm report [34] it was discussed to place a pump either in the storage tank, in the combustion chamber, or in between. It is required that the pump is able to sustain a very accurate flow rate of around 4.3 grams per second, depending on the Mach number and altitude. Furthermore, the pump must be able to heat the ethanol solution, as was explained in section 5.4.2, and the pump must be corrosion resistant. Lastly, it must be connected to the avionics in the aircraft so it can regulate the flow rate for different values of altitude and speed. Based on these requirements, the pump and its location are chosen.

The pump will not be stored inside the storage tank as the ethanol solution is very corrosive and will damage the pump if this configuration is chosen. It will not be placed inside the combustion chamber as temperatures are high and this will affect the pump, as most pumps are not able to sustain temperatures higher than $300°$C [7]. Consequently, the pump will be placed between the storage tank and the combustion chamber. The pipelines that ensure payload flow in and out of the pump will be elaborated upon in section 5.5.3.

The pump that fits these requirements, except for heating the solution, is the Magnetic Drive Gear Pump 2222, manufactured by Flight Works Inc. This pump is able to handle corrosive alcohol solutions. Furthermore, it

[5] Retrieved from: http://www.haynesintl.com/alloys/product-forms/sheet-and-plate [06/06/18]
[6] Retrieved from: https://www.azom.com/article.aspx?ArticleID=1547 [06/06/18]
[7] Retrieved from: https://www.witte-pumps.com/ [08/06/18]

can regulate the flow very accurately with a maximum of 400 ml/minute. The pump costs $3000 and weighs approximately 300 grams including housing[8]. Micro pumps generally have an accuracy of ±1% [9]. This pump is small and lightweight, but it can not heat the solution. Therefore, a heating element must be considered in addition to this pump. A cartridge heater for liquids will be used for this. This can be inserted into the tube just before the pump, to heat the liquid to $25°$C. Such a device is cheap and can be easily implemented and regulated[10].

5.5.3. Payload Storage Tank

An important aspect of the mechanical design of the payload system is the payload storage tank. The material that was determined as best suitable is high density polyethylene (HDPE) which is further developed into an actual structural design. To maintain adequate pressure in the tank, the tank has to be equipped with a venting system with emergency air vents as back-up. Using the venting system will cause for no pressure differential to exist between the inside and outside of the tank.

The dimensions of the payload tank are determined by considering a cylindrical vessel with spherical end caps to avoid stress concentrations along sharp corners of tank that would exist in a non-spherical design. [38] The payload tank is positioned inside the aircraft fuselage above the main landing gear, the rationale for this location is presented in chapter 6.

As no pressure differential exists between the inside and outside of the tank and the payload acts in a similar fashion to fuel contained in a tank, the pressure resulting from the maximum loads caused by the tank content are determined using equation (5.9) from [30] §25.963, where k is the load factor defined for every direction in table 5.2 [30], ρ is the payload solution density in kg/m^3, g is the gravitational acceleration in m/s^2 and L is the reference distance between the point of pressure application and the furthest distance to the tank boundary in m. The pressure is converted to necessary thickness of the separate aspects of the tank using equation (5.10) for the stress in the tank in the radial direction and equation (5.11) for the stress in the tank in the longitudinal direction [38]. The material yield strength is a key parameter in determining the tank thickness, as for HDPE the yield strength varies with temperature, the yield strength considered for determining the tank thickness is the worst case temperature in the operational scenario. [60] The resulting design parameters of the storage tank are shown in table 5.3.

$$V_{cylinder} = \pi \cdot r_{inner}^2 \cdot L_{cyl} \quad (5.7) \qquad V_{sphere} = \frac{4}{3}\pi \cdot r_{inner}^3 \quad (5.8) \qquad P = k\ \rho\ g\ L \quad (5.9)$$

$$\sigma_\theta = \frac{P \cdot r}{t} \quad (5.10) \qquad \sigma_x = \frac{P \cdot r}{2 \cdot t} \quad (5.11)$$

Table 5.2: Load factor (k) for fuel tank

Direction	Load factor [-]
Forward (Outside Fuselage)	4.5
Forward (Inside Fuselage)	9
Aft	1.5
Inboard - Outboard (Outside Fuselage)	3
Inboard - Outboard (Inside Fuselage)	1.5
Downward	6
Upward	3

Integrating the storage tank in the fuselage, particular care should be given to the fact that HDPE has a melting point of 110 degrees Celsius [11] and is shielded from warm components of the payload system. To avoid stability issues in abrupt manoeuvres, the tank will be equipped with slosh baffles that delay the movement of

[8]Retrieved from: https://www.flowlink.nl/ [08/06/18]
[9]Retrieved from: https://www.lewa.com/en/pumps/metering-pumps/micro-metering-pumps/ [08/06/18]
[10]Retrieved from: https://nl.rs-online.com/ [08/06/18]
[11]Retrieved from: http://www.plasticmoulding.ca/polymers/polyethylene.htm [07/06/2018]

Table 5.3: Payload Storage Tank Design Parameters

Parameter	Value	Unit
Material	HDPE	-
Mass	2.23	kg
Thickness	0.5	mm

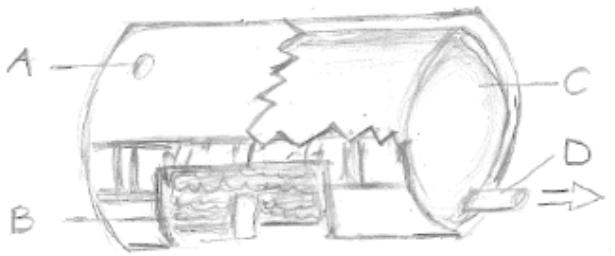

Figure 5.2: Payload Storage tank - A: Vent hole - B: Landing Gear Stowage - C: Payload Storage Tank - D: Connection Pipe to Pumping System

the content of the payload tank.

In the midterm report [34] it was determined that the storage tank will be placed inside the aircraft to minimise drag. It was not decided whether to place the tank in the wing or in the fuselage. Since the combustion chamber is placed at the tail end of the fuselage, the storage tank will not be placed in the wing. This will complicate the wing and fuel tank design and will require more energy to transport the ethanol solution to the combustion chamber. Therefore, the storage tank will be placed in the fuselage. The avionics will be stored in the front of the aircraft, fuel in the centre and tail end and the combustion chamber is placed in the tail end of the aircraft. In order to reduce the c.g. range to an acceptable distance, the storage tank will be located in the centre of the fuselage.

The payload tank feeds to the pumping system through a HDPE pipe, that extends from the storage tank and has been reinforced locally to account for stress concentrations and is 0.88 m in length and 0.005 m in diameter. From the pumping system to the combustion chamber the pipe runs along the upswept part of the tailcone and is made of Haynes 188 and connected directly to the combustion chamber.

5.6. Monitoring System and System Initiation Tests

To ensure an optimum cirrus cloud thinning system, local monitoring of the ice nuclei concentration as well as remote monitoring of the system effectiveness is necessary. For in-situ checking of the particle concentration, in the midterm report [34] it was stated that both Ultra-High Sensitivity Aerosol Spectrometer (UHSAS) and Passive Cavity Aerosol Spectrometer (PCAS) must be used to monitor particle size and concentration. However, after more research, it became clear that the UHSAS is able to measure concentrations. Therefore, the PCAS will be redundant and will no longer be used. The UHSAS can measure particles between 0.06 and 1 μm. It has a price of $120,000 and requires one to two hours of maintenance per month[12].

If the seeding concentration is not correct, an increase in net cloud forcing might occur, or the effect will be minimal and money has been wasted. Therefore it is of high importance to have an accurate model. At the start of the detailed design phase a testing program will be initiated as shown in chapter 16. This is done to check the design assumptions by in-situ measurements using weather modification aircraft prepared to use BiI_3 solution as IN. These aircraft however are not optimised for the mission like AT1 and hence will only be able to cover a small area per seeding test, however, they are helpful in executing system tests on short timescale.

The characteristics found in the initial test will serve as a basis to determine the need for monitoring and drive

[12]Retrieved from: http://www.dropletmeasurement.com/ [07/06/18]

the detailed design. The concentration in the seeded area should be measured several times at different times. This will then be used to validate the dispersion model described in section 5.2. If major discrepancies are found, the model must be revised or a new model should be made which complies with the experimental data. If minor discrepancies occur, the model should be scaled accordingly. The UHSAS will also be used in the test program on every measurement flight.

If atmospheric residence of the IN is found to be highly variable and subject to large fluctuation based on local (weather) phenomena, it could be decided that every seeding aircraft should be equipped with the UHSAS for monitoring. This would allow for immediate adjustment of the injection rate. Whereas if it is found to be fairly stable, only a few aircraft will be equipped with the device to ensure no changes in the model developed from test occur over time. The data that is collected using these measurements will be used to make an accurate model. It can be used to investigate the influence of the weather to the dispersion and determine whether there are large differences in seeding width and depth in different seeded areas. The UHSAS will be integrated in the nose of the AT1 as in this position the device will have the minimum possible negative impact on aircraft drag.

As previously described in the midterm report, the overall effect of CCT has to be monitored as well to validate that the method is working. Several satellite missions which are able to measure aerosols and ice crystals in Earth's atmosphere are considered. For example, the CALIPSO satellite is able to measure relative differences in concentrations of ice crystals. This can be used to study the effect of CCT and also the possible unknown side effects. The GOES-16 and GOES-17 satellites are also able to measure these ice crystal concentration differences. CALIPSO was launched together with the CloudSat satellite. Together they can observe how cirrus clouds and aerosols in the atmosphere behave [13]. Therefore, this will be a suitable option to monitor the effects of CCT on the short and long term.

5.7. Integration into Existing Aircraft

The required payload weight is relatively small compared to the maximum take-off weight. For a seeding range of 12605 km, only 300 kg of payload is required. This makes it interesting to evaluate the possibility of equipping existing aircraft with the payload system. Existing aircraft are not optimised for the mission like AT1 which may lead to a higher overall system cost, for example in terms of fuel use and need for human operators, however if a short-term need for CCT arises before the AT1 is operational, this option may need to explored at the expense of less efficient and more costly daily operations.

Several integration possibilities are possible. The tank in the original design is located in the fuselage and can be separated from the aircraft easily. It can be easily installed into other aircraft fuselages, for example by converting small existing passenger aircraft and replacing the cabin content by the payload system. Where in conventional passenger aircraft bleed air from the engine is used to pressurise the cabin, part of the bleed air could be used to supply oxygen for the combustion process. A simpler solution will be to additionally store an oxygen tank next to the payload tank which is then connected to the combustion chamber. The combustion chamber however, is integrated into the aircraft skin. Therefore, if the same configuration as the original design is used, adaptations to the tail end of the aircraft should be made, such as creating a hole and prevent excessive heating of the aircraft structure. Another possibility is to combine the combustion chamber and storage tank into one. As such, this system can be placed as pods under the wing. This will increase drag and will lower the amount of payload which can be injected, but it is effective for shorter ranges and can be easily used to conduct experiments for the dispersion. This is also the method which is performed for weather modification programs [50]. Another option is again to place the combustion chamber as a pod under the wing and place the storage system in the fuselage. This will however increase the complexity of the placement as the connection between the tank and combustion chamber must be integrated into the wing. Depending on the aircraft, urgency and applicability one of these options can be considered.

The cost of using other aircraft is hard to estimate. It will consist of the purchase or hiring costs of the aircraft and equipping it with the payload system. The entire payload system cost in estimated to be in the order of $300,000 per aircraft. This will be added to the price of a new aircraft. However, most small aircraft will

[13] Retrieved from: https://www.nasa.gov/mission_pages/calipso/main/index.html [19/06/18]

not achieve the range that the AT1 will achieve, as they are designed for a larger payload mass percentage. This will result in an inefficient system, as the number of aircraft will be enormous and so will be the fuel consumption. It will however be a good option to conduct initial experiments or in case of an emergency when more aircraft are urgently required.

5.8. Compatibility with Silver Iodide

In section 5.3 it was determined that the payload system should be made compatible with silver iodide. This was done to mitigate the risk of bismuth tri-iodide not being able to perform its function properly. Silver iodide has been proven to be an effective IN in weather modification programs, increasing its reliability [50]. It is very expensive however; if silver iodide would be chosen, this would lead to a yearly cost of $204 million dollar instead of $17 million dollar [63] for the IN material. Furthermore, it is toxic to aquatic life when it is dissolved in water [81]. It should be noted that silver iodide will only be used in case of an emergency and in any other case, bismuth tri-iodide will be used.

When silver iodide is used, it will be dissolved in an acetone solution instead of an ethanol solution [50]. Silver iodide is not corrosive when it is dissolved in acetone [14], so no extra measures have to be taken for this. However, the storage tank should be made from a different material, as acetone reacts with HDPE [15]. Since silver iodide dissolved in acetone is not corrosive, the material of the storage tank can be a metal.

It is convenient that the density of acetone is almost the same as ethanol (0.78 vs 0.79 g/cm^3) and the density of silver iodide is almost the same as bismuth tri-iodide (5.7 vs 5.8 g/cm^3). The only thing that differs significantly is the solubility. Silver iodide is dissolved in acetone at a solubility of 5.63 grams per 100 millilitres [64], instead of 3.5 grams per 100 millilitres for bismuth tri-iodide. As a result, the total payload mass decreases by 35%. This will save approximately 100 kg per flight, which can be used for extra fuel and extra payload which reduces the total number of sorties. The storage tank mass will however increase, as a metal will be used which has a higher density. The aircraft system is not optimised for this configuration, but since the change in maximum take-off weight is not considerable (about 2%), it is expected that the performance will not be influenced heavily.

The combustion rate will also decrease from 4.3 to 2.7 grams per second at 10 km altitude. The combustion chamber is large enough for this and the pumping system is able to micro dose these rates. Therefore, the combustion chamber and pumping system remain the same. The monitoring system can also be used to monitor the silver iodide concentration. The flash point of acetone is -20^{o}C, which is 35^{o}C lower than ethanol, so less heat needs to be added to warm up the solution.

Concluding, using silver iodide as IN will decrease the payload weight. Corrosion is no longer an issue, but the storage tank material must be changed to a metal. Furthermore, the combustion chamber, pumping system and sensor remain the same. However, the use of silver iodide will increase the payload cost by a factor of twelve and it is toxic when large quantities are dissolved in water. Therefore, silver iodide will only be used in case of an emergency.

[14] Retrieved from: https://www.materials.sandvik/en/materials-center/corrosion-tables/silver-bromide-silver-iodide/ [21/06/18]

6 Aircraft Design

Development of the aircraft for IN delivery aircraft started with the selection of the conventional operations concept. With this concept selected, new requirements specific to the seeding aircraft were established. The most driving requirements the aircraft had to meet was the range of at last 14,000 km, the required altitude of at least 10 km, and operations in very harsh weather conditions, such as strong cross-winds and low temperatures. Since the CCT seeding aircraft has to obtain a very long range and will migrate between the polar regions, it was given the name Arctic Tern (AT1) after the migratory bird species. Arctic terns traverse the globe from polar regions in the north to polar regions in the south and back every year, similarly to the seeding aircraft.

First, the class I weight estimation using statistical data and fuel fractions is presented in section 6.1. Next, the thrust and wing loading diagram is described in section 6.2. section 6.3 elaborates upon the aircraft configuration trade-off. The wing is sized in section 6.4 and the preliminary sizing of the fuselage and tail is presented in section 6.5. Drag estimation is carried out in section 6.6. section 6.7 describes the landing gear sizing and positioning. Next, section 6.8 presents the selected engine. The Class II weight estimation is carried out in section 6.9 and the loading diagram is obtained in section 6.10. The stability and control with empirical relations is done in section 6.11. The aircraft parameters obtained after the last iteration are presented in section 6.12. Finally, the electrical system and fuel and payload systems lay-out are presented in section 6.13 and section 6.14, respectively.

6.1. Class I Weight Estimation

The class I weight estimation was done with fuel fractions and a linear regression relating OEW to MTOW of reference aircraft, presented in table 6.1. Since the range was the driving parameter, reference aircraft were selected based on their focus on long range. All of the reference aircraft achieve a range above 10,000 km. Nevertheless, they differ greatly in MTOW, since the approximate weight of the IN delivery aircraft was still unknown.

Table 6.1: Reference aircraft data[1]

Plane	Cruise Mach	MTOW [t]	OEW [t]	Range [km]
Boeing 777-200LR	0.84	348	145	17,445
Airbus A340-500	0.82	380	170	16,668
Airbus A350-900ULR	0.85	280	135	18,000
Bombardier Global 8000	0.85	47.5	24.6	14,631
Gulfstream G650	0.85	45.2	24.5	12,960
Boeing B-52	0.84	220	83.3	16,232
Tupolev TU-95MS	0.67	188	90.0	15,000
RQ-4 Global Hawk	0.54	14.6	6.78	22,779
Lockheed U-2	0.56	18.1	6.49	10,308
Virgin Atlantic Globalflyer	0.51	10.0	1.69	41,466

To estimate the fuel fraction for the cruise it was necessary to assume the exact design range, corresponding payload, Mach number and L/D. First, a comparison was done between subsonic and transonic cruise. Subsonic cruise Mach number offered much better fuel efficiency which was the main optimisation parameter due to its importance in environmental and economic sustainability. The initially selected aircraft cruise Mach number is 0.6. Lowering the mach number was expected to yield diminishing return in efficiency and would increase the required fleet size significantly. Furthermore, reference long range subsonic aircraft also fly at

[1] Retrieved from: https://janes.ihs.com/ [17/05/2018]

this mach, supporting the expectation. This assumption will later be validated by analysing the L/D at different speeds. The L/D estimate of 25 followed from subsonic reference aircraft list. The selected design range was 20,000km, which allowed for 4 movements in one hour per base. With this information the class I weight estimate was obtained. The first iteration estimation of MTOW and OEW are 7650kg and 5160kg, respectively. The corresponding payload mass was 480kg, where payload refers to only the BiI_3-Alcohol solution and the payload tanks and dispersion system were at this stage assumed to be included in the operational empty weight. The payload weight was in this phase used as a driving requirements where in the next phase the volume will be taken into account when defining the aircraft lay-out. The fuel weight accounts for 2010kg. With such an aircraft the mission could be done with 122 aircraft operating continuously.

6.2. Thrust and Wing Loading Diagrams

After the class I weight estimation the wing and thrust loading diagram was produced to established the the wing surface area and required thrust. To obtain those, wing and thrust loading diagrams have been produced. The CCT delivery aircraft will most likely not be a commercially available, but rather a governmental or internationally owned and/or controlled aircraft. Therefore, it does not have to adhere to the EASA or FAA regulations. Consequently, the constraints on wing loading and thrust come from operational aspects like base airport operational procedures. For instance, the stall speed requirement follows from landing distance requirement of 2500m. For preliminary estimate a statistical relation for CS25 aircraft was used for the stall speed requirement and returned vale of 65.4 m/s to add a safety margin this speed was lowered to 60m/s at MTOW. Similarly, the take-off distance of 2500m constrains the minimum thrust loading. The cruise of 0.6M and altitude between 7 and 10km that the aircraft will be designed for also imposed a constraint on thrust and wing loading. Drag and wetted area were estimated from statistical relations. Finally, climb rate and climb gradient were analysed for the last two constraints. Climb rate was limited by the fact that the aircraft shall reach the seeding altitudes in a reasonable time. Since it is still unknown what the optimum climb rate will be it was assumed to be 10m/s, similar to airliners. Nevertheless, this constraint was left as a design variable for future iterations. Climb gradient, however, was given by the airport instrumental departure routes. Out of four selected airport bases Christchurch is the most constraining with the gradient of 8.1%. Due to possible changes in the base airports a contingency of 20% was applied to the gradient. The obtained thrust and wing loading diagram gives the possible design space for the aircraft from where the design point was selected. Currently, climb rate and stall speed are the most constraining factors. The initial selected wing loading was W/S = 4650 N/m2, but that produced a relatively small wing which required complex high lift devices. After the last iteration the selected design point giving wing loading value of W/S = 4150 N/m2. The thrust to weight ratio T/W was initially 0.172 N/N, but was later also revised to 0.215 N/N. This was done to allow the aircraft to reach seeding altitudes sooner. The thrust and wing loading diagram and the initial design point can be seen in figure 6.1.

6.3. Aircraft Configuration Trade-off

Concurrently with the wing and thrust loading diagram, the design option tree for the aircraft was developed. First, the decision was made on the autonomy of the aircraft. The unmanned option was selected over a manned aircraft because of lower operational cost, higher reliability, better operational flexibility and system weight. Possible fuselage configurations were analysed next. The options evaluated were single fuselage, double fuselage, blended wing body and flying wing. Blended wing body and flying wing were discarded based on low TRL. Double fuselage would mostly benefit structurally for a very high aspect ratio wing. Although the CCT delivery aircraft is likely to have such a high aspect ratio wing it would be harder to land at the base due to cross-winds. Moreover, it was decided to use a single engine which is easier to attach to a single fuselage. A decision to use a single engine was made based on the higher efficiency and the fact that the aircraft will be operating autonomously over non-populated regions where safety is not the highest concern. It was decided to use fossil fuel because of overall good performance, especially good energy density and high TRL. The best performing engine type for the mission was the turbofan engine. Finally, the empennage selection was made in combination with engine positioning, since they have a strong influence on each other. It was decided to place the engine on top of the aircraft since the aircraft can have shorter landing gear and the engine is better

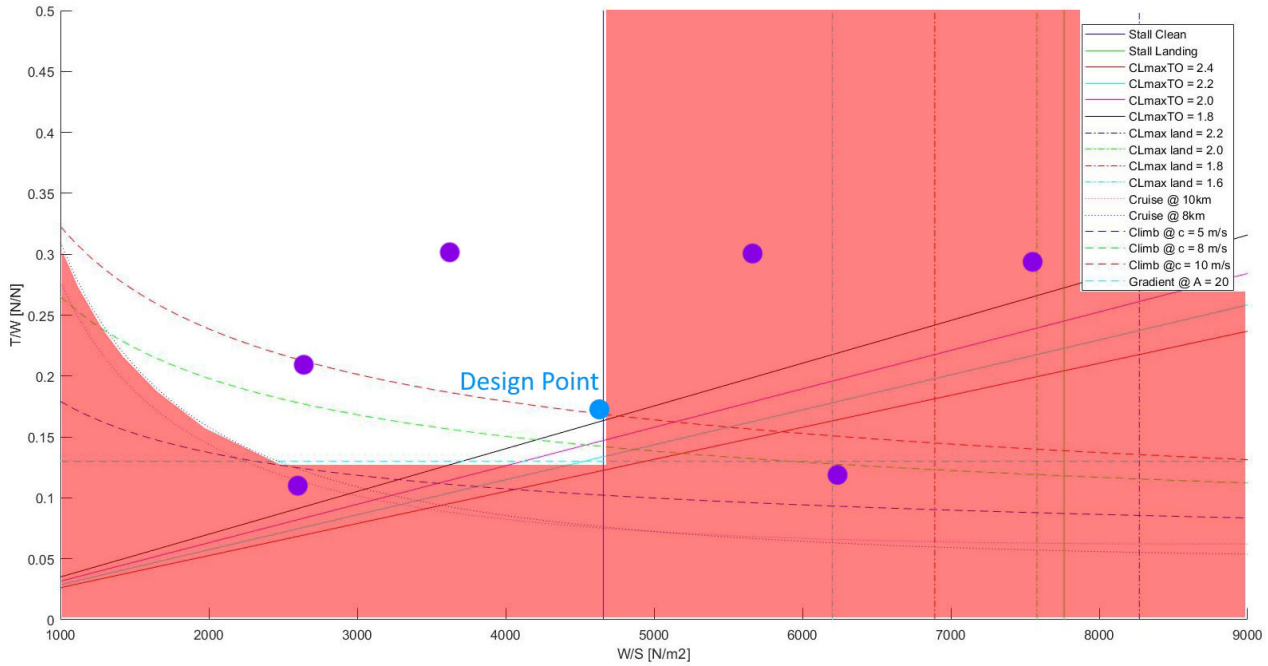

Figure 6.1: Thrust and wing loading diagram. The red area displays the non-allowable region for the design point and limits the design area. The blue dot denotes the chosen design point.

protected from runway contaminants. The tail configurations were selected with the engine position in mind. Conventional and T-tail would have to have the engine integrated into the vertical tail which is structurally undesirable. Poor stability performance discarded the canard. Finally, a double tail is structurally heavy and a vertical stabiliser redundancy is not critical. The most optimal configuration was a V-tail with the engine mounted in between both stabiliser fins. This allows the tail to be out of the engine exhaust without mounting the engine into the vertical tail fin. Moreover, the engine position could be moved fairly independently of the tail position. Nevertheless, the V-tail control surfaces combine the elevator and rudder into a ruddervator. This introduces additional complexity and undesirable yaw-roll coupling.

6.4. Wing Design

With the MTOW estimation, selected wing loading and aircraft configuration the wing design was initiated. First the wing planform was designed and the airfoil was selected. Next, the wing lift curve was calculated. Finally, the high lift devices (HLD's) were sized for the selected stall speed at MTOW.

6.4.1. Wing Planform Design

The first wing geometry parameter - the surface area - was calculated by dividing the MTOW with the wing loading of $4150 N/m^2$ obtained from the wing and thrust loading diagram. The required wing surface area is then 10.22 m^2. Secondly, the aspect ratio was selected. Based on statistical data, the aircraft achieving best range performance had aspect ratios above 20. As an example the RQ-4 Global Hawk had an aspect ratio of 25 and Virgin Atlantic Globalflyer achieved an aspect ratio of 32.5[2]. Nevertheless, those aircraft lack the ability to operate from shorter runways and severe crosswind conditions, which would be detrimental for CCT Arctic Tern. The commercial aircraft that have demonstrated crosswind operations at around 35 knots have aspect ratios of around 13. Therefore, to achieve a balance between range and crosswind performance an aspect ratio of 15 was selected. Next, the taper ratio was analysed. To approach the ideal elliptical lift distribution over the wing a taper ratio of 0.4 was chosen. Finally, the sweep angle at quarter chord was kept

[2]Retrieved from: https://janes.ihs.com/ [17/05/2018]

at 0, since the cruise Mach of 0.6 allows for an unswept wing, which is structurally favourable. The surface area, aspect ratio, taper ratio and sweep fully define the wing platform geometry and the results are presented in section 6.12.2.

6.4.2. Airfoil selection

It was decided to select a NACA airfoil for the aircraft since a lot of data is available for these airfoils and because they can be evaluated relatively easy with JAVAfoil. Next, it was decided to analyse the different families of airfoils in order to choose a suitable family. It was decided not to evaluate the 16-series since its main application is in propellers. 7-series and 8-series airfoil are also not analysed since they are seldom used and minimal data is available. 4-Digit, 5-Digit and 6 series airfoils are further analysed. The advantage, disadvantages and applications of these airfoil families can be found in table 6.2.

Family	Advantages	Disadvantages	Applications
4-Digit	1. Good stall characteristics 2. Small center of pressure movement across large speed range 3. Roughness has little effect	1. Low maximum lift coefficient 2. Relatively high drag 3. High pitching moment	1. General aviation 2. Horizontal tails Symmetrical: 3. Supersonic jets 4. Helicopter blades 5. Shrouds 6. Missile/rocket fins
5-Digit	1. Higher maximum lift coefficient 2. Low pitching moment 3. Roughness has little effect	1. Poor stall behavior 2. Relatively high drag	1. General aviation 2. Piston-powered bombers 3. Commuters 4. Business jets
6-Series	1. High maximum lift coefficient 2. Very low drag over a small range of operating conditions 3. Optimized for high speed	1. High drag outside of the optimum range of operating conditions 2. High pitching moment 3. Poor stall behaviour 4. Very susceptible to roughness	1. Piston-powered fighters 2. Business jets 3. Jet trainers 4. Supersonic jets

Table 6.2: Comparison of different NACA airfoil families [3]

From table 6.2 it was decided to go for a 6-series airfoil. The advantages of such an airfoil is the good performance over a small range of operating conditions. Since the aircraft will spend most of its time in cruise, this is favourable. The disadvantages of these airfoils is the poor stall behaviour, this is deemed to be acceptable.

A comparison between 8 airfoils from the NACA 6-series is presented in table 6.3. The selection was based on the desired airfoil performance characteristics and the analysis was performed with JavaFoil software that is based on the panel method. Within the NACA 6-series family, The following parameters can be controlled: maximum thickness, location of maximum thickness, design C_l number and the drag bucket size. For the CCT AT1 it was estimated that the cruise C_l will be in range from 0.37 to 0.56. Therefore, the design C_l of the considered airfoils is either 0.4 or 0.5. Moreover, the drag bucket of was 0.2 is required to stay inside the bucket throughout the cruise. For comparison, a drag bucket of 0.1 was used on one of the airfoils analysed. Thickness was limited to a maximum of 17% to stay below the drag divergence Mach number.

The main trade-off parameters were the maximum cruise C_l/C_d, $C_{l_{max}}$ and $(t/c)_{max}$. It was found that NACA 65_2416 offered the best overall performance in the aforementioned parameters and was therefore selected as the design airfoil. It has to be noted, however, that the detailed design stages might choose different airfoils along the wing span for better performance. Moreover, NASA LRN 1015 airfoil used on RQ-4 Global Hawk was found to have a very favourable characteristics, but was designed for different flying regime and would have to be modified to be applied on CCT Arctic Tern.

[3]Retrieved from; http://www.aerospaceweb.org/question/airfoils/q0041.shtml [05-04-2018]

Table 6.3: Comparison between NACA 6-series aerofoils

Aerofoil	NACA 64_2416	NACA 63_2416	NACA 64_1516	NACA 65_2416	NACA 64_2415	NACA 64_2417	NACA 65_2415	NACA 64_2415
$\mathbf{C_l/C_d}$ $[C_l = 0.46; Re = 15 \cdot 10^6]$	70	67	70	74	71	69	77	72
$\mathbf{C_{l_{max}}}$ $[Re = 5 \cdot 10^6]$	1.34	1.41	1.45	1.34	1.33	1.44	1.29	1.33
$\mathbf{M_{dd}}$ $[C_l = 0.56]$	0.613	0.604	0.611	0.621	0.618	0.606	0.627	0.618
$\mathbf{C_{m_{0.25}}}$ $[C_l = 0.46; Re = 15 \cdot 10^6]$	-0.040	-0.039	-0.044	-0.042	-0.040	-0.040	-0.042	-0.040
$\mathbf{(t/c)_{max}}$	0.16	0.16	0.16	0.16	0.15	0.17	0.15	0.15
$\mathbf{C_l}$ **drag bucket**	+/-0.2	+/-0.2	+/-0.1	+/-0.2	+/- 0.2	+/-0.2	+/-0.2	+/-0.2

6.4.3. $C_L - \alpha$ curve

The $Cl - \alpha$ curve of the airfoil needs to be corrected to obtain a $CL - \alpha$ curve which represents a three-dimensional wing. This was done using the DATCOM method [26]. First, the linear part of the cure had to be estimated. The slope reduction for the 3D wing is calculated by taking into account the aspect ratio A, Mach number and sweep $\Lambda_{0.5c}$. The empirical relation is presented in equation (6.1) with A=15, η=0.95, $\Lambda_{0.5c}$= -1.64° and $\beta = \sqrt{1 - M^2}$.

$$\frac{dC_L}{d\alpha} = \frac{2\pi A}{2 + \sqrt{4 + \left(\frac{A\beta}{\eta}\right)^2 \cdot \left(1 + \frac{\tan^2 \Lambda_{0.5c}}{\beta^2}\right)}} \tag{6.1}$$

For cruise Mach number of 0.6 the slope equals to approximately 6.37 and for landing conditions it equals to approximately 5.33. The α = -2.2° is where the Cl equals to 0. This number is the same for CL=0. Therefore, the linear part of $Cl - \alpha$ curve can now be constructed. Secondly, the CL_{max} had to be determined for landing conditions and to size the HLDs. The DATCOM method gives an estimate of $C_{L_{max\_clean}} = 1.2$ from equation (6.2)[26], where the $C_{l_{max}}$ from NACA 65_2416 is 1.343 and the $\Lambda_{0.25c}$ equals 0.

$$C_{L_{max}} = 0.9 \cdot C_{l_{max}} \cdot cos\Lambda_{0.25c} \tag{6.2}$$

6.4.4. High lift device selection and sizing

Since the regulation does not impose limits on stall speed it had to be constraint to a reasonable value. It was established that the approach speed should not be higher than the approach speed of the commercial airliners. This was deemed necessary to ensure a safe insertion into traffic and the ability to execute standard approach and departure routes. It was decided to constrain the stall speed at MTOW to 60m/s. This gives the approach speed of around 38m/s with the aircraft at landing weight.

To achieve those speeds the HLD's had to be added to the CCT Arctic Tern. Specifically, the additional aircraft lift $\Delta C_{L_{max}} = 0.67$ was required. To keep the OEW low and reliability high the design of the chosen HLD's had to be as simple as possible. Therefore, two possible options were examined: plain trailing edge flaps and single slotted trailing edge flaps. Both options produced a required affected wing surface area via equation (6.3)[26], where Λ_{hinge_line} is taken at 3/4c and results in an angle of -3.3. $\Delta C_{l_{max}}$ is the additional lift coefficient the wing cross section can deliver due to the HLD's and is dependant on their type. For plain flaps it is approximately 0.9 and for single slotted flaps it is approximately 1.3[26].

$$\frac{Swf}{S} = \frac{\Delta CL_{max}}{0.9\Delta Cl_{max} \cdot cos\Lambda_{hinge\_line}} \tag{6.3}$$

The resulting ratio $\frac{Swf}{S}$ required for plain and slotted flaps was 0.84 and 0.58, respectively[26]. The plain flap would occupy almost the entire available wingspan allowing little room for possible flap enlargements during design iterations. Therefore, the slotted flap solution was selected, spanning from 0.92m to 4.02m of the wing half span and occupying 25% of the wing chord. This produces a ratio $\frac{Swf}{S}$ of approximately 0.60 gives a slight margin over the minimum requirement of 0.58.

6.5. Preliminary Fuselage & Empennage Sizing

The fuselage and empennage sizing are closely related. As the avionics, payload subsystem and fuel is only setting the required fuselage volume but is not constraining the fuselage dimensions, the optimum diameter over length (D/L) of the fuselage has to be found. The optimum will be found by minimising the zero-lift drag of the aircraft as this parameter has a large effect on the lift over drag, which is key to the mission. The structural effects are not considered in the optimisation but the D/L is constrained to be above 0.08, as typical subsonic jet transports have their D/L in the range of 0.08 and 0.12, and therefore are still in the realm of feasibility.[90] There is expected to be an optimum as an increased fuselage length, a lower D/L, will increase the zero-lift drag of the fuselage but decrease the required tail surface area, therefore decreasing the zero-lift drag effects of the empennage.

6.5.1. Volume budget

Before the optimisation the required fuselage volume had to be determined. A volume budget was made consisting of three categories: avionics, fuel, and the payload subsystem. Furthermore, 10% of the fuselage volume is reserved for empty space and structures. The volume budget and total volume can be seen in table 6.4.

Table 6.4: Volume budget for the fuselage. Volumes are divided into three categories: Avionics, Fuel and Payload subsystem.

Section	Parts included	Volume
Avionics	Camera, Antenna, On-board flight computer, Nose landing gear & IN measurement	0.65 m^3
Fuel	Fuel tank	1.8 m^3
Payload subsystem	Tank with solution & combustion chamber	0.39 m^3
Total Volume with 10% reserve space		3.88 m^3

The avionics volume is estimated to be 0.65 m^3 by comparing to other UAVs and validating with the volume of the required avionics components as identified in chapter 8. The fuel volume is calculated by subtracting the estimated wingbox volume designated for fuel from the total fuel volume. For the estimation of the wing volume designated for fuel, a front and aft spar were chosen to be at 20% and 75%, respectively. Furthermore, 80% of the total wingbox volume is estimated to be used for fuel, taking into account the main landing gear storage inside the wing. The payload volume is estimated from the summation of the estimated tank and combustion chamber volume and the volume from the specifications of the monitoring system.

6.5.2. Fuselage length optimisation

As the required fuselage volume is estimated, the fuselage length optimisation can be performed. The optimisation trade-offs fuselage surface area and tail surface area, therefore a relation has to be set-up to calculate the tail surface area for a given fuselage length. Firstly, the horizontal and vertical tail volumes were retrieved from statistical data on business jets. Business jets were chosen as they usually have long range and small payload weights, similar to the AT1, and as there is not enough data on empennages of UAVs which are

all-weather operational. An average tail volume was then found to be 0.0729 for the vertical tail and 0.721 for the horizontal tail with a standard deviation of 0.0115 and 0.129, respectively. [90] The tail sizes can then be calculated with equation (6.4) and equation (6.5). [90]

$$S_h = \frac{S \cdot MAC}{X_h - X_{aft,cg}} \qquad (6.4) \qquad S_v = \frac{Sb}{X_v - X_{aft,cg}} \qquad (6.5)$$

S_h is the horizontal tail surface area, S_v is the vertical tail surface area, S is the wing surface area, b is the wing span, MAC is the mean aerodynamic chord length and $X_{h/v} - X_{aft,cg}$ is the tail arm. The tail arm is assumed to be 40% of the fuselage length.

The zero-lift drag is then estimated by adding the zero-lift drag of the wing, nacelle, fuselage and tail with equation (6.6). [90]

$$C_{D_0} = \frac{1}{S}\Sigma C_{D_c} A_c + C_{D_{misc}} \qquad (6.6)$$

C_{D_0} is the total zero-lift drag, C_{D_c} is the skin-friction coefficient for a specific component and $C_{D_{misc}}$ is the zero-lift drag increment for interference, roughness and excrescence. The zero-lift drag estimation does not take into account the pressure drag. This will result in an underestimation of zero-lift drag, more so for shorter fuselage lengths than for longer lengths. Therefore, the optimum fuselage length will also be underestimated. The skin-friction coefficients used for each category are displayed in table 6.5. [90]

Table 6.5: Skin-friction coefficients for different aircraft components. [90]

Aircraft component	C_{D_c}	A_c
Wing	0.0030	Wing wetted area
Fuselage	0.0024	Fuselage wetted area
Nacelles	0.0060	Wetted area of nacelles
Tailplane	0.0025	Tailplane wetted area
$C_{D_{misc}}$		Add 10% to C_{D_0}

The calculated zero-lift drag values were plotted against fuselage length and can be seen in figure 6.2.

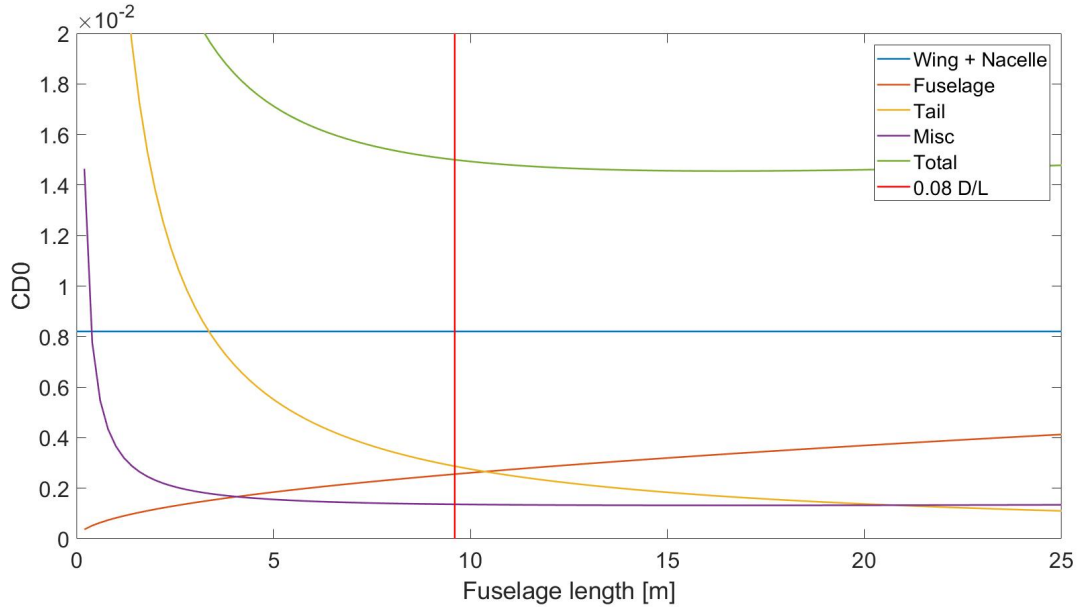

Figure 6.2: Estimated zero-lift drag of the total aircraft and components for different fuselage lengths. The red vertical line marks the diameter over length ratio of 0.08 which constraints the region of structural feasibility.

In the figure it can be seen that the fuselage length corresponding to the least amount of zero-lift drag is far beyond the maximum fuselage length of 9.55 meters, corresponding to the minimum D/L of 0.08. Therefore, it was first chosen to have a 9.55 meter fuselage with a diameter of 0.76 meter.

After having drawn out the fuselage with these preliminary values it was noticed that the slenderness might give problems for the structure. The CCT Arctic Tern will have a relatively large empennage due to the high crosswind requirement and due to the nature of V-tails opposing the rolling moment during a coordinated turn which might give rise to problems for the torsional loads on the fuselage. Therefore, it was decided to use a more reserved D/L of 0.1, which corresponds to the middle of the range of D/L reference subsonic jet airliners have. [90] The increase of optimum cruising L/D for a D/L of 0.1 compared to the lower D/L of 0.08 is estimated to be 1%, which is acceptable.

The nose is chosen to have a fineness ratio of 0.5 as this is the recommended value for 0.6-0.65 Mach cruising aircraft. [90] The tail cone is chosen to have a length of 2.5 times the diameter, as this is the optimum value for minimal zero-lift drag. [90] The tail cone first housed the total payload subsystem but after analysing the longitudinal stability the payload tank was moved to the centre of the fuselage, as described in section 6.10. Out of the payload subsystem, only the combustion chamber is positioned in the tail cone, as described in section 5.5.3. The tail cone has more volume than the required payload subsystem volume and therefore a part of the fuel is stored in the tail cone as well. The avionics and fuel sections will be positioned at the front and in the middle of the fuselage, respectively. The fuel is chosen to be stored in the middle of the fuselage as the emptying of the fuel tank should have minimal effects on the centre of gravity.

The verification and validation of this optimisation is presented in section 13.4

6.5.3. V-tail sizing

The horizontal stabiliser surface area is estimated to be 5.02 m^2 and the vertical stabiliser surface area is estimated to be 7.18 m^2. As the CCT Arctic Tern has a V-tail, the total tail surface with equal stability parameters can be computed by adding the horizontal and vertical tail surfaces together. [72] Furthermore, the angle of the V-tail can be computed with equation (6.7). [72]

$$S_h = S_{vtail}\ cos^2(\mathrm{T}) \tag{6.7}$$

S_{vtail} is the total V-tail surface area and T is the angle of the V-tail with respect to the horizon when the pitch is zero. The angle is computed to be 50.1°.

6.5.4. Preliminary fuselage & empennage dimensions

The aspect ratio, taper ratio and sweep angle of the empennage were chosen from reference aircraft and consecutively the empennage was sized. [90] The final fuselage and empennage dimensions are summarised in section 6.12.2.

6.6. Drag Estimation

With the preliminary outer dimensions of the aircraft and some aerodynamic characteristics it was possible to obtain a drag polar, which is presented in equation (6.8). Aircraft drag is composed of two main components: the zero-lift drag C_{D_0} and the induced drag which is dependant on the square of the wing lift coefficient and a factor K.

$$C_D = C_{D_0} + K \cdot C_L^2 \tag{6.8}$$

The C_{D_0} was already estimated in section 6.5.2. However, now that the outer dimensions of the aircraft are

known a better drag estimate can be obtained. C_{D_0} itself is a sum of the drag introduced by different aircraft components. In the case of AT1 those are the fuselage, the wing, the empennage, the nacelle and the engine pylon. Each of those components can introduce drag in 3 different ways. The skin friction drag C_f is the most prominent one. The other two are the form factor FF and the interference factor IF. All of those factors are multiplied together. Moreover, they are multiplied by the wetted area of the specific component and divided by the reference wing area S_{ref} to obtain a dimensionless drag coefficient. The drag of different components is simply added together. The table of contributions from individual components is presented in table 6.6. Finally, the miscellaneous drag is added to the estimate. In the case of CCT Arctic Tern it accounts for excrescence and leakage (factor of 1.05) giving the total final C_{D_0} estimate of 0.0135. The full drag estimation relation is presented in equation (6.9)[25].

$$C_{D_0} = \frac{1}{S_{ref}} \sum_c C_{f_c} \times FF_c \times IF_c \times S_{wet_c} + C_{D_{misc}} \tag{6.9}$$

Table 6.6: Zero-lift drag by main aircraft components

Component	$C_{D_0}[\cdot 10^{-3}]$
Wing	4.849
Fuselage	4.409
V-tail	1.980
Nacelle	0.568
Pylon	0.259
Sum	12.065
Miscellaneous $[1.04 \cdot C_{D_0}]$	12.548
Contingency $[1.10 \cdot C_{D_0}]$	13.803

The factor K is computed as per equation (6.10) with Oswald efficiency factor e as defined in equation (6.11)[25]. The factor K is then approximately 0.0334.

$$K = \frac{1}{\pi A e}, \tag{6.10}$$

$$e = 1.78(1 - 0.45A^{0.68}) - 0.64 = 0.635 \tag{6.11}$$

6.7. Landing Gear Positioning and Sizing

The landing gear ensures that the aircraft can take-off and land without damage. There are many different options for the landing gear depending on the surface it will use as a base. Skis, skids or floats for example can be used for surfaces such as snow, water and other soft surfaces. For hard surfaces wheels are commonly used. The design of the undercarriage takes into account the balance, stability and control of the aircraft [88].

First, a Class I weight estimation is done to determine the wing position and the centre of gravity range. With this, an approximation of the loads on the front and main landing gear was determined. The undercarriage needs to be capable of handling the taxi and landing loads and transmitting part of them to the fuselage. Furthermore, it should also provide the ability for ground manoeuvring, braking, aeroplane towing and protecting the landing surface.

Second, the number of wheels and struts are determined. This is done using the maximum take-off weight. It is rounded up to the nearest number of 2, for the main landing gear two wheels are sufficient and for the nose gear there will be one wheel.

The position of the nose landing gear is determined using static equilibrium which results in equation (6.12), where P_m is the load on the main landing gear, P_n is the load on the nose landing gear, X_{cg} is the distance from the nose to the approximated location of the centre of gravity, and X_w is the approximated distance from the nose to the main landing gear attachment point in the wing.

$$X_n = -2 \cdot \frac{P_m}{P_n}(X_w - X_{cg}) + X_{cg} \quad (6.12)$$

$$Y_{MLG} > \frac{l_n + l_m}{\sqrt{\frac{l_n^2 \cdot tan(\psi)^2}{z^2} - 1}} \quad (6.13)$$

The nose landing gear should have a minimum of 8% of the maximum take-off weight to enable steering and braking capabilities. [77] Taking 20% nose landing gear load and a 80% main landing gear load based on their respective arms to the aircraft centre of gravity, the static loads per tire/strut are determined using the aircraft's MTOW to allow for landing even when at maximum take-off weight. Wider tires with a lower tire pressure allow for better landing on runways with a low surface hardness. Even though the majority of take-offs and landings of the CCT Arctic Tern are planned to take place on a paved runway, the aircraft is equipped with similar tires as aircraft in the same weight range that are able to land on unpaved airfields to allow for versatile landing options in case of emergencies without causing further structural damage due to tire blowout.

After the selection of the tire is done, the strut length has to be determined, the strut length includes the length needed for the landing gear shock absorber. The strut length has to be determined considered the following constraints: overturn angle, the geometric constraint for landing gear stowage after retraction, the tip-back constraint and the scrape angle constraint. The tire deflection on impact and shock absorber stroke have to be considered to ensure the constraints are met as well on landing impact. The tire deflection is taken from The Goodyear Tire and Rubber Company [85]. The shock absorber stroke for the nose and main landing gear was determined using methods from Roskam [77]. The design of the landing gear was performed in parallel with the design of the aircraft, the approach taken was to first determine the landing gear geometry based on the class I weight estimation, linking any known dependent parameters in the parameter sheet to the parameters in the landing gear design and check the design for compliance after the design freeze.

The overturn angle (ψ) as defined in equation (6.13) [77] must be at least 55° to ensure that the aircraft does not tip over in the lateral direction when performing manoeuvres on ground.

The tip-back angle is defined as the angle between the line running from the mid of the main landing gear at a right angle with the ground and the line running from the main landing gear ground contact point to the most aft CG position, this angle has to be at least 15° to avoid the aircraft tipping back, the aircraft is determined with uncompressed shock absorbers.

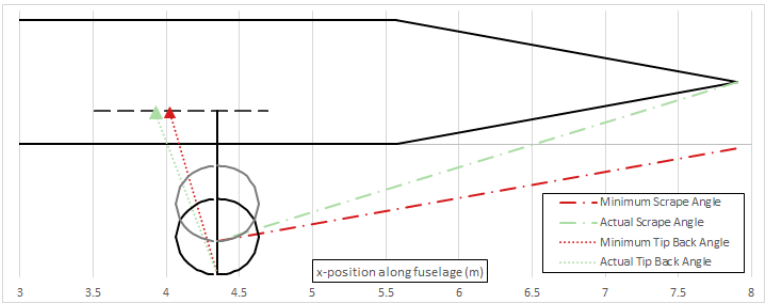

Figure 6.3: Check of tip-back and scrape angle of landing gear design

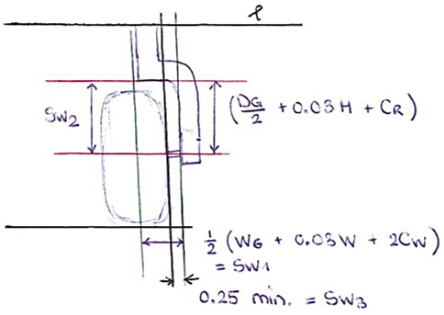

Figure 6.4: Landing Gear Tire Clearance

The positioning and length of the landing gear and struts design of the tail section of the fuselage have to be done such that the aft part of the fuselage does not scrape the ground on take-off. The scrape angle as defined in figure 6.3 should be bigger than the tip-back angle and at least 15°. [77] The strut lengths of the main and nose landing gear need to be designed such that both these angles meet their requirements.

Since the fuselage diameter is determined to be 0.935m, the landing gear will only fit partly into the fuselage, but the tires will not fit into the wing as the wing $\frac{t}{c}$ is too small at all values for c. The length of the landing gear struts are determined taking into account all the constraints mentioned above.

The maintenance of the landing gear is important to investigate as it contains moving parts and is exposed to a dirty environment. Due to the high stresses and pressure the maintenance of the landing gear should be a continuous process. During maintenance the landing gear should be cleaned to ensure that no irregu-

Table 6.7: Landing Gear Design Parameters

Part	Parameter	Value	Unit
Main LG	Load	1729.62	kg
Main LG	Tire	9.00-6	-
Main LG	Tire Maximum Inflation Pressure	58	psi
Main LG	Shock Absorber Stroke	0.246	m
Main LG	Strut Length	0.96	m
Nose LG	Load	864.21	N
Nose LG	Tire	7.00-6	-
Nose LG	Tire Maximum Inflation Pressure	38	psi
Nose LG	Shock Absorber Stroke	0.135	m
Nose LG	Strut Length	0.98	m

larities remain undetected. Also, the trunnion, shock struts, brace assemblies and bearings, wheels, shimmy dampers, wheel bearings, brakes and tires should be inspected. [4].

6.8. Engine Selection

The four main engines used in aircraft, turbojet, turbofan, turboprop, and propeller, were all considered when deciding which type of engine will be most appropriate. Turbojet and propeller were discarded for their low efficiency at the AT1 cruise mach. Between turbofans and turboprops, turbofans were chosen for their better efficiency at the seeding altitudes near the tropopause. Furthermore, the turbofans are less sensitive to a change in altitude requirements which can occur when the seeding region expands to lower latitudes. There are three inputs in selecting the engine: the type, the number of engines on the aircraft, and the thrust required, derived from the thrust-to-weight ratio. This resulted in one turbofan engine, which must provide 1.733 kN of thrust at the cruise altitude of 10km. This is on the smaller side of the turbofan aircraft engines, so engines used on small business jets are considered. The chosen engine is the GE Honda HF120, used on the HondaJet. The rest of this section will evaluate the chosen engine on its most important parameters: thrust, mass, size, reliability, and efficiency.

Most importantly, the engines must provide enough thrust that the requirements are met. The thrust produced by a turbofan engine decreases with altitude, due to the density of air decreasing. While the exact relationship between maximum thrust provided and altitude are different for each engine, a general relationship can be found using equation (6.14) [5]. Using this relationship, the required maximum thrust provided by the turbofan engine at sea level must be approximately 5.8 kN, which the HF120 far exceeds with a maximum sea level thrust of 9.1 kN. Reliability can be evaluated by looking at the time between overhaul (TBO), which indicates the allowable amount of flight hours before the engine should be removed from the aircraft, taken apart, cleaned, inspected, and repaired if necessary. While this does not directly relate to reliability, this indicates the ability of the engine to perform without failure. The manufacturers of the HF120 recommend a TBO of 5000 hours, which leans on the more reliable side of the spectrum of turbofan engines. Lastly, the efficiency can be evaluated from the specific fuel consumption (SFC). Since the SFC is one of the most important parameters in turbofan engines, the engine manufacturers are reluctant to release this information, however, Honda have said that the SFC at cruise is less than 0.7 $\frac{lb}{lbf \cdot hr}$. We have assumed this to be approximately 0.68 $\frac{lb}{lbf \cdot hr}$ [41]. The SFC varies with altitude, so to estimate the SFC at lower altitudes a rough statistical relationship between SFC at sea level versus cruise altitude was taken. This relationship was taken to be $SFC_{cruise} = 1.5 \cdot SFC_{SL}$.

$$Thrust = Thrust_0 \cdot \frac{p}{p_0} \cdot \sqrt{\frac{T_0}{T}} \tag{6.14}$$

[4] Retrieved from: https://www.faa.gov/regulations_policies/handbooks_manuals/aircraft/amt_airframe_handbook/media/ama_Ch13.pdf [15/06/2018]

[5] Retrieved from: https://www.grc.nasa.gov/www/k-12/Missions/Jim/Project1ans.htm [26-06-2018]

Table 6.8: Engine Specification

Engine	**GE Honda HF120**
Max. sea level thrust	9100 N
Time between overhaul	5000 hr
Dry mass	211.3 kg
Length	1.1 m
Diameter	0.54 m
Specific fuel consumption at cruise	~0.68 $\frac{lb}{lbf \cdot hr}$
Accessory power extraction	18 kW (24.2 hp)

6.9. Class II Weight Estimation

Accurate estimations of the aircraft subsystems is of the utmost importance in aircraft design. If the mass of a subsystem or part increases throughout the design process, the snowball effect comes into play and results in a disproportionately large increase in operation empty weight. This can be mitigated by carrying out accurate class II weight estimations, which will be elaborated in this subsection. The estimation procedure stems from statistical data on existing aircraft that has been collected and the relationships between the most basic aircraft parameters and subsystem masses being quantified. This enables mass estimates of the subsystem within the Arctic Tern aircraft from parameters such as max take-off weight, wing area, and aspect ratio.

First the V-N diagram for the aircraft was created. Next, the chosen method to perform the weight estimation is described and the calculations are carried out. Finally, the OEW iteration process is described.

6.9.1. V-N Diagram

The first step in class two weight estimation is creating a V-N diagram applicable to CCT Arctic Tern. With this diagram the maximum load factor, n_{max}, on the aircraft can be determined. In this V-N Diagram, two cases will be evaluated: the load factor during manoeuvres and during gusts. The gusts will also be evaluated for empty-wing loading case, as this is usually critical. Even though the aircraft will probably not have to adhere to certain regulations, the maximum load factors presented in CS25 are taken as a reference. The maximum manoeuvring load factor is assumed to be 2.1. The maximum gust velocities were assumed to be 55 f/s for high angles of attack, 43 f/s for cruise conditions and 20 f/s for dive conditions. The V-N Diagram is presented in figure 6.5

From this diagram the maximum negative en positive load factor can be determined. The maximum positive load factor is 2.6, the maximum negative load factor is -1. With a safety factor of 1.5, the maximum loads to design for are 3.9 and -1.5.

6.9.2. Class II Weight Estimation Method

The next step in the weight estimation procedure was selecting one of the available methods. Raymer's method outlined in 'Aircraft Design: A Conceptual Approach' by Raymer [74] was eventually selected, as it utilised more parameters than the other two options, Roskam and Torenbeek, so it is assumed to be more accurate. Within Raymer's method, there are three sets of equations to use corresponding to three types of aircraft: fighter/attack aircraft, cargo/transport aircraft, and general aviation aircraft. Of these, the most applicable for the ACT system is the general aviation category. The results were verified by obtaining an OEW estimation using relations for the cargo/transport aircraft, which gave a 2.2% higher OEW estimate.

The equations for the class II weight estimations were then put into an excel file where one could change the inputs and be left with the subsystem weights. After verifying and validating the programme, which is explained in detail in section 13.3, the programme can be used. Below, in table 6.9, the results of class II weight estimation are shown.

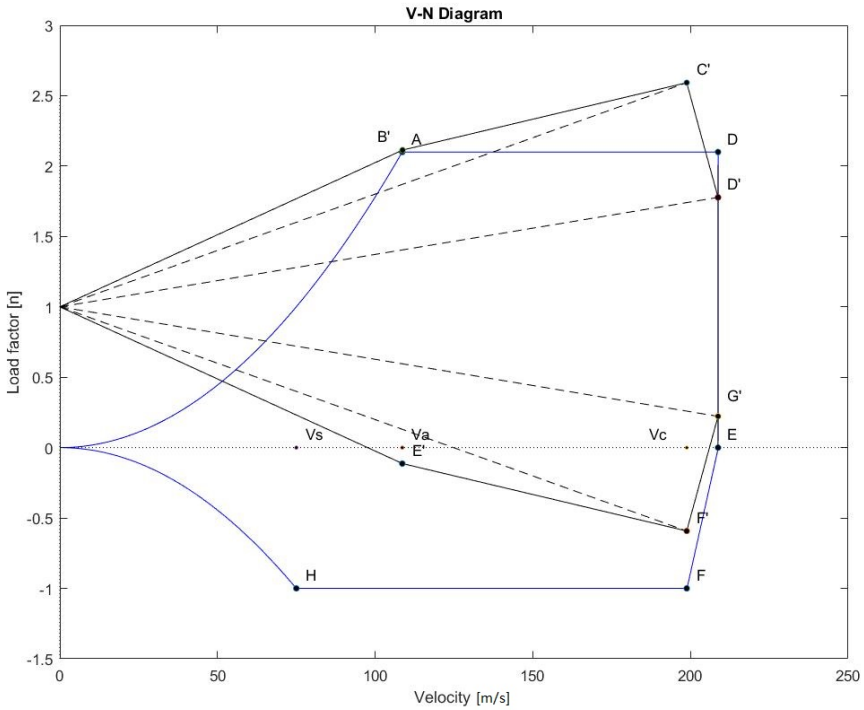

Figure 6.5: V-N Diagram

Table 6.9: Results of class II weight estimation

Output parameters	Mass [kg]	% of MTOW	Output parameters	Mass [kg]	% of MTOW
Main wing	224.7	16.2	Horizontal tail	11.5	0.83
Vertical tail	18.3	1.3	Fuselage	143.3	10.4
Main landing gear	62.6	4.6	Nose landing gear	5.2	0.38
Installed engine	336.9	24.4	Fuel system	72.3	5.2
Flight controls	402.5	29.1	Hyrdraulics	4.3	0.31
Electrical	84.5	6.1	Avionics	17.2	1.2

• Class I Cost Estimation & Optimisation • Class I Weight Estimation	• OEW • Fuel Weight • MTOW	• OEW
• L/D • SFC • Cruise speed	• Engine selection • Fuselage Sizing • Wing Sizing & Aerofoil Selection & Preliminary Positioning • Preliminary tail sizing & positioning	• 3D views • Ultimate load
• OEW		• Class II weight estimation • c.g. determination

Figure 6.6: Section of the N2 chart that encompasses the Class I and II weight estimation iteration.

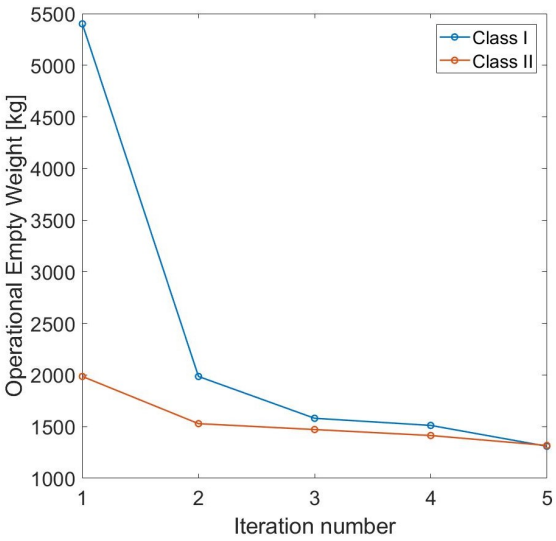

Figure 6.7: Operational Empty Weight estimation with Class I and Class II weight estimation plotted for each iteration.

6.9.3. Operational Empty Weight Iteration

The OEW estimated with the Class II weight estimation has a significant different value than the OEW of the Class I weight estimation. These two weight estimations have to be iterated to converge to a single estimate of the OEW. The N2 chart section of this iteration is displayed in figure 6.6. As can be seen in the N2 chart, during the OEW iteration, iterations for L/D, SFC and cruise speed were integrated as well. It was decided to iterate the OEW until the two class estimations differed less than 1%.

For every iteration the new wing area and thrust were determined for the new mass estimation, using the same thrust and wing loading. Thereafter, the planform, fuselage, empennage, and control surfaces were sized with the methods as described before and a new engine was selected if relevant. If the new estimated L/D, SFC and/or cruise speed was increased or decreased more than 1%, it was iterated in the Class I weight estimation again until this difference converged to a less than 1% difference. Consecutively, the OEW was iterated until the OEW converged to less than 1% of a difference as well. The OEW converged within 5 iterations to an OEW of 1411 kg. The class I and class II OEW estimates for every iteration are displayed in figure 6.7.

In the figure, it can be seen that the first Class I OEW estimate was highly overestimated but quickly converged to the final OEW. The initial overestimation of the OEW can be explained by the overestimated statistical OEW/MTOW used for the first Class I weight estimation. The OEW/MTOW was determined from reference aircraft with most of them having smaller range and most of them having a cockpit, furniture, and a pressurised fuselage, which all contribute to a higher OEW/MTOW compared to the CCT Arctic Tern. The Class II weight estimation takes into account the higher L/D, the lack of cockpit and furniture and corrected for this overestimation of the OEW in the first iteration. With the iterated OEW and aircraft subsystem weights, the empennage sizing and landing gear positioning could be further developed.

6.10. Loading Diagram

Since the aircraft has a low OEW and MTOW, and a depleting payload weight during operations, it is very susceptible to centre of gravity shifts during loading and in-air operations. To prevent it from being loaded incorrectly in which case it might tip over or have too much weight on the front landing gear and to prevent instability and uncontrollability during flight, a loading diagram has been made. First the x_{cg} of the OEW is determined in section 6.9.3 and was found to be 1411kg with a c.g. location at 4.120 m from the nose of the aircraft.

In case of emergency the aircraft will stop seeding and will return to the airbase. In this case the most extreme option of a full payload tank with total empty fuel tanks might occur. To prevent that the aircraft will become very hard to control or even become uncontrollable it was chosen to put the payload compartment above the main landing gear to be as close as possible to the x_{cg} of the OEW. The total weight of the payload is equal to 296kg and the c.g. location will shift with the wing as the main landing gear is placed below the main wing.

The fuel has been placed into different compartments placed at various locations through out the aircraft. The tanks in the fuselage of the aircraft have a volume that is equal to the fuselage cross section times their total length minus 10% to accommodate for cabling and structures. In table 6.10 an overview of the fuel tanks and their total volume, weight, and location can be found. The location of the wing is not included in this table since it will shift with the placing of the wing and is thus part of the iteration.

Table 6.10: Fuel tanks

	Location x_{cg} (m)	Length (m)	Volume (L)	Weight (kg)
Forward fuel tank	2.460	2.682	1674.2	1346.0
Aft fuel tank	5.128	0.881	550.1	442.3
Tailcone fuel tank	6.166	1.380	452.9	364.2
Wing			618.4	497.2

With this data a maximum loading diagram of the aircraft can be made. This is given in figure 6.8.

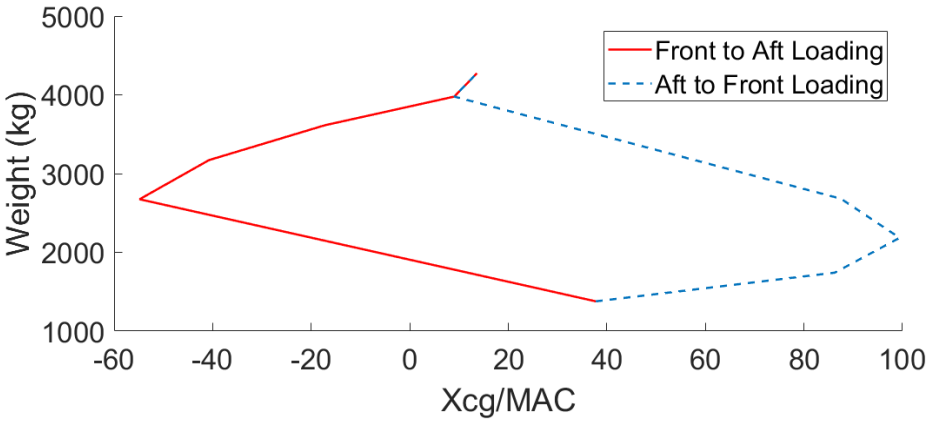

Figure 6.8: Loading diagram c.g. range

From the loading diagram it can be seen that a huge centre of gravity range would be required to fulfil the maximum and minimum loading cases. Therefore, the decision was made to distribute the fuel over all the tanks in the aircraft during every phase of the flight such that the optimum c.g. is obtained. Doing this results in the most aft loading case of the $x_{cg_{OEW}}$ and the most forward case of $x_{cg_{MTOW}}$. Since the centre of gravity of the payload is the same as $x_{cg_{OEW}}$ it barely influences the aircraft c.g. When the c.g. range is plotted against different possible locations of the main wing this results in the graph found in figure 6.9. This data is used in section 6.11.1 to determine the final wing location.

Since not every loading strategy is possible a special strategy is designed to load the aircraft. Deviating from this strategy results in the risk of the aircraft tipping over resulting in unnecessary damages and maintenance. From section 6.7 it results that the loading on the front landing gear is 20% of MTOW, thus equalling 865kg. A simple static calculation on the front to aft loading strategy shows that for the maximum case of -57.3% x_{cg}/MAC at a weight of 2674kg results in a load on the front landing gear of 738kg. This thus means that the front to aft loading strategy is always possible. The aft to front loading strategy is not possible since the maximum loading case at 96.4% x_{cg}/MAC exceeds the location of the main landing gear and thus tipping over the aircraft. To make sure that this could never go wrong the fuel inlet was placed in the front of the aircraft as can be seen in section 6.14 resulting in a correct loading. The payload is always loaded after the fuel.

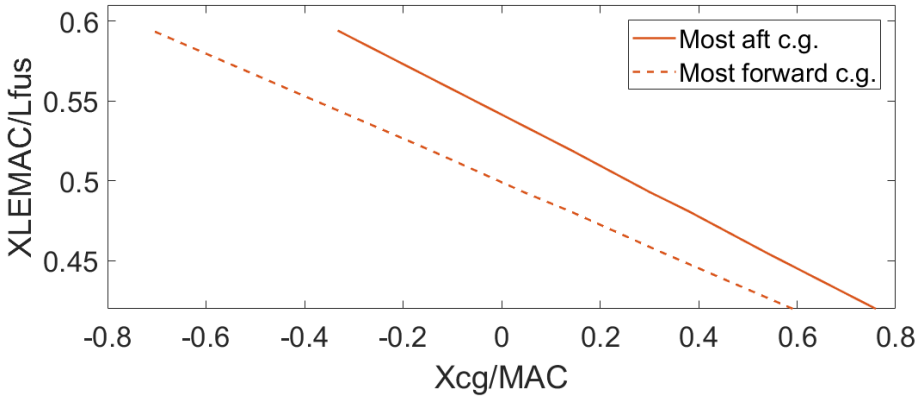

Figure 6.9: Loading Diagram

6.11. Sizing for Stability and Control

Although the tail surfaces were already sized based on statistical data it is important to evaluate the stability and stabiliser surfaces based on the actual design parameters of the CCT Arctic Tern. Moreover, the control surfaces are sized in this section. Because of the limited resources the mixed rudder/elevator control surfaces on the V-tail are analysed only for the yaw requirement, since it was concluded that this would be more constraining than the elevator size due to the high cross-wind requirement. Also, the lateral stability is not addressed here, however, it is addressed in chapter 7 with XFLR5 analysis.

6.11.1. Longitudinal Stability, Wing Positioning and Pitch Control

The scissor plot including both the longitudinal stability and control constraints, is created. After that, the wing position is adjusted to match the scissor plot with the c.g. range and minimise the required horizontal tail size.

First, the stability is evaluated. The centre of gravity, x_{cg}, of the aircraft must at all times be in front of the neutral point of the aircraft to grant longitudinal stability of the aircraft.[46] In this case if the angle of attack increases, the change in lift from the resulting lift will create a nose-down moment which will result in a decrease of the angle of attack and therefore levelling out the aircraft again, making it stable. This implies that C_{m_α} must also be negative. This gives equation (6.15) for the change of lift around the neutral point, with ΔL_{A-h} as per equation (6.16) and ΔL_h as per equation (6.17).

$$\Delta L_{A-h}(\bar{x}_{np} - \bar{x}_{ac}) - \Delta L_h(\bar{x}_h - \bar{x}_{np}) = 0 \tag{6.15}$$

$$\Delta L_{A-h} = C_{L_{\alpha_{A-h}}} \Delta\alpha \frac{1}{2}\rho V^2 S \tag{6.16}$$

$$\Delta L_h = C_{L_{\alpha_h}} (\Delta\alpha - \Delta\epsilon) \frac{1}{2}\rho V_h^2 S_h \tag{6.17}$$

Rewriting and adding a safety margin this gives the stability formula.

$$\bar{x}_{cg} = \bar{x}_{np} - SM = \bar{x}_{ac} + \frac{C_{L_{\alpha_h}}}{C_{L_{\alpha_{A-h}}}} \left(1 - \frac{d\epsilon}{d\alpha}\right) \frac{S_h l_h}{S\bar{c}} \left(\frac{V_h}{V}\right)^2 - SM \tag{6.18}$$

Secondly, the controllability of the aircraft was assessed. The trim condition is the equilibrium condition of the aircraft, which means that all moments equal zero. This results in the following formula.

$$C_m = C_{m_{ac}} + C_{L_{\alpha_{A-h}}} \frac{x_{cg} - xac}{\bar{c}} - \frac{C_{L_h} S_h l_h}{S\bar{c}} \left(\frac{V_h}{V}\right)^2 \tag{6.19}$$

During the flight there must be a combination of wing-fuselage and tail lift for the configuration of the aircraft that results in a total moment coefficient of zero ($C_m = 0$). If this is the case the aircraft is trimmed and the following formula holds.

$$C_{m_{ac}} + C_{L_{\alpha_{A-h}}} \frac{x_{cg} - xac}{\bar{c}} = \frac{C_{L_h} S_h l_h}{S\bar{c}} \left(\frac{V_h}{V}\right)^2 \tag{6.20}$$

Rewriting equation (6.18) and equation (6.20) to a function of x_{cg} with S_h/S as outcome this results in equation (6.21) and equation (6.22) respectively. The safety margin in the stability formula was set on 5%.

$$\frac{S_h}{S} = \frac{1}{\frac{C_{L_{\alpha_h}}}{C_{L_{A-h}}}\left(1 - \frac{d\epsilon}{d\alpha}\right)\frac{l_h}{\bar{c}}\left(\frac{V_h}{V}\right)^2}\bar{x}_{cg} - \frac{\bar{x}_{ac} - 0.05}{\frac{C_{L_{\alpha_h}}}{C_{L_{\alpha_{A-h}}}}\left(1 - \frac{d\epsilon}{d\alpha}\right)\frac{l_h}{\bar{c}}\left(\frac{V_h}{V}\right)^2} \tag{6.21}$$

$$\frac{S_h}{S} = \frac{1}{\frac{C_{L_h}}{C_{L_{A-h}}}\frac{l_h}{\bar{c}}\left(\frac{V_h}{V}\right)^2}\bar{x}_{cg} + \frac{\frac{C_{m_{ac}}}{C_{L_{A-h}}} - \bar{x}_{ac}}{\frac{C_{L_h}}{C_{L_{A-h}}}\frac{l_h}{\bar{c}}\left(\frac{V_h}{V}\right)^2} \tag{6.22}$$

Plotting equation (6.21) and equation (6.22) gives a scissor plot. Combining it with the loading diagram from figure 6.9 results a graph, presented in figure 6.10.

From the graph the most optimum centre of gravity range can be seen. This range is found to be between 0.132 and 0.378 x_{cg}/MAC with a S_h/S of 0.161 and the location of the wing at 0.481 x_{LEMAC}/l_{fus}. The x_{LEMAC} is then 3.8 m from the nose of the AT1.

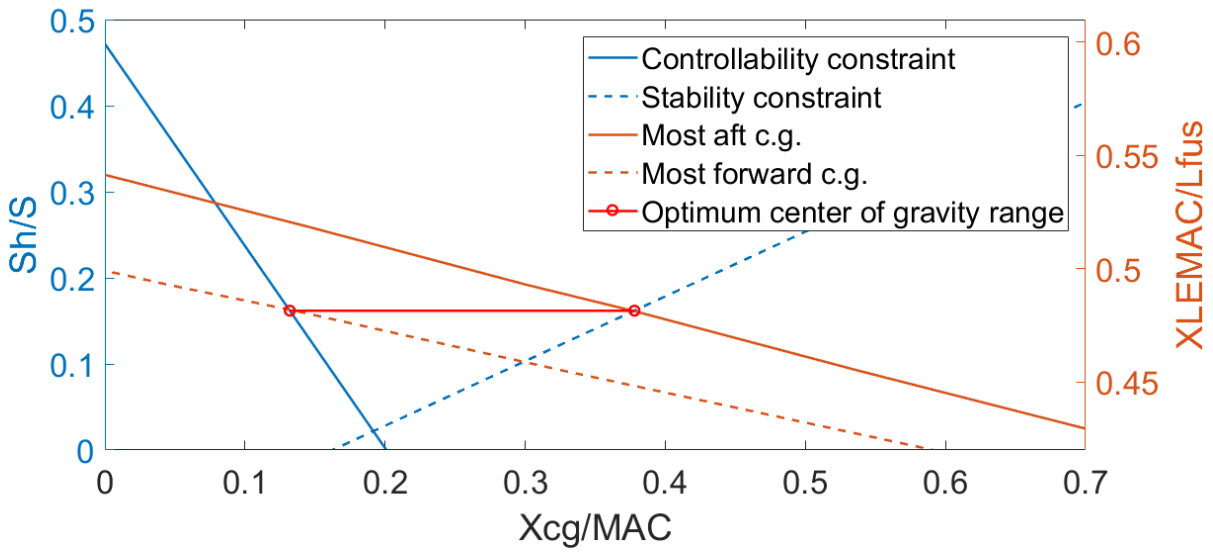

Figure 6.10: Stability & Control and c.g. plot

6.11.2. Roll Control

The ailerons were sized based the requirement for Class II aircraft which applies to light and medium transport aircraft [24]. Therefore, the required constant roll rate for CCT Arctic Tern is 45 degrees in 1.4s. The ailerons were first sized from statistics and later adjusted to meet the requirement. The maximum aileron deflection δ_a selected was 20° upwards and 15° downwards. The difference in aileron deflections was imposed to fight

the adverse yaw. The average deflection δ_a is 17.5°. The final position of the ailerons is from 70% to 97% of the span and the area of 0.328m^2 per wing giving a steady roll rate at approach speed of 32.5°/s.

The steady roll rate is obtained by equation (6.23)[24].

$$P = -\frac{C_{l_{\delta a}}}{C_{l_p}}\delta a\left(\frac{2V}{b}\right) \qquad (6.23) \qquad C_{l_{\delta a}} = \frac{2C_{l_\alpha}\tau}{S_{ref}b}\int_{b_1}^{b_2} c(y)ydy \qquad (6.24)$$

The stability derivatives $C_{l_{\delta a}}$ and C_{l_p} are calculated with equation (6.24) and equation (6.25), respectively.

C_{l_α} for the selected airfoil is 5.3285, obtained by JavaFoil analysis. It was assumed that the aileron spans 25% of the chord, which gave a τ of 0.48, according to Sadraey [78]. The wing chord as a function of the span-wise position is $c(y) = c_{root}\left(1 - \lambda\frac{y}{b}\right)$. With those inputs the $C_{l_{\delta a}}$ is 0.273 for an approach speed of 37.4 m/s.

$$C_{l_p} = -\frac{4(C_{l_\alpha} + C_{d_0})}{S_{ref}b^2}\int_0^{b/2} y^2 c(y)dy \qquad (6.25)$$

The value of c_{d_0} for the airfoil is approximately 0.005, according to JavaFoil analysis. Other inputs stay the same as in the $C_{l_{\delta a}}$ calculation. The C_{l_p} is then approximately -0.889.

6.11.3. Directional Stability and Yaw Control

The weathercock stability requires C_{n_β} to be larger than zero. [67] The main contributions to this derivative are the fuselage, the wing and the vertical stabiliser. The sum of these determines the stability of the aircraft, as displayed in equation (6.26). [67] For a circular fuselage the contribution is obtained as per equation (6.27). The contribution of an un-swept wing is computed as given in equation (6.28).

$$C_{n_\beta} = C_{n_{\beta_{VT}}} + C_{n_{\beta_{fuselage}}} + C_{n_{\beta_{wing}}} \qquad (6.26) \qquad C_{n_{\beta_{fuselage}}} = -1.3\frac{V_{fuselage}}{S_{ref}b} \qquad (6.27)$$

$$C_{n_{\beta_{wing}}} = C_L^2\left[\frac{1}{4\pi A} - \frac{1}{\pi A(A+4)}\left(1 - \frac{A}{2} - \frac{A^2}{8} + \frac{6y_{MAC}}{A\bar{c}}\right)\right] \text{[67]} \qquad (6.28)$$

The C_L of 1.8 used was taken from landing with MTOW, since it proved the most constraining. The parameter y_{MAC} is the span-wise position of MAC. The tail contribution, according to Nicolai [67], is calculated as perequation (6.29) with $\overline{V}_{VT}$ as defined in equation (6.30).

$$C_{n_{\beta_v}} = \overline{V}_{VT}C_{L_{\alpha_v}}\left(1 + \frac{d\sigma}{d\beta}\right)\left(\frac{V_{VT}}{V}\right)^2, \quad (6.29) \qquad \overline{V}_{VT} = \frac{l_V S_v}{bS_{ref}} \qquad (6.30)$$

$C_{L_{\alpha_v}}$ is estimated with the DATCOM method described in Elham [26]. The aspect ratio of the vertical tail is 1.5, but the presence of the fuselage makes the apparent aspect ratio increase by a factor of 1.55[67]. Furthermore, the η is assumed to be 0.95[26], β is approximately 1 during landing and $\Lambda_{VT_{0.5c}}$ is 30°.

$$C_{L_{\alpha_{VT}}} = \frac{2\pi A_v}{2 + \sqrt{4 + \left(\frac{A_{VT}\beta}{\eta}\right)^2 \cdot \left(1 + \frac{\tan^2 \Lambda_{VT_{0.5c}}}{\beta^2}\right)}} \qquad (6.31)$$

The side-wash factor $\left(1 + \frac{d\sigma}{d\beta}\right)$ is very hard to estimate. Nevertheless, the CCT Arctic Tern features a very

high aspect ratio wing which is a feature that drastically decreases the side-wash according to Phillips [70]. Therefore, the side-wash was neglected for this estimation. The $\left(\frac{V_{VT}}{V}\right)$ ratio used for the calculation was 0.85. This value was taken from the ratio for the fuselage mounted horizontal tail sizing.[69]

Having determining the values for the individual contributions, the weathercock stability C_{n_β} could be determined as stated below.

$$C_{n_\beta} = C_{n_{\beta_{VT}}} + C_{n_{\beta-fuselage}} + C_{n_{\beta_{wing}}} = 0.0969 - 0.0609 + 0.0168 = 0.0529 \tag{6.32}$$

The obtained value is positive, therefore, the aircraft is directionally stable.

To ensure safe decrab manoeuvres before touch-down it had to be confirmed that a sufficiently effective rudder can be incorporated in the design. The aircraft was designed to handle cross-winds of up to 20m/s and a landing speed of 35 m/s. This gives a side-slip angle $\beta = 30°$. To be able to handle such decrab manoeuvre equation (6.33) has to be satisfied. [67]

$$C_{n_\beta}\beta \leq C_{n_{\delta r}}\delta r \tag{6.33}$$

$$C_{n_{\delta r}} = 0.9 C_{L_{\alpha_{VT}}} \overline{V}_{VT} \tau \tag{6.34}$$

The $C_{n_\beta}\beta$ that CCT Arctic Tern is designed for equals 0.0277. The $C_{n_{\delta r}}\delta r$ has to equal or exceed this number. The maximum rudder deflection is taken from statistics. According to Sadraey [78] the average rudder deflection is $+/-30°$. However, it has to be noted that the presence of the combined elevator and rudder control surface, called the ruddervator, inflicts some special design considerations. One of them is the fact that the ruddervator deflection contribution to yaw control is only the sine of the V-tail dihedral angle (Γ) [72]. Because the deflection of the control surfaces cannot be further increased to compensate for that, the required ruddervator surface is increased with a factor of $1/sin(\Gamma)$. The $C_{n_{\delta r}}$ is obtained using equation (6.34) [67].

The only parameter that could be altered to meet the design goal was the rudder effectiveness which is a function of the rudder-to-vertical-fin area ratio. The required ratio was 0.28 which results in a τ of 0.47[67]. Therefore, the $C_{n_{\delta r}}$ of CCT Arctic Tern was determined to be approximately 0.053. The $C_{n_{\delta r}}\delta r$ obtained is then 0.0277, which satisfies the requirement. The required rudder surface would then be 0.659 m^2. Therefore, the total ruddervator area is 0.859 m^2.

6.12. Final Aircraft Wing, Fuselage & Empennage Sizing

After having generated the loading diagrams and scissor plots, new wing & landing gear positions and new landing gear & empennage sizes have been determined. Consecutively, the new positions and dimensions call for a new iteration in the aircraft design process. In section 6.12.1, the effects of the alterations of the empennage and landing gear on the design of the aircraft are discussed. Afterwards in section 6.12.2, the final Aircraft design dimensions calculated in the final iteration are presented.

6.12.1. Effects of Re-sizing Empennage & Landing Gear

During the landing gear sizing, as described in section 6.7, it was determined that the main landing gear had to be stored in the fuselage. As the main landing gear was expected to be stored in the wing during the fuselage sizing, the fuselage sizing has to be iterated with the main landing gear housing in mind. Furthermore, the newly estimated centre of gravity range changes the landing gear positioning and sizing as well, altering their estimated weight. The new dimensions of the landing gear have to be inputted in the class II weight estimation and in the fuselage sizing.

Furthermore, the generation of the scissor plot allows for the determination of the new horizontal tail size and wing position. The vertical tail size is found by multiplying the horizontal tail area with the statistical ratio of vertical tail surface area to horizontal tail surface area. The new tail areas are found to have halved in size compared to their statistical preliminary estimate. The new tail dimensions have to be inputted in the class II

weight estimation. With the new tail sizes, a new L/D is estimated by estimating the the trim drag and zero-lift drag of the empennage. The new L/D will be inserted in both the class I and class II weight estimation.

The changed parameters and their place within the iteration process are marked as red and schematically displayed in the N2 chart section displayed in figure 6.11.

• Class I Cost Estimation & Optimisation • Class I Weight Estimation	• OEW • Fuel Weight • MTOW	• OEW	
• L/D • SFC • Cruise speed	• Engine selection • Fuselage Sizing • Wing Sizing & Aerofoil Selection & Preliminary Positioning • Preliminary tail sizing & positioning	• 3D views • Ultimate load	
• OEW		• Class II weight estimation • c.g. determination	• OEW • c.g. range
• L/D	• Landing gear size and position	• Tail size and position • Wing position • Landing gear size and position	• Tail Sizing & positioning • Wing positioning

Figure 6.11: Section of the N2 chart that encompasses the aircraft iteration process with the parameters from the second empennage & landing gear positioning and sizing marked as red.

6.12.2. Final Aircraft Dimensions

The iterations have been finalised to the dimensions of the wing, fuselage, empennage, and landing gear. The aircraft dimensions are presented in table 6.11. Furthermore, a drawing of three perspectives of the aircraft can be seen in figure 6.12.

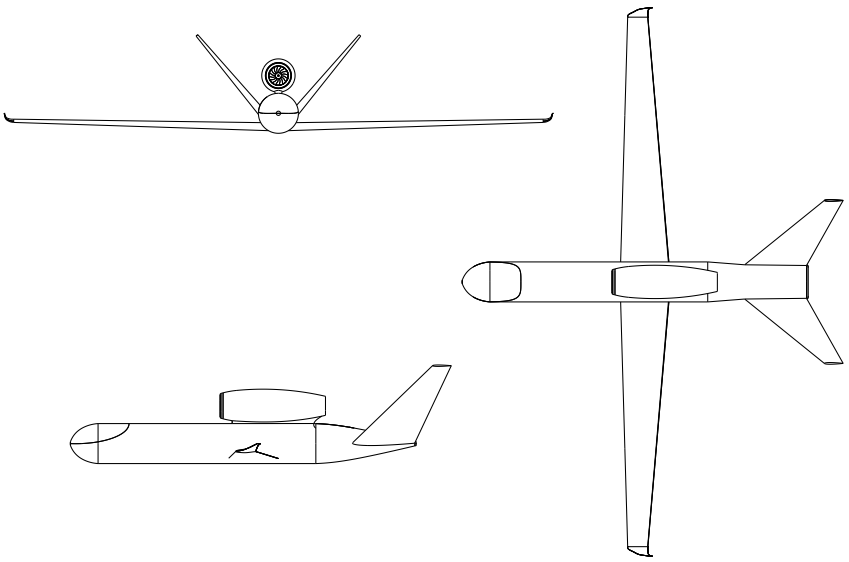

Figure 6.12: Drawing of the aircraft from three perspectives.

Table 6.11: Final values for the aircraft parameters

Parameter	Value
Mass & Balance	
MTOW	4323 kg
OEW	1378 kg
Maximum fuel weight	2650 kg
Maximum payload weight	297 kg
Most forward c.g. position	13 MAC%
Most aft c.g. position	38 MAC%
Fuselage dimensions	
Fuselage length	7.90 m
Fuselage diameter	0.935 m
Nosecone length	0.468 m
Tailcone length	2.34 m
XLEMAC	3.80 m
Landing gear	
Nose gear position from nose	0.49 m
Main gear position from nose	4.27 m
Wheel base	3.78 m
Main landing gear track	1.23 m
Nose gear tire diameter	0.46 m
Main gear tire diameter	0.54 m

Parameter	Value
Wing dimensions	
Surface area	10.2 m^2
Aspect Ratio	15
Span	12.4 m
Taper ratio	0.4
MAC	0.88 m
Quarterchord sweep angle	0°
Airfoil	NACA$65_2$416
Empennage dimensions	
Configuration	V-tail
Dihedral	50°
Surface area	4 m^2
Aspect ratio	2.5
Span	2.24 m
Taper ratio	0.3
Leading edge sweep angle	40°
Control surfaces	
High-lift device type	Single-slotted flap
Aileron surface area	0.33 m^2 per wing
Total ruddervator surface area	0.86 m^2

6.13. Electrical System

To determine the total required power for the aircraft three statistical formulas were found based on the MTOW and maximum amount of passengers of the aircraft [73]. Figure figure 6.13 shows these formulas are a reasonably good estimation of the actual total engine mounted generator ratings. The formulas used, Equation 6.35 to Equation 6.37, can be seen below.

$$f(M_{TOW}) = 9 \cdot 10^{-15} \cdot M_{TOW}^3 - 7 \cdot 10^{-9} \cdot M_{TOW}^2 + 0.0022 \cdot M_{TOW} \tag{6.35}$$

$$f(PAX) = 2 \cdot 10^{-6} \cdot PAX^3 - 0.002 \cdot PAX^2 + 1.1208 \cdot PAX \tag{6.36}$$

$$f(M_{TOW}, PAX) = 115.0983 + 0.0012 \cdot M_{TOW} - 0.6849 \cdot PAX + 7.2401 \cdot 10^{-9} \cdot M_{TOW}^2 - 9.8505 \cdot 10^{-6} \cdot M_{TOW} \cdot PAX + 0.004 \cdot PAX^2 \tag{6.37}$$

Equation 6.36 can be discarded immediately, since it is only dependent on the number of passengers and the AT1 will have none. Since this will give a wrong estimation, only the other two formulas are evaluated. Verifying the appropriateness of using these equations for the AT1 by filling in the weight of the Global Hawk RQ-4 and comparing the estimation to the actual results. The power generated from the engine by the Global Hawk is equal to 5.2kVA and it has a hydraulic generator which delivers another 8.3kVA.[6] When the the MTOW of the Global Hawk, 11612kg, is entered in the formulas it is clear that the 130kVA outcome of Equation 6.37 is wrong. Due to the way the formula is set up it can never be lower than 115.0983kVA. Therefore, for passengerless aircraft this formula cannot be used. The f(M_{TOW}) calculation is significantly more accurate, returning a total required power of 24.6kVA, however, this is still considerably higher than the actual value of 13.5kVA. The dispersion system, which the Global Hawk does not have, will require a significant amount of power and the weight of the AT1 is low compared to the reference aircraft, therefore the safety factor is considered reasonable. For the ACT aircraft with a MTOW of 4136.5kg this would result in a total required generator power of 8.9kVA.

[6] Retrieved from: https://www.nasa.gov/centers/armstrong/aircraft/GlobalHawk/performance.html [2-7-2018]

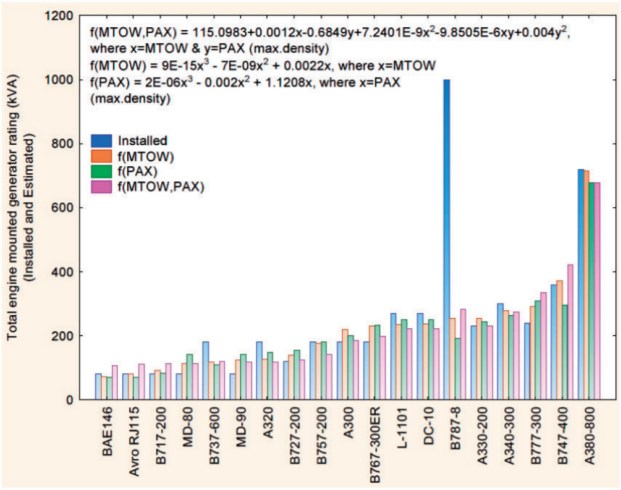

Figure 6.13: Estimated versus published total engine mounted generator ratings. [73]

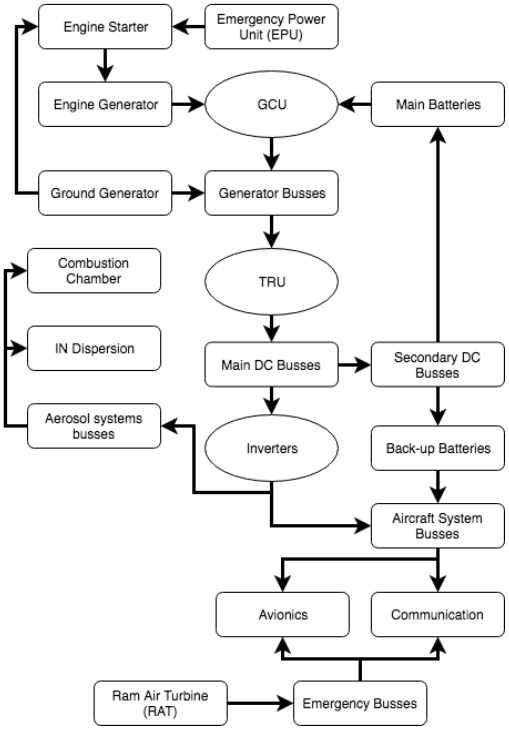

Figure 6.14: Electrical system lay-out

Besides the generators on the engines, most aircraft also have an Auxiliary Power Unit (APU) to power the aircraft when the main engines are shut off and the aircraft is on the ground. This is not necessary for the AT1 since it does not matter that it has no power when it is parked after landing as it has no passengers, and thus no systems requiring high amounts of power will still running. The communication systems will be able to run on the batteries in the aircraft for the time between shutting of the engines and plugging in the ground generator. For redundancy, the aircraft will be equipped with an Emergency Power Unit (EPU) which is able to restart the engine in case the engine fails and needs to be restarted. Finally, in case the generator itself fails, a Ram Air Turbine (RAT) will be installed on the aircraft. A RAT is a simple fan which generates power due to the airflow around the aircraft. This RAT will only power the most essential systems such as the avionics, communications, and flight controls. In case the main generator fails, the aircraft will stop seeding and attempt to safely bring the aircraft back to the base. The lay-out of the electric system of the ACT aircraft can be seen in figure 6.14.

6.14. Fuel and Payload Systems Lay-out

In this section, the layout of the payload and fuel systems will be discussed. The graphical layout of these systems can be found in figure 6.15 where the fuel system is depicted as black solid lines and the payload system as red dotted lines. It is important to note that the large tanks depicted in the figure are actually a lot of smaller tanks combined to prevent large shifts in weight location. This means that there will be 2 pumps in each section and not just the 2 pumps in the large tanks as depicted in the figure.

The fuel system is separated in a left and right section. This way it is guaranteed that the engine will be able to still run if there is a blockage in either the left or right section. Because the weight distribution during flight is important to keep the plane controllable, each pump is able to both pump fuel out of a section as it is to pump it in to optimise the overall centre of gravity. To do this, the left and right sections are connected to each other with two crossfeed pumps that are able to let fuel flow from left to right and vice verse. Finally two jettison valves are installed at the tips of the wing to allow the aircraft to dump fuel in case too much fuel is still in the tanks to land the aircraft. Also a defuel valve was added to allow on-ground defuelling.

The payload system is more simple. It has a single inlet from where the IN can be refilled and a valve which can be used to empty the payload tank on the ground. Since the IN must only be dispersed within the seeding area no jettison valve for the payload system is installed. The rest of the system simply exists out of pumps to keep the IN flowing through the system and a low pressure tank to prevent fuel flowing back from the combustion chamber.

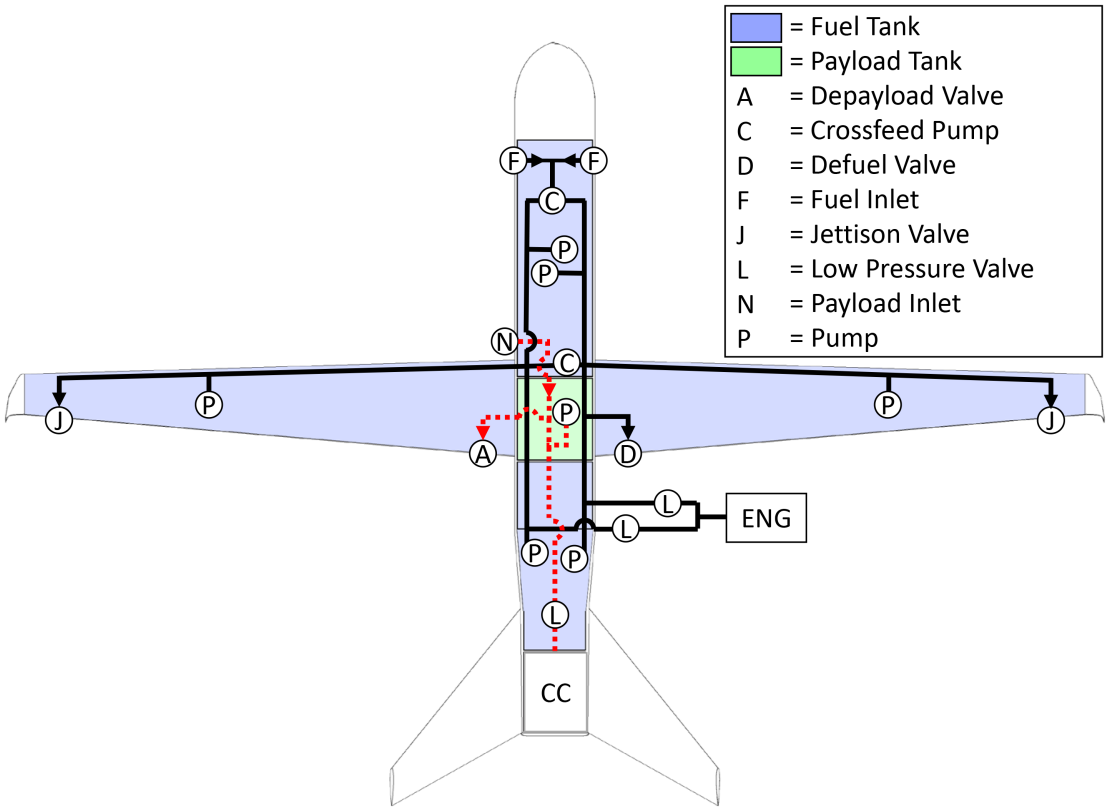

Figure 6.15: Fuel and Payload systems layout

7 Aircraft Performance

Now that the design of the aircraft has been established in chapter 6, its performance can be further analysed to build upon the first and second level estimations. This is necessary to ensure all the system requirements are met. First, the aerodynamic performance of the wing and tail, stability and control analysis, and aeroelasticity will be analysed in section 7.1, section 7.2, and section 7.4 respectively. The aircraft's take-off, climb, ceiling, range, turn, cruise, descent and landing performance will then all be calculated in as much detail as possible. These, along with the flight altitude envelop will be discussed in sections 7.6 to 7.13. Lastly, in section 7.3, a detailed structural analysis will be performed where the wing box and fuselage can be further designed, followed by evaluating if the AT1 can in fact perform in all weather conditions.

7.1. Aerodynamic Analysis

In order to analyse the aerodynamic performance of the AT1 and optimise the aircraft dimensions, a model was created in XFLR5. This model does not include the fuselage or the winglets. First, the airfoils are analysed in 2D. Then, the model is evaluated in 3D so that the trim point can be determined. From this, the stability and control of the airplane can be analysed.

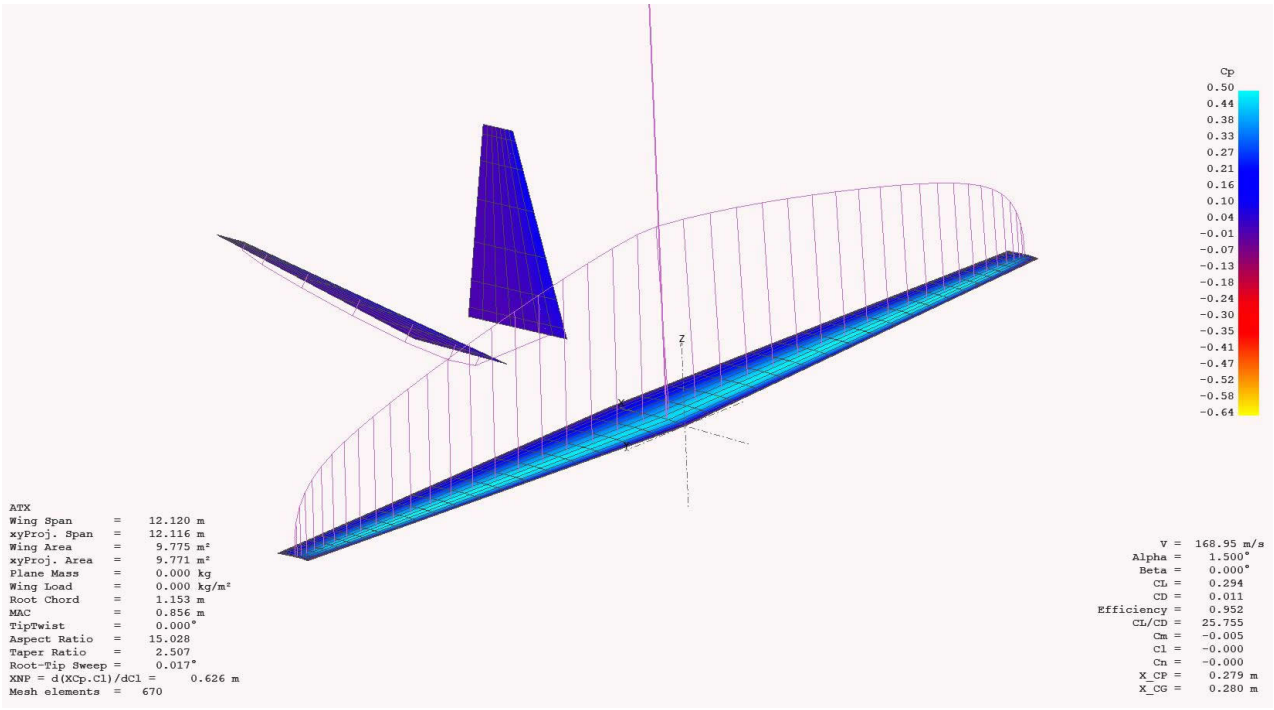

Figure 7.1: XFLR5 Model of the AT1

Figure 7.1 shows the model that was used for the analysis. It also shows the lift distribution over the wing and the Cp distribution. This lift distribution was used to validate earlier assumptions of the lift distribution. The analysis was done using the Ring Vortex VLM2 method in XFLR5. This method has some limitations that affect the accuracy of the outputs, which should be considered. The VLM2 method is derived from non-viscous assumptions for the fluid. For the AT1 the viscous drag cannot be ignored. To account for viscosity a 2D analysis is done, the results of this analysis are then extrapolated to the 3D analysis. Furthermore, the fuselage is not part of the aircraft model, as it is not taken into account when using the VLM2 method.

However, fuselage drag, found from the fuselage drag coefficient and surface area of the cross section, is added to the analysis manually. The accuracy of the results is also dependent on the mesh used. For the analysis a mesh is defined over the wing and fin surface. The standards mesh given by XFLR5 is used to do the analysis. The mesh is more dense over the area of the wing that has more curvature, and closer to the tip of the wings and he change in spacing of the mesh should be gradual to get the optimal results. Since number of panels in XFLR5 in the direction of the chord is quite limited and defining an optimal mesh is outside the scope of this project the standard mesh is used initially. Refining the mesh and comparing results can be done to study the accuracy of the model. This model was then used to find the trim point, associated velocity, and L/D in a T2 analysis. These graphs could then be used to design the angle of incidence of the tail and the position of the centre of gravity. In order to get maximum range, the angle of incidence of the V-tail was set to -2.1°, which corresponds to the leading edge rotating outwards. This gives a negative C_{m_α} and a positive C_{m_0}. The trim point is then at an angle of attack of 1.4°, which corresponds to the maximum L/D of 26.3, as can be seen in figure 7.2. Due to the absence of the fuselage, this prediction is more positive than in reality. The induced drag that was found using XFLR5 was used to improve the analytical model that estimates drag.

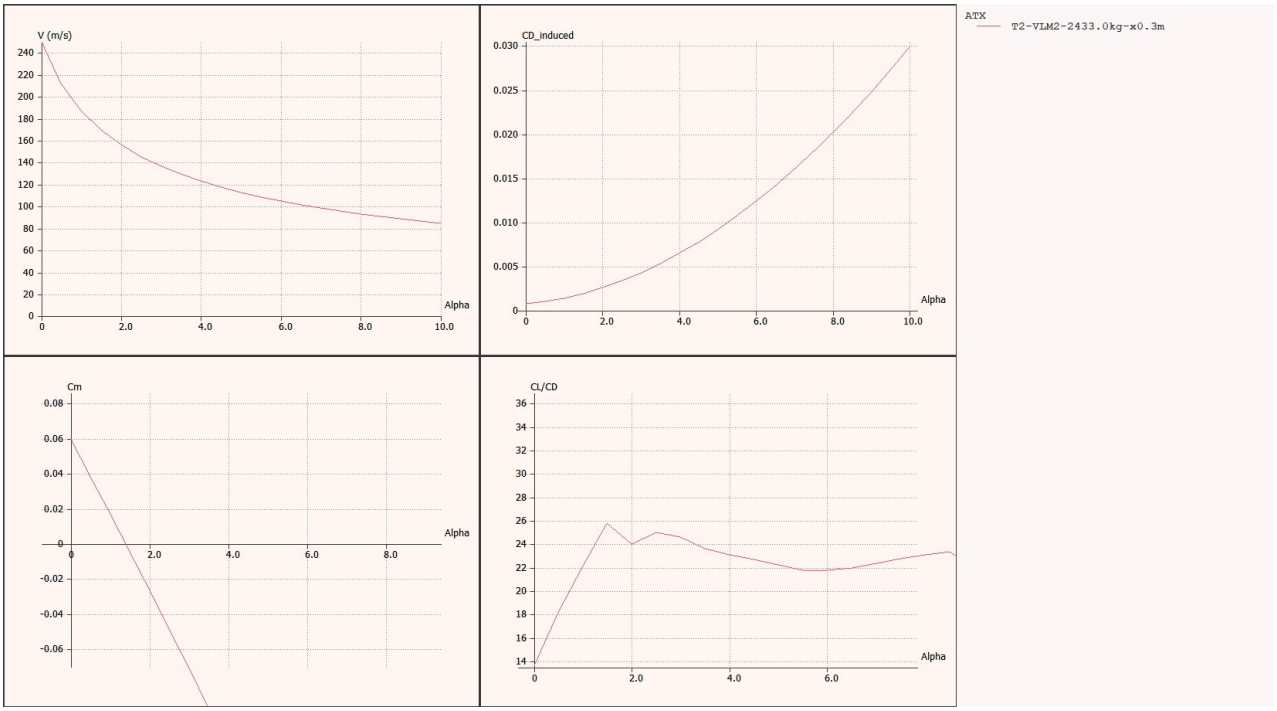

Figure 7.2: V/α curve, $C_{d_{induced}}/\alpha$ curve, C_m/α curve and L/D curve

7.2. Stability and Control Analysis

After finding the trim point for the required L/D a T7 analysis was performed in XFLR5 to determine the stability and control characteristics of the aircraft. The aircraft response to the short period, phugoid, roll subsidence, dutch roll and spiral motion are evaluated in two cases: Both the stability during cruise and in landing, just before deployment of the flaps will be analysed. To do the analysis the centre of gravity location and mass moments of inertia are needed. The centre of gravity range that could be used is defined in section 6.10, the stability margin is 0.39 but decrease to 0.05 in later stages of the flight. The moments of inertia in during cruise and landing are calculated with relation from Raymer [74]. It should be noted that the destabilising effect of the fuselage on the lateral stability of the aircraft is not taken into account. The damping ratios and time constant for the different modes during cruise can be found in table 7.1. The damping ratios and time constants for the aircraft just before landing can be found in table 7.2 and the root locus plots for symmetric and asymmetric motions in cruise can be seen in figure 7.3 and figure 7.4. The aircraft was found to be stable

without any dihedral of the wing, still, a 1.5°angle was added to increase the ground clearance of the wings.

The outcomes from the stability analysis are compared to handling quality requirements. Handling qualities of an aircraft are determined by studying the stability and control characteristics [14]. Classification for the handling quality of an aircraft is based on the type of aircraft and flight phase. For each classification three levels are defined, the level of flying qualities seek to indicate the severity of the pilot workload during the flight. Each level can be linked to the Cooper-Harper rating scales for demands on the pilot. Most aviation authorities provide regulations for the required level of flying quality for different types of manned aircraft. Currently, for unmanned aircraft regulation is not available. However, several studies have been done into UAVs ability to counter disturbances, concluding that new regulation is necessary when the pilot response is taken out of the loop, and the UAV performs better than manned flight since response time and fitness are no longer an issue [16].

In the cruise phase for the short period, phugoid, and dutch roll the AT1 is stable and adheres to the level 2 requirement which is defined as: ”Flying qualities adequate to accomplish the mission flight phase, but with an increase in pilot workload and, or, degradation in mission effectiveness.” Which is considered acceptable as there is no pilot involvement. The spiral mode is unstable but because of the large time constant this is considered acceptable since there is enough time to counter this motion. When analysing the landing phase the AT1 is found to be more stable for the dutch roll and roll subsidence mode and short period. For the short period the damping mode is within the level I criteria. For the phugoid and dutch roll the aircraft still adheres to the level II requirements. Different than for the cruise phase the AT1 can be controlled pilot in the loop during landing and take-off. This means that the argument of not having the pilot response in the loop, as was made for the cruise phase, is no longer valid. When further developing the aircraft it is important to critically assess the stability and control characteristics in more detail. At this stage the time and resources are not sufficient to do such an analysis and with the assumptions made the accuracy of the outcomes is hard to quantify. To increase the handling qualities of the aircraft a fly-by-wire system or yaw damper could be imposed.

Table 7.1: Stability modes characteristics during cruise

Mode	**Short period**	**Phugoid**	**Dutch Roll**	**Spiral**	**Roll subsidence**
Damping/Time constant	ζ_s: 0.273	ζ_p: 0.026	ζ_d: 0.075	T_s: 122.7 sec	T_r: 0.033
Frequency	2.694 Hz	0.009 Hz		1.001 Hz	

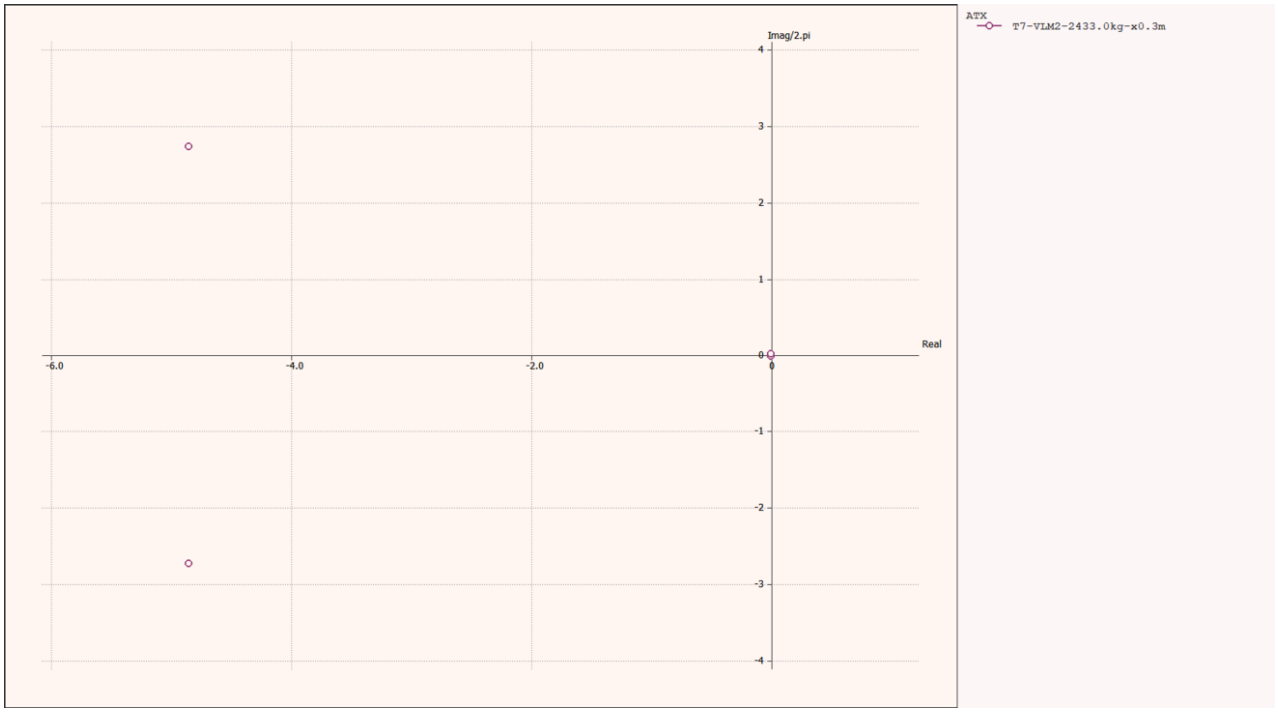

Figure 7.3: Root locus for symmetric motion

Figure 7.4: Root locus for asymmetric motion

Table 7.2: Stability modes characteristics during landing

Mode	**Short period**	**Phugoid**	**Dutch Roll**	**Spiral**	**Roll subsidence**
Damping/Time constant	ζ_s: 0.414	ζ_p: 0.024	ζ_d: 0.095	T_s: 28.515 sec	T_r: 0.047
Frequency	0.915	0.023		0.518	

7.3. Structural Characteristics

In this section a preliminary design of the fuselage and wing will be presented. First, the material of the fuselage and wing is selected. Next, different load cases are analysed and after that, the stresses in the fuselage and wing are determined. These are then used to make a preliminary sizing of the wing and fuselage, such as skin thickness and spars. A contingency is included for future design considerations. In the end, the model that is used for this design is verified and validated.

7.3.1. Material selection

For the material selection the following materials are compared: Aluminium alloys, Titanium allows, Carbon Fibre Reinforced Polymers and Glass Fibre Reinforced polymers. These materials have been chosen because they have very favourable material properties for aerospace applications and are therefore often used in aircraft design. Their material properties are given in table 7.3. [65]

Table 7.3: Material Properties

Material	Density $[g/cm^3]$	Young's modulus [GPa]	Yield stress [MPa]	Structural efficiency E/ρ $[GPa \cdot m^3/kg]$	Cost [$/kg] [1]
Al Alloys	2.7	70	525	0.026	1.7
Ti Alloys	4.5	110	1000	0.024	16.25
CFRP	1.7	120	700	0.071	110.00
GFRP	2.1	22	600	0.01	3.90

The most important important criteria in the selection of the material are:

- **Material weight** The material weight is extremely important in the selection of the material, this is because the fuel-consumption of the aircraft is highly dependent on the aircraft weight.
- **Material strength** The material strength is important to make sure the aircraft is able to carry all loads experienced during flight and ground operations. The structure shall not fail under the applied loads.
- **Cost** The cost of the material consists of both the raw material cost as-well as the production cost of the aircraft. These costs determine the cost of the fleet and therefore a large portion of the initial cost of the mission.

First we compare the metals, aluminium and titanium, we find that aluminium has a better structural efficiency and lower cost. Titanium can therefore quickly be discarded. Secondly we compare the composites, CFRP and GFRP. We find that GFRP has a stiffness and structural efficiency which are too low, it is therefore also discarded. The comparison of aluminium and CFRP is not as straight forward. CFRP has a far higher structural efficiency but also a very high cost. To properly trade-off between these two materials an estimation of the cost-benefits of the lower weight of CFRP was performed.

According to Kennedy and Martins [49], the use of CFRP in aircraft design can decrease the structural weight of an aircraft by up to 40%. This weight reduction causes the fuel-consumption to decrease which will then decrease the cost of the operations. To estimate this reduction in fuel consumption the results of the class II weight estimations were altered and reused in the Class I weight estimation to get a new estimate for the fuel use. The results of these calculations are given in table 7.4. These estimates assume a very high price for CFRP of $110/kg, this means that in reality the cost savings can possibly be even larger. However these estimates do not include the cost of production which can possibly increase quite significantly for CFRP with respect to aluminium.[98]

In the end CFRP comes out on top. Even though the raw material cost is far larger than for aluminium, the reduced fuel usage makes up for this because of the annual cost savings. Also with respect to sustainability CFRP is a better option, for a mission of 20 years the fuel usage will reduce by roughly 165 thousand tonnes.

[1] Retrieved from: http://web.mit.edu/course/3/3.11/www/modules/props.pdf [13-06-2018]

Table 7.4: The effect of a reduction in weight

Weight reduction	Structural weight [kg]	Raw material cost [$]	Fuel usage reduction per sortie [kg]	%	Annual fuel cost reduction [$]	Total mission cost reduction [$]
0%	382	649	0	0.0%	0.00E+00	0
10%	344	37824	60	2.4%	1.51E+06	2.46E+07
40%	229	25216	241	9.5%	6.04E+06	1.17E+08

This reduces the total CO_2 emissions by 496 thousands tonnes [2]. For these reasons CFRP is chosen as the main material for the CCT Arctic Tern. Some parts of the aircraft, where CFRP is not suitable due to high temperatures or possible impacts materials such as aluminium might still be used.

7.3.2. Assumptions

Fuselage
To find the most critical load on the fuselage, a few load-cases were analysed. The first load case considers the aircraft at MTOW cruising at cruise altitude, it experiences the maximum load-factor, determined in section 6.9.1, due to a gust and the tail has a rudder deflection which applies a torque to the fuselage. This torque is counteracted by the wing. The second load-case considers the aircraft in taxi. In order to analyse the loads on the fuselage, a few assumptions had to be made to get a good first estimate of the loads. These assumptions are given below.

- The maximum loading factor is applied.
- A safety-factor of 2.0 is applied.
- The fuselage structure is idealised.
- The fuselage is modelled as a beam.
- Drag is very small compared to the lift, so it is neglected.
- The aircraft is flying at MTOW.
- All weights act as point loads at their centre of gravity.
- All aerodynamic loads act as point loads at their AC.
- During cruise the wing induces a reaction moment which causes static equilibrium.
- The fuselage has no cut-outs.
- Loads due to bending around z are negligible w.r.t the bending around y.
- Normal stresses due to drag and thrust are negligible w.r.t. the normal forces due to bending.
- The fuselage has a round nose and an empennage which is tapered in z.
- The tensile strength of CFRP is equal to the compressive strength.
- No buckling or delamination occurs.

Wing
Several loading conditions have been analysed to identify the most critical loading condition. The loading factors are obtained from loading diagram in figure 6.5. It can be seen that the maximum loading conditions are 2.5g and -1g. Two conditions have been further analysed, the first of which is during maximum loading conditions and no fuel stored in the wing. The second loading condition is with maximum fuel in the wing during ground operations, for which a loading factor of 1.5 will be applied resulting from a taxi bump. The first condition will be analysed to determine the skin thickness and number of spars in the wing box. The second condition will be analysed to compare with condition 1. This will be done to determine the maximum deflection both upward and downward. Before the loading diagrams of condition 1 will be presented, the assumptions for the model are stated first.

- The maximum loading factor is applied.
- The wing box structure is idealised.
- The wing is modelled as a beam.
- Drag is very small compared to the lift, so it is neglected.

[2]Retrieved from: https://www.engineeringtoolbox.com/co2-emission-fuels-d_1085.html [14-06-2018]

- The fuel tanks in the wing are empty.
- The lift is modelled as an elliptical distribution.
- The wing box is symmetrical.
- The wing is weightless.
- The aircraft is flying at MTOW.
- The wing has no cut-outs.
- The tensile strength of CFRP is equal to the compressive strength.
- No buckling or delamination occurs.

As said above, the lift is assumed to be elliptically distributed. The lift is modelled with equation (7.1). Here, *b* is the maximum point of the function and *a* is the semi-span of the aircraft. *y* is the variable along the aircraft span.

$$L = \frac{a_{ellipse}}{a_{ellipse}}\sqrt{a^2 - y^2} \tag{7.1}$$

b is found by integrating equation (7.1) and setting equal to the aircraft weight multiplied with the maximum loading condition and a safety factor of 1.5. The reaction force of the lift is modelled as a point load in the centre of the fuselage.

7.3.3. Loading diagrams

The loads on the fuselage as a function of the x-position in the fuselage is given in figure 7.5. Due to the assumption of the point-loads, the shear force varies in discrete steps. The bending moment is simply the integral of the shear and it therefore varies linearly with x. The torsion moment is a constant moment between the wing and tail. Comparing the cruise condition, figure 7.5(a), with the taxi condition, figure 7.5(b), we find some interesting resemblances and differences. The magnitude of the shear in cruise is very similar to the shear in the taxi case although the loads for cruise are slightly higher. The largest difference occurs in the magnitude of the bending moment and torsion moment. For the cruise case the bending moment is almost an order of magnitude larger than in the taxi case. Furthermore the magnitude of the torsion is two orders of magnitude smaller than for the cruise case. For these reasons the cruise at MTOW is taken as the critical case for the analysis of the fuselage structure.

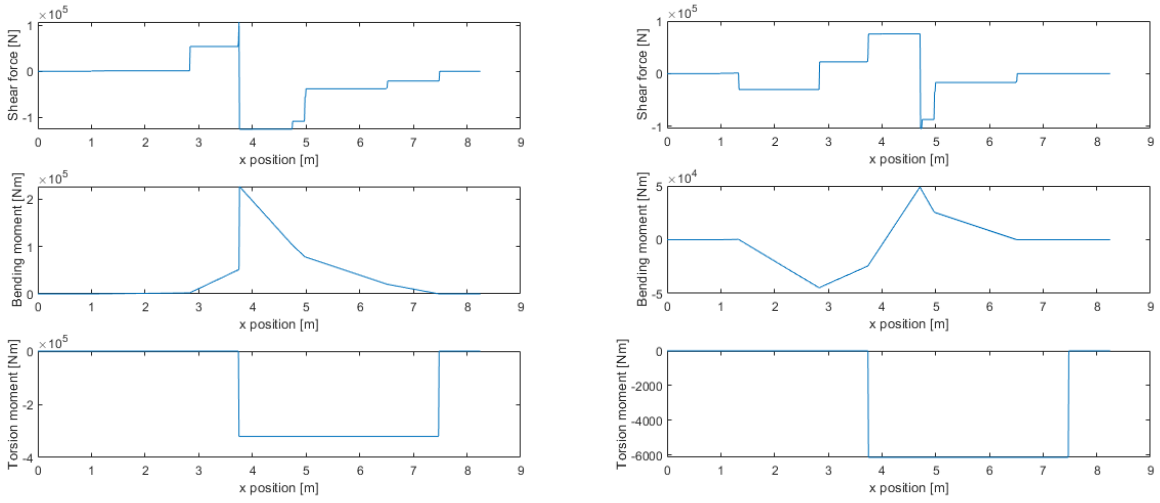

(a) Cruise with rudder deflection

(b) Taxi with crosswind

Figure 7.5: Fuselage loading diagrams for different load cases

The loads on the wing as a function of half the wing span is given in figure 7.6. The loading diagrams are symmetrical along the y-axis for the entire wing span. Figure 7.6(a) shows the distribution of the shear force and the bending moment for maximum loading conditions with empty wing fuel tanks so all fuel is stored in the fuselage. Figure 7.6(b) shows again the distribution of the shear force and bending moment, but now during ground operations with full wing fuel tanks and landing gear not retracted.

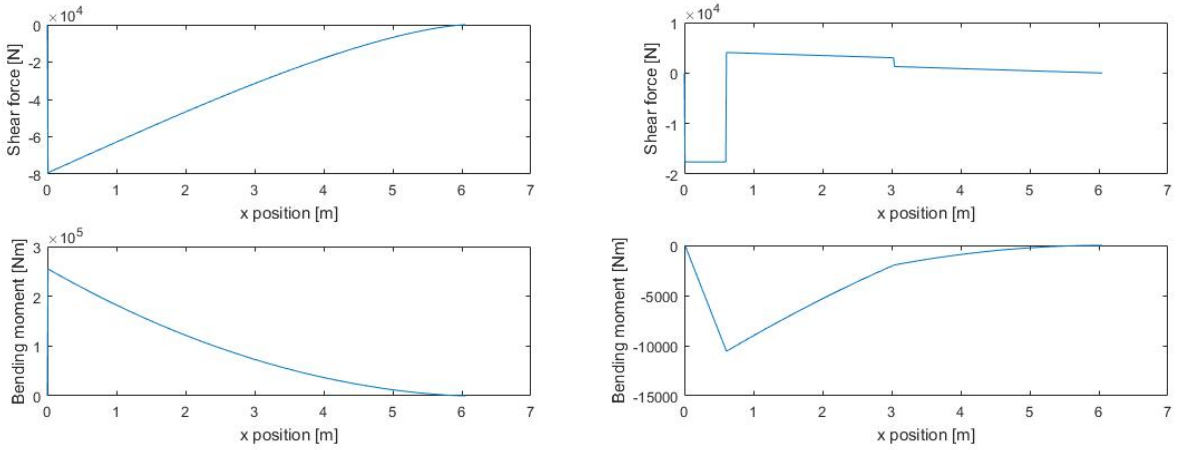

(a) Shear and moment diagram for maximum loading condition of n=2.6 on the wing

(b) Shear and moment diagram for the wing during ground operations for which n=1.5

Figure 7.6: Wing loading diagrams for two load cases along the semi-span of the aircraft

These diagrams will be used to make a prediction of the stresses along the span of the wing and the length of the fuselage. The deflection of the wing can be modelled using the moment diagram. The deflection is obtained by integrating the bending moment function twice. Four scenarios are plotted, as can be seen in figure 7.7. The first is condition 1, as described previously, where a loading factor of 2.6 is applied. The second scenario is condition 2, which is also described previously. A loading factor of 1.5 is applied, which is the result of a taxi bump. The last 2 scenarios are the deflections during cruise for which a loading factor of 1 is applied and during the scenario with the lowest possible loading factor of -1, which is derived from figure 6.5. It should be noted though, that for these deflections the tip of the wing is strengthened to increase the structural rigidity. This is required due to the taper of the wing. If this part would not be strengthened, the deflections will become too extreme. This will be elaborated upon in section 7.3.5.

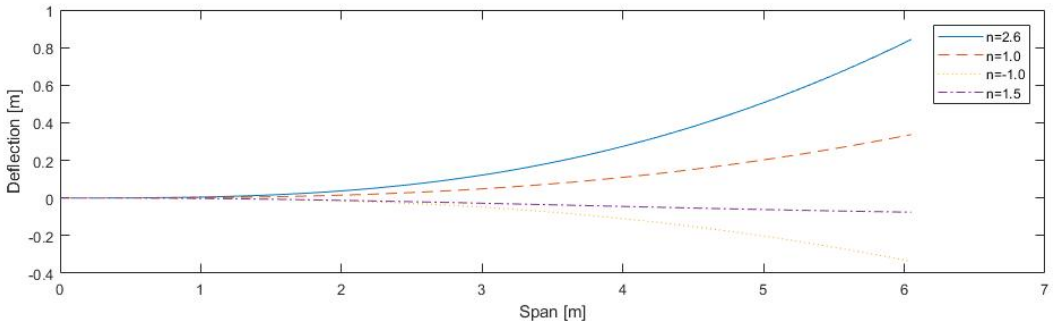

Figure 7.7: Deflections for several loading conditions along the semi-span of the aircraft

7.3.4. Stress Analysis

Now the general methodology to determine the stresses in both the fuselage and the wing will be elaborated upon. Both structures are first idealised according to the methods described in Megson [56]. The cross section of the structure is replaced by booms with a certain boom area, which is optimised in the program in

section 7.3.5. The fuselage is a cylinder which is rounded at the nose and tapered in the z-axis in the tail. The wing box is first defined as a tapered symmetrical box with 8 spars, which will be modelled as booms. The model will have the wingspan as variable, so the stresses will be determined for the number of booms located along the span. The fuselage is defined as a cylinder with a round nose and the rear part is flattened out as a tube. Again, the spars will be modelled as booms. The fuselage length is the variable in this model to obtain an accurate stress distribution along the entire length. The number of spars and skin thickness will be varied later in this section to determine the best configuration for the wing and fuselage. Now onto the bending stress analysis. The bending stress will be analysed for each boom with equation (7.2) for which the moment of inertia is calculated according to equation (7.3).

$$\sigma = \frac{M \cdot z}{I} \qquad (7.2) \qquad I = B_{area} \cdot z^2 \qquad (7.3)$$

Here, *M* is the local moment derived previously and *z* is the distance to the symmetrical axis. B_{area} is the boom area. Next, the shear flow is determined with equation (7.4) and consequently, the shear stress is determined with equation (7.5).

$$q = -\frac{S_z}{I}\sum B_{area} z + q_{s,0} \qquad (7.4) \qquad \tau = \frac{q}{t} \qquad (7.5)$$

The shear and bending stresses will used to determine the Von Mises stress according to equation (7.6). The Von Mises stress will be the stress which will be used to design the structure, i.e. the number of spars and skin thickness.

$$\sigma = \frac{1}{\sqrt{2}}\sqrt{\sigma_y^2 + 6\tau_{yz}} \qquad (7.6)$$

The resulting Von Mises stress can be plotted to have a graphical point of view of the stress distribution and the location of the maximum stresses. This can be seen in figure 7.8. Figure 7.8(a) shows the stress distribution of the fuselage and figure 7.8(b) shows the stress distribution of wing along the semi-span of the aircraft.

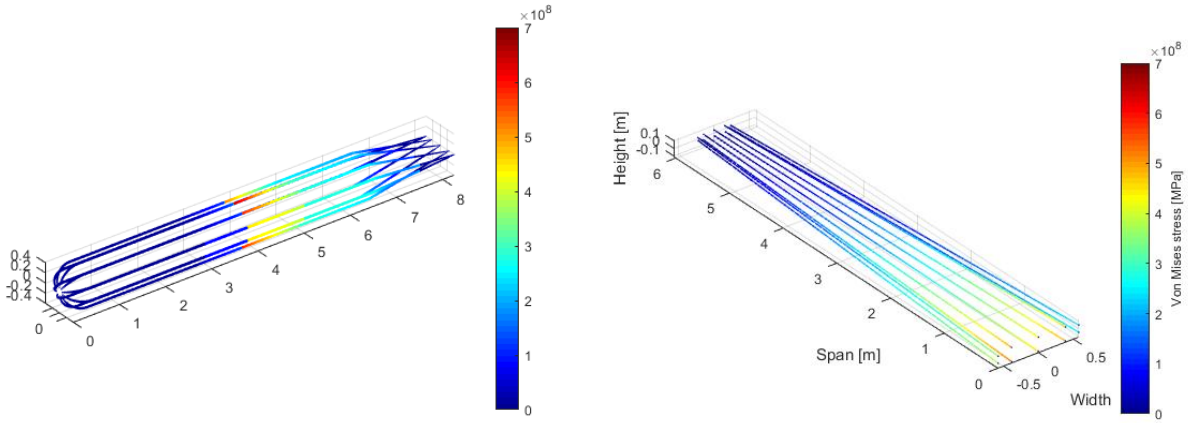

(a) Fuselage in critical loading condition (b) Wing at critical loading condition

Figure 7.8: Graphical representation of Von Mises stresses [Pa]

7.3.5. Sizing of the Wing Box and Fuselage

To get an estimate of the weight of the fuselage a few preliminary designs were made and their performance estimated. For these calculations the number and dimensions of the stringers as well as the skin thickness were varied. The weight was then estimated using the volume of the skin and stringers combined and multiplied with the density of CFRP. The stresses were then estimated using the boom theory described in section 7.3.4.

The maximum allowable stress was taken to be the yield-stress of quasi-isotropic CFRP of 700 MPa. The results of these design options are given in table 7.5. Structural weights ranging from 23kg for the ”most optimised” design and 102 kg for the over-designed design are found. The first thing which stands out is that all these weights are far lower than the fuselage weight in the class II weight estimation, this has two main causes. The first cause is the fact that the class II weight estimations are based on aluminium aircraft which has almost twice the density of CFRP. The second reason is the fact the fuselage is not pressurised which greatly reduces both the hoop- and normal stresses in the fuselage. The weights in table 7.5 should not be seen as the final weights for the fuselage structure. This is because these estimates do not include the effects of skin and stringer column buckling. These calculations also do not include the effects of stress concentrations in areas where the wings or engine are attached to the fuselage. However there are also opportunities to reduce the structural weight by varying the stringer dimensions or even the skin thickness along the length of the fuselage. Also areas where impact such as bird strike etc. can be expected the structure will need to be reinforced with tougher materials such as aramid fibres or aluminium plates.

Table 7.5: Fuselage design options

Option	# Stringers	Stringer area [mm^2]	Skin thickness [mm]	Mass [kg]	Maximum stress [MPa]
1	10	28	0.6	23	659
2	10	28	0.7	27	576
3	22	28	0.7	31	498
4	10	80	0.7	34	477
5	50	28	0.7	42	401
6	10	80	2	76	202
7	22	120	2	102	159

Several design options for the wing box are considered. Here, the number of stringers, stringer area and skin thickness are varied. These are varied such that the structure is capable of handling the most critical loads and having a structural rigidity such that the wing does not deform to extreme positions. Furthermore, it is driving that the mass should be kept as low as possible. A few options can be seen in table 7.6. It can already be noted that a design with 8 stringers will not be used, as the mass is much higher than the other options in order to carry all the loads. Furthermore, the deflection is higher than the other options, which is also unfavourable. Option 2 and three have the same mass, while option 3 is not loaded until the yield strength. It seems that the mass of option 3 can be even more reduced. However, as this affects the structural rigidity enormously, this will not be done. The resulting maximum deflections become too severe, which will affect the aircraft performance. However, the local thickness and stringer area along the span of the wing can be adapted. The root section can be decreased as the maximum stress occurs here and the stringer area at the tip can be increased as the structural rigidity is lowest here. As a result, the maximum deflection can be further decreased, making the wing more rigid. Therefore, the configuration of option 3 will be chosen.

As could also be noticed for the design of the fuselage, the weight of the wing is considerably lower than was estimated at the class II estimation. This is because the class II weight estimation is based on aluminium aircraft. CFRP is used for the wing, for which the density is almost 40% less and the yield strength almost 40% higher. The fuel tank weight is not included. Furthermore, a contingency of 20% should be taken into account for future design considerations, because skin and stringer buckling have not yet been analysed. Furthermore, deicing systems, wing-fuselage interactions, cut-outs, high-lift device attachments etc., have not been analysed and should be analysed in a later design stage.

Table 7.6: Wing box design options (mass is of half a wing)

Option	# Stringers	Stringer area [mm^2]	Skin thickness [mm]	Mass [kg]	Maximum stress [MPa]	Maximum deflection [m]
1	8	550	1.6	74.2	662	0.97
2	10	400	1.0	59.3	663	0.84
3	14	300	0.9	59.5	521	0.80

7.4. Aeroelasticity

A preliminary investigation into aeroelasticity is being performed using empirical relationships in this section. The two main aeroelastic phenomena can be divided into two parts: static and dynamic phenomena. Static aeroelastic problems come in the form of divergence and control reversal. Dynamic aeroelastic problems come in the form of flutter and is harder to model than static aeroelastic behaviour. First, static aeroelasticity will be discussed after which dynamic aeroelasticity will be discussed.

7.4.1. Static Aeroelasticity

Now, torsional divergence and control reversal will be analysed. The analysis will be performed at the MAC.

Torsional divergence
The increments of the lift vector on a wing generate a moment about the centre of twist. The angle of incidence increases, which increases the lift again and a snowball effect occurs. This process converges for air speeds below a certain value, called the divergence speed. The conversion means that the torsional rigidity of the wing and the torsion created by the aerodynamic forces are in equilibrium. If the wing experiences an air speed which is larger than the divergence speed, this process diverges and aircraft performance characteristics are negatively affected. The divergence speed of a finite wing can be calculated analytically with equation (7.7) [56]. Note that the solutions resulting from this equation are not the exact divergence speeds, but give rather an approximation of the order of the divergence speed. This gives a conservative estimation of the divergence speed.

$$V_{div} = \sqrt{\frac{\pi^2 GJ}{2\rho ec^2 s^2 (\partial c_l/\partial \alpha)}} \qquad (7.7) \qquad GJ = \frac{4A^2 G}{\int \frac{ds}{t}} \qquad (7.8)$$

Here, GJ is the torsional rigidity of the wing which is determined with equation (7.8) [56], ρ is the air density, s is the semi-span of the wing and $\partial c_l/\partial \alpha$ is the lift slope. ec is the distance between the aerodynamic centre and the flexural point, which is estimated to be 0.25 MAC, as the aerodynamic centre is located at 0.25 MAC and the flexural point is estimated to be at 0.5 MAC for a straight wing [56]. A is the enclosed area of the wing and the thickness t is integrated along the circumference of the wing. The results of the divergence speed for several air speeds can be seen in table 7.7. According to CS 25.629, the divergence speed may not approach $1.15V_c$ or $1.15V_d$ [3]. From table 7.7 it can be seen that this requirement is met.

Control reversal
The next static aeroelastic phenomenon is control reversal. The flexibility of different surfaces of the aircraft such as wing surface and tail surface adversely influence the effect of the corresponding control surfaces such as ailerons and elevators. Ailerons and elevators become less effective at larger speeds. A downward deflection of the aileron creates a nose down moment of the wing, which reduces the incidence angle of the aileron and thus the lift difference generated. When the aircraft reaches the reversal speed, the deflection of the aileron does not generate a rolling moment anymore. The reversal speed can be estimated analytically with equation (7.9). Just as for the torsional divergence, this is a conservative estimation. The spring stiffness of the wing can be calculated with equation (7.10).

$$V_{rev} = \sqrt{\frac{-K(\partial C_L/\partial \delta_a)}{\frac{1}{2}\rho Sc(\partial C_m/\partial \delta_a)(\partial C_L/\partial \alpha)}} \qquad (7.9) \qquad K = \frac{GJ}{0.5C} \qquad (7.10)$$

Here S is the wing surface area and c is the chord length. $\partial C_L/\partial \delta_a$ is determined to be 2.56 in section 6.11.2. $\partial C_m/\partial \delta_a$ is the derivative of the moment coefficient w.r.t. the aileron deflection, which is generally around -1 [46]. Therefore, a value of -1 is assumed here. Larger values for this derivative favour the design, however, if smaller values are found at a later stage, the torsional stiffness of the wing should be adapted in order to prevent control reversal. The results for the reversal speed can be seen in table 7.7. It can be seen that the reversal speed is not always more than 1.15 the cruise speed. This has to be dealt with in order to not have

any control reversal issues during flight. This can be solved by increasing the wing spring stiffness, which can be increased by increasing the thickness. With a wing skin thickness of 12 mm instead of 0.9 mm, the reversal speed is increased such that it will not be a problem. This will increase the wing mass from 59.5 kg to 64.9 kg.

Table 7.7: Divergence and control reversal speed for different flight conditions

	V [m/s]	1.15 x V	Density [g/m^3]	Divergence speed [m/s]	Reversal speed [m/s]
Take off	63.0	72.45	1.225	152.8	127.5
Cruise at 8 km	178	204.7	0.525	233.5	194.7
Cruise at 9 km	184	211.6	0.466	247.8	206.6
Cruise at 10 km	180	207.0	0.412	263.4	219.7
Landing	61.8	71.07	1.225	152.8	127.5

7.4.2. Dynamic Aeroelasticity

Just like in aircraft stability, a wing which is aeroelasticly stable in a static sense, might not be dynamically stable. Aeroelastic dynamic instability is called flutter. Flutter occurs when the aerodynamic forces on a wing-surface cause it to twist but the structure return to the initial position, however it then overshoots and twists in the other direction. This then continues and causes harmonic motion. When this harmonic motion is no longer dampened the deformations increase over time, ultimately resulting in failure of the structure [56].

A way to prevent flutter is to prevent aerodynamic, inertial and elastic coupling. This can be achieved by making sure the centre of gravity, centre of impedance and flexural axis of the aircraft coincide [56]. However this is often not possible in practice, therefore the critical flutter speed needs to be calculated to make sure it's sufficiently different from the speeds which are found in the flight envelope.

The method that is used to obtain an estimate of the flutter speed is described in [42]. This method is called the 'k method'. The 2D analysis will be performed at 75% of the span which is sufficient for a preliminary estimate for the flutter speed [42]. The result of this estimation is not the exact flutter speed, but it gives an estimate for the order of magnitude. The flutter speed is analysed using a script provided by the course staff of the course *"AE4ASM506 Aeroelasticity"*, taught at Delft University of Technology. This script is assumed to be verified and validated. The parameters in the script are changed to the proper parameters of the wing of the Arctitc Tern at 75% of the wing span. Furthermore, different altitudes and thus densities are considered, as well as different speeds. At 9 km altitude and at a cruising speed of 184 m/s, the flutter diagram which plots the fictitious damping versus the speed can be seen in figure 7.9.

An estimate for the flutter speed can be obtained by finding the roots of this graph [42]. Using interpolation it is found that for this particular case the flutter speed is equal to 638 m/s. The flutter speed for different speeds and altitudes can be seen in table 7.8.

Table 7.8: Flutter speeds at different flight conditions

	V [m/s]	Density [g/m^3]	Flutter speed [m/s]
Take off	63.0	1.225	432
Cruise at 8 km	178	0.525	618
Cruise at 9 km	184	0.466	638
Cruise at 10 km	180	0.412	682
Landing	61.8	1.225	432

From table 7.8 it can be seen that the flutter speed will be orders of magnitude larger than the speed at which the aircraft flies. This means that the aircraft will not experience flutter issues.

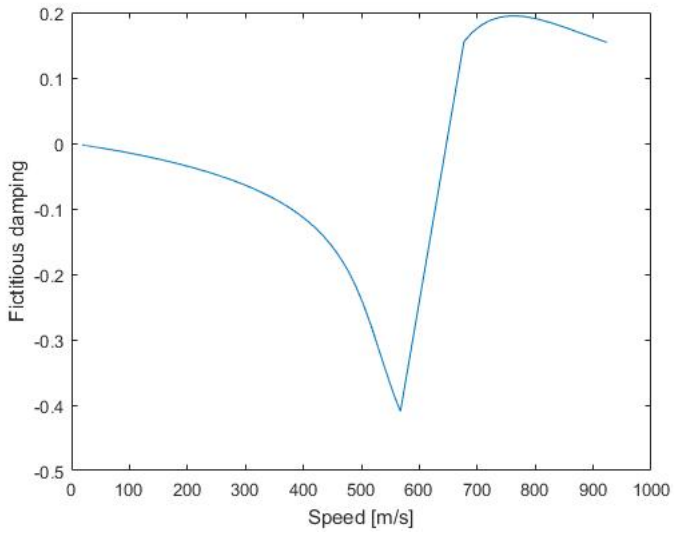

Figure 7.9: Flutter diagram in which the fictitious damping is plotted against the speed

7.5. Flight Profile Diagram

The composition of the flight profile can be seen below, in figure 7.10. For most of these sections, computer programs were written to assess the AT1's performance taking into account as much as possible. For each section, the program would estimate the time taken, fuel burnt, and distance covered. For some of the sections, however, fuel fractions taken from statistical data were used. These are: taxi, climb for loiter, descent for loiter, and taxi-in. The fuel fraction, distance covered, and time taken for each phase is shown in table 7.9.

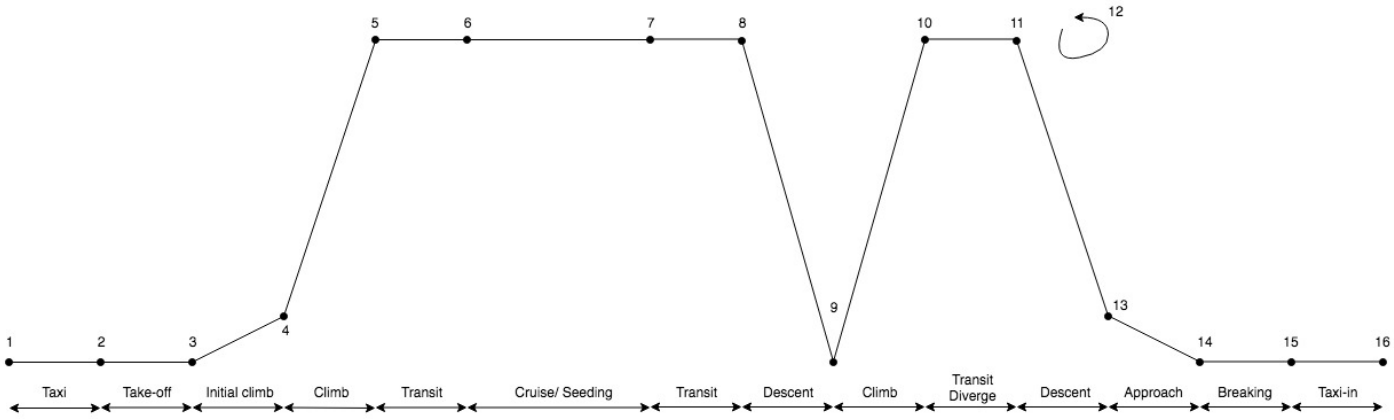

Figure 7.10: Flight Profile

7.6. Take-off

The take-off performance of the aircraft is investigated to ensure that the aircraft can operate at the chosen airports from section 4.2. The take-off performance is divided into the ground run phase and the airborne phase, which will be discussed below.

Ground run
Using static equilibrium and assuming a friction coefficient of 0.02, for asphalted runway [91], the take-off performance can be investigated. The average speed during take-off is assumed to be a function of the

Table 7.9: Breakdown of each phase of flight during the mission

Phase	Total mass at end of phase [kg]	Fuel fraction [-]	Distance covered [km]	Time taken [s]
Taxi	4237.98	0.980	-	-
Take-off	4233.75	0.999	1.25	36
Climb	4168.80	0.9846	123.9	697
Transit departure	4039.57	0.969	680	3690 (1.0 hr)
Seeding	1547.15	0.383	15827	85861 (23.9 hrs)
Transit return	1469.80	0.950	680	3690 (1.0 hr)
Descent	1468.18	0.999	152.3	993
Climb	1438.82	0.980	36.1	204
Transit diverge	1414.36	0.983	182.5	990 (17 mins)
Loiter	1407.28	0.995	111	600
Descent	1393.21	0.990	101.4	695
Landing	1391.82	0.999	0.296	6
Taxi	1380.68	0.992	-	-
Total	-	-	17191	27 hr 4 mins

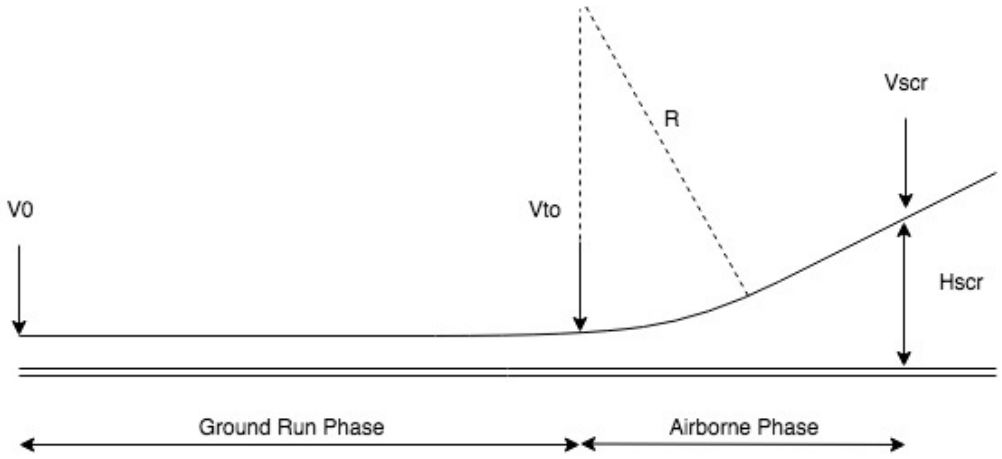

Figure 7.11: Take-off profile

take-off speed as shown in equation (7.11)

$$\bar{V}_{to} = \frac{V_{to}}{\sqrt{2}} \quad (7.11) \qquad V_{to} = 1.05 \cdot V_{stall} \quad (7.12)$$

This results in a take-off speed of approximately 63 m/s and an average speed during take-off of 44.55 m/s. Knowing the maximum take-off weight and assuming maximum thrust the acceleration and runway distance can be determined using equation (7.13) and equation (7.14).

$$\bar{a} = \frac{g_0}{MTOW} \cdot \mu \cdot (MTOW - L) \quad (7.13) \qquad s = \frac{V_{to}^2}{2\bar{a}} \quad (7.14)$$

This results in a ground run distance of approximately 1438.8 m using an acceleration of 1.38 m/s^2.

Airborne phase
The airborne consist of the transition phase which can be divided into the first transition phase and the second transition phase as can be seen in figure 7.11. The first transition phase follows a curve until the desired climb angle is reached, at which point the aircraft travels on a quasi-rectilinear path until the screen height is cleared. Calculating the radius of climb for the first transition phase, the horizontal distance can be determined using equation (7.15) and equation (7.16) for the first transition phase, resulting in 18.4 m.

$$R_{cl} = \frac{V_{to}^2}{(n \cdot T_0 \cdot g_0)} \quad (7.15) \qquad x_{trans_{tot}} = R_{cl} \cdot sin(\gamma_{cl}) + (h_{scr} - \frac{R_{cl} - R_{cl} \cdot cos(\gamma_{cl})}{tan(\gamma_{cl})} \quad (7.16)$$

The distance for the second transition phase is found by calculating the corresponding horizontal distance for the height gain required. This came to be 194 m. When summed with the distance of the first transition phase and the ground-run distance, the total take-off distance becomes 1260 m. This is significantly lower than the shortest runway length of the selected airports (2319m at Svalbard Airport, Longyear). The margin of safety is crucial considering the possibility for poor weather conditions at the selected airports.

7.7. Climb

The strategy for climbing will be to minimise fuel used. This is done by maintaining a constant indicated air speed (V_{IAS}) [92] while staying within the critical Mach limit. This results in flying at an indicated air speed of 180 m/s, until a 1km altitude at which point the aircraft flies just below the divergence mach number, at 0.55. The thrust, which decreases with altitude, will be at 90% of the maximum setting for the duration of climb. The relationship between thrust and altitude can be seen in equation (7.17). Using this relationship and derivations of the lift equation, drag polar, and flight conditions, the rate of climb can be found, as shown in equation (7.18).

$$Thrust = Thrust_0 \cdot \frac{p}{p_0} \cdot \sqrt{\frac{T_0}{T}} \quad (7.17) \qquad ROC = \frac{P_a - P_r}{W} = \frac{V(T - D)}{W}$$

The result is climb lasting just under 12 minutes, covering 124 km, and burning 66 kg of fuel. At the start of climb, the rate of climb is 22 m/s and the true air speed is 180 m/s. The climb rate decreases to 6 m/s at 8000 m altitude.

7.8. Turn

Turning performance is a key characteristic to fulfil the seeding requirements. The time it takes to make the turn, the bank angle, and the maximum load factor will be found as a function of the most stringent turn radius requirement and flight conditions.

The smallest possible turn radius for our mission is 5000m, since that is the distance the aircraft must turn if it wishes to seed a parallel path directly next to the path it has just seeded. For this to happen, the aircraft must turn with a bank angle of 30.5°, and it will take 3 minutes and 5 seconds. The load factor experienced during this turn will be 1.6. This is well within the maximum load factor of 2.6, and since there won't be a pilot or passengers on the aircraft, the amount of the g-force experienced during the turn is not significant.

7.9. Cruise

The cruise consist of three phases: The transit to the seeding area, the seeding, and the transit back to base. For the transit, the range is known and the fuel fraction can be calculated. Contrarily, for the seeding the fuel fraction is known and the range can be calculated. This section will present the two transit phases together in section 7.9.2 and the seeding phase in section 7.9.3.

7.9.1. Lift over drag during cruise

The CCT Arctic Tern will cruise with constant speed, and as such its lift coefficient and lift over drag will change during cruise. To calculate the fuel fractions of the transit range and the range for the seeding phase, the mean lift-over-drag has to be found for each phase. The mean of the lift-over-drag can be determined with equation (7.19), assuming a parabolic drag polar.

$$\overline{\frac{L}{D}} = \frac{1}{C_{L_{end}} - C_{L_{start}}} \int_{C_{L_{start}}}^{C_{L_{end}}} \frac{L}{D} dC_L = \int_{C_{L_{start}}}^{C_{L_{end}}} \frac{C_L}{C_{D_0} + kC_L^2} dC_L = \frac{1}{2k(C_{L_{end}} - C_{L_{start}})} ln\left(\frac{C_{D_0} + kC_{L_{end}}^2}{C_{D_0} + kC_{L_{start}}^2}\right) \quad (7.19)$$

In this equation, $\overline{\frac{L}{D}}$ is the mean lift-over-drag. If the aircraft flies with MTOW, a mean L/D of 20.6 is calculated.

7.9.2. Transit cruise

The fuel fraction of the transit cruise can be calculated with the Brequet range equation for jet aircraft as displayed in equation (7.20). [45]

$$R = \frac{V_{cruise}}{g \cdot SFC} \overline{\frac{L}{D}} ln\left(\frac{W_{initial}}{W_{final}}\right) \quad (7.20)$$

In this equation, R is the range and V_{cruise} is the cruise speed. The transit range for each base can be found from the distance to the seeding area for each airport as presented in table 7.10.

Table 7.10: Distance to seeding area for each airport

Airport	Distance to seeding area
Ushuaia	669 km
Christchurch	1895 km
Svalbard/Thule	0 km

The fuel fractions for the transit cruise can then be calculated for each base location with equation (7.20).

7.9.3. Seeding cruise

During seeding cruise, the payload mass depletes. To account for the depleting mass in the range equation, the Brequet range equation with depleting payload mass has to be derived.

Depleting payload mass range equation derivation The depletion of the aircraft weight during cruise is described by the differential equation shown in equation (7.21). Using the fact that during cruise the aircraft performs a steady, straight, level, and symmetric flight, the fuel mass flow can be rewritten as in equation (7.22).

$$\frac{dW}{dt} = -g\dot{m}_F - g\dot{m}_{PL} \quad (7.21) \qquad \dot{m}_F = T \cdot SFC = D \cdot SFC = \frac{W \cdot SFC}{\frac{L}{D}} \quad (7.22)$$

Substituting the equation (7.22) in equation (7.21) yields the first-order non-homogeneous linear differential equation as displayed in equation (7.23).

$$\frac{dW}{dt} = -\frac{g \cdot SFC}{\frac{L}{D}} w - g\dot{m}_{PL} \tag{7.23}$$

Solving this differential equation with the initial condition of $W = W_{initial}$ yields equation (7.24).

$$W(t) = \dot{m}_{PL} \frac{L}{D} \frac{1}{g \cdot SFC} \left(1 - e^{-\frac{g \cdot SFC}{\frac{L}{D}} t}\right) + W_{initial} e^{-\frac{g \cdot SFC}{\frac{L}{D}} t} \tag{7.24}$$

Rewriting equation (7.24) for t and multiplying with the cruise velocity yields the final range equation with depleting payload mass and is displayed in equation (7.25).

$$R = \frac{V}{SFC \cdot g} \frac{\overline{L}}{D} ln\left(\frac{W_{initial} + \dot{m}_{PL} \frac{\overline{L}}{D} \frac{1}{SFC \cdot g}}{W_{final} + \dot{m}_{PL} \frac{\overline{L}}{D} \frac{1}{SFC \cdot g}}\right) \tag{7.25}$$

The final weight and initial weight are known of this phase as they can be calculated with the fuel fractions of the other mission phases, assuming MTOW at the start of the mission and OEW at the end of the mission. The payload mass flow rate is dependant on the speed, required seeding concentration, and dispersion characteristics and is constant during the mission.

7.9.4. Total Range Analysis

Using the calculated fuel fractions for transit cruise and the fuel fractions for each phase without cruise, the total range of the aircraft can be analysed.

As the payload mass flow rate is a constant, the payload weight that should be brought aboard should be directly coupled to the required fuel weight to have enough seeding range to inject all the payload. If these two are coupled, the payload and fuel reserved for seeding cruise will be depleted at the same time and will yield the most optimum performance. Furthermore, for every mission either the payload tank or fuel tank will be filled up to get the most out of the aircraft's capability and to minimise the fleet size.

Considering the maximum take-off weight and the maximum payload and fuel volumes, the payload weight, fuel weight and total range can be calculated for different scenarios. The range performance will be calculated for the following scenarios:

- Initial and refreshing seeding concentrations.
- Operations from Ushuaia, Christchurch, and Svalbard/Thule.
- Cruising altitude at 8, 9, and 10 km.
- Hemisphere migration with zero payload weight.

The first scenario that will be evaluated is the most critical one. The most critical scenario is expected to

happen at a cruising altitude at 8 km, departure from Christchurch and with the initial seeding concentration. The same scenario is evaluated for Ushuaia and Svalbard/Thule in the northern hemisphere. The results for this scenario are displayed in table 7.11. Finally, the most generic scenario of a seeding altitude of 9 km, departure from Ushuaia and a refreshing concentration has been analysed.

Table 7.11: Cruise Scenario

No	Scenario	Payload Weight	Fuel Weight	Total Transit Range	Seeding Range	Total Range
1	-Initial concentration -8 km altitude -Christchurch departure	292 kg	2650 kg (Maximum)	3800 km	12320 km	16120 km
2	-Initial concentration -8 km altitude -Ushuaia departure	296 kg (Maximum)	2258 kg	1380 km	12495 km	13855 km
3	-Initial concentration -8 km altitude -Northern hemisphere (Svalbard/Thule)	296 kg (Maximum)	2038 kg	0 km	12492 km	12492 km
4	-Refreshing concentration -9 km altitude -Ushuaia departure	281 kg	2650 kg (Maximum)	1380 km	15773 km	17133 km
5	-Hemisphere migration	0 kg	2650 kg (Maximum)	19013 km	-	19013 km

Scenario 1: It can be seen that the aircraft fuel tanks are filled up till the maximum and that the payload weight is also almost at its maximum, which is making most use of the maximum take-off weight and therefore efficient. The total range also exceeds the minimum range to reach all points within the seeding area.

Scenario 2: In scenario 2, the transit range becomes much less than scenario 1. The reduction in transit range allows for more seeding range and therefore more payload weight can be brought along. The increased payload weight increases the required seeding range but its increase is smaller than the decrease in transit range. Therefore, the fuel brought along is less than in scenario 1.

The total range is seen to be less than 14000 km, the range required to reach all points within the seeding area. This can simply be resolved by bringing more fuel and practically increasing your transit range. The downside of this solution is the fact that the aircraft will fly the first kilometres in the seeding area without seeding, which is not as efficient as when the aircraft immediately starts seeding once it enters the seeding area. However, this is only for the initial seeding phase.

Scenario 3: This scenario is limited by its maximum payload carrying capability just as for scenario 2. There is no fuel required for transit as the airport location is already in the seeding area. The total range of 12492 km is enough to reach all points within the seeding area, as such it can always seed while flying through the seeding area, which is optimum.

Scenario 4: In scenario 4, the fuel is maxed out and its payload weight is also close to the maximum. The seeding range is almost 16000 km and this scenario therefore allows for a very efficient flight, as it can cover a lot of seeding area with one sortie.

Scenario 5: For the hemisphere migration, the range of the aircraft with zero payload weight and maximum fuel weight, the ferry range, is analysed. The maximum distance between the airports is between Christchurch and Svalbard with a distance of 16128 km. The total range of the aircraft is determined to be 19013 km which is more than enough to migrate from the northern hemisphere to the southern hemisphere, and vice-versa, in one flight.

7.10. Descent

Descent is conducted at a constant glide angle, 3°, chosen to minimise fuel spent and maximise horizontal distance travelled. Much like the climb calculations, the aircraft will be flying at a constant indicated airspeed or at the critical Mach number, which ever is lower. Once the speed is known for a given altitude, the rate of climb can be calculated in order to maintain the same glide angle. Using the rate of climb and velocity, the required thrust can be found, which indicates the fuel burnt. The AT1 will burn 1.5 kg of fuel to descend from the lowest level of seeding to the start of the landing phase, travelling a distance of 101.6 km in the process.

7.11. Diversion

The aircraft should be able to divert to another airport in case the weather at one of the airports is too severe to allow a safe landing. Furthermore, there may not be space for the aircraft to land as soon as it arrives at the airport, so it will then have to loiter above the airport. The limiting factor for the diversion is the distance between the two airports, assuming the aircraft does not know it has to land at the other airport until it reaches the airport with poor weather. This distance was taken to be 320 km. This is not the distance to the other operational base, but rather, to another usable airport. Airports near each operational base were evaluated on their ability to receive diverted AT1 aircraft, and one was selected for each base. This is further explained in subsection 4.2.4.

The loiter phase is limited by having to be in the air an additional 600 seconds. To calculate the ascent and descent from the diversion and loiter altitude, the same programs used in section 7.7 and section 7.10 were used. The distance that was travelled in these two phases were taken away from the required 320 km diversion range. The results for this can be seen in table 7.9.

7.12. Landing

The landing phase begins at the screen height, travelling just above the stall speed with the maximum lift devices applied. The most important aspect of the landing phase that must be evaluated is the total landing distance. The shortest runway length is found at at Svalbard Airport, Longyear, with a length of 2319m. All airports will experience poor weather conditions, so a safety factor must be applied.

Much like the take-off analysis, the landing can be split into two phases, airborne phase and ground run. The airborne phase corresponds to the transition from screen height to touch-down. This takes 2.5 s and covers a distance of 156 m. The other phase is the ground run, for which aircraft mass and friction between the runway and wheels are deciding factors. Assuming a coefficient of friction of 0.02, which is standard for asphalt runways in good conditions [93]. This results in a braking distance of 140.3 m. The two phases combined result in a total distance of 296.3 m, time of 5.7 s, and fuel burn of 0.0126 kg.

7.13. Altitude Envelope

The altitude envelope gives insight in the flight envelope regarding the minimum and maximum speed for every altitude. The altitude envelope encompasses three constraints: the stall speed, the maximum speed due to thrust required or drag divergence, and the service ceiling.

7.13.1. Stall speed with altitude

The stall speed is calculated with equation (7.26) for different densities related to the different altitudes.

$$V_{stall} = \sqrt{\frac{2W}{C_{L_{max}} \rho S}} \tag{7.26}$$

The maximum lift coefficient for a clean configuration is used, furthermore the MTOW is used as weight.

7.13.2. Maximum speed with altitude

The maximum speed is either constrained by the maximum thrust at given altitudes or by the drag divergence mach number. For the CCT Arctic Tern it was found that the maximum speed is only constrained by the drag divergence number for each altitude within the envelop. The maximum speed due to the drag divergence mach is given by equation (7.27).

$$V_{max,dd} = M_{dd}a = M_{dd}\sqrt{\gamma RT} \tag{7.27}$$

In this equation, $V_{max,dd}$ is the maximum speed due to the drag divergence limit, M_{dd} is the drag divergence mach number, a is the speed of sound, γ is the specific heat ratio, R is the specific gas constant for air, T is the International Standard Atmosphere (ISA) temperature at the respective altitude.

7.13.3. Service ceiling

The service ceiling is identified to be the altitude for which the rate of climb is 500 feet per minute [29]. The service ceiling can then be found by solving equation (7.28) for different speeds.

$$P_a - P_r = ROC_{sc}W \tag{7.28}$$

In this equation, P_a is the available power, P_r is the required power, and ROC_{sc} is the rate of climb at the service ceiling and equal to 500 feet per minute. The post-climb weight is chosen for the service ceiling equations.

7.13.4. Altitude envelope plot

The constraints are plotted against altitude and speed to generate the altitude envelope. The altitude envelope is plotted and can be seen in figure 7.12.

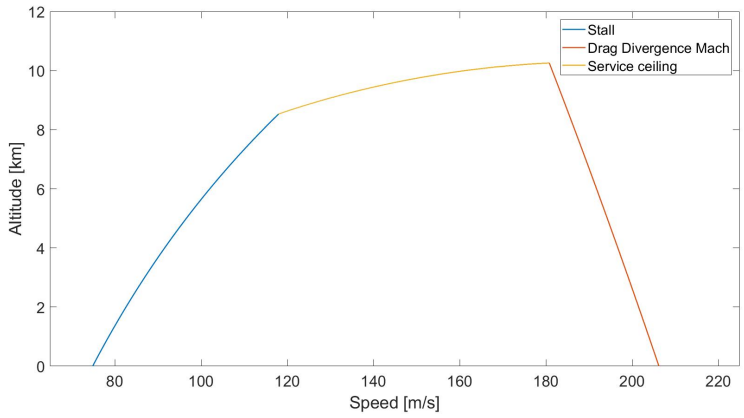

Figure 7.12: Altitude envelope of the AT1 aircraft.

It can be seen that the service ceiling exceeds 10 kilometres altitude at the maximum speed, which is the required altitude as this is the height of the tropopause above 60 degrees latitude [40].

7.14. All Weather Operations

The ACT system has to be all weather operational. Therefore, multiple measures have been taken to ensure this requirement is met. The CCT Arctic Tern will be equipped to operate through most foreseeable weather scenarios. When the weather conditions will be to extreme to design for, however, the fleet redundancy will ensure the system performs as prescribed.

Low temperature operations

The aircraft was designed to withstand temperatures down to -65°C. Some aircraft systems therefore required heating. The avionics, electrical equipment and fuel must remain operational during the entire flight. The avionics and electrical components can only be used when the temperature is higher than -40°C. The fuel that is used is jet B fuel, as it has a low freezing temperature of -60°C. So, the aircraft cabin must be warmer than -40°C at all times. As the minimum temperatures might reach -65°C, the aircraft must be heated to remain operational.

In section 5.5.1 it was determined that air is bled from the engine. This air has a temperature of 578 K and should be cooled down 250 K in order to not exceed the maximum allowable temperature of the payload combustion chamber after combustion has taken place. The cooling of this air can be used to heat the fuselage. For this process a heat exchanger will be used which transports heat from the bled air to air in the fuselage. This is in essence an air conditioner which cools down the air and in the process heats up the air of the fuselage, as the exhaust of the conditioner blows hot air into the fuselage. To ensure that the fuselage is well isolated, the inside of the fuselage should be covered with an isolating layer. Many companies develop complex heat exchangers, of which one is MSM Aerospace Fabricators. They produce heat exchangers which can heat up aircraft cabins using bled air[3]. In a later design stage the company shall be involved in the design process to design a heat exchanger which is able to heat up the cabin to at least -30°C and cool the air required for combustion of the payload so the aircraft will remain operational at all expected temperatures during flight.

Low visibility operations

The visibility approach during landing will be explained in control and communications in section 8.3.2.

Cross-wind operations

The maximum cross wind component the aircraft was designed for is 20 m/s. It has to be noted however, that this will have to be demonstrated by the aircraft during flight testing.

Icing conditions

Since the fleet will operate during the winter months at high latitudes it is expected that icing conditions are expected on ground and during flight. Anti-ice systems were included into the preliminary aircraft design to protect the CCT Arctic Tern from ice build-up.

Ice formation is mostly accumulated on the wings, especially on the leading edge. This influences the wing profile and thus affects the lift performance of the wing. This should be avoided since this lowers the stall speed and could cause dangerous scenarios which can potentially lead to loss of aircraft. For this reason, a de-icing system is required. For this choice, different possibilities are researched. The three main de-icing methods will be briefly described now. First, ice can be removed by pneumatic de-icing boots [39]. They consist of a rubber layer which is mostly located on the aircraft's leading edge of the wing and horizontal stabilisers. When ice has formed on the leading edge, the rubber inflates and expands which causes the ice to be released from the wing. The second option is using an electro-thermal system [32]. A current is applied

[3]Retrieved from: http://www.msm-aero.com/products/head_exchanger_pipes/ [23/06/18]

through a resistive circuit in an air frame structure which results in heat generation and the ice will melt. This can be applied continuously or only when ice forming has been observed. Thirdly, bleed air from the engine can be used [32]. The hot air is blown through the wing after which it is exhausted through the lower surface of the horizontal stabilisers and wings.

The last option will not be utilised since the bleed air is almost entirely utilised by the payload combustion chamber as was determined in section 5.4.2. The first option which considers de-icing boots has the advantage that it is easy to implement. However, it has the risk of ice forming behind the boot and the aerodynamic behaviour changes when the boot is inflated [39]. The second option which uses an electro-thermal system has the advantage that de-icing can be performed over the entire wing and not only the leading edge. Furthermore, as the wing of AT1 is made of carbon fibre reinforced plastic, this can be used to integrate the electro-thermal system inside the skin since it has high electrical resistance. This was also done for the wing of the Boeing 787 Dreamliner[4]. Because of this advantage and boots only being able to be implemented at the leading edge, an electro-thermal system will be implemented in the Arctic Tern for de-icing purposes. The system of the Boeing 787 Dreamliner requires a power supply of 3.61 kW/m^2 [57]. Since this is rather high, the de-icing system will not be active at all times, only when ice is forming.

Before take-off during the turn around time, the aircraft should be de-iced as well if ice is present. This is also stated in section 4.3.1. It will consist of spraying the aircraft with propylene glycol before take-off. This substance is widely used by airliners as well. Therefore, the same procedures will be performed for the AT1 as for airliners concerning propylene glycol.

Fleet redundancy

If all aircraft design considerations taken still prove insufficient there is redundancy in operations. The ACT system is designed in such a way that the fleet can be grounded for up to 2 days every 9 days with no visible impact on the seeding quality. Moreover, the fact that the operations will be carried out from 2 bases simultaneously and the aircraft is designed to be able to change the base location in one flight gives system ability to only operate from the base with less severe weather conditions.

[4]Retrieved from: http://www.boeing.com/commercial/aeromagazine/articles/qtr_4_07/article_02_4.html [25/06/18]

8 Communication and Navigation

This chapter elaborates on the communications and navigation systems needed for the AT1. As the aircraft is an unmanned aerial vehicle the communication system is an important aspect for the mission. This includes a navigation system and flight data recorder which can be found in section 8.1. For safety, an in-air collision avoidance system is also included in the communication system, which is discussed in section 8.2. The control of the aircraft is discussed in section 8.3, followed by the line of sight control and beyond line of sight control in section 8.4 and section 8.5 respectively.

8.1. Navigation System and Flight Data Recorder

To be able to determine the drift free long-term stability of the aircraft, a navigation system is needed. Global Navigation Satellite Systems (GNSS) are commonly used to navigate around the world. Since these systems have an inclination around 55° for GPS and Galileo, and 65° for GLONASS, the systems are not predominately focused on the poles and are therefore less accurate at high latitudes. However they will still be able to operate [89]. For the Galileo system, the probability that at any given time at any given place on Earth there are at least 4 satellites in sight is over 90%.[1] This will result in sufficient accuracy to determine the location of the plane.

Besides a GNSS system the aircraft is equipped with an Inertial Navigation System (INS) to determine the aircraft's position, velocity, and attitude. To be able to do so accurately, a complete 6-degree of freedom inertial sensor consisting of 3-axis accelerometers and 3-axis gyros is required. INS will also be used as back-up of the GNSS system if there are not enough GNSS satellites in sight. Another benefit of the INS system is that it is able to compensate for the relatively low update frequency of GNSS.

The selected device to perform these operations is the LaserefVI micro IRS from Honeywell Aerospace. This system is proven to work on large airliners like the Boeing 787 as well as small aircraft like the PC-21 and various helicopters. With a size of only 165x163x163mm and a total weight of 4218g, it is ideal for this design since it is industry's smallest and lightest package.[2]

The flight data recorder chosen for the mission is the Curtiss-Wright Fortress OEM. It is a compact lightweight flight data recorder of 3.7kg designed to be able to withstand a crash.[3] It is equipped with a 90 day Ultrasonic Locator Beacon to TSO-C121. Therefore the recorder can be located for up to 90 days after the crash.

8.2. Collision Avoidance System

The UAV should be equipped with an in-air collision avoidance system. Many aircraft are operating in the same area simultaneously, therefore it is important that the aircraft are spaced sufficiently to avoid wake interference and potential collision. An onboard system has been tested on the Barracuda Unmanned Aerial System (UAS) demonstrator in July 2010 by Air4All [6]. Since collision avoidance capability is only required in the A-C airspace classes, the TCAS II system is considered a suitable technology. The cooperative collision avoidance system will include an 'opt out' logic. This enables the ground-based pilot to input another manoeuvre than the TCAS system advises for the autopilot, ensuring safety when interaction with a commercial aircraft occurs. Independent of the data link availability, the system has full authority to execute the TCAS II defined avoidance manoeuvres. However, in case of data link availability, the ground operator has the ability to override this

[1] Retrieved from: https://www.esa.int/Our_Activities/Navigation/Galileo/Galileo_a_constellation_of_navigation_satellites [05/06/2018]
[2] Retrieved from: https://aerospace.honeywell.com/en/ /media/aerospace/files/datasheet/laservi-productdescription.pdf [05/06/2018]
[3] Retrieved from: https://www.curtisswrightds.com/products/electronic-systems/crash-protected-recorders/fortress-oem.html#tabbed-table1 [24/06/2018]

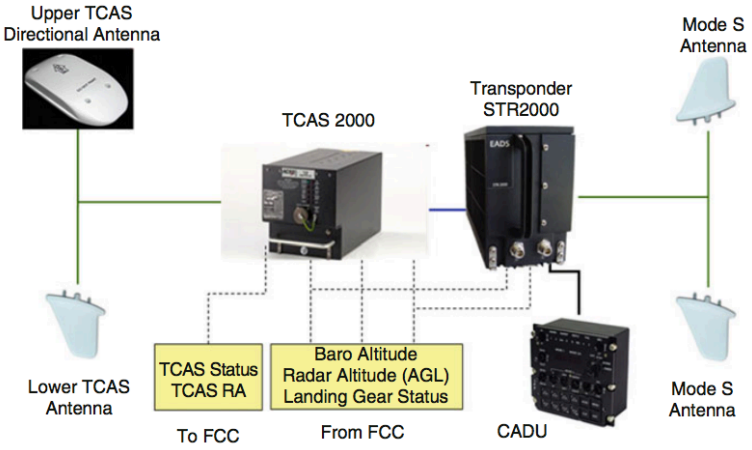

Figure 8.1: System Architecture of cooperative collision avoidance system

automatic execution and input alternative commands. This is necessary in case the aircraft flies in the airspace of a commercial aircraft for example. This specific system has been tested on the UAS, and consists of several elements shown in figure 8.1.

In figure 8.1 the interaction of the different elements in the cooperative collision avoidance system is represented. On the left a TCAS directional antenna is shown which is mounted on the top of the UAV. Other traffic is typically shown in a limit to a vertical volume of ±2,700 ft. As the autopilot assigned for the avoidance manoeuvre is far more accurate than a pilot could execute it, the manoeuvre is carried out in less time and more accurately, reducing the vertical and/or lateral deviation from the predetermined trajectory. Furthermore, in a crowded airspace the precise execution of the autopilot reduces the risk of new collision threats caused by the manoeuvre. The airborne collision avoidance system (ACAS) risk ratio is calculated using equation (8.1), the risk ratio is 0.18 when the intruder is not ACAS equipped, 0.32 when the intruder is equipped but not responding and 0.04 when the intruder is equipped and responds. [28]

$$\text{ACAS Risk Ratio} = \frac{\sum \text{probability of a collision with ACAS installed}}{\sum \text{probability of collision without ACAS installed}} \tag{8.1}$$

8.2.1. Emergency Locator Transmitter

The single fleet elements will be equipped with an emergency locator transmitter (ELT). This is a battery powered transmitter which is activated when high G-forces occur, for example during a crash. Every 50 seconds a digital signal is transmitted with a frequency of 406.025 MHz at 5 watts for at least 24 hours. This signal is received anywhere in the world by satellites in the COSPAS-SARSAT satellite system. [4] This system makes use of both LEOSATs and GEOSATs, the signal is partially stored in the satellites and then sent to ground stations known as local user terminals (LUTs). Here, the signal from the satellites is deciphered and a retrieval plan can be put in place.

The emergency locator transmitter mass is approximately 907.2 g and has dimensions of 13.97 x 9.65 x 8.63 cm. The ELT system can only last for 6 years [5] so it should be replaced after this time, this is included in the maintenance schedule introduced in chapter 9. Also, the operating temperature is between -20 $^{\circ}C$ and 55 $^{\circ}C$, this could cause a problem as the north and south pole have temperatures outside of this range, however the emergency locator beacon is expected to function properly for the first couple of hours, in which the aircraft can be located, storing the location of the emergency signal.

[4] Retrieved from: https://www.faa.gov/regulations_policies/handbooks_manuals/aircraft/amt_airframe_handbook/media/ama_Ch11.pdf [04/06/2018]
[5] Retrieved from: https://www.dallasavionics.com/artex/elt3000_spec.pdf [04/06/2018]

8.3. Control and Communications

For Unmanned Aerial Systems (UAS) especially, the design of the control and communications system is very important. In order to design the C&C system, first the pilot involvement was identified. [37]

The fact that an Unmanned Aircraft (UA) has no pilot on board does not mean that no pilot is involved in the control of the aircraft. In fact some UAs have multiple pilots controlling a single UA. Three levels of pilot involvement can be identified.

Pilot in the loop control In Pilot-in-the-loop control the pilot is part of the control loop. This means that the pilot receives the information on the required flight path and current condition of the aircraft. The pilot then controls the aircraft as if he or she is in the cockpit. This method requires at least one pilot per UA.

Pilot on the loop control Pilot-on-the-loop is most similar to a conventional aircraft flying on autopilot. The aircraft is flying autonomously but its state is monitored by the pilot. This level of control allows for one pilot to control/monitor multiple UAs at the same time.

Autonomous control In fully autonomous control there is no pilot involvement. The aircraft flies completely autonomously without pilot interaction or monitoring. The UA knows the required flight path and then determines the required control actions.

The control of ACT will use all three levels of pilot involvement. The amount of pilots is minimised in order to keep the cost as low as possible while maintaining a good level of safety. In order to analyse the required pilot involvement the mission is split into three different parts, the take-off and landing part, the cruise part and the seeding part. Furthermore, a loss of communication situation can occur for which a handling strategy has to be established. During take-off and landing, pilot-on-the-loop will be used as much as possible, where the regulations and weather allow it. Whenever pilot-on-the-loop is not possible, pilot-in-the-loop will be used during take-off and landing. During cruise and seeding, pilot-on-the-loop will be used to control the UAs, this allows for one pilot to monitor multiple UAs, minimising the amount of pilots while assuring the mission is performed correctly and safely. During emergency situations such as possible collisions or system malfunctions during cruise or seeding the UAs will switch to pilot-in-the-loop momentarily until the crisis is averted. Lastly, if communication with a UA is lost the aircraft will operate in a safe mode, in this safe mode the aircraft will continue its mission fully autonomously while trying to reconnect to the ground-station. If the UA is unable to reconnect but has finished its seeding mission it will return to base where it will try to reconnect using the LOS communications. If this is also not possible the aircraft will land fully autonomously in an area away from the airport to ensure the safety of the airport personnel as well as the runway.

8.3.1. Data-rate analysis

The data which will be sent and received by the UAs consists of the Control and Non-Payload Communications (CNPC) and the payload control and communication (C&C). This section analyses the data-rates required for these two types of communication. After the total required data-rate is determined the required data-rate for the Line Of Sight and Beyond Line Of Sight system are determined.

Control and Non-Payload Communications The CNPC data-rate was estimated using statistical data[37]. The CNPC consists of the Control, Navigation aids, ATC voice and Data, Target avoidance/tracking, airborne weather radar and video. Their values are presented in table 8.1. The data-rate of video in *Handbook for unmanned aerial vehicles*[37] was determined to be too low, therefore a more realistic calculation of the required data-rate for video was made.

Payload In surveillance aircraft such as the Global Hawk, the payload takes up most of the communications data-rate[6]. However, for the CCT Arctic Tern this will not be the case since it will not have any high definition surveillance footage. The data from the payload consists mostly of the measurements on the IN concentration and particle size mentioned in section 5.6. These values will be updated at a rate of 10Hz. Other parameters were determined to be the rate at which the payload is used, the current storage of payload and some pa-

[6]something about the global hawk

rameters on the combustion's on the payload. Assuming these values would fit in 16-bit floats the down-link data-rate was calculated to be 960 bps. The up-link data-rate consists only of the control parameters of the payload combustion, it was calculated to be 320 bps.

Table 8.1: Estimated required data-rates during operations in bps

Data source	Up-link	Down-link	Transmission
Payload	320	960	BLOS
Control (manual)	4600	7600	LOS/BLOS
Control (autonomous)	440	650	BLOS
Navaids	670	1100	LOS/BLOS
ATC voice	4800	4800	LOS
ATC Data	50	60	LOS
Target tracks		9100	LOS/BLOS
Airborne weather radar		8700	LOS/BLOS
Video		7000000	LOS
LOS total	10120	7031360	-
BLOS total	5590	27460	-

8.3.2. Low visibility landings

The aircraft has to be all weather operational, therefore the aircraft shall be able to both take off and land in low visibility. For conventional aircraft, procedures are in place to ensure safety of the crew and passengers[7]. These procedures are in place for two reasons: the aircraft should be visible to other aircraft and ground personnel and the pilot should be able to see the landing strip clearly. In order to make the aircraft visible the aircraft will be fitted with light on the wings and fuselage to ensure its visibility.

To make sure the aircraft is able to land in low visibility, the aircraft will use a combination of ILS (Instrument landing system), GPS and INS (Inertial Navigation System). And in case those fail infra-red imaging and computer vision based on Wang Xiao-hong [96] can be used as a means of redundancy. ILS and GPS will be used to determine the glide-slope to the landing strip. Once the UA is sufficiently close to the landing strip the INS combined with GPS will be used for the final phase of the landing. In case Either one of these fails the infra-red system will perform the last phase of the landing. The combination of ILS, GPS and INS is relatively conventional while and therefore need minimal adjustments to protocol and the airports in order to be implemented.

The infra-red system is more unconventional and therefore some small aircraft and airport adjustments are needed. The aircraft will be fitted with an infrared camera and the landing strips will be fitted with so called cooperative objects[96]. The aircraft will be able to land fully autonomously with a pilot on the loop and also with a pilot in the loop by transmitting the Infra-red images to the ground-station. This way the aircraft will still be able to land even if LOS communications are lost temporarily.

8.4. LOS Communications Design

Since the aircraft will only be controlled by a pilot on take-off and landing this is the only time that it is in the line of sight. To be able to perform the landing the aircraft must be able to land with ILS. For the selected airports this results in the need to have the following ILS receivers. For both the localiser and the glide-path slope, frequency receivers with a range of 90-150Hz are required. Also a marker beacon receiver will be added with a frequency range of 400-3000Hz. To be able to communicate with the airfield there must also be a radio on board. This radio must at least be able to transmit and receive on frequencies of 118.1-134.1Hz as this is the frequency range of the various airports.[8] For the pilot being able to land the aircraft there is, besides the aforementioned systems, also a high definition video feed required to have a visual on the take-off and

[7] Retrieved from: https://www.skybrary.aero/index.php/Low_Visibility_Procedures_(LVP) [25-06-2018]
[8] Retrieved from: apxp.info [06/06/2018]

landing procedure. Since the landing procedures are quite straightforward not the most high-end technology is required for this. The chosen resolution is therefore regular high-definition of 720p with a frame rate of 60fps. The screen dimensions are 16:9. This results in a required data flow from the aircraft to the ground station of 7Mb/s. This is higher than a 3g data connection is able to handle, but would be perfect for a 4g data connection.

8.5. BLOS Communications Design

The operational area of the aircraft is very remote, especially in the North and South-pole. The communication with the UA will use Beyond Line Of Sight communication or Satcom. This means that the communications will go through a network of in orbit sattelites. Section 8.5.1 discusses these different satellite systems and selects the most useful one.

8.5.1. Satcom System Selection

A number of these satellite systems are operational, each with their own advantages and disadvantages. The analysis for the possible systems is shown below along with the final decision of the most suitable system for the mission.

Geostationary Ka/Ku band satellites Most military UAS's use geostationary satellites communicating on the Ka or Ku frequancy band for BLOS data transfer. The advantages of these systems are the high data-rate which are possible due to the high frequencies used and Geostationary nature of the satellites makes the pointing of an antenna towards the satellite fairly straightforward. These systems also have their drawbacks, Geostationary Sat's can only orbit around the equator. Their coverage at the poles is therefore extremely poor which excludes them as an option for ACT.

Inmarsat Inmarsat is a system of satellites which are also in geostationary orbits using the L-band frequency to communicate to ground. Their Geostationary orbits again gives them poor coverage, as shown in figure 8.2(a), which makes them in-feasible for use in ACT.

Iridium Iridium is a system of satellites in a lower Earth orbit with an inclination of 86.4°, communicating on L-band frequencies. These satellites have excellent coverage of the Earth, especially at the poles where the orbits overlap. The coverage of the Iridium system is given in figure 8.2(b). A drawback of the Iridium system is however that the LEO orbit makes the satellites fly over relatively quickly making the pointing of an antenna directly at the satellite very challenging. This problem can however be solved by changing the type of antenna used by the aircraft. Another drawback of Iridium is the limited data-rate it can supply, this is however not a problem due to the low bit-rate required for BLOS communications.

Leosat Leosat is a system very similar to Iridium in coverage but promising higher data-rates due to the usage of the Ka frequency band. This system is however not operational at the time of this report and is therefore not considered in the design but it seems very promising for future design iterations.

From the different options which were analysed Iridium is the best option and is therefore the system which will be used for BLOS communications.

8.5.2. Antenna design

In many UAVs, such as the Global Hawk, Reaper, Predator, etc., the antenna dish is fairly large and requires a bulge on the front of the fuselage. To determine whether the CCT Arctic Tern will also have such a bulge, the antenna to be used needs to be determined. First the type of antenna that will be used need to be determined. The types of antenna that are considered are a parabolic, horn and helical antennas.

Parabolic Antenna Parabolic antennas typically have very high gain which allows for fast data-rates with little transmitter power. However they also require very high pointing accuracy's to achieve this high gain.[12]

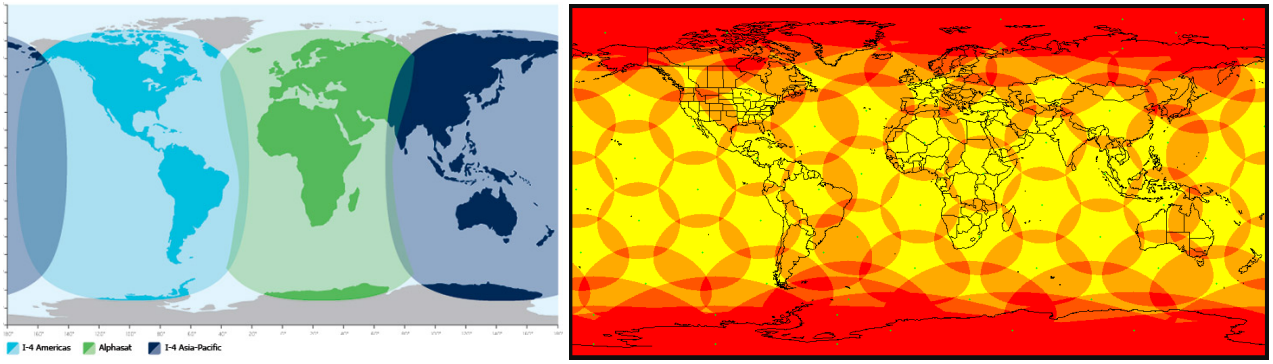

(a) Coverage of the geostationary (Inmarsat) satellites [9]

(b) Coverage of the Iridium satellite constellation (red is covered more than once)[11]

Figure 8.2: Satellite coverage

Since the Iridium satellites fly over at extremely high speeds a high pointing accuracy is hard to achieve and will require a large space in the aircraft to point the dish. Due to the difficulty of requiring a very high pointing accuracy, parabolic antenna's are deemed unfeasible.

Horn Antenna Horn antenna's generally have lower gains than parabolic antenna's but still in the order of 5 - 10 dB. They are, however, also still very directional which again causes issues with the pointing accuracy.[12] They are therefore also deemed unfeasible for use in the CCT Arctic Tern.

Helix Antenna Helical antenna's typically have a low gain in the order of 0 dB in the normal direction to helix and 10 dB in the axial direction. The greatest advantage of helix antenna is the almost unidirectional nature of the signal.[12] Helix antenna's therefore require very small pointing accuracy's and are therefore very useful in the CCT Arctic Tern. The lower gain does limit the data-rate which can be transmitted but this is not an issue for the low requirements for BLOS communications.

Off-the-shelf Iridium transceivers Iridium offers some off-the-shelf transceivers which can work with their system[12]. These transceivers can offer very quick implementation and a very small form factor in the order of centimetres. Some of these systems, such as the *ICG NxtLink ICS-400*[13] can offer data-rates of up to 80 kbps which would be sufficient for use in the Arctic Tern.

8.6. Communication System Integration

The integration of the navigation, communication and payload command system is visualised in the communication flow diagram in figure 8.3. The different segments of the system can be distinguished by their different colours. The options for communication LOS and BLOS are also made visible with an OR function in the loop. The diagram shows the inputs from the environment and the different sensors and transmitters in the communication flow. The latency in the BLOS system is 1.76s on average[54] and at most 20 seconds.[14]. This is sufficient for monitoring the fleet but it should be investigated whether this is also sufficient for the collision avoidance systems.

The payload sensors measure the current density of IN at the location of the aircraft, this information is combined with weather prediction to decide on a dispersion and flight plan. The plan is then transmitted back to the aircraft where the payload dynamics system steers the dispersion of the IN. This data handling process is shown in figure 8.4. The figures used the some colour scheme as figure 8.3, the data transmitted is shown in the white boxes.

[12]Retrieved from: https://www.iridium.com/products [07-06-2018]
[13]Retrieved from: https://www.iridium.com/products/icg-nxtlink-ics-400-aviation/ [07-06-2018]
[14]Retrieved from: https://www.iridium.com/download/?dlm-dp-dl=24127 [21-06-2018]

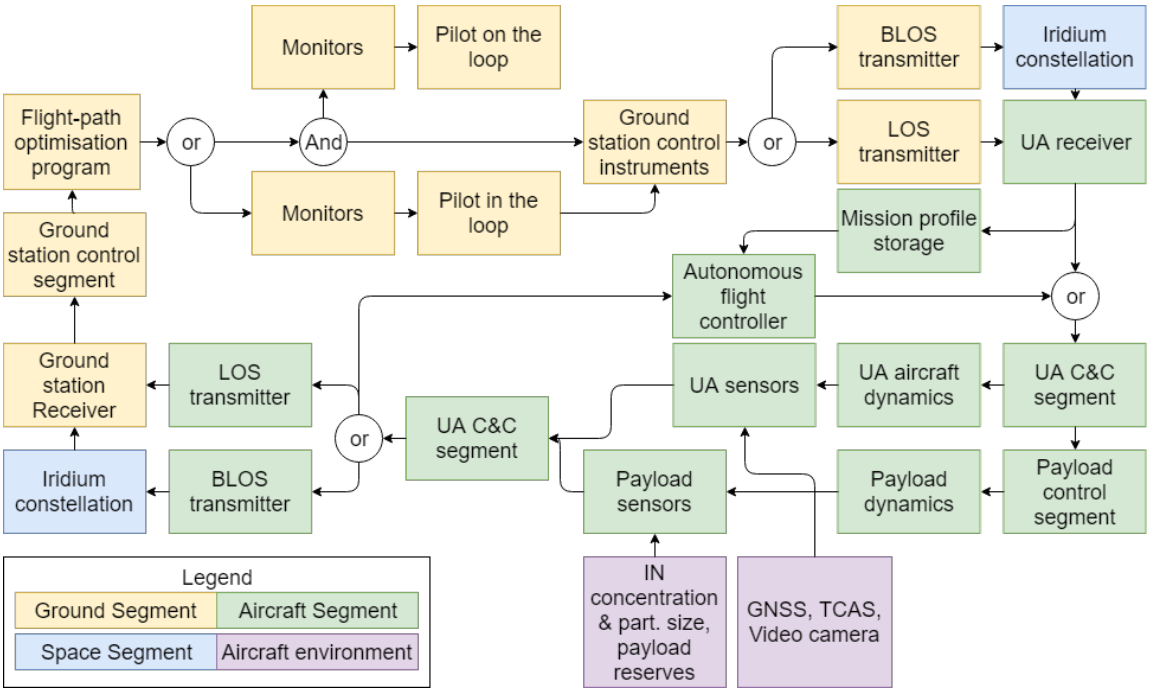

Figure 8.3: Communications and control loop diagram

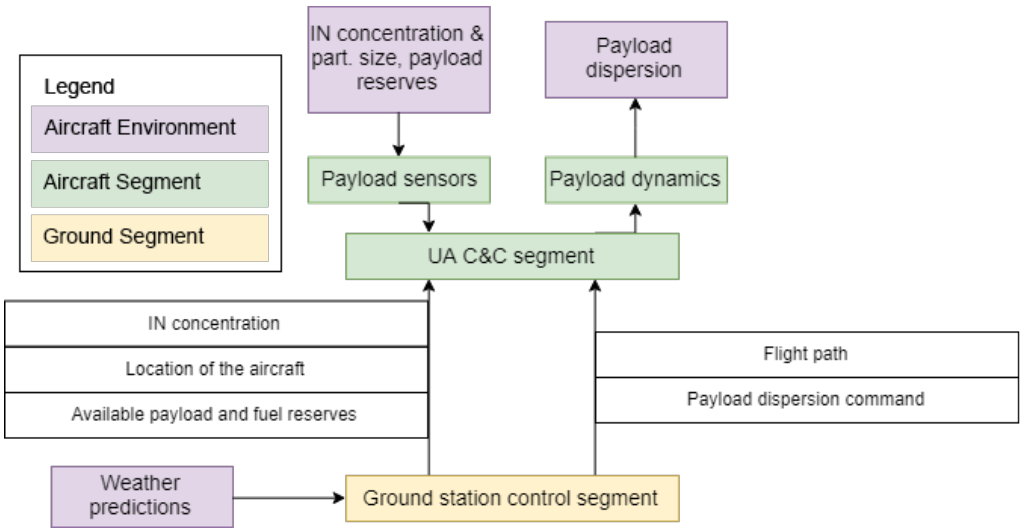

Figure 8.4: Payload data handling diagram

9 Reliability, Availability, Maintainability and Safety Characteristics

During the design of ACT the required availability level of the system has to be considered during all different phases of the project. In this chapter the reliability, aircraft and payload maintenance and safety assessment of the system are discussed in section 9.1 to section 9.4, respectively. These characteristics combined determine the availability of the system in section 9.5.

9.1. Reliability

The project is in a too early stage to come up with reliability functions. Some components of major importance, such as the engine, have been analysed on their reliability. In this section, a Failure Mode and Effect Analysis (FMEA) will be performed and the redundancies in the design will be explained.

9.1.1. Failure Mode and Effect Analysis

In an attempt to quantify the change of aircraft functions failing a Failure Mode and Effect Analysis (FMEA) was done. The FMEA includes a list of possible function that are sensitive to failure, which can be subdivided into different modes. For each of the modes the causes and effects are listed. The causes and effects evaluated in terms of likelihood and severity, using the same scale as used for the risk assessment. The scaling is also shown in table 9.1.

Table 9.1: Scaling severity and likelihood

Value	Severity	Likelihood
1	Negligible	Rare
2	Marginal	Unlikely
3	Critical	Likely
4	Catastrophic	Very likely

Function	Mode	Effects	Severity	Causes	Probability
Aircraft measures velocity incorrectly	Aicraft flies too fast	Induced flutter	4	Sensor frozen	3
		Incorrect seeding	3	Sensor broken	2
	Aircraft flies too slow	Stall	2	Wiring failure	3
		Spin entry	3		
Aircraft measures altitude incorrecly	Aircraft flies too high	Seeding on wrong altitude	3	Sensor frozen	3
	Aircraft flies too low	Seeding on wrong altitude	3	Sensor broken	2
		Aircraft hits ground object	4	Wiring failure	3
Loss of contact	Loss of contact	Unable to land pilot in or on the loop	4	Navigation satellite unavailable	2
		IN density measurements not communicated	3	Aircraft communication antenna broken	3
		Aircraft collides with other aircraft	4	Ground control station antenna broken	2
Hydraulic failure	Gear does not deploy	Plane cannot land	4	Leaking pipes	3
	Flaps do not retract/deploy	Plane lands with overspeed	2	No hydraulic fluids	1
	Control surfaces cannot be controlled	Plane cannot be controlled	4	Broken pumps	2
Electric failure	Loss of contact	Crash	4	Wiring failure	2
	Loss of control	Collision with ground object	4	Engine failure	2
Engine failure	Complete engine failure	Crash	4	No fuel	1
	Overheating	Eventual engine failure	4	No cooling	2
	Thrust uncontrolable	Loss of control	4	Bird strike	3
IN concentration measured incorrectly	Measured concentration too high	Underseeding	4	Broken sensor	3
	Measured concentration too low	Overseeding	4		

Figure 9.1: Overview FMEA

9.1.2. Redundancy Philosophy

The probability of occurrence of some of the safety critical functions can be decreased by implementing redundancies in the system. Table figure 9.1 shows these critical functions. Failures that can be prevented using redundancies are listed below:

- **Aircraft measures velocity incorrectly** The probability of this failure can be decreased by using a second pitot tube. Either one of these pitot tubes would be able to function independently.
- **Aircraft measures altitude incorrectly** This probability can also be decreased using multiple pressure sensors.
- **Aircraft measures IN concentration incorrectly** As explained in chapter 5, there will be no redundancy on the aircraft itself, but there will be redundancy throughout the fleet. If the sensor fails on one of the aircraft, another aircraft can take over its measuring.
- **Loss of contact** A loss of contact can have detrimental effects. Therefore, redundancies are implied in the system. Line of sight communication is of such importance that an extra system will be added for redundancy.
- **Electric Failure** An extra battery will be added for redundancy. If the electrical system fails as a whole, a Ram Air Turbine (RAT) can be deployed to keep the most important systems running.
- **Airport redundancy** As discussed in chapter 4 due to weather conditions the airports could temporarily be unavailable, for each of the hemispheres two airports are chosen to ensure that the operation can continue at all times from at least one of the bases.

Another redundancy that is not linked to any of the failures listed in 9.1 is software redundancy. N-version programming might be used in the detailed design phase. N-version programming is a method where multiple functionally equivalent programs are independently generated from the same initial specifications to prevent common bugs in the code.

9.1.3. Accident rate

The aircraft accident rate is necessary to know to make sure there are enough spare aircraft to carry out the mission. Before any figures can be stated, the definition of an accident must be established. According to Boeing [10], an accident is when the aircraft is substantially damaged or missing. Substantial damage is when the aircraft's performance is compromised and major repairs or replacing the failed component is required. The failure rate will be measured against departures, since there is a stronger statistical correlation between accidents and departures compared to accidents and flight hours. The accident rate of commercial jet aircraft was estimated to be approximately 1 accident per 1,000,000 departures from the early 1980's until now [10]. The ACT mission will require 816,600 departures over its lifetime, meaning the most likely case is one aircraft accident over the mission duration. The discrepancy in this estimate might arise from the fact that the seeding aircraft are equipped with only one engine and are therefore more likely to have an accident due to engine problems. Moreover, the aircraft will be operating in extreme weather conditions and will therefore be more prone to accidents.

9.2. Aircraft Maintenance

To ensure the availability of the aircraft to meet the mission requirements, proper maintenance planning is required. As the fleet size is limited and flight planning is such that the aircraft are required to be used to their full capacity, flying full range with short turn around times, an efficient maintenance schedule is vital for the operational part of the CCT mission. The number of spare aircraft needed for the mission is largely dependant on the maintenance planning. This section gives an overview into the structure of the maintenance planning manual and the specific focus point for ACT. As advised by the FAA [1] a maintenance planning manual should include at least the following sections:

a. Administrative Policies and Procedures. This section gives a description of how the maintenance

[1] Retrieved from: https://www.faa.gov/documentLibrary/media/Advisory_Circular/AC%20120-16F.pdf [11/06/2018]

program is organised, directed, amended and controlled. It includes function descriptions and relations of all personnel working on the maintenance of the fleet. The hierarchy within the organisation should be clearly defined, as well as, the responsible people for all parts of the program. As ACT will operate from smaller, remote, bases maintenance facilities will need to be build at the airports and personnel should be trained to maintain both the aircraft and the ground payload system.

b. Instructions for the Administration, Management, and Accomplishment of the Maintenance Program. This section includes an overview of all scheduled and unscheduled maintenance performance. The scheduled maintenance planning includes a schedule of how and when an aircraft has to be checked. For scheduled maintenance tasks four different categories are identified [51].

- 'A' Check: This check includes visual inspection of the aircraft structure for evidence of damage, deformation and missing parts. Furthermore, access panels are opened to further inspect item such as lights, gears and brakes. For this check limited tooling is needed. It is performed every 400-600 flight hours. The flight time per sortie for this mission is over 20 hours, therefore a type 'A' check is required every 20-30 flights. It requires 50-70 man hours on average to perform this check.
- 'B' Check: For this check the component and systems are checked more extensively. However, as most of the former 'B' check items are currently integrated under 'A' and 'C' checks this is not discussed in more detail. This does mean that 'A' checks become more extensive.
- 'C' Check: This check requires the dissembling of critical parts and is usually carried out once every 12-18 months. It includes among others checking of the door seals, operation of the DC bus tie control unit, and inspection of the engine inlet for cracks. This check can take up to 6000 man hours.
- 'D' Check: The heaviest check type is the type 'D' check, also known as heavy maintenance visit, during which the stabiliser attach bolts, floor beams and win box are inspected. This check takes the aircraft out of service for several weeks, up to 50000 man hours. The check is performed every 5-7 years.

The unscheduled maintenance planning is required to include procedures for unusual flight and ground events. These events are, for instance, several turbulence, extreme manoeuvres, hard or overweight landings. Instructions should be present for inspection when these type of events occur.

c. Technical Data that Describe Maintenance Standards, Methods, Techniques, and Procedures. This section should include a detailed description of how certain task are to be performed. Methods, techniques and standards for measurements and calibrations are described in detail. Maintenance manuals for specific parts are usually provided by the manufacturer. Furthermore, the handling of the aircraft in different operational scenarios, such as harsh weather, are included.

Furthermore, the maintenance planning manual can include work cards, or any other description of how the work on the aircraft is checked and documented. If the part of the maintenance is carried out by a subcontractor, the details of such an agreement should be included in the manual.

9.3. Payload Maintenance

The payload components require the same maintenance as the aircraft components, except for the sensor. The combustion chamber will require the same maintenance schedule as the engine, as the high temperatures degrade the combustion chamber quickly and corrosion must be monitored. The payload storage tank and pipes require the same maintenance schedule as the aircraft fuel tanks. Since corrosion is not an issue for the HDPE storage tank, there is no need for more maintenance than for the fuel tank. The sensor requires 1-2 hours of maintenance each month for cleaning.

The personnel which will transport the payload to and on the airport should be well informed about the consequences of coming in contact with the payload. The payload can cause skin damage if the skin is exposed to the payload. Therefore, personnel has to wear protective clothing. Furthermore, all components in contact with the payload such as trucks, pipes, storage facility, etc., should be protected from the corrosive effects of the payload by adding a protective layer.

9.4. Safety

A common way to assess the safety of a system is defining a Failure Mode and Effect Analysis as described in section 9.1.1. Furthermore, for unmanned aerial vehicles the damage on the ground in case of a failure that leads to a crash is considered important. To quantify this damage the concept of expected level of safety (ELS) can be used. ELS is defined as:

$$ELS = \frac{A_{exp}\rho P_{pen}(1 - P_{mit})}{MTBF} \tag{9.1}$$

In which $(1/MTBF)$ is the failure rate of safety, so the estimated rate of "crash". A_{exp} is the territorial area damaged by the crash, ρ is the population density of the area on which the UAV is operating, P_{pen} is the probability for people to be hit by debris, even if they are protected by houses, buildings or vehicles in which they eventually find themselves in the timeframe when the crash occurs. P_{mit}, is the probability that crash effects are decreased by systems of safe flight termination (i.e., ballistic parachutes, autonomous guidance systems on uninhabited places) [37].

In this phase of the design, ELS will not be calculated. But, this formula does give an insight how this expected level of safety can be increased. For 'ACT' ρ will be very low since the system operates in very remote areas. P_{mit} can be increased by incorporating safe flight termination systems. An example of this might be a total engine failure. The system can then determine the new flight pattern and direct the Arctic Tern to a safe place to crash.

9.5. Availability

The availability of the system is largely dependent on the reliability in combination with the level of maintenance. Critical functions are identified so that proper redundancy measures can be put into place and extra maintenance can be performed to further improve the reliability of the aircraft. However, the availability of the aircraft is not the sole factor that influences the availability of the system. As discussed in chapter 4 weather conditions at the airports could be a cause reduce availability of the system. Furthermore, the system might be subjected to changes in the mission requirements, possible changes are described in chapter 15. As is concluded in this chapter the fleet can be scaled to meet the different mission requirements, if adequate resources are available.

10 Resource Allocation, Budget and Cost Breakdown

An important aspect in projects is the management of resources. This is often done through budgets such as a mass and power budget. This chapter will first discuss the cost analysis of ACT in section 10.1. Then it will discuss the other budgets and the contingency strategy used to adhere to these budgets in section 10.2.

10.1. Cost Breakdown Structure

To get a good estimate of the mission cost, a cost breakdown structure was made in the baseline report [33]. This cost breakdown was then updated and adjusted to new insights. The updated cost breakdown structure is given in figure 10.1. The top level cost was divided into initial cost, annual cost and end-of-life cost. These were then subdivided into their contributors. The initial cost is analysed in section 10.1.1, the annual and end-of-life costs are analysed in table 10.2 and section 10.1.3 respectively. The total initial cost is equal to €2 Billion and the annual operating cost is €762M.

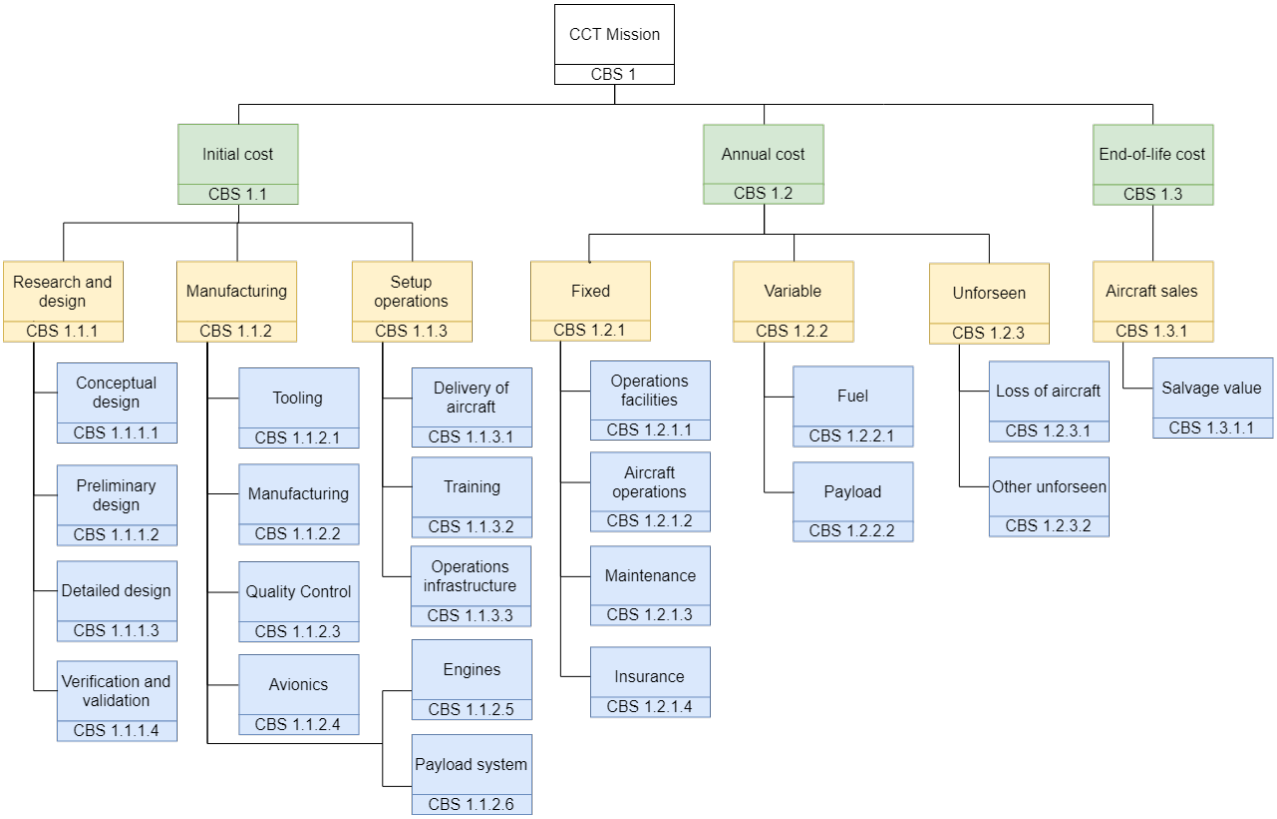

Figure 10.1: Graphical representation of the cost breakdown structure

10.1.1. Initial Cost

The initial costs are divided into three sub categories: Research & Development (R&D), Manufacturing, and Operational setup costs. In table 10.1 the cost breakdown for the initial cost can be found. Below a short explanation for the various costs per sub category is given.

Research & Development: The total Research & Development costs are found to be equal to €423M. The conceptual design phase and preliminary design phase both contribute €300k to the R&D. This is based on the total time that the DSE took and the amount of people working on the design during these phases. The next phase, the detailed design is estimated to cost €356M. This value was estimated using the Raymer development cost estimation [74] and an assumed total cost per engineer of €150 per hour. The same thing was done to predict the cost of the flight test part during the V&V. Combined with the research required to validate the functioning of the payload, which was assumed to be €30M, this adds up to €66M.

Manufacturing: The tooling, manufacturing and related quality control costs were estimated using Raymer [74] and found to contribute €216M, 906M, and 62M respectively. For the avionics all prices of the installed systems were added up together and were found to add €30.9M to the manufacturing costs. For the engines a conservative estimate was made to account for their value and was set at a total of €1M per engine and thus a total sum of €204M. The payload system costs are made up by the cost for the sensors required in the payload system and the estimated price of the combustion chamber and payload tanks, which adds up to €40M. All this combined leads to a total manufacturing cost of €1,459M.

Setup operations: The setup operations is mainly made up out of the changes required in the infrastructure on the airfields. It is assumed that all four airports used will need modifications to their runway and control tower. For this, a total of $15M per runway, $6M per tower, and $ 15M per apron are assumed. This adds up to a total of €125M. The remainder of the €135.9M of the setup operations costs consist out of personnel training of €10.6M.

Table 10.1: Initial Cost Breakdown

Initial cost	**€ 2,017,389,312.96**				
R&D	**€ 422,993,040.31**	**Manufacturing**	**€ 1,458,526,185.60**	**Setup operations**	**€ 135,870,087.04**
Conceptual design	€ 300,000.00	Tooling	€ 216,223,474.05	Training	€ 10,590,087.04
Preliminary design	€ 300,000.00	Manufacturing	€ 905,526,009.76	Operations	€ 125,280,000.00
Detailed design	€ 356,397,622.64	Quality control	€ 61,694,967.76	Infrastructure	
V&V	€ 65,995,417.67	Avionics	€ 30,971,253.89		
		Engines	€ 204,000,000.00		
		Payload system	€ 40,110,480.00		

10.1.2. Annual Cost

The annual costs are the costs of the system once its operational. These costs consist of fixed, variable and unforeseen costs. Fixed costs are the cost that are always incurred independent of the ”production quantity” in this case that would be the amount of seeding which is performed. The fixed costs which were identified are: The cost of operations facilities, aircraft operation, maintenance and insurance. The variable costs are the cost of fuel and IN solution, since these depend directly on the seeding operations. Lastly the unforeseen cost consist of the cost incurred by the loss of an aircraft and a margin for costs which might have been forgotten during the cost analysis. A summary of the annual cost can be found in table 10.2. The total annual cost is then € 762,371,888.83

Fixed Costs The first factor of the fixed cost is the cost of facilities, this includes the cost of the airport and the cost of the control towers used to operate the fleet. The airport cost was estimated to be $8.88 based on the airport fees at Christchurch airport[1]. The aircraft operations are the second part of the fixed cost, this exist of the aircraft operators, supervisors and ground personnel. The quantities and wages for these employees are described in section 4.3.

[1]Retrieved from: http://www.christchurchairport.co.nz/media/873623/cial_pricing_disclosure_1_july_2017_to_30_june_2022.pdf [02-07-2018]

The maintenance cost is very difficult to analyse because no similar aircraft or mission exist. The aeroplane is very small but has a huge range which is very unconventional. To get the most accurate estimate, several methods were used which produced very different results. The first methods are based on Raymer, these methods base the maintenance material cost on the total aircraft cost and the flight hours or flight cycles. The material cost is only 17% of the total maintenance cost[19], therefore the total maintenance cost is calculate by dividing the material cost by 0.17. These cost estimates produce and annual maintenance cost of €544M based on the flight hours and €12M based on the flight cycles. Since this cost range is so large a third method was used to estimate the cost of maintenance based on the required labour. However this estimate was even higher than the estimates from Raymer [74] (in the order of €700M per year) because it's based on aircraft which are far larger than the AT1. Therefore this third cost estimate is discarded. To validate the maintenance cost it was compared to conventional airliner maintenance cost[44], this is described in section 13.10.

There is no straightforward way to calculate the insurance cost based on the size and cost of the aircraft. Therefore the insurance cost is estimated to be 1% of the annual operating cost. This estimate is based on the cost analysis in Raymer [74]. The annual insurance then is €6.8M. This estimate however does not take the fact that the aircraft lacks certification into account which means the insurance cast might rise significantly. This possible increase in cost in taken into account in the unforeseen cost but in the further stages of the project a more accurate estimate of the insurance cost is needed.

Variable Cost The fuel usage per aircraft is calculated in chapter 7, this is then multiplied by the amount of sorties per year to get the annual fuel cost. The cost of fuel is estimated to be $ 0.685 per kg [2] resulting in a fuel cost of €63.1M. The IN quantity and price is discussed in chapter 5. Its final cost is equal to €20.4M.

Unforeseen Costs As in any project, there is a chance some things don't go according to plan. An example of this is the loss of an aircraft, in section 9.1.3 the rate at which aircraft are lost is roughly 0.04 aircraft per year. Multiplying this with the aircraft production price of roughly €9.2M the annual cost of aircraft loss is €369k. Furthermore there are always cost which have not been identified in the cost breakdown. To have a conservative estimate these costs are assumed to be 10% of the annual operating costs, this is an extra €69.2M per year.

Table 10.2: Annual Cost Breakdown

Annual Cost	**€ 762,371,888.83**				
Fixed cost	**€ 609,261,781.53**	**Variable costs**	**€ 83,468,182.28**	**Unforeseen costs**	**€ 69,641,922.02**
Operations facilities	€ 2,748,069.59	Fuel	€ 63,095,710.24	Loss of aircraft	€ 368,925.34
Aircraft operations	€ 24,939,679.91	IN solution	€ 20,372,710.24	Other unforeseen costs	€ 69,272,996.68
Maintenance	€ 574,715,322.49				
Insurrance	€ 6.858,712.54				

10.1.3. End of Life

After 25 years of service the aircraft will be decommissioned. Due to the amount of flight hours made during those years, take-offs and landings performed, and its specific design to this mission it is unlikely that the aircraft will find a second life. If after 25 years it appears that they are still in good shape or the mission ends earlier than expected a plan for a second life could be made and the aircraft could be sold to an external party that could give it its second life. But this is very unlikely.

The assumed case is that the aircraft will be sold to a parting out facility who will sell off all useful items still present on the aircraft such as the engine, avionic systems, and all other assets that can still be used. The remainder will be fully taken apart and separated by material so that it can be recycled and can be used for other products. However the salvaged funds acquired by selling of the aircraft will be quite low. Currently

[2]Retrieved from: http://www.iata.org/publications/economics/fuel-monitor/Pages/index.aspx [24/06/2018]

even large passenger jets are sold for a few million dollars while their original unit prices were up to a few hundreds of million dollars.[3] For older narrow body aircraft even less than a few percent of their initial value is salvaged. Taking into mind that this aircraft has no similar aircraft in the market which would make it even harder to sell of the parts it is assumed that the total salvaged value will be about 1% of the initial production cost of the aircraft. Therefore a total of €92 231 can be retrieved per aircraft.

10.2. Budget Breakdown and Contingencies

In the future design phases of the AT1, different teams will design different parts of the aircraft. These teams all need requirements that their components need to meet. Requirements such as the component weight and volume can be derived from budgets. These budgets are created to make sure that the entire system will meet the requirements for the entire system. The mass and volume budget are discussed in section 10.2.1 and the contingency strategy which are used as a tool to meet the requirements are given in section 10.2.2.

10.2.1. Mass and Volume budget

For the future design of the AT1 the different design groups will have to design their components within certain weight specifications in order to make sure that the aircraft does not become too heavy or an unexpected location of the centre of gravity. For this mass budget the class II weight estimations, which were calculated in section 6.9 and presented in table 6.9 are used.

For the available volume in the aircraft something similar to the mass budget was done. Since the space in the fuselage and wings is very limited the allowable volume for the different subsystems is also limited. Therefore a volume budget was created. This volume budget is discussed in more detail in section 6.5.

10.2.2. Contingency strategy

To make sure the budgets discussed in section 10.2.1 are met contingencies are used. These contingency can be viewed as a buffer between the design value and the required value for the components. The magnitude of the contingencies are dependent on the level of detail in the design. As the detail of the design increases the contingency decreases. The contingencies for the future design phases of the AT1 are given in table 10.3. Since some components of the aircraft are already designed in more detail others their initial contingencies are lower, such as the installed engine, which has already been chosen.

Table 10.3: Mass-budget contingencies for the different aircraft components

	Mass budget contingency %											
Design maturity	Wing	Horizontal tail	Vertical tail	Fuselage	Main landing gear	Nose landing gear	Installed engine	Fuel system	Flight controls	Hydraulics	Electrical	Avionics
Preliminary calculations	20	20	20	20	15	15	10	15	20	20	15	15
Layout calculations	15	15	15	15	10	10	7	10	10	15	10	10
Pre-release Drawings	7	7	7	10	5	5	5	5	7	10	5	5
Released Drawings	5	5	5	7	3	3	3	3	5	5	3	3
Specifications (subcontractor)	5	5	5	5	5	5	5	5	5	5	5	5
Actual measurement qualification hardware	1	1	1	1	1	1	1	1	1	1	1	1
Actual measurement flight hardware	0	0	0	0	0	0	0	0	0	0	0	0

[3]Retrieved from: http://www.aircraftvaluenews.com/scrap-values-start-to-fall-for-some-narrowbodies/ [20/06/2018]

11 Technical Risk Assessment

Potential risks have to be identified in order to reduce the change of project failure, delay or financial issues. In this chapter the risk identification, analysis, and handling are discussed. The risks are divided into payload, operational, aircraft, and development risks. For each of these risk categories risks are identified, analysed, mapped, and mitigated where needed.

The risks identified are analysed based on their likelihood and severity. The likelihood is measured on a scale from rare to very likely, while the severity is measured on a scale from negligible to catastrophic. On this scale, negligible represents events which do not effect the rest of the mission. This means that the mission, as mentioned in the mission statement, can be performed as planned. If a risk occurs and has an impact on the quality with which the mission is performed but does not cause a threat to the mission as a whole, it is labelled as a marginal event. Meanwhile, critical events have a large impact on the mission, to the point where the mission is not performed for a period of time. The events with the catastrophic label could potentially cause the mission to fail, or even be performed in such a way that the results are worse than if no mission was performed. High risk items, identified as such because of either severity, likelihood of occurrence, or both are presented along with their mitigation strategy.

The risks from the previous report [34] have been addressed earlier, but are added in this section for completeness. Please note the risk identifiers have been changed compared to the midterm report, as previously payload risks were covered as operational risks as well. because The new risks that have been identified in the preliminary design of the concept will be handled in this chapter and are listed in italic.

11.1. Payload

Payload Risk Analysis

The payload risks can be seen in table 11.1. The risk map can be seen in table 11.2.

Table 11.1: Payload Risks

Risk ID	Description	Source
PY1	The payload leaks during ground operation.	SYS-16
PY2	The target area is under or over seeded.	SYS-04
PY3	The aircraft is damaged by the IN.	SYS-03
PY4	The exit material of the combustion chamber negatively influences the dispersion of the IN.	SYS-04
PY5	The seeding subsystem fails.	SYS-04
PY6	The seeding density is measured incorrectly.	SYS-04
PY7	Payload leaks during in-air operation.	SYS-04
PY8	*Bismuth tri-iodide is found to be ineffective as IN material.*	*SYS-17*
PY9	*The particle size density is incorrect after combustion.*	*SYS-17*
PY10	*The payload pump does not function.*	*SYS-04*
PY11	*The combustion chamber does not function.*	*SYS-04*
PY12	*The actual IN dispersion differs from the modelled dispersion.*	*SYS-04*

Table 11.2: Payload Risk Map

		Severity			
		Negligible	Marginal	Critical	Catastrophic
Likelihood	Very Likely				
	Likely		1	12	
	Unlikely		5, 10	4, 9, 11	2, 8
	Rare			7	3, 6

Payload Risk Mitigation

There are three risks in the high risk zones of the risk map, which can be seen in table 11.2. The mitigation procedures are as described below. The updated risk map after risk mitigation can be seen in table 11.3.

2. The target area is under or over seeded. This risk is mitigated by regularly checking and maintaining the regulating system. Furthermore, the payload monitoring system should result in an accurate model for the dispersion width and height. The results of this model should be coupled correctly to the resulting injection rate, also if the dispersion varies over the seeding area. This will lower the likelihood of the risk.

8. Bismuth tri-iodide is found to be ineffective as IN material. A substitute IN material can be selected such as silver iodide, which has been proven to be suitable for cirrus cloud thinning. This will increase the cost of the mission significantly, and the payload subsystem in the sorties might have to be altered. The severity of the risk is hereby lowered to critical.

12. The actual IN dispersion differs from the modelled dispersion. To mitigate this risk, test flights should be performed prior to the start of the mission to ensure that the dispersion behaves as predicted. The test measurements should be performed in all conditions representative of the mission environment. The results of the test measurements should be incorporated in the detailed design. This would decrease both the likelihood and the severity of this risk.

Table 11.3: Payload Risk Map Post Risk Mitigation

		Severity			
		Negligible	Marginal	Critical	Catastrophic
Likelihood	Very Likely				
	Likely		1		
	Unlikely		5, 10, 12	4, 9, 11,8	
	Rare			7	2,3,6

11.2. Operations

Operations Risk Analysis

The operational risks can be seen in table 11.4. The risk map can be seen in table 11.5.

Table 11.5: Operations Risk Map

		Severity			
		Negligible	Marginal	Critical	Catastrophic
Likelihood	Very Likely	7			
	Likely		5, 13	8, 11, 15	
	Unlikely	10	6, 14	2	
	Rare	12	9	1, 4	3

Table 11.4: Operational Risks

Risk ID	Description	Source
OP1	The fleet of aircraft can not function as required due to maintenance.	SYS-10
OP2	Aircraft can not take off because of weather conditions.	SYS-01
OP3	The operations can not be switched from the North to the South hemisphere, or vice versa.	SYS-06
OP4	Airports cannot support the additional flights to properly carry out the mission.	SYS-16
OP5	The seeding area or location changes during the operational period.	SYS-05
OP6	An aircraft is not able to operate for 25 ± 5 years.	SYS-07
OP7	The annual operations cost surpass requirement.	SYS-13
OP18	*The aircraft's take-off and landing distance increase due to snow and/or rainfall.*	*SYS-AC-02*
OP9	*There is a lot of other air-traffic in the seeding area during operation.*	*SYS-04*
OP10	*The noise levels of the aircraft is exceeding limits.*	
OP11	*Weather effects on the flight path are not taken into account.*	*STK-CUS-15*
OP12	*The aircraft collision avoidance system fails.*	*SYS-AC-06*
OP13	*Maintenance cannot be provided in the amount required.*	*SYS-OPS-07*
OP14	*Communication with an aircraft is lost.*	*SYS-AC-06*
OP15	*The communication system is inoperable because of lack of satellite coverage over the poles.*	*SYS-AC-06*

Operations Risk Mitigation

There are two risks identified in the high risk zone of the risk map which can be seen in table 11.5. The mitigation procedures are as described below. The updated risk map after risk mitigation can be seen in table 11.6.

8. The aircraft's take-off and landing distance increase due to snow and/or rainfall. This risk could be critical for the mission if it is for take-off. However, the take-off distance of the aircraft is determined using a margin for on the take-off distance for take-off in less favourable conditions. For landing, the aircraft can diverge to a different airport if the conditions at one airport are such that landing is no longer possible. Thus the severity can be decreased by taking a margin on the take-off distance and increasing the range for divergence to another airport.

11. Weather effects on the flight path are not taken into account. The weather conditions when seeding over the poles can be quite extreme, if the particles are moved by the weather at the seeding area this could have a critical effect on the mission. However, research was done on the weather conditions and will be done in more detail at a later stage of the project. This will decrease the severity of this risk.

15. The communication system is inoperable because of lack of satellite coverage over the poles. The risk of loss of communication is critical for the operation and likely as the satellite coverage for the poles is not optimal. This risk is mitigated by using the Iridium satellite system which has good coverage over the poles chapter 8. The risk will then still have the same severity, but the likelihood is mitigated to unlikely.

Table 11.6: Operations Risk Map Post Mitigation

		Severity			
		Negligible	Marginal	Critical	Catastrophic
Likelihood	Very Likely	7			
	Likely		5, 8, 11, 13		
	Unlikely	10	6, 14	2, 15	
	Rare	12	9	1, 4	3

11.3. Aircraft

Aircraft Risk Analysis

The aircraft risks can be seen in table 11.8. The corresponding risk map can be seen in table 11.7.

Table 11.7: Aircraft Risk Map

		Severity			
		Negligible	Marginal	Critical	Catastrophic
Likelihood	Very Likely	5			
	Likely	13	23		
	Unlikely		2, 4	3, 7, 14, 15, 16, 18, 20	19, 22
	Rare			6, 8 , 9, 10, 11, 12	1, 5, 17, 21, 24

Table 11.8: Aircraft Risks

Risk ID	Description	Source
AC1	Aircraft does not function properly at the required operating conditions.	SYS-02
AC2	Operational conditions are different from the conditions that the aircraft was designed for.	SYS-02
AC3	An aircraft is unable to return to a base station.	SYS-14
AC4	An aircraft breaks down due to unforeseen effects as a result of the flying frequency.	SYS-10
AC5	The system seeds the air at the wrong altitude.	SYS-05
AC6	Payload is too heavy to carry.	SYS-04
AC7	The fuel freezes.	SYS-AC-01
AC8	The engine fails.	SYS-AC-15
AC9	The autopilot fails.	SYS-AC-15
AC10	There is catastrophic structural failure.	SYS-AC-04
AC11	Inability to take-off and land due to size of aircraft.	SYS-14
AC12	Inability to climb to desired altitude due to lack of engine power.	SYS-AC-14
AC13	Requires more maintenance than planned.	SYS-AC-18
AC14	The aircraft measures its position incorrectly.	SYS-AC-12
AC15	The aircraft cannot take-off or land due to weather conditions.	SYS-AC-02
AC16	The aircraft does not meet required range.	SYS-06
AC17	The aircraft does need CS certification.	SYS-AC-10
AC18	The aircraft is lost due to an engine failure.	SYS-10
AC19	The engine flow disturbs the flow around the empennage to such an extent that the controllability becomes unacceptable.	
AC20	*Fatal design flaws are detected during structural testing.*	*SYS-AC-04*
AC21	*The subsystems cannot be integrated in the aircraft.*	*SYS-04*
AC22	*The aircraft does not have enough range to reach any point within the seeding area.*	*SYS-AC-14*
AC23	*The aircraft is not able to take-off due to weather conditions.*	*SYS-AC-02*
AC24	*The aircraft is unable to pump the fuel around the aircraft.*	*SYS-AC-14*

Aircraft Risk Mitigation

Two risks have been identified to be in the red zone in the risk map in table 11.7 and should thus be mitigated. The mitigation strategy is shown below. The updated risk map after risk mitigation can be seen in table 11.9.

20. The engine flow disturbs the flow around the empennage to such an extent that the controllability becomes unacceptable. This risk can be mitigated by creating a small scale model of the aircraft to be tested in a wind tunnel and investigate its stability in detail before the actual aircraft is built. This would result in more time to develop the aircraft design as it would have to be changed, however extra time is calculated in the project plan.

23. The aircraft does not have enough range to reach every point within the seeding area. As described in chapter 4 this only occurs when Ushuaia can not be used to take-off due to weather conditions. Part of the seeding area is unreachable from Christchurch airport. However, the seeding replenishment strategy is defined such that a margin is left for the seeding concentration not to drop below critical levels even if the area is not seeded again after 7 days as planned.

Table 11.9: Aircraft Risk Map Post Mitigation

		Severity			
		Negligible	Marginal	Critical	Catastrophic
Likelihood	Very Likely	5			
	Likely	14	24		
	Unlikely		2, 4	3, 8, 15, 16, 17, 19, 21	
	Rare			7, 9 , 10, 11, 12, 13	1, 6, 18, 22, 25, 20, 23

11.4. Project Development

Project Development Risk Analysis

The risks related to project development can be seen in table 11.10. The risk map is shown in table 11.11.

Table 11.10: Project Development Risks

Risk ID	Description	Source
PD1	The environment is adversely impacted.	SYS-08
PD2	The certification of the aircraft is delayed.	SYS-15
PD3	Testing takes longer than expected.	SYS-15
PD4	An acceleration of climate change causes an urgent need for CCT.	SYS-15
PD5	The development cost surpasses requirements.	SYS-12
PD6	Seeding dispersion width and depth are found to differ from initial design assumptions.	SYS-04
PD7	Selected supplier of parts or materials is no longer available.	SYS-10
PD8	Another project with similar goals has a cheaper design/solution.	SYS-07
PD9	The project development takes longer than 6 years.	SYS-15
PD10	The modular payload system is not ready in the required time.	Section 3.2
PD11	The modification of the airports takes longer than anticipated.	SYS-15

Table 11.11: Project Development Risk Map

		Severity			
		Negligible	Marginal	Critical	Catastrophic
Likelihood	Very Likely	4, 5			
	Likely		1, 3, 6	9, 11	
	Unlikely			7	8
	Rare		10	2	

Project Development Risk Mitigation

Three risks have been identified in the red zone of the risk map in table 11.11. The mitigation strategy is shown below. The updated risk map after risk mitigation can be seen in table 11.12.

8. Another party with similar goals has a cheaper design/solution. This risk would be catastrophic, but unlikely. Should there be another company or party with a cheaper design/solution, the modular system can be implemented in existing aircraft which would give a significantly lower cost for the project. This would decrease the severity of the risk, however the likelihood cannot be mitigated and thus this risk moves to the marginal and unlikely block in the risk map.

9. The project development takes longer than 6 years. As the project is very complicated and the amount of information available on IN dispersion in contrails is limited, there is a severe risk that the project development time will be more than initially expected. The likelihood of this risk can be mitigated by making a detailed project plan for each phase of the design and production of the aircraft and ensuring more resources are available instantly to deal with unforeseen issues in the project.

11. The modification of the airports takes longer than anticipated. This would mean that the time to operation will be longer than anticipated, this can be mitigated by contacting the airports at an early stage of the project development to investigate the modification possibilities.

Table 11.12: Project Development Risk Map Post Mitigation

		Severity			
		Negligible	Marginal	Critical	Catastrophic
Likelihood	Very Likely	4, 5			
	Likely		1, 3, 6		
	Unlikely		8	7, 9	
	Rare		10	2, 11	

12 Sustainable Development Analysis

To limit the amount of resources, time and money used to complete the CCT mission successfully a sustainable development strategy is set-up. This strategy was developed in the early stages of the project but runs through all phases from project planning to final implementation and operation. A widely used method to evaluate the sustainability of a project is used for this mission: the triple-P (profit, planet and people) also known as the bottom line concept [53]. When applying this method during the different phases of the project, economic, environmental, and social criteria have to be considered and, if possible, design choices can be graded on performance with respect to these criteria. An optimally managed project is such that all three indicators are respected. This chapter elaborates on the sustainability analysis that was done during the project and how the triple-p approach will play a role in the future of ACT.

12.1. Economic Sustainability

The economic performance of a project can be determined in terms of profit. In the early stage of the project the mission was analysed and the requirements for the system were identified [33]. The first step to investigate the economic sustainability is to perform a market analysis. This analysis investigates the market presence and economic feasibility of the mission, the results of the market analysis can be found in chapter 2. Even though, in general, economic performance is considered to be a vital element for any mission for this particular case it is assumed to be less significant. The reason for this is that the mission is set up as a necessary measure to prevent a severe temperature rise that would cause catastrophic changes in weather conditions on earth. Therefore, the economic feasibility is considered secondary aspect to the goal of this mission. However, during all design phases the costs for the different options are used as an important trade-off parameter for the different concepts. In any case it is important to design an affordable system, that meets all customer requirements. As explained in the market analysis, if this is not achieved other parties could present solutions at a lower cost, which might not be able to correctly perform the mission, and could have an adverse effect on the environment.

12.2. Environmental Sustainability

For environmental sustainability the use of materials is a critical indicator, furthermore, transport efficiency and effects on the climate are considered important.

Materials and resources

The use of raw material was considered when deciding on the material that is to be injected into the atmosphere in the early conceptual phase. Several materials have been considered. They were traded-off by looking at effectiveness for the mission, but also cost and environmental side effects. This approach was also be used when choosing the material to use for manufacturing other parts of the system. Something to consider here is the option to reuse materials or even entire products. For the manufacturing of the aircraft the most commonly used aircraft materials were evaluated for their material performance, cost and their environmental sustainability. The reuse of materials can be implemented at the end-of-life phase of the mission. As the aviation industry grows, so does the number of decommissioned aircraft. Currently around 80% of an aircraft is recycled, several organisations are pushing to further increase this number [1].

Waste and emissions should be kept to a minimum during the manufacturing and operating phase of the mission. For manufacturing, this is done by implementing the lean principle. This means that during all stages of the process the resources and materials should be used in an efficient manner, as well as minimising waiting

[1] Retrieved from: ttps://www.thebalancesmb.com/airplane-recycling-and-value-extraction-2877922 [20-06-2018]

times during the process.

CES Edupack's Eco Audit is used to quantify the sustainability of the mission. The carbon footprint and energy can be estimated for the material production, manufacture, transport, use, and disposal with this program. However, for the ACT system, the environmental impact of the transport phase will be ignored. Firstly, the location of assembly hasn't been chosen yet, and furthermore, since there will be scores of aircraft flying continuously, transporting the manufactured product will be negligible on the full system scale. To perform the Eco Audit, both aircraft and mission parameters are needed. The material, mass, manufacturing method, and quantity for the various parts that make up the aircraft are required. For the mission parameters, the operational time per week, power of the engine and type of fuel used are required. The table below shows the results from the Eco Audit.

As expected, the use of the system requires the most energy. Since this is the most crucial contribution determining the system's environmental impact (aside from the seeding effect), this must be verified. This is done by calculating the CO_2 output with a different method. Using the fuel mass burned and the CO_2 emitted per kilo of kerosene burnt [68], the CO_2 emitted throughout ACT's lifetime was estimated to be 5.5×10^9 kg. Since this is in the same order of magnitude as the estimation from CES Edupack, it can be assumed that this is a reliable enough estimate. If this amount of CO_2 was released into the atmosphere, the global temperature would increase by $9.35 \cdot 10^{-6} °C$ [55].

Table 12.1: Results from Eco Audit, for whole lifetime of mission

	Energy use (MJ)	CO_2 footprint (kg)
Material	3.73×10^7	2.6×10^6
Manufacture	1.48×10^6	1.11×10^5
Use	5.16×10^{10}	3.67×10^9
Disposal	6.23×10^4	4.36×10^3
Reclaimed through end-of-life	-1.12×10^7	-7.16×10^5
Total	5.17×10^{10}	3.67×10^9

Emissions during operation are minimised by optimising the flight pattern such that the minimal amount of fuel is burned. ACT does this by operating the fleet from different airports in different areas, flying optimal routes and keeping track of the current IN density to further optimise the seeding. The process of optimising the flight pattern is described in chapter 4. The usage of Bio-fuel was discarded during the design trade-off due to the bad freezing characteristics, however during final design this decision should be reevaluated since in the meantime a new type of bio-fuel might be developed with good characteristics and this could decrease the total emissions for the mission as well.

Transport

The CCT mission is carried out on a global scale. This results in the need to efficiently manage transport during manufacturing, set-up, and operational phase of the mission. An obvious way to do this is to make use of existing production sites, airports and transportation options. The existing transportation options from the private sector are assumed to be optimised for economical performance. However, decisions on where the aircraft fleet is manufactured and transportation to the mission site lie outside the scope of the DSE project and should be developed in the next design stages.

Climate

The most direct effect of this mission on the climate should be a drop in global temperature which is also the main goal of the mission. The climate side effects for the CCT mission have to be studied extensively during the design phase. The severity of the side effects will be weighed against the necessity to stop global warming. As the objective of the mission is to change the global temperature, any other local changes to the climate are considered to be side effects. These local changes will have to be identified and procedures should be put into place to minimise their impact, if prevention is not possible.

Since climate predictions are a timely and costly procedure, it is important to research this. Even with intensive study it will not be entirely clear what the direct and indirect results of this mission will be. These unknown effects should be accounted for by creating a certain flexibility in the implementation of the mission, this could

be in terms of seeding density or seeding location. The sensitivity of the system to these kind of changes is considered in the design phase of the project. Lowering global temperatures via CCT should in any case be considered to be a temporary measure. For the results to be sustainable, procedures that lead to a reduction of emission of greenhouse gasses should be implemented simultaneously. It is of great importance that steps toward the reduced emission are not delayed or terminated because of this mission.

12.3. Social Sustainability

When considering the social sustainability of the CCT mission the impact on society and the ethical aspect of the mission are taken into account. This section explains the importance of societal, labour and ethics parameters for this project.

Society

CCT will have an impact on an individual, community, and global level, thus directly or indirectly affecting the livelihood of all people. This will have to be well understood before any seeding can take place. Open communication with the community and actions to mitigate the adverse climate effects are necessary to gain community support for this mission. This is partly due to the ethical responsibility of geo-engineering, but also to ensure public opinion is sufficiently positive for the project to be executed and not be halted due to a public outcry.

It is not immediately clear how the effect of CCT will be received. If the system is successful, the most noticeable impact will be a decrease in global temperature, which, depending on the impact on crop growth, may or may not benefit agriculture. Furthermore, the predictions of the effects of CCT on global precipitation levels are not fully in agreement: two models made by the same author presented in different reports indicate an increase [82] and decrease [84] in precipitation. Furthermore, the effect will not be the same for everyone, so evaluating the impact on society becomes even harder. Storelvmo and Herger [82] showed how some areas will receive substantially more rain, for instance South and South-East Asia will be particularly affected. However, due to the severity of the global warming effects, for the research and design phase of this project the main objective is designing an effective CCT system. During the implementation and operation the effects of CCT should be closely monitored and the mission execution could then be altered to avoid adverse impact on certain areas.

Labour

The CCT mission will create a lot of employment opportunities distributed around the globe, especially in the production and operational phase. This will favourably influence the community support of the mission. As the operational part of the mission is done in remote areas, the availability of employees should be considered during the set-up of the operations. Another important sub category is the operator safety. As this is a new type of operation the staff should be properly trained to work with the payload and sensitive equipment. This is done to avoid accidents and ensure that the correct seeding concentrations are achieved.

Ethics

The ethical aspects of climate engineering is a very delicate subject to discuss. However, if the CCT mission is carried out, the negative effects of global warming will be of such severity that, considered unethical or not, CCT is to be perceived as a necessary evil by the majority of the global population. However, the scope of this project does not cover this aspect of the CCT mission, and therefore this will be considered by external parties.

13 Verification & Validation

In this chapter the verification and validation procedures for the software that is used for designing the aircraft is presented. First, the operations optimisation model is verified in section 13.1. The class I and class II weight estimations are verified and validated in section 13.2 and section 13.3, respectively. In section 6.5.2 the fuselage length optimisation is treated. In section 13.5 until section 13.9 the scissor plot, drag estimation, V-N diagram, landing gear design and structural analysis are verified and validated, respectively. Finally, in section 13.10 the cost analysis verification and validation is presented.

13.1. Operations Optimisation Model

The Design of the operations is very unique to this specific mission, a program to model the operation was therefore made. This model is described in section 4.1.3. This model was made independently of the model which was used to perform the initial fuel estimation for the trade-off of the operations concepts[34]. The results of these two models were the same and both models are therefore considered to be verified. These models were also tested with extreme inputs to check whether the model would feedback an error. During these test the model still behaved as expected.

13.2. Class I Weight Estimation

The Class I weight estimation is done using the Roskam methods[90]. These models are validated and therefore need not to be validated again. The numerical implementation of these methods was however verified by comparing the numerical results to analytical results. Also the method of finding the OEW was done with a method described by Roskam, using existing aircraft. In the Class I weight estimations, the payload is treated as a dead mass while for this specific mission the payload is dispersed and therefore decreases during the flight. This does not pose a problem in the design since it will only make the mass estimate more conservative.

13.3. Class II Weight Estimation

An Excel program was built to carry out the class II weight estimation and, as explained in section 6.9, it is imperative this produces accurate results. Due to the sheer volume of parameters and equations, this is a hotbed for errors and must be thoroughly verified and validated. The methods of which will be elaborated upon throughout this section.

Verification

The main task of verification is making sure the program accurately represents the class II weight estimation procedure, outlined in 'Aircraft Design: A Conceptual Approach' by D. Raymer [74]. The most common cause for discrepancies stem from typos due to the long equations and many parameters. Thankfully, these errors can be minimised easily by having someone unfamiliar with the program check that each of the equations corresponds to the equations used by Raymer. Unit tests can also be utilised. This was done by checking that a particular equation results in the same weight estimation in both the programme and when done externally on a calculator.

Validation

Validation is performed to confirm the program accurately solves the problem, which is estimating the weights of various aircraft subsystems from the most basic aircraft parameters. This was done by using the class II

weight estimation program on an existing aircraft and comparing its results to the aircraft's actual subsystem masses. The Gulfstream G550 was the aircraft this was performed on, mainly due to being a light, long-range aircraft, similar to the Arctic Turn aircraft. After comparing the results of the program to the actual aircraft specifications [1], it was found that the program's output for operational empty weight was 8.9% larger than the actual value. Since these two values were within the acceptable range of 10%, it can be concluded that the program is valid.

13.4. Fuselage Length Optimisation

The fuselage length optimisation performs three functions: calculating length of fuselage for a given volume and diameter, calculating the tail area with a given tail volume and tail arm, and estimating the zero-lift drag of the wing, fuselage, and empennage.

13.4.1. Length calculation

The length of the fuselage calculation for a given volume and diameter is simple geometry and can be verified with limit tests and validated by inserting the fuselage section dimensions into a volume calculator tool and comparing the calculated volumes with the required volumes.

Limit tests are applied to the volumes for the length calculation. In table 13.1, the results of the limit tests are shown for the particular case of 0.79, corresponding to a D/L of 0.08.

Table 13.1: Results of limit test on the required fuselage volume for the fuselage length, using a diameter of 0.79 meters.

Volume	**Length**
0 m^3	2.37 m = 3 X D
1E12 m^3	2.04E12 m

In case of zero required volume, the calculated fuselage length is 3 times the diameter. This makes sense, as the nosecone and tail cone have a fixed length related to the diameter, with the nosecone being half the diameter and the tail cone 2.5 times the diameter. The cylindrical section of the fuselage will be zero, as the volume is zero.

In the case of a very high volume of 1E12 m^3, the length has the same order of magnitude. Moreover, at such a volume the cylinder section of the fuselage will be much larger than the nose and tail cone section. Therefore, the length can be approximated with just a cylinder using equation (13.1), with a diameter of 0.79 meters.

$$L = \frac{4V}{\pi D^2} = 2.04V \tag{13.1}$$

The length is then 2.04 times the volume, which is exactly what was shown in the limit test for the second limit.

For the validation of the length calculations, the volume of the nosecone, cylinder and tail cone were calculated by inputting the calculated lengths and diameters. The sum of these volumes can be calculated and compared with the required fuselage volume. The results of the validation are displayed in table 13.2. It can be seen that no discrepancies are found.

13.4.2. Tail area calculation

The tail area is calculated with a statistical tail volume coefficient for business jets and with the assumption that the tail arm is 40% of the fuselage length. As the calculation entails one equation, the verification is very

[1] Retrieved from: http://www.lissys.demon.co.uk/samp2/index.html [25-6-2018]

Table 13.2: Validation of length calculations for the example of a diameter of 0.79 meters.

Section	**Volume**
Nosecone (hemispherical cap)	0.129 m^2
Cylinder	3.785 m^2
Tail cone (Cone)	0.323 m^2
Total	4.237 m^2
Required volume	4.237 m^2
Discrepancy	0.000 m^2

elemental, and has been verified with hand calculations. The validation can be done by calculating the tail area with the code using reference aircraft for the span, MAC, wing surface area and comparing this to their actual tail area. The results are shown in table 13.3.

Table 13.3: Validation results of tail area calculation for six reference aircraft. [45]

Aircraft	**Calculated** S_h	**Actual** S_h	**Discrepancy in** S_h	**Calculated** S_v	**Actual** S_v	**Discrepancy in** S_v
Falcon 50	12.7 m^2	14.2 m^2	-10.7 %	8.5 m^2	11.1 m^2	-23.1 %
Cessna Citation II	7.8 m^2	7.6 m^2	1.7 %	6.0 m^2	5.8 m^2	2.5 %
Gates Learjet 55	5.5 m^2	5.1 m^2	8.0 %	3.6 m^2	4.1 m^2	-12.9 %
Bombardier Challenger 601	12.4 m^2	10.6 m^2	17.4 %	7.1 m^2	7.9 m^2	-9.2 %
IAI Westwind	7.5 m^2	7.9 m^2	-5.3 %	4.5 m^2	4.6 m^2	-3.9 %
British Aerospace 125-700	8.8 m^2	9.3 m^2	-5.4 %	5.6 m^2	7.1 m^2	-21.3 %

In the validation results it can be seen that the discrepancy for the horizontal tail area ranges from -10.7% to 17.4 % with a standard deviation of 10.4 % and the vertical tail area ranges from -23.1 % to 2.5 % with a standard deviation of 9.9 %. The statistically calculated values are close to the actual values and are good enough for the preliminary drag estimation used in the fuselage length optimisation.

The discrepancy is likely dominated by the assumption of the tail arm being 40% fuselage length, which in practice is either more or less. Furthermore, the vertical tail area is most of the time underestimated as the same tail arm is used as for the horizontal tail, in practice the vertical tail is more forward than the horizontal tail. However, the assumption of using the same tail arm for both horizontal and vertical tail is valid for the case of a V-tail configuration, which the CCT Arctic Tern has. The discrepancy poses not a problem for the further development of the aircraft concept, as a more advanced tail area calculation has been iterated as presented in section 6.11.1.

13.4.3. Zero-lift drag estimation

To validate the zero-lift drag, the dimensions of a reference aircraft are inputted in the zero-lift drag estimation and the calculated zero-lift drag is compared with the actual zero-lift drag of the aircraft. The Boeing 727-100 is chosen as reference aircraft, as the zero-lift drag is known and it fits the statistical group of aircraft for which the estimation is based on, namely subsonic jet engine aircraft. Furthermore, the zero-lift drag of this reference aircraft is taken at 0.6 mach as the CCT Arctic Tern also flies at this mach and for that speed the zero-lift drag should be aimed to be accurately estimated. The results of the zero-lift drag estimation and the discrepancy are displayed in table 13.4.

Table 13.4: Validation results of preliminary zero-lift drag estimation.

Aircraft name	Calculated zero-lift drag coefficient	Actual zero-lift drag	Discrepancy
Boeing 727-100	0.0196	0.0171 [67]	14.6 %

The discrepancy is shown to be 14.6%. This is an acceptable discrepancy for a very preliminary zero-lift drag

estimation. Furthermore, the absolute value of the zero-lift drag is less important than the actual relationship between its fuselage length and tail size for the fuselage length optimisation.

13.5. Scissor Plot

In section 6.11.1 a scissor plot was made to determine the final location of the main wing and the horizontal tail area over the main wing surface area ratio (S_h/S). The location of the wing was found to be at 0.481 x_{LEMAX}/l_{fus} and a (S_h/S) of 0.161. To validate these outcomes they are checked with reference aircraft.

The chosen reference aircraft RQ4 Global Hawk, MQ1 Predator, and MQ9 Reaper all have a similar fuselage lay-out and mission profile of long range UAV's. The only noticable difference between the aircraft is that the MQ1 has the tail below the fuselage and the MQ1 and MQ9 are propeller powered. Even though the aircraft are all slightly larger than the AT1, this makes these aircraft perfect reference material. The comparison between the AT1 Arctic Tern and the reference aircraft can be found in table 13.5.

Table 13.5: Scissor plot reference aircraft comparison

Aircraft	S_h/S	**Δ%**	x_{LEMAC}/l_{fus}	**Δ%**
AT1 Arctic Tern	0.1610		0.4810	
RQ4 Global Hawk[2]	0.1141	-29.13	0.4889	1.64
MQ1 Predator[3]	0.2918	81.24	0.4627	-3.80
MQ9 Reaper[4]	0.2654	64.84	0.4589	-4.59

From the table it is clear that the location of the main wing is very similar to the reference planes with only a maximum of 4.59% difference. This implies that for this type of aircraft it is very normal to have a wing at almost the centre of the fuselage. This is mainly explained by the amount of fuel the aircraft need to take along and the avionic systems in the nose of the aircraft. The S_h/S differs more compared to the other aircraft as it is slightly smaller than the average of the combined data of the reference data. However since the RQ4 has an even lower ratio it can be concluded that this is unlikely to become a problem and further detailed design will determine if the current value indeed complies with the requirements.

The calculations leading to the results presented in section 6.11.1 were verified by checking the performed calculations by hand. This way the mistakes which were initially made in the programming were able to be detected and removed from the equations, leading to a solid and feasible design.

13.6. Drag Estimation

An Excel spreadsheet was developed to calculate the drag estimation presented in section 6.6. The outcome had to be verified and validated because of the complexity of the calculations. Moreover, the aircraft range is closely related to the aircraft drag in cruise. Therefore, a reliable drag estimate was important to ensure a sufficient range of the aircraft.

13.6.1. Verification

In order to verify the results from the program hand calculations were performed on all the relations in the spreadsheet. Moreover, input values for which the results were known were used to see if the program performs as expected.

[2]Retrieved from: https://www.nasa.gov/centers/armstrong/aircraft/GlobalHawk/performance.html [21/06/2018]
[3]Retrieved from: http://www.armyrecognition.com/us [21/06/2018]
[4]Retrieved from: https://www.nasa.gov/centers/armstrong/news/FactSheets/FS-097-DFRC.html [21/06/2018]

13.6.2. Validation

Reference aircraft data for Boeing 727-100 from section 13.4.3 was reused to validate the C_{D_0} in this program. Again, the zero-lift drag was estimated at 0.6 Mach. The output underestimated the C_{D_0} by 1.25%. This discrepancy was deemed sufficiently low to consider the sheet validated.

13.7. V-N Diagram

This model is relatively simple and so it was verified by hand. The maximum load factors can be obtained by three separate calculations. The obtained stall speed was crosschecked with the stall speed in the wing/thrust loading diagram. Next to this, this model was compared to a model created by Abbott Aerospace[5].

13.8. Landing Gear Design

Compared to conventional cargo and passenger aircraft, CCT Arctic tern has a higher fuselage content density as the majority of the fuselage content is jet fuel and liquid payload, therefore the tires may to the unknowing observer appear as *too big* where the tires are actually the correct fit for the design. When comparing the tire selection for AT1 to the tires used on the Cessna Grand Caravan II [85], it is found the Cessna Grand Caravan has similar tires (Cessna GC Nose: 22x8.0*8 AT1 Nose: 7.00-6 / Cessna GC Main: 8.50-10 AT1 Main: 9.00-6) and the minor difference can be attributed to a different weight distribution along main and nose landing gear between the different aircraft.

To verify whether the results of the calculations for the landing gear are an accurate representation of the real life scenario a brief weight estimation of the landing gear is done using the first method for weight estimation from Currey [20]. Using this method to estimate the weight assuming a short strut length, the landing gear weight is determined to be approximately 5.106% of the maximum take-off weight. According to Roloff [76] the landing gear weight is typically withing 2.5-5% of the take-off weight. As the method from Currey [20] is a preliminary calculation, the weight will be in the range of 2.5-5% from Roloff [76].

13.9. Structural Analysis

In order to verify the loading calculations and the stress calculations the calculations were repeated by hand on critical points such as the position of the wing in the fuselage. The method used for the idealisation of the structures comes from Megson [56] and is therefore assumed validated. For as well as the wing as the fuselage, a point is chosen for which the loading, shear force, bending moment, shear stress, bending stress, moment of inertia and deflection are determined analytically along the whole cross section. The model is adapted until no discrepancies are found. The model is then verified to do what it is supposed to do along the entire length for the fuselage and span for the wing.

The assumptions which are made in section 7.3.2 can be validated properly by performing a FEM analysis or testing. This is not possible in this stage of the design process. Therefore, the models will be validated using the mass approximation from Raymer [74]. The mass of both the fuselage and the wing are estimated using this method. These are then compared with the resulting mass of the model which is able to carry all stresses. Using the class II weight estimation, a fuselage and wing structural mass of 143 kg and 112 kg are found, respectively. However, this estimation is based on the assumption that the aircraft is made from aluminium. Since the aircraft is made mostly from CFRP, the estimation must be changed. Research performed by Kennedy and Martins [49] shows that use of CFRP can have a structural mass reduction of up to 40%. Consequently, a mass estimation of 85.8 kg and 67.2 kg are obtained for the fuselage and wing, respectively. The wing box mass resulting from the numerical model is 59.5 kg. A discrepancy of 13% is found. This is due to the fact that a contingency is required for future design considerations, as was explained in section 7.3.5. The same procedure can be done for the fuselage when a the design is more detailed.

[5]Retrieved from: https://www.abbottaerospace.com/v-n-diagram-spreadsheet [11-06-2018]

13.10. Cost Analysis

In the preliminary design phase the cost analysis is a very difficult practice, there are still many unknowns which and assumptions which have to be made. Especially in the aircraft R&D, manufacturing, and the maintenance cost many assumptions had to be made. Therefore these costs need to be validated using different methods.

For the RDT&E cost the cost per aircraft was compared to the aircraft list price of aircraft with similar size. This was done using methods described in Tim Lammering [86]. This method uses the MTOW and fuselage length to estimate the list price of an aircraft. These estimates came to €6.1M and €8.7M respectively accounting for inflation[6] and conversion[7] from dollars to euro's. This means that the €8.8M estimated in section 10.1.1 is a good conservative estimate for the cost per aircraft.

The maintenance cost estimated in section 10.1.2 was based on the cost of the maintenance materials [74] and the material fraction[19] in the total cost of maintenance. This method gave a very wide range of estimates for the maintenance cost per flight hour and per cycle. Therefore the maintenance cost was compared to the maintenance cost of conventional airliners.[44]. The costs are compared on a basis of maintenance per flight hour, per flight and per aircraft. The results of this comparison is given in table 13.6. For the AT1 estimate based on the flight-hour method the cost per flighthour and per aircraft are within the bounds of the conventional airliners. The cost per cycle is however far higher than the conventional airliner, this is caused by the extraordinarily long endurance of the AT1. The cost estimates per flight cycle for the AT1 is far lower than the conventional airliners. This is especially true for the cost per flight hour and per aircraft, this is again caused by the long endurance of the AT1. The overall lower maintenance cost is most likely to be due to the fact that the smallest aircraft in the airliner sample is the Bombardier Q400 with a Maximum take-off weight of 27 tons[8].This is over 6 times the MTOW of the AT1, besides this the Q400 has 2 engines where the AT1 only has a single engine. Therefore the maintenance cost for the AT1 can be expected to be lower than the cost for the airliner. From the airliner data we find that the cost estimate based on flight hours of the AT1 is too high while the estimate based on the flight cycles is too low. Thus the airliner data can not be used to validate either of the maintenance cost estimates. It can however be used to find a range within which the maintenance cost for the AT1 should lie. This range is found by multiplying the flight hours, cycles and number of aircraft with the minimal and maximum values found for the airliners. Annual maintenance costs ranging from $ 341M up to $ 491M would lie within all bounds for the airliner maintenance cost. To keep a conservative cost estimate the flight hour cost estimate calculated in section 10.1.2 is kept.

Table 13.6: Maintenance cost comparison

Maintenance cost	Average	Min	Max	AT1 (FH)	AT1 (cycle)
per flight hour	$ 1,087.00	$ 287.00	$ 2,841.00	$ 548.81	$ 11.82
per flight cycle	$ 2,681.00	$ 465.00	$ 11,937.00	$ 15,852.42	$ 341.44
per aircraft	$ 3,600.00	$ 670,000.00	$ 9,300,000.00	$ 3,813,108.91	$ 82,128.53

[6]Retrieved from: https://www.bls.gov/data/inflation_calculator.htm [20/06/2018]
[7]Retrieved form: Google Search [20/06/2018]
[8]Retrieved from: https://commercialaircraft.bombardier.com/content/dam/Websites/bca/literature/q400/BCA_5446_03_Q400_Factsheet_Update_EN_vF.pdf [22/06/2018]

14 Requirements Compliance Matrix

In this chapter, the requirements compliance matrices are presented in section 14.1. Some requirements can only be met at a later design stage or are identified as killer requirement in the baseline report[33]. These are presented in section 14.2.

14.1. Requirements Compliance Matrices

In table 14.1 up to and including table 14.5 the requirements matrices are presented. If a requirement is met, a check mark is given. In the fourth column it can be seen in which section in the report the requirement is verified.

Table 14.1: Stakeholder requirements

Req. ID	Requirement	✓	Source
Customer			
STK-CUS-01	The CCT system shall deliver payload at altitudes from 3km below the tropopause to the start of the tropopause.	✓	Section 7.13
STK-CUS-02	The CCT system shall be capable of injecting at least $15l^{-1}$ concentrations of ice nuclei (IN) over the specified global cirrus formation areas.	✓	Section 5.1
STK-CUS-03	The CCT system fleet shall be able to operate using existing airports and facilities.	✓	Section 4.2
STK-CUS-04	The CCT system fleet size shall include some spares for aircraft under maintenance.	✓	Section 4.3.1
STK-CUS-07	The CCT system shall have adequate hardware and software redundancy to meet safety-critical levels of reliability.	✓	Section 9.1.2
STK-CUS-09	The negative effects of the seeding of IN by the CCT system should be orders of magnitude less than benefits of earth radiation management.	✓	Section 12.2
STK-CUS-10	The CCT system shall incorporate appropriate materials, fuels and low-drag technologies to minimise the environmental impact of ice nuclei delivery.	✓	Section 5.3, Section 6.1, Chapter 12
STK-CUS-11	The CCT system shall seed the specified areas during late fall / winter / early spring.	✓	Chapter 4
STK-CUS-12	The CCT system shall seed in alternating hemispheres at latitudes greater than $60°$ North and greater than $60°$ South.	✓	Chapter 4
STK-CUS-13	The CCT system shall refresh the seeding locally at least once a week.	✓	Chapter 4, Section 5.1
STK-CUS-14	The CCT system shall have minimal indirect environmental effects.	✓	Chapter 12
STK-CUS-16	The CCT system shall operate for 25 ± 5 years.	✓	Section 10.1.3, Chapter 16
STK-CUS-17	The CCT system shall have a development time of 4 to 6 years.	✓	Chapter 16
Certifying Bodies			
STK-CRT-01	The CCT air segment shall comply to the (safety) regulations.	✓	See below

TU Delft			
STK-TUD-01	Publication of the project shall take into account the controversy surrounding climate engineering.	✓	Chapter 1

Table 14.2: Top-level system requirements

Req. ID	Requirement	✓	Source
SYS-02	The CCT system shall be able to perform seeding at air temperatures ranging from -60°C to 45°C	✓	Section 7.14
SYS-03	The CCT system shall be protected from the damaging effects of the IN.	✓	Section 5.5
SYS-04	The CCT system shall provide a seeding concentration of at least 15 and a maximum of 100 particles with an optimum of 18 particles per litre in the specified seeding volume.	✓	Section 5.1
SYS-05	The CCT system shall be able to seed at altitudes from 3 km below the tropopause up to the tropopause.	✓	Section 7.13
SYS-06	The CCT system shall be able to distribute the seed at latitudes larger than 60° on both hemispheres.	✓	Chapter 4
SYS-07	The CCT system shall operate for ±25 years.	✓	Section 10.1.3, Chapter 16
SYS-08	The effect of the total CO2 emissions of the CCT system on the global temperature increase shall be at least two orders of magnitude less than the effect of the CCT mission on the global temperature decrease.	✓	Section 12.2
SYS-09	The CCT system shall have a communications system.	✓	Chapter 8
SYS-11	The CCT system shall comply to the regulations set by certifying bodies.	✓	See below
SYS-14	The CCT system shall operate from existing airports.	✓	Section 4.2
SYS-15	The CCT system shall have a maximum development time of 6 years.	✓	Chapter 16
SYS-16	The CCT system shall be able to refresh the seeding once a week.	✓	Chapter 4
SYS-17	The CCT system shall be able to measure the current IN concentration.	✓	Section 5.6

Table 14.3: Payload subsystem requirements

Req. ID	Requirement	✓	Source
SYS-PAY-01	The payload of the CCT payload subsystem shall remain operative at air temperatures ranging from -60^{o}C to 45^{o}C.	✓	Section 5.4.2, Section 5.5.1
SYS-PAY-02	The CCT payload subsystem shall be able to determine the payload injection flow rate with an accuracy of ±1%.	✓	Section 5.5.2
SYS-PAY-03	The injection element of the CCT payload subsystem shall be able to achieve a regulated payload flow rate of no more than 400 ml/minute.	✓	Section 5.5.2
SYS-PAY-04	The injection of the CCT payload subsystem shall have at least one level of redundancy.	✓	Section 4.3.1
SYS-PAY-05	The payload of the CCT payload subsystem shall not directly harm organisms on earth.	✓	Section 5.3
SYS-PAY-06	The CCT payload subsystem shall fit into the CCT aircraft subsystem.	✓	Section 5.5, Section 6.5
SYS-PAY-07	The CCT payload subsystem shall be able to to sustain a net IN flow of 4.26 g/s at 10 km altitude.	✓	Section 5.5.2

Table 14.4: Aircraft subsystem requirements

Req. ID	Requirement	✓	Source
SYS-AC-01	The CCT aircraft subsystem shall be able to operate with an outside air temperature between -65^{o}C to 40^{o}C	✓	Section 7.14
SYS-AC-03	The CCT aircraft subsystem shall have a capability of delivering at least 300 kg payload to the specified area.	✓	Section 6.12.2
SYS-AC-04	The structure of the CCT aircraft subsystem shall be able to cope with the operational loads.	✓	Section 7.3
SYS-AC-05	The CCT aircraft subsystem shall be protected from the damaging effects of the payloads.	✓	Section 5.5
SYS-AC-06	The CCT aircraft subsystem shall have an on-board communications system.	✓	Chapter 8
SYS-AC-07	The CCT aircraft subsystem shall communicate its position at least every 0.3 minutes.	✓	Section 8.6
SYS-AC-08	The CCT aircraft subsystem shall be able to communicate the results of IN measurements to the base.	✓	Section 8.3
SYS-AC-09	The CCT aircraft subsystem shall be able to communicate its current flight profile.	✓	Section 8.3-Section 8.5
SYS-AC-10	The CCT aircraft subsystem shall comply to the regulations set by certifying bodies.	✓	See below
SYS-AC-11	The manufacturing cost of the CCT aircraft subsystem including payload components shall not exceed 95% of initial development cost.	✓	Section 10.1
SYS-AC-12	The CCT aircraft subsystem shall be able to determine its altitude.	✓	Section 8.1
SYS-AC-13	The CCT aircraft subsystem shall be able to determine its horizontal position.	✓	Section 8.1
SYS-AC-14	The CCT aircraft subsystem shall be able to reach an altitude equal to the altitude of the tropopause within the seeding area.	✓	Section 7.13
SYS-AC-15	The CCT aircraft subsystem shall be able to operate a minimum of 200 flights per year.	✓	Chapter 4
SYS-AC-16	The CCT aircraft subsystem shall be able to operate for a minimum of 25 years.	✓	Section 10.1.3
SYS-AC-17	The CCT aircraft subsystem delivery vehicle shall carry a flight data recorder at all times.	✓	Section 8.1
SYS-AC-18	The CCT aircraft subsystem shall be able to house the CCT payload subsystem.	✓	Section 6.12

Table 14.5: Operations subsystem requirements

Req. ID	Requirement	✓	Source
SYS-OPS-07	The CCT operations subsystem shall provide maintenance to the CCT aircraft subsystem.	✓	section 9.2
SYS-OPS-08	The CCT operations subsystem shall provide an A check every 200-300 cycles to every aircraft.	✓	section 9.2
SYS-OPS-09	The CCT operations subsystem shall provide a B check every 6-8 months to every aircraft.	✓	section 9.2
SYS-OPS-10	The CCT operations subsystem shall have a C check every 20-24 months to every aircraft.	✓	section 9.2
SYS-OPS-11	The CCT operations subsystem shall provide a D check every 6 years to every aircraft.	✓	section 9.2
SYS-OPS-12	The CCT operations subsystem shall have at least one spare aircraft.	✓	section 4.3.1
SYS-OPS-14	The annual cost of payload shall not exceed 15 % of annual operating cost.	✓	Section 10.1.2

SYS-OPS-15	The annual cost of fuel shall not exceed 45 % of annual operating cost.	✓	Section 10.1.2

STK-CRT-01/SYS-11/SYS-AC-10: the CCT delivery aircraft will operate for government and/or military purposes and does not have to adhere to the certifications set by these authorities[1]. Therefore this requirement is considered to be met.

14.2. Feasibility Analysis

The feasibility analysis includes an elaboration on the identified killer requirements and requirements which are to be verified at a later design stage.

14.2.1. Identified killer requirements

The following requirements have been identified as a killer requirement in the baseline report[33].

STK-CUS-05/SYS-12: The initial development cost for the CCT system fleet shall not exceed 1 Billion Euros. The supervisors of the project have agreed on a higher margin on this, thus this is no longer a requirement that has to be met. However the cost shall still be kept to an absolute minimum while still complying with the other requirements.

STK-CUS-06/SYS-13: The annual direct operating cost for the CCT system fleet shall not exceed 300 Million Euros.
The supervisors of the project have agreed on a higher margin on this, thus this is no longer a requirement that has to be met. However the cost shall still be kept to an absolute minimum while still complying with the other requirements.

STK-CUS-15: The CCT system shall be all-weather operational from the chosen airports.
SYS-01: The CCT system shall be able to perform in all expected operational weather conditions.
SYS-AC-02: The CCT aircraft subsystem shall be able to operate in the expected weather conditions during operations.
This stakeholder requirement was identified as a killer requirement in the baseline report[33]. The other two requirements were derived from this requirement. After consultation of the supervisors, it was agreed that this requirement is not feasible as the aircraft is not able to take-off at all airports during all weather conditions such as storms. At the airport in Ushuaia severe cross winds and storms can occur and therefore, the aircraft was designed for this airport. In section 7.14 it was explained that the aircraft is designed to handle cross winds of 20 m/s. If higher cross winds occur, which happen rarely but do happen, the aircraft will not be able to take off. A payload margin is included for these occasions, so seeding can be postponed by 1.3 days while still maintaining the required minimal seeding concentration. While the aircraft is in the air, the aircraft is able to operate during all expected weather conditions, as verified in section 7.14. Concluding, the aircraft can take off in almost any weather condition, except when rare storms and cross winds occur which was approved by the supervisors.

14.2.2. Requirements to be verified at a later design stage

The requirements stated in table 14.6 must still be validated, as these requirements are beyond the scope of the project. The storage facilities will be decided on at a later stage, as well as the transportation of the IN to the base. This also holds for personnel considerations. Validating that the system does not fail can only be done by testing.

[1] Retrieved from: https://www.sciencedirect.com/science/article/pii/S1877705814012041?via%3Dihub [21-06-2018]

Table 14.6: Requirements to be met in future stages of the project development

Req. ID	Requirement
SYS-OPS-01	The CCT operations subsystem shall provide <tbd.> kg IN during operations to the base.
SYS-OPS-02	The CCT operations subsystem shall have storage facilities on ground to store <tbd.> kg of payload.
SYS-OPS-03	The CCT operations subsystem shall have an emergency batch of <tbd.> kg of IN.
SYS-OPS-04	The CCT operations subsystem shall protect the IN storage facilities from the corrosive effects of the IN.
SYS-OPS-05	The transportation system between the storage facility and delivery system shall be protected from the damaging effects of the IN.
SYS-OPS-06	All personnel handling the IN shall be protected from the damaging effects of the IN.
SYS-OPS-13	The CCT operations subsystem personnel shall be trained to be able to perform their task.
SYS-10	The CCT system shall have no single points of failure.

15 Sensitivity Analysis

Since there are many unknowns in the field of cirrus cloud thinning, it is important to see whether the design is robust to changes in the mission. To analyse this robustness a sensitivity analysis was performed. All analyses in this chapter are performed based on the current AT1 design and determining the sensitivity of changes in both seeding requirements and airplane performance to the overall mission costs. Since ACT consists of a fleet of aircraft, scaling the number of aircraft can solve many of the problems. However, if the fleet is scaled to a too large extent, a complete redesign might be more efficient.

15.1. Sensitivity to Seeding Requirements

In this section the sensitivity to the seeding requirements will be discussed, these requirements mainly come from the customer requirements. Since CCT is a technique that has not been performed yet, these requirements have a high chance of changing. Therefore, a sensitivity analysis to the seeding requirements is very important.

15.1.1. IN Concentration

The target IN concentration is a particle concentration of 35 particles per litre as described in section 5.1, which decays to 17.5 particles per litre after seven days considering seven days of atmospheric half-life. The target seeding concentration may be subject to change because of either experiment findings that lead to the conclusion the desired particle concentration for effective cirrus cloud thinning is different. As the AT1 is designed for the fleet to be able to seed the initial build-up concentration needed, there is room for a higher maintenance concentration than anticipated, which will of course increase the overall payload (and fuel) costs. For the current AT1 design, the ceiling of concentration is 48 particles per litre right after seeding, decaying to a concentration of 24 particles per litre after seven days. The resulting impact on system costs (accounting for fleet purchase, fuel expense and payload) is shown in figure 15.1.

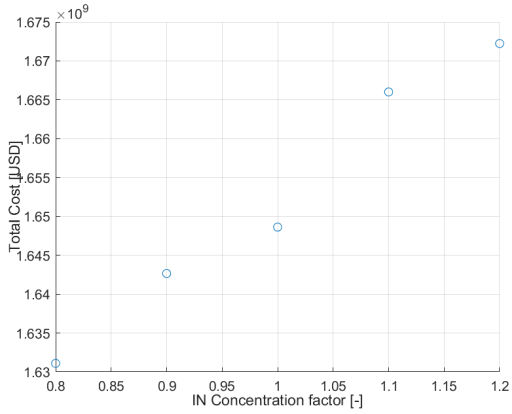

Figure 15.1: System costs versus IN Concentration (from 80% to 120%)

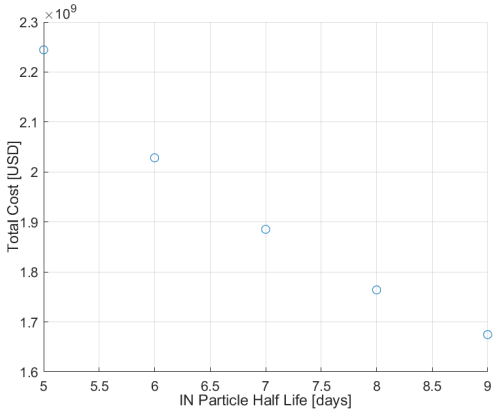

Figure 15.2: Systems costs versus IN Atmospheric Residence (Half-life in days)

15.1.2. IN Atmospheric Residence

The target seeding concentration and interval are based on the assumption of an atmospheric half-life of 1 week [62] and the particle concentration outlined in section 5.1. The target seeding concentration may be subject to change because of either experimental findings that lead to the conclusion that the desired particle concentration for effective cirrus cloud thinning is different, or findings that the atmospheric residence time of particles differs from the initial assumption, or both. If the seeding concentration decays faster than expected, it could be resolved by shortening the replenishment interval or using a higher maintenance IN quantity. The seeding at higher quantities needs to be evaluated carefully as having higher concentration involves the risk of over-seeding with adverse effects on cloud forcing. The fleet and range of the AT1 are designed to cover all seeding area nodes in a single week. The result on the overall system costs of having a different residence time (half-life in days) is shown in figure 15.2.

15.1.3. Seeding Altitude

In this phase of the design, it is assumed that seeding will be done at heights of 8 to 10 km, since it is assumed that CCT would be most efficient there. But, since relatively little research has been done to the technical implementation of CCT, this might be subject to change. If the seeding height is decreased, performance goes down because of the higher density. If the seeding height is increased, the performance is better since a higher L/D can be reached. As described in section 7.13, the ceiling of the aircraft in the later stages of the mission is 12 km, that is, when the aircraft is lighter due to burnt fuel. Therefore, if the requirements would be altered to seed above 12 km, a new engine would have to be selected. If the height is decreased, the fleet size increases, this is because the aircraft flies through thicker air and has a lower ground speed at this lower height. If the seeding altitude would be even lower than 6 km, the range of the AT1 would approach the minimum range of 14000 km and the fleet size would approach infinity, as less and less payload can be brought along per sortie in order to achieve the minimum range. This would increase the amount of sorties, and therefore the fleet size, dramatically to still get a fixed amount of payload in the air every week. This is shown in figure 15.3.

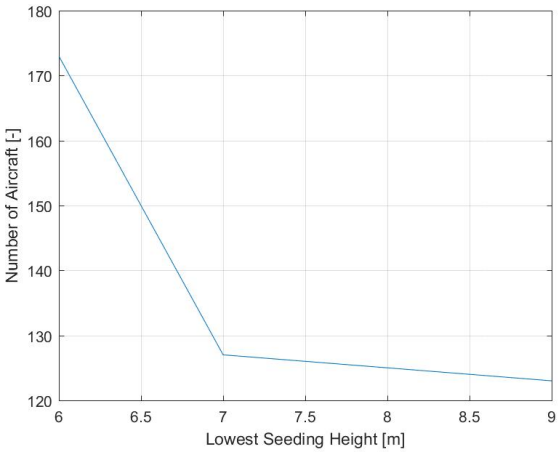

Figure 15.3: Fleet size plotted against the minimum seeding height

15.1.4. Seeding Area

The latitude for which IN seeding is required for ACT is above 60° and below -60° for this project. However, in the future, the climate may develop in such a way that the seeding area needs to be extended. Since this is a likely scenario, a more detailed analysis is performed to investigated a change from 60°to 45°. An increase to 45° would mean the surface area seeded increasing by a factor of 2.18. at first glance this may be solved by scaling the fleet by a factor 2.18. Figure 15.4 displays a map of seeding area position with a

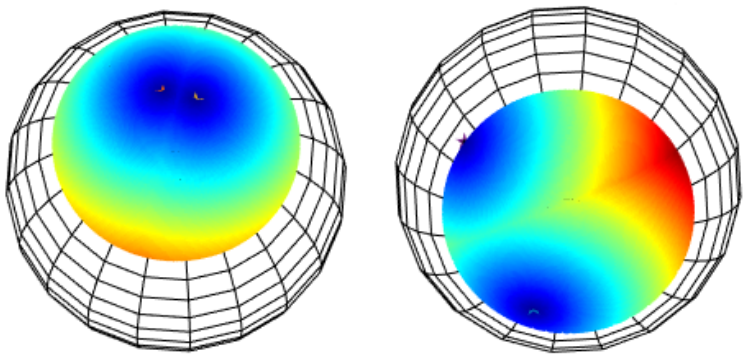

Figure 15.4: Seeding area nodes distance to closest base for 45 degrees latitude - Left: North Pole - Right: South Pole

colour scale showing the distance of seeding area points to the closest base with the bases marked with a star. Further analysis using a grid of seeding area points shows that when extending the seeding area from 60 to 45 degrees latitude both on the North and South Pole distance to base of the ”outer” points in the seeding area are even further away which poses a challenge for AT1 in terms of range. To decrease the distance-to-base for the outer points in the seeding area as well as alleviate the bases in the number of movements on a single base are more than doubled, a third base needs to be selected to allow for extension of the seeding area. In the northern hemisphere, there are multiple airports available to use as third base. In the southern hemisphere, which is the most constraining for the design, Cape Town International Airport would be best fit to serve as third airport. The costs for fleet plus single-year payload and fuel costs would be $2.88 billion for the 45 °latitude seeding area scenario.

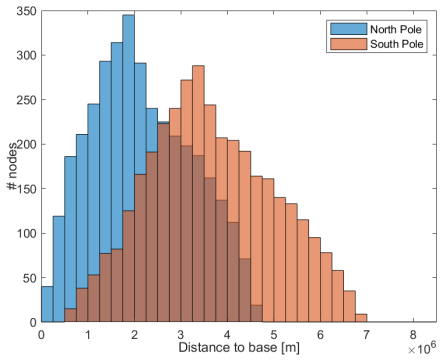

Figure 15.5: Seeding area nodes distance to closest base for 60 degrees latitude

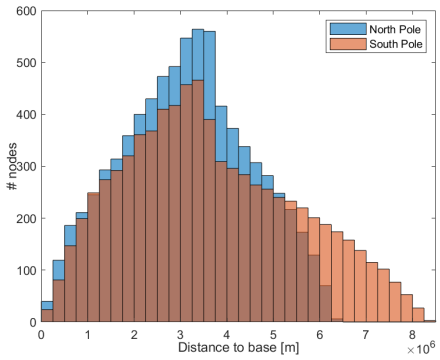

Figure 15.6: Seeding area nodes distance to closest base for 45 degrees latitude

15.2. Sensitivity to Airplane Performance

The preliminary design of the AT1 is done using statistical data and simplified models. If these assumptions turn out to be oversimplified, the performance of the airplane might be less then what was assumed earlier. A sensitivity analysis was performed see changes with respect to L/D and Dispersion Area.

15.2.1. L/D

Statistical data and aerodynamic models in XFLR5 have been used to estimate the aircraft’s L/D. Since L/D and range are heavily linked, a sensitivity analysis was done to show the change in fleet size if L/D would be less than estimated. In figure 15.7, the L/D is plotted over the fleet size. Figure 15.7 shows that the fleet size will increase drastically if the L/D drops below 13. This is because the aircraft range approaches the

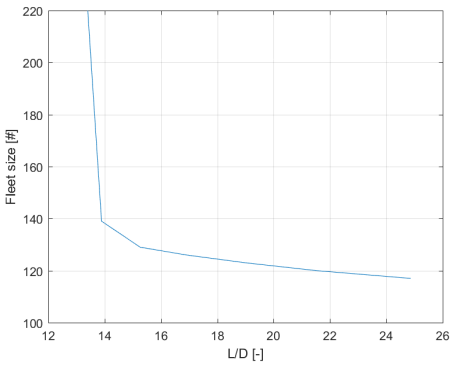

Figure 15.7: Fleet size plotted over Aircraft L/D

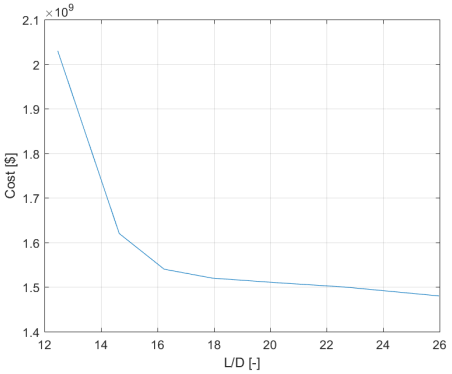

Figure 15.8: Total cost plotted over Aircraft L/D

minimum range that is required to seed the entire area. This figure also shows that the fleet size will not increase drastically if the L/D is close to the initial approximation. This is because the aircraft with less L/D have less range, return earlier to the base and can therefore fly more sorties. However, they would use more fuel since their efficiency is lower. That is why L/D is plotted against total cost in figure 15.8. This cost is build up out of initial purchasing cost, fuel cost, and statistical maintenance cost. Figure 15.8 shows that the L/D does not heavily influence the cost except for when the L/D drops below 14. The use of CFD in the detailed design phase will eliminate some of the uncertainty in the L/D estimate.

15.2.2. Dispersion Area

The dispersion area is the width and height to which the IN material is spread and is one of the most important assumptions in the design of the AT1. Very little specific data is available on this subject and so it is very likely that the initial assumption of a width of 10km and a height of 1 km is subject to change based on the initial payload test that will be executed. Fortunately, a change in the dispersion area varies linearly with the fleet size. If the dispersion width turns out to be 5 km instead of 10 km, twice as many aircraft will have to be used. The same happens if the dispersion depth is 0.5 km instead of 1 km. This is not true for the cost of the fleet because of the effect of the learning curve [1]. This is visualised in figure 15.9. This graph shows that the

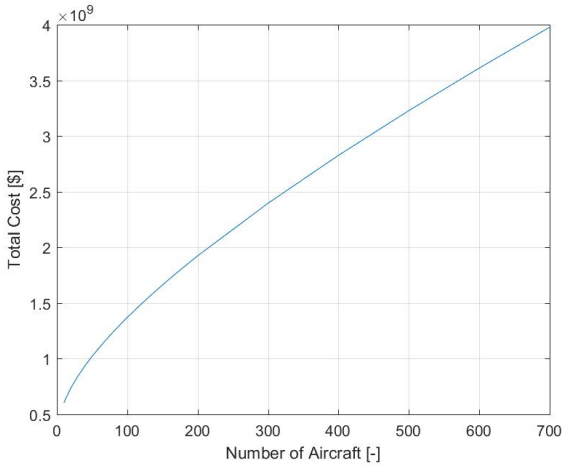

Figure 15.9: Total cost plotted over Fleet size

design is very robust to a change in dispersion width. The only thing that isn't taken into account in this figure is the fact that there is a limitation to the number of aircraft the airports can handle. If the initial assumption of 10 km is orders of magnitude less than expected, more than two airports will need to be selected.

[1] Retrieved from http://strategosinc.com/downloads/learning-curves-dl1.pdf [24-06-2018]

16 Post-DSE Planning

This chapter contains an overview of the activities that will be executed for implementation after the preliminary design is concluded in the DSE. The sequence of activities are represented in a logic diagram along with a separate time planning showing estimated duration of activities as well as project milestones. Please note that the dates presented are based on start of the detailed design phase at the beginning of Q3 2018, immediately proceeding the DSE.

During this project, the conceptual design and preliminary design of the delivery system for CCT have been performed. The next phases until the start of operations will be detailed design, followed by the production, test and certification, and operational phase. The final dispersion characteristics used to generate the preliminary design have a high level of uncertainty and start of operations might be needed earlier than would be possible with a full new aircraft design. ACT has therefore decided on parallel development of a modular design that could be used on existing aircraft (foreseen start of operations in Q1 2021) and the AT1 aircraft design with integrated payload system (foreseen start of operations Q1 2024).

The logical flow of activities is presented in figure 16.1, this diagram shows the steps in the post-DSE phases for both the AT1 and the modular system design on a time line. An important aspect is that at the start of the next phase a test program is initiated to check the design assumptions as described in section 5.6. The tests encompass both lab tests for IN effectiveness as well as in-situ tests using weather modification aircraft to determine the atmospheric dispersion characteristics and system efficacy. As the system needs to be available rather sooner than later unfortunately it is not possible to commence the detailed design only when the uncertainties have been cleared out, therefore ACT strives to adapt the design in the best possible way to the test findings and scale the fleet such that the seeding requirements are met with no adverse effect on net cloud forcing.

While the finer details of the design are worked out, the first steps of the production phase like manufacturing of tooling and part manufacturing are started to ensure the AT1 is available as soon as possible. These steps in the production phase are continued by assembly of parts to sub-assemblies and integration of sub-assemblies and third party supplies to the final aircraft. The test and certification phase entails component testing (e.g. structural testing) as well as quality checking of third party supplies and ends with the flight test program. While the flight test program runs, the bases will be prepared for seeding operations and the fleet control and ground crew are trained.

The development of the modular system is started with the detailed design as well, in this phase as well fleet will have to be acquired if CCT operations need to start earlier than Q1 2024. The test program described is considered to be part of the modular system development as the modular system will be used by ACT to continue the refinement of system characteristics while the AT1 is developed. From 2030, the first parts of the system are expected to be decommissioned whereas aircraft will be recycled where possible as described in section 12.2.

A time planning of the high-level activities in the following project phases is depicted in the Gantt chart presented on the next page.

ID	Task Name	Start	Finish
1	Conceptual Design	Mon 23-4-18	Mon 28-5-18
2	Preliminary Design	Tue 29-5-18	Thu 5-7-18
3	**Payload (Modular) System Detailed Design**	**Mon 9-7-18**	**Fri 26-6-20**
4	Design Modular Payload System in Detail	Mon 9-7-18	Fri 26-6-20
5	Prepare Weather Modification Aircraft for In-Situ Tests	Mon 9-7-18	Fri 24-5-19
6	Perform Lab Test for Payload	Mon 9-7-18	Fri 15-2-19
7	Performing Payload Dispersion System Testing	Mon 14-1-19	Mon 15-7-19
8	Perform In-Situ Dispersion System Tests	Mon 3-6-19	Mon 27-4-20
9	**Payload (Modular) System Production Phase**	**Mon 14-10-19**	**Fri 1-10-21**
10	Manufacture Modular System	Mon 14-10-19	Thu 2-7-20
11	Acquire Existing Aircraft for Fleet	Mon 1-6-20	Fri 27-11-20
12	Integrate Modular System in Existing Aircraft	Mon 3-5-21	Fri 1-10-21
13	**Payload (Modular) System Test Phase**	**Fri 1-1-21**	**Tue 1-6-21**
14	Perform Modular System Testing	Fri 1-1-21	Tue 1-6-21
15	**Payload (Modular) System Operational Phase**	**Mon 3-1-22**	**Tue 31-12-30**
16	Commence Seeding Operations	Mon 3-1-22	Tue 31-12-30
17	Initiate Fleet Maintenance	Mon 3-1-22	Tue 31-12-30
18	Operate Fleet in Daily Operations	Mon 3-1-22	Tue 31-12-30
19	Initiate Day-to-Day Fleet Maintenance	Mon 3-1-22	Tue 31-12-30
20	Monitor System Performance Continuously	Mon 3-1-22	Tue 31-12-30
21	Re-Supply Payload to Bases	Mon 3-1-22	Tue 31-12-30
22	**AT1 Detailed Design**	**Mon 9-7-18**	**Thu 5-11-20**
23	Design of all Aircraft Structural Elements	Mon 9-7-18	Thu 5-11-20
24	Perform Detailed Design Check	Mon 6-8-18	Wed 2-9-20
25	Produce Production Drawings for Aircraft Components	Mon 4-2-19	Mon 2-11-20
26	Select and Purchase of 3rd Party Supplies	Mon 4-2-19	Mon 20-4-20
27	**AT1 Production Phase**	**Thu 25-4-19**	**Fri 23-9-22**
28	Manufacturing of Tools	Thu 25-4-19	Mon 23-3-20
29	Manufature Parts	Mon 4-11-19	Fri 19-3-21
30	Assemble Parts to Subassemblies	Mon 15-2-21	Fri 26-11-21
31	Assemble Subassemblies to Aircraft	Mon 3-1-22	Tue 5-7-22
32	Integrate 3rd Party Systems	Mon 3-1-22	Fri 23-9-22
33	Install Aircraft Systems	Mon 3-1-22	Fri 23-9-22
34	**AT1 Testing and Certification Phase**	**Mon 3-5-21**	**Fri 29-12-23**
35	Test Components	Mon 3-5-21	Fri 25-2-22
36	Perform Quality Check on 3rd Party Supplies	Mon 3-5-21	Fri 25-2-22
37	Perform Static Load Test on Aircraft Structural Assembly	Fri 1-7-22	Thu 1-9-22
38	Perform Maiden Flight	Mon 9-1-23	Mon 9-1-23
39	Perform Flight Test Program	Mon 2-1-23	Fri 27-10-23
40	Perform Airworthiness Certification	Sat 1-4-23	Fri 29-12-23
41	Prepare Base Stations	Mon 2-1-23	Fri 27-10-23
42	Perform Airworthiness Certification	Mon 6-3-23	Fri 1-12-23
43	**AT1 Operational Phase**	**Mon 1-1-24**	**Mon 31-12-29**
44	Commence Seeding Operations	Mon 1-1-24	Mon 31-12-29
45	Initiate Fleet Maintenance	Mon 1-1-24	Mon 31-12-29
46	Control Fleet in Daily Operations	Mon 1-1-24	Mon 31-12-29
47	Initiate Day-to-Day Fleet Maintenance	Mon 1-1-24	Mon 31-12-29
48	Monitor System Performance Continuously	Mon 1-1-24	Mon 31-12-29
49	Re-Supply Payload to Bases	Mon 1-1-24	Mon 31-12-29

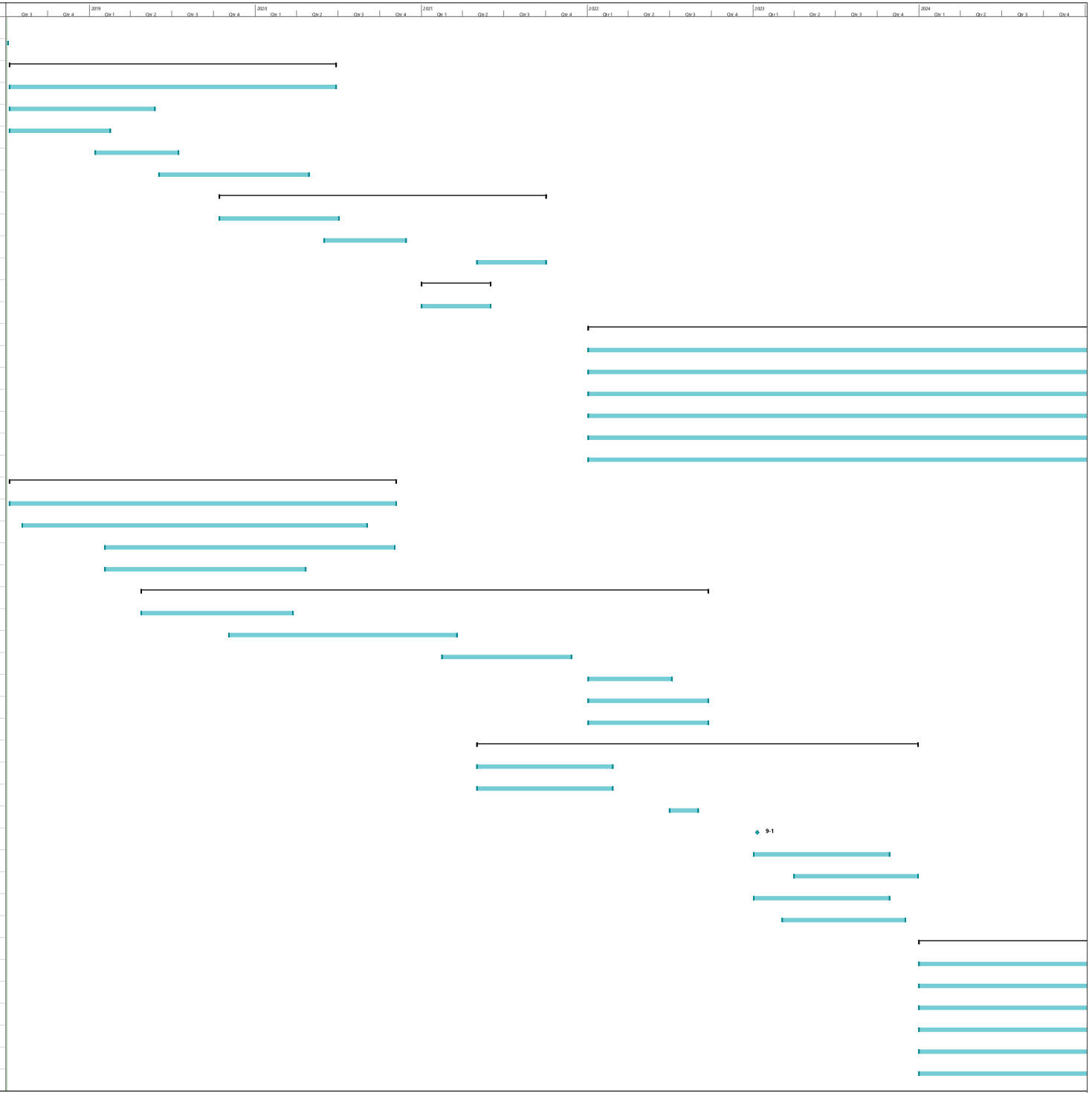

Project: PostDSEGantt
Date: Tue 3-7-18

Task | Split | Milestone | Summary | Project Summary | Inactive Task | Inactive Milestone | Inactive Summary | Manual Task | Duration-only | Manual Summary Rollup | Manual Summary | Start-only | Finish-only | External Tasks | External Milestone | Deadline | Progress | Manual Progress

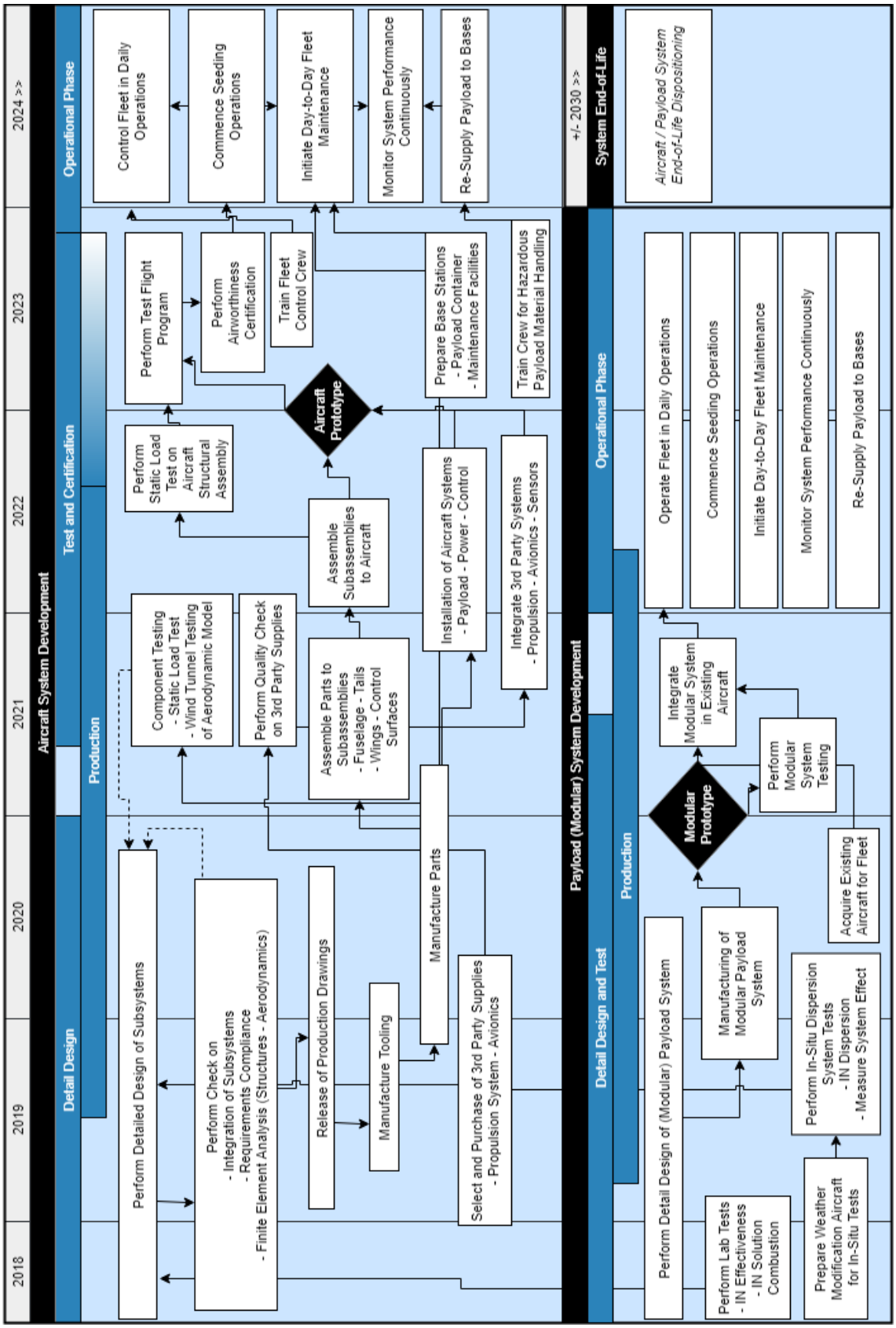

Figure 16.1: Project Design and Development Logic - Post DSE

17 Conclusion and Recommendations

Current climate simulation models indicate an exponential increase in the global temperatures. To prepare for the worst outcomes, the feasibility of geo-engineering methods are investigated. One of these geo-engineering methods is cirrus cloud thinning (CCT), a method which uses ice nuclei (IN) seeding to thin cirrus clouds, thereby increasing the Earth's albedo. The goal of this project was to investigate the feasibility of such an aerial cloud thinning (ACT) system. This report aimed to elaborate on the design of such a system which uses a fleet of aircraft to inject the IN at the seeding altitudes. The aircraft (AT1) as well as the support and maintenance of such a system has been preliminary designed and analysed.

To successfully perform CCT, both the Northern and Southern hemisphere above $60°$ latitude need to be seeded at altitudes varying between 7 and 10 km. The seeding has to be performed during late fall, winter and early spring on each side of the globe, alternating the fleet of aircraft between the poles. The ACT mission requires 205 aircraft that will seed the area by flying 786 sorties per week. This is done operating from the following airports: Ushuaia in Argentina, Christchurch in New Zealand, Svalbard in Norway, and Thule in Greenland. These airports were chosen based on their location, capacity, ability to expand and local weather conditions.

The IN material chosen was bismuth tri-iodide, as this material is relatively cheap, has a low effectivity threshold and is not toxic for the environment. A weekly concentration of 35 particles per litre has to be injected into the cirrus clouds. The yearly amount of bismuth tri-iodide (not dissolved in ethanol) required was found to be 422 tons. The material is transported in a solution form, consisting of bismuth tri-iodide and ethanol, which is combusted before dispersion into the troposphere. To ensure that the desired concentration of IN at the seeding altitudes is maintained, an Ultra-High Sensitivity Aerosol Spectrometer is installed. The overall effect of CCT is monitored using the CALIPSO, GOES-16, and GOES-17 satellites. A modular payload system is designed to integrate on existing aircraft for a short term implementation of CCT.

The driving design factor for the aircraft was having a minimum range of 14,000 km. This resulted in an aircraft with a high aspect ratio of 15, and a wing surface area of 10.22 m^2. This wing design ensures a good lift to drag ratio performance. The engine selected to ensure that the required thrust can be provided given a preferable low operational empty weight is the GE Honda HF120, providing a thrust of 9.1kN at sea level. This turbofan engine will run on jet-B fuel to ensure the fuel doesn't freeze at the low temperatures during aerial operation. With this engine placed on top of the fuselage a V-tail was found to offer the best performance. The aircraft design resulted in an aircraft with an operational weight of approximately 1378 kg and capability to carry and inject a maximum of 296 kg of IN-ethanol solution per flight.

Using a mission cost analysis it was found that the initial cost is approximately €2 billion, the annual cost was approximated to be €770 million, and the end-of-life cost to be an income of €19 million. The initial costs of the project are high but they are still far lower than the cost for other possible solutions, such as equipping existing aircraft with a modular CCT seeding system. Moreover, due to the highly specific nature of the mission no existing aircraft will be able to meet the performance of the AT1 in terms of operations cost and environmental impact.

Recommendations

The market should be analysed on a regular basis to ensure that the estimated time for the mission to be operational is still accurate. A decrease in the available development time could require the implementation of the modular payload subsystem on existing aircraft, to overlap the time until the AT1 will be operational.

The CCT process should first be tested on a small scale basis in order to quantify the environmental impact of the ice nuclei injection, such as the research performed by the Desert Research Institute [21]. This is to further ensure that cirrus cloud thinning does not have any negative affects that have not been accounted for in previous studies. Furthermore, several tests should be performed to confirm whether the assumption of a dispersion width of the ice nuclei of 10km and height of 1 km is indeed a feasible assumption. Also, a small scale experiment should be set up to test the effect of using bismuth tri-iodide as the injection material, as its technology readiness level for cirrus cloud thinning is currently very low. The particles per litre is now established at 35, but the effect of this should be analysed using experimental data. The effects of these payload aspects can be analysed using the CALIPSO, GOES-16, and GOES-17 satellites, which can observe the cirrus clouds behaviour in the atmosphere.

The range is one of the most important characteristics of the aircraft design. As a result, the parameters that affect this the most must be reevaluated in more detail. The engine's specific fuel consumption is currently a relatively rough estimate that can easily be validated by HondaJet aircraft which use the same engine. Moreover, a small scale model of the aircraft should be produced to analyse the aircraft drag, aerodynamic performance, and stability and control. Such a test would generate more accurate values for the lift-to-drag ratio resulting in a more feasible design. Since the V-tail configuration with the engine located in between the fins is prone to unexpected airflow interactions, it should be analysed with advanced CFD software or, preferably, a wind tunnel experiment. Another step to be taken before continuing with the design process is an in-depth evaluation of whether the engine can provide enough auxiliary power to heat the aircraft up during the operations in the low temperature extremes. Furthermore the flutter of the wing needs to be analysed in more detail to ensure that the wing does not fail in this mode.

For the operational aspect of the project, an algorithm should be developed to determine the most optimal flight path for the fleet of aircraft to cover the seeding area. This could potentially lead to a shorter and more accurate range, resulting in a lower fleet size required to seed the entire area, consequently in a lower cost and higher sustainability for the mission. Furthermore, a more detailed support system should be investigated regarding the monitoring of the aircraft and the take-over from ground control during severe landing conditions. Lastly, the maintenance, which is found to be the main driver in the annual operating cost, should be analysed in more detail to get a more accurate cost estimate. The same holds for the Insurance cost, it needs to be estimated in more detail due to the rough estimate of 1% of the operational cost which it is based on now.

Bibliography

[1] Design Synthesis Exercise Group 2. *Stratosperic Aerosol Geoengineering Aircraft*. Delft University of Technology, "Delft, Kluyverweg 1, The Netherlands", 2016.

[2] Federal Aviation Administration. Aircraft noise and noise monitoring, Sep 2017.

[3] European Aviation Safety Agency. *Certification Specifications for Large Aeroplanes CS-25*. EASA, September 2008.

[4] European Aviation Safety Agency. *Certification Specifications for Engines CS-E*. EASA, December 2010.

[5] European Aviation Safety Agency. *Type-Certificate Data Sheet for GE Honda Aero Engines HF120 Series Engine*. EASA, April 2016.

[6] European Defence Agency. European defence agency, annual report 2009. Technical report, European Defence Agency, 2009.

[7] The European Aviation Safety Agency. Easa certification noise levels, Jan 2018.

[8] Christchurch International Airport. Christchurch international airport airport noise management plan, May 2018.

[9] C.M. Archuleta, P.J. DeMott, and S.M. Kreidenweis. Ice nucleation by surrogates for atmospheric mineral dust and mineral dust/sulfate particles at cirrus temperatures. *Atmospheric Chemistry and Physics*, 5(10):2617–2634, 2005.

[10] Boeing. Statistical summary of commercial jet airplane accidents. Technical report, Boeing, July 2017.

[11] T.C. Bond, S.J. Doherty, D.W. Fahey, P.M. Forster, T. Berntsen, B.J. DeAngelo, M.G. Flanner, S. Ghan, B. Kärcher, D. Koch, Kinne S., Y. Kondo, P.K. Quinn, M.C. Sarofim, M.G. Schultz, M. Schulz, C. Venkataraman, H. Zhang, S. Zhang, N. Bellouin, S.K. Guttikunda, P.K. Hopke, M.Z. Jacobson, J.W. Kaiser, Z. Klimont, U. Lohmann, J.P. Schwarz, D. Shindell, T. Storelvmo, S.G. Warren, and C.S. Zender. Bounding the role of black carbon in the climate system: A scientific assessment. *Journal of Geophysical Research: Atmospheres*, 118(11):5380–5552, 2013.

[12] A. Cervone. *Aerospace Design and Systems Engineering Elements II – AE2111-II - Telecommunications*. TU Delft, September 2015.

[13] P. Colonna and W.C. Reynolds. *Thermodynamics*. Cambridge University Press, first edition, 2016.

[14] M.V. Cook. *Flight Dynamics Principles*. Butterworth-Heinemann, 2007. Chapter 10.

[15] CDF Corporation. Polyethylene chemical resistance chart. , July 2004.

[16] M.C. Cotting. Evolution of flying qualities analysis: Problems for a new generation of aircraft. *Virginia Polytechnic Institute*, March 2010.

[17] National Research Council. *Advancing the Science of Climate Change*. The National Academic Press, "Washington, DC 20001, 500 Fifth Street N.W., United States of America", 2010.

[18] J. Cozic, S. Mertes, B. Verheggen, D.J. Cziczo, S.J. Gallavardin, S. Walter, U. Baltensperger, and E. Weingartner. Black carbon enrichment in atmospheric ice particle residuals observed in lower tropospheric mixed phase clouds. *Journal of Geophysical Research: Atmospheres*, 113(D15), 2008.

[19] Geraldine CROS. *FY2013 Maintenance Cost Preliminary Analysis*. IATA, September 2014.

[20] N. S. Currey. Aircraft landing gear design: Principles and practices, - 1988.

[21] W. Finnegan D.L. Mitchell. Modification of cirrus clouds to reduce global warming, Oct 2009.

[22] Prof. dr. D. G. Simons. Ae4431 aircraft noise and emissions, chapter 6: Noise metrics, December 2017.

[23] A.J. Durant, R.A. Shaw, W.I. Rose, Y. Mi, and G.G.J. Ernst. Ice nucleation and overseeding of ice in volcanic clouds. *Journal of Geophysical Research: Atmospheres*, 113(D9), 2008.

[24] A. Elham. *Aerospace Design and Systems Engineering Elements II – AE2111-II - Aileron design*. TU Delft, September 2016.

[25] A. Elham. *Aerospace Design and Systems Engineering Elements II – AE2111-II - Aircraft aerodynamic analysis - Drag*. TU Delft, September 2016.

[26] A. Elham. *Aerospace Design and Systems Engineering Elements II – AE2111-II - Aircraft aerodynamic analysis - Lift*. TU Delft, September 2016.

[27] EUMETRAIN. Clean air turbulence, chapter 2- the significance of jet streams for clean air turbulence, 2012.

[28] Eurocontrol. Acas ii post-implementation case, 2011.

[29] FEDERAL AVIATION ADMINISTRATION, DEPARTMENT OF TRANSPORTATION. *Pilot's Handbook of Aeronautical Knowledge*. Federal Aviation Administration, 2016.

[30] FEDERAL AVIATION ADMINISTRATION, DEPARTMENT OF TRANSPORTATION. *Electronic Code of Federal Regulations*. Federal Aviation Administration, 2018.

[31] H Gersmann. Public supports geoengineering research, survey finds. *The Guardian*, October 2011.

[32] Zdobyslaw Goraj. An overview of the deicing and antiicing technologies with prospects for the future. *Warsaw University of Technology*, 2004.

[33] Group 11. Baseline report- delivery system for cirrus cloud thinning. Technical report, TU Delft, 2018.

[34] Group 11. Midterm report - delivery system for cirrus cloud thinning. Technical report, TU Delft, 2018.

[35] Group 11. Project plan- delivery system for cirrus cloud thinning. Technical report, TU Delft, 2018.

[36] Jay Gundlach. *Designing Unmanned Aircraft Systems: A Comprehensive Approach*. American Institute of Aeronautics and Astronautic, 2012.

[37] Stephen B. Heppe. *Handbook of Unmanned Aerial Vehicles*. Springer, Dordrecht, 2014. Chapter 32, Problem of UAV Communications.

[38] R.C. Hibbeler. *Mechanics of Materials*. Pearson, 2014.

[39] Eugene Hill, Manny Rios, Galdemir Boturaand, James T. Riley, Christopher J. Dumontand, Decio Pullin, Sudhindra Uppuluri, Andrew Broeren, Michael S. Selig, and David N. Anderson. Investigations of performance of pneumatic deicing boots, surface ice detectors, and scaling of intercycle ice. Technical report, U.S. Department of Transportation - FAA, 2006.

[40] K.P. Hoinka. Temperature, humidity, and wind at the global tropopause. *Monthly Weather Review*, 127(10):2248–2265, October 1999.

[41] Honda. Hf120 turbofan engine. Technical report, Honda, 2018.

[42] S.J. Hulshoff. *AE4930 Aeroelasticity*. Faculty of Aerospace Engineering, TU Delft, Kluyverweg 1, Delft, eleventh edition, 2011.

[43] S.J. Hulshoff. *Project Guide Design Synthesis Exercise - Delivery System for Cirrus Cloud Thinning*. TU Delft, 2018.

[44] IATA. Airline maintenace cost executive commentary. Technical report, IATA, 2015.

[45] Roskam J. *Airplane design- Part I - Preliminary Sizing of Airplanes*. Roskam Aviation and Engineering Corporation, 1985.

[46] J.A. Mulder, W.H.J.J. van Staveren and J.C. van derVaart and E. de Weerdt and C.C. de Visser and A.C. in 't Veld and E. Mooij. Flight dynamics. Technical report, TU Delft, 2013.

[47] A. Janes and J. Chaineaux. Experimental determination of flash points of flammable liquid aqueous solutions. *Chemical Engineering Transactions*, 31:943–948, 05 2013.

[48] H. Schmidt J.E. Kristjánsson, H. Muri. The hydrological cycle response to cirrus cloud thinning. *Geophysical Research Letters*, December 2015.

[49] G. Kennedy and J. Martins. A comparison of metallic and composite aircraft wings using aerostructural design optimization. *American Institute of Aeronautics and Astronautics*, 09 2012.

[50] C.G. Keyes, G.W. Bomar, T.P. DeFelice, D.A. Griffith, and D.W. Langerud. *Guidelines for Cloud Seeding to Augment Precipitation*. American Society of Civil Engineers, third edition edition, 2016.

[51] Harry Kinnison. *Aviation Maintenance Management*. McGraw-Hill, 2011.

[52] A.H. Lefebvre and D.R. Ballal. *Gas Turbine Combustion*. Taylor & Francis Group, third edition, 2010.

[53] H Linger and J Owen. *The project as social system : Asia-Pacific perspectives on project management*. Monash University PublishFdatcming, "Clayton, Victoria 3800, Australia", 2012.

[54] Robert Rathburn Margaret M. McMahon. Measuring latency in iridium satellite constellation data services. *Researchgate*, March 2015.

[55] H. Damon Matthews. Regional estimates of the transient climate response to cumulative co2 emissions, Jan 2016.

[56] T.H.G. Megson. *Aircraft Structures for Engineering Students*. Elsevier Aerspace engineering series. Elsevier, fourth edition, 2007. Chapter 10.

[57] O. Meier and D. Scholz. A handbook method for the estimation of power requirements for electrical de-icing systems. *Hamburg University of Applied Sciences*, September 2010.

[58] J. Melkert. *AE2230-II Propulsion and Power lecture slides*. TU Delft, 2017. Lecture 4, Slide 34 and Lecture 5.

[59] J. Melkert. *AE-2230-II Propulsion and Power lecture slides*. TU Delft, 2017.

[60] N. Merah, F. Saghir, Z. Khan, and A. Bazoune. Effect of temperature on tensile properties of hdpe pipe material. *Plastics, Rubber and Composites*, 35(5):226–230, 2006. Cited By :12.

[61] Sharp J Mercer M, Keith D. Public understanding of solar radiation management. *Environmental Research Letters*, October 2011.

[62] D.L. Mitchell. Estimation of seeding material requirements. , September 2010.

[63] D.L. Mitchell and W. Finnegan. Modification of cirrus clouds to reduce global warming. *Environmental Research Letters*, 4(4): 045102, 2009.

[64] S.C. Mossop and C. Tuck-Lee. The composition and size distribution of aerosols produced by burning solutions of agi and nai in acetone. *Journal of Applied Meteorology (1962-1982)*, 7(2):234–240, 1968.

[65] Adrian P. Mouritz. *Introduction to Aerospace Materials*. Woodhead Publishing Limited, 2012. Chapter 25, Materials selection for aerospace.

[66] F. Möller, C. Thomy, F. Vollertsen, P. Schiebel, C. Hoffmeister, and A.S. Herrmann. Novel method for joining cfrp to aluminium. *Physics Procedia*, 5:37 – 45, 2010.

[67] L. M. Nicolai. *Fundamentals of Aircraft Design*. American Institute of Aeronautics & Astronautics, first edition edition, 1984.

[68] Senter Novem. The netherlands: list of fuels and standard co2 emission factors, December 2004.

[69] Fabrizio Oliviero. *AE3221-I Systems Engineering and Aerospace Design: Requirement Analysis and Design principles for A/C stability & control (Part 1)*. TU Delft, March 2018.

[70] W. F. Phillips. Estimating the low-speed sidewash gradient on a vertical stabilizer. *Journal of Aircraft*, 39(4):600–608, 2002. URL https://doi.org/10.2514/2.3042.

[71] K.A. Pratt, P.J. Demott, J.R. French, Z. Wang, D.L. Westphal, A.J. Heymsfield, C.H. Twohy, A.J. Prenni, and K.A. Prather. In situ detection of biological particles in cloud ice-crystals. *Nature Geoscience*, 2(6):398–401, 2009.

[72] P.E. Purser and J.P. Campbell. Report 823: Experimental verification of a simplified vee-tail theory and analysis of available data on complete models with vee tails. *National Advisory Comittee for Aeronautics (NACA)*, 1944.

[73] R. Sheresinhe and C. Lawson. Electrical load-sizing methodology to aid conceptual and preliminary design of large commercial aircraft. Technical report, Institution of Mechenical Engineers, 2014.

[74] D. P. Raymer. *Aircraft Design: A Conceptual Approach*. AIAA, 1992.

[75] P. Roberts and J. Hallett. A laboratory study of the ice nucleating properties of some mineral particulates. *Quarterly Journal of the Royal Meteorological Society*, 94(399):25–34, 1968.

[76] G. Roloff. Aircraft landing gear, April 2002.

[77] J. Roskam. *Airplane design- Part IV - Lay-out and Design of Landing Gear and Systems*. Roskam Aviation and Engineering Corporation, 1985.

[78] Mohammed H. Sadraey. *Aircraft Design, A Systems Engineering Approach*. John Wiley & Sons Ltd., The Atrium, Southern Gate, Chichester, West Sussex, PO19 8SQ, United Kingdom, 2013. ISBN 978-1-119-95340-1.

[79] T.L. Schindler. The polar jet stream, Oct 2011.

[80] U. Schumann, R. Baumann, D. Baumgardner, S.T. Bedka, D.P. Duda, V. Freudenthaler, J.F. Gayet, A.J. Heymsfield, P. Minnis, M. Quante, E. Raschke, H. Schlager, M. Vázquez-Navarro, C. Voigt, and Z. Wang. Properties of individual contrails: a compilation of observations and some comparisons. *Atmospheric Chemistry and Physics*, 17(1):403–438, 2017. doi: 10.5194/acp-17-403-2017.

[81] *Safety data sheet silver iodide*. Sigma-Aldrich, July 2006.

[82] T. Storelvmo and N. Herger. Cirrus cloud susceptibility to the injection of ice nuclei in the upper troposphere. *Geophysical Research Letters*, March 2014.

[83] T. Storelvmo, J.E. Kristjansson, H. Muri, M. Pfeffer, D. Barahona, and A. Neses. Cirrus cloud seeding has potential to cool climate. *Geophysical Research Letters*, 40:278–182, January 2013.

[84] T. Storelvmo, W.R. Boos, and N. Herger. Cirrus cloud seeding: a climate engineering mechanism with reduced side effects? *The Royal Society*, 372(2031), November 2014.

[85] The Goodyear Tire and Rubber Company. *Global Aviation Tires*. Goodyear, 2016.

[86] Kristof Risse Ralf Hoernschemeyer†and Eike Stumpf Tim Lammering, Katharina Franz. Aircraft cost model for preliminary design synthesis. *American Institute of Aeronautics and Astronautics*, January 2012.

[87] S. Unterstrasser and N. Görsch. Aircraft-type dependency of contrail evolution. *Journal of Geophysical Research*, 119(24):14,015–14,027, 2014. Cited By :10.

[88] W. Verhagen. *AE3221-I Systems Engineering and Aerospace Design: Lecture 8 - Risk Management & Reliability Engineering*. TU Delft, March 2018.

[89] P.N.A.M. Visser. Ae2233-ii experimental design & data analysis space topic reader, June 2017.

[90] R. Vos. *Aerospace Design and Systems Engineering Elements I – AE1222-II - A/C Preliminary Sizing*. TU Delft, March 2018.

[91] Dr. Ir. M. Voskuijl. Climb and descent - flight and orbital mechanics lectures, 2017.

[92] Mark Voskuijl. Ae2230-i lecture sldies- climb and descent, Feb 2017.

[93] Mark Voskuijl. Ae2230-i lecture sldies- take-off and landing, Feb 2017.

[94] R. Wagner, J. Kaufmann, O. Möhler, H. Saathoff, M. Schnaite, R. Ullrich, and T. Leisner. Heterogeneous Ice Nucleation Ability of NaCl and Sea Salt Aerosol Particles at Cirrus Temperatures. *Journal of Geophysical Research: Atmospheres*, 123(5):2841–2860, 2018.

[95] P.P. Walsh and P. Fletcher. *Gas Turbine Performance*. Blackwell Science Ltd, second edition, 2004.

[96] Tian Yu-peng Wang Biao Wang Jing-dong Wang Xiao-hong, Xu Gui-li. Uav's automatic landing in all weather based on the cooperative object and computer vision. *Second International Conference on Instrumentation & Measurement, Computer, Communication and Control*, pages 1346–1351, January 2012.

[97] M.E. Wise, K.J. Baustian, T. Koop, M.A. Freedman, E.J. Jensen, and M.A. Tolbert. Depositional ice nucleation onto crystalline hydrated nacl particles: A new mechanism for ice formation in the troposphere. *Atmospheric Chemistry and Physics*, 12(2):1121–1134, 2012.

[98] Y. Xu R. Curran-S. Raghunathan D. Gore J. Doherty X. Tan, J. Wang. Cost-efficient materials in aerospace: Composite vs aluminium. *Collaborative Product and Service Life Cycle Management for a Sustainable World*, pages 259–266, 2008.

A Appendix A: Work Division

A.1. Evaluation of PM/SE tool use

During the entire DSE many PM/SE tools were used. Some of these tools were used more effectively than others, this section reflects on the use of the PM/SE tools. For each PM/SE tool it is described how it was used, what went right and what could have been better.

A.1.1. WBS & WFD

The work breakdown structure was initially used to identify the work which needed to be performed throughout the entire project. In the first version of the WBS the first weeks of the DSE were described in detail while for the later phases only the higher levels were identified. The WBS proved to be very useful for the initial identification of the work, however as expected some things were forgotten in the initial version WBS, in case this happened the new task was added to the whiteboard planning which will be discussed later. The WBS was not updated very frequently, it was updated whenever we entered an new phase in the design. The largest updates to the WBS were done for the Baseline review and the Mid-term review. The infrequent updating of the WBS caused it to often be outdated and not very useful continuously throughout the phases. However, the identification of the work at the beginning of each of the phases was very useful for the generation of the WFD and for the initial determination of the tasks for the Gantt chart, which was updated more frequently. the large update during the Mid-term proved particularly useful. Large amount of work which required the design of the aircraft to be fixed was identified. This meant we needed to have an internal deadline on which the design was frozen, which helped tremendously in our planning.

The WBS was used to create the Work Flow Diagram and the Gantt chart. The Work flow Diagram was mostly used to identify the order in which certain design phases had to be performed and where concurrent engineering is possible. Furthermore it was used to identify bottlenecks in the design process which could then be used in the resource allocation. The WFD was updated whenever the WBS was updated, so like the WBS it was often outdated and it could be more useful if updated more frequently.

A.1.2. Gantt-chart

The Gantt chart was used to make the initial planning of the project. The Gantt chart was not updated on a daily basis, instead it was used to determine internal deadline when certain parts of the project needed to be finished. The day to day planning was done through the whiteboard planning and internal meeting.

A.1.3. Whiteboard planning & internal meetings

The Whiteboard planning was very similar to a Gantt chart, but instead of digital it was made on a whiteboard. This planning included all task that needed to be performed during the week, and presented part of the planning of the design phase. It showed the task, progress and deadline of the task. The advantage of the whiteboard planning over the Gantt chart was the fact that it was visible for all group members at all times and it is easier to adjust quickly. These advantages were especially useful during the internal meetings. Every day started with a ”stand-up” during this stand up all team-members tell what they will work on that day and every day was ending with a slightly longer ”wrap-up meeting” where everybody gave an update on their progress. The stand-up’s made sure all tasks were covered and no tasks would be covered twice, if people needed to work together on a task this was also ironed out during the stand up. The wrap up served more as a way to make sure the project was still going according to the planning, this was also the moment where the resources for

the next day were assigned and points of discussion could be addressed.

A.1.4. Functional analysis & Requirements

The functional breakdown and functional flow diagram have been very useful in the identification of the functions of the system and especially the subsystems. The tools were used to identify many of the requirements and risks of the system. The FBD and FFD were first made for the baseline and then reviewed for the final report.The FBD and FFD were at first very non-specific, as the concept was not selected yet. Throughout the preliminary design the FBD and FFD could be updated as more design options were traded off and selected. The FBD and FFD were used especially at the initial set-up of the requirements. However, they were not consistently used for the later stages, which should have been done to generate halfway the project subsystem requirements.

The requirements were first set up during the baseline, and then reviewed for the mid-term and final report. However throughout the design process too little attention was paid to the requirements. This meant that during the first set-up of the compliance matrix some of the requirements were not yet met. Fortunately there was enough time to change parts of the design such that the system met all requirements.

A.1.5. N2 chart

The N2 chart was used to identify the models to be made for the design of the system and the interfaces between these models. The N2 chart gave a good overview of where the iterations should happen and where it is not required. After a model was finished and the outputs were calculated, the N2 chart was checked to see where the inputs should go to. In case an iterative loop was seen, the respective models were iterated until the values converged and the iterated output was then used for the next model on the N2 chart. The N2 chart should have been checked a bit more thoroughly as a mistake was found during the aircraft design process at the end of the design phase. An element was missing between the landing gear design and the fuselage design which caused us to miss the increased dimensions of the landing gear to not iterate with the fuselage dimensions. In the end we had to enlarge the fuselage and had to do a final iteration, which delayed our design freeze by one day. However, there could have been way more issues similar to this scenario but the N2 chart prevented such issues very effectively.

A.2. Personal contributions to the project

In this section all team-members will discuss their personal contribution to the project. A detail task division of the sections and the people who worked on them is given in table A.1.

A.2.1. Max Aalberse

My contribution for this report starts at the Market Analysis, after this I joined the aircraft design team with the first weight estimations and the Thrust and Wing Loading section. When this was finished i continued into programming the loading diagram and scissor plot calculations and afterwards the final location of the wing. This took a lot of effort since we had a difficult load case and it took some time to find the final solution. The electrical system, fuel, and payload system lay-out were also performed by me. Also the navigation system section and the LOS communications as well as a few small other sections in the communications chapter were performed by me. Finally I also worked on the final cost estimation of the mission.

A.2.2. Elja Ebbens

I started the final report phase by revising the N2 chart with Maaike as it was important for the aircraft design phase to have a proper N2 chart, and to identify the points of iterations.

Afterwards I focused on the initiation of the aircraft design. I started working on the fuselage design and with it the preliminary empennage design. As all the separate subsystems had to be integrated into the aircraft fuselage, I made sure to assess the size constraints for the avionics from the operations subsystem team and the size constraints for the payload subsystem from the payload subsystem team. A volume budget was also made. I optimised the fuselage dimensions for zero-lift drag and made sure that everything fitted into the fuselage. I also did V&V on this model. After having set-up the fuselage design model, I worked with Miha on the iterations of the OEW and the final aircraft iteration which incorporates the more advanced empennage sizing. I also worked on the plots of the scissor plot and loading diagrams. Lastly, I worked on the cruise performance analysis and the altitude envelope.

A.2.3. Simon van den Eijkel

I contributed to this report in both a technical and an organisational way. I started the final phase of the DSE and have done the initial planning for these weeks. In this report, I have worked on the Aerodynamics and Stability in XFLR5 to validate Aerodynamic assumptions and to design for Stability. After this, I created a model for the V-N diagram in Matlab, I have analysed the RAMS of ACT together with Amber, I have analysed the selected airports and I have conducted the Sensitivity analysis together with Madelon.

A.2.4. Kees ’t Hooft

The first area I worked on for the final report was updating the work breakdown structure so it was up-to-date for the remainder of the DSE. Following this, I worked with Amber on the class II weight estimation, and then spent a long time looking into the engine selection. The two remaining areas I studied was the noise pollution at the airports, and the aircraft performance analysis, for which I focused on all aspects of the flight profile except for cruise, and worked in conjunction with Maaike and Elja.

A.2.5. Niels Schiettekatte

During the first week I continued working on the payload concepts with Madelon. We tried to finish as much as possible so we could start working on the aircraft analysis and design. During the second week I started working on the structural analysis model together with Joris. We also selected the material that the aircraft will be made of. Next, Joris and I briefly worked on the aeroelasticity. I updated the FFD and FBS after that, together with Amber. Madelon and I revisited the payload to finish the chapter, because some parameters had changed over the weeks and some things could only be finished after some parameters were known. After that I worked on the compliance matrix together with Maaike. Finally, I worked on the heating and the de-icing system of the aircraft.

A.2.6. Maaike Sickler

For the final report I contributed by first updating the N2 chart together with Elja for the remainder of the DSE. I then briefly worked on the communication collision avoidance system, after which I started on the Class I weight estimation for the landing gear. After this I worked on the landing gear sizing, tire selection and positioning with Madelon. Following this I analysed the aircraft performance with Kees, on which Kees reported. Then I briefly joined Madelon to assist her with the post-DSE planning. Niels and I worked on the compliance matrix together. After this I reorganised and wrote the technical risk assessment, based on the current stage of the report. Apart from these tasks I have been involved with the group organisation and resource allocation.

A.2.7. Amber Stienstra

In this report I updated the functional flow analysis, to match the new insight we have for this project. I spent a large part of my time on the operations concepts description, working on the analysing the effects of weather

and setting up the ground logistics. Together with Kees I set up the initial model for the Class II weight estimation. Next I worked on the aerodynamic and stability and control analysis with Simon. Furthermore I did the RAMS and sustainability analysis, which included the maintenance plan and CO_2 emissions analysis.

A.2.8. Madelon Stol

For the payload section I worked mainly on the dispersion characteristics, payload storage tank and system testing. After this was finished I worked on the landing gear design and tire selection with Maaike, further I worked out the post-DSE project development and Gantt chart and finally I worked on the sensitivity analysis together with Simon. A considerable part of my day-to-day work was LaTeXmaintenance (set-up templates - issue fixing) and MATLAB troubleshooting.

A.2.9. Joris Vlasblom

During this project I have contributed both in organisational as well as a technical aspects. My organisational contribution is most evident in my co-chairmanship with Simon. Furthermore I set-up the WBS and Gannt chart for the final phase of the project and evaluated the use of PM/SE tools. My technical contribution to the project starts with optimisation of the operations and fleet-size using the class I weight estimations. Then I worked together with Amber and Madelon on the routing of the aircraft. The next thing I worked on was the communications system of the aircraft, here I focused on the integration of the entire communications system and the BLOS communications. When this was finished I set-up the structural analysis for the fuselage, Niels joined the structures and analysed the structure of the wing. During the analysis of the structure we also performed a trade-off for the materials. Later we analysed the aeroelasticity of the wings. Finally I made the cost analysis, analysed the maintenance procedures with Amber and worked on the budgets and contingencies.

A.2.10. Miha Zupanič

After the midterm report I planned and organised the work on aircraft design. Together with Elja I established a ”Parameter sheet” where all the relevant design parameters for the aircraft, as well as the payload subsystem and operations were gathered. I encouraged the group members to add and update the parameters daily. The parameters in the sheet were accompanied by the date of update, the method and responsible person. During the aircraft design phase I worked on the class I and class II weight estimation, wing planform, wing airfoil, detailed drag estimation, HLD’s, loading diagram, aileron and rudder design and directional stability. Moreover, I worked with Elja on the aircraft class II weight estimation iterations and the wing positioning with Max. I worked on the verification and validation of the aircraft design methods I used. When the design was frozen I made the CATIA model of the aircraft. From this model I made 3-view drawings and renderings for the DSE poster. Moreover, I helped with the overall poster design and written the text for it. In the end I have written the recommendations for the post-DSE aircraft design.

Table A.1: Work Division per Section

Section:	Max	Elja	Simon	Kees	Niels	Maaike	Amber	Madelon	Joris	Miha
Executive Overview		x		x		x	x		x	x
1. Introduction						x				
2. Market Analysis	x									
2.1 Potential Users and Buyers	x									
2.2 Suppliers	x									
2.3 Competition	x						x			
2.4 Existing Aircraft	x									
2.5 Funding	x									
2.6 Public Opinion	x									
3. Operations Concept										
3.1 Operations and Logistics							x			
3.2 Airport Operations			x	x			x			
3.3 Logistics and Ground Support							x		x	
3.4 Mission Profile							x		x	
3.5 Flight Path							x		x	
4. Functional Analysis										
4.1 Functional Breakdown					x		x			
4.2 Function Flow Diagrams				x	x		x			
5. Payload Concept										
5.1 IN Strategy					x					
5.2 Dispersion of IN								x		
5.3 IN Material					x					
5.4 Injection System					x					
5.5 Payload System Components					x			x		
5.6 Monitoring System					x			x		
5.7 Integration into Existing Aircraft					x			x		
5.8 Compatibility with Silver Iodide					x					
6. Aircraft Design										
6.1 Class I Weight Estimation	x		x			x			x	x
6.2 Thrust and Wing Loading	x	x								
6.3 Aircraft Configuration Trade-off				x						x
6.4 Wing Design				x						x
6.5 Preliminary Fuselage & Empennage		x								
6.6 Drag Estimation										x
6.7 Landing Gear Positioning						x		x		
6.8 Engine selection	x			x						
6.9 Class II weight estimation		x	x	x			x			x
6.10 Loading Diagram	x	x								x
6.11 Sizing for Stability and Control	x	x								x
6.12 Final Aircraft Wing, Fuselage & Empennage Sizing		x								x
6.13 Electrical System	x									
6.14 Fuel and Payload System Lay-out	x									
7. Aircraft Performance										
7.1 Aerodynamic Analysis			x				x			
7.2 Stability and Control Analysis			x				x			
7.3 Structural Characteristics					x				x	
7.4 Aeroelasticity					x				x	
7.5 Flight Profile Diagram		x		x		x				
7.6 Take-Off				x		x				
7.8 Turn						x				
7.9 Cruise		x								
7.10 Descent				x		x				
7.11 Diversion				x						
7.12 Landing				x		x				
7.13 Altitude Envelope		x								
7.14 All Weather Operations					x					x
8. Communication and Navigation										
8.1 Navigation System	x									
8.2 Collision Avoidance System						x				
8.3 Control and Communications	x								x	
8.4 LOS Communications Design	x									
8.5 BLOS Communications Design									x	
8.6 Communication System Integration							x		x	

Table A.2: Work Division per Section

Section:	Max	Elja	Simon	Kees	Niels	Maaike	Amber	Madelon	Joris	Miha
9. Reliability, Availability, Maintainability and Safety										
9.1 Reliability			x				x			
9.2 Aircraft Maintenance			x				x		x	
9.3 Payload Maintenance							x			
9.4 Safety			x				x			
9.5 Availability			x				x			
10. Resource Allocation, Budget and Cost Breakdown										
10.1 Cost Breakdown Structure	x								x	
10.2 Budget Breakdown and Contingencies									x	
11. Technical Risk Assesment										
11.1 Payload						x				
11.2 Operations						x	x			
11.3 Aircraft						x				
11.4 Project Development						x				
12. Sustainable Development Analysis										
12.1 Economic Sustainability							x			
12.2 Environmental Sustainability				x			x			
12.3 Social Sustainability							x			
13. Verification and Validation										
13.1 Class I Weight Estimation									x	x
13.2 Class II Weight Estimation				x			x			x
13.3 Fuselage Length Optimisation		x								
13.4 Scissor Plot	x									
13.5 Drag Estimation										x
13.6 V-N Diagram			x							
13.7 Landing Gear Design						x				
13.8 Structural Analysis					x				x	
13.9 Cost Analysis									x	
14. Requirements Compliance Matrix										
14.1 Requirements Compliance Matrices					x	x				
14.2 Feasibility Analysis					x	x				
15. Sensitivity Analysis										
15.1 Sensitivity to Seeding Requirements			x				x	x		
15.2 Sensitivity to Airplane Performance			x							
16. Project Design and Development Logic and Post-DSE Planning						x		x		
17. Conclusion and Recommendation						x				x
A. Work Division	x									
A.1 Evaluation of PM/SE Tool Use									x	
A.2 Personal Contributions to the Project	x	x	x	x	x	x	x	x	x	x